ADSORPTION OF ADENINE AND PHENYLGLYCINE ON Cu(110) SURFACES STUDIED USING STM AND RAIRS

Lanxia Cheng

A Thesis Submitted for the Degree of PhD
at the
University of St Andrews

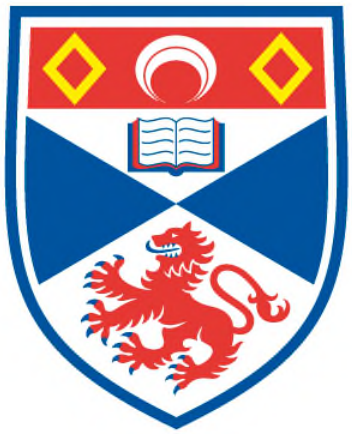

2011

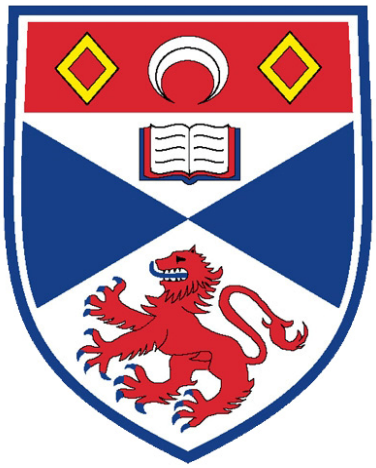

University
of
St Andrews

Adsorption of adenine and phenylglycine on Cu(110) surfaces studied using STM and RAIRS

Lanxia Cheng

Thesis submitted in accordance with the requirements of the University of St-Andrews for the degree of Doctor of Philosophy

November 2010

Declaration

I, Lanxia Cheng, hereby certify that this thesis, which is approximately 25,7793 words in length, has been written by me, that it is the record of work carried out by me and that it has not been submitted in any previous application for a higher degree.

DATE **SIGNATURE OF CANDIDATE**

I was admitted as a research student in September 2006 and as a candidate for the degree of Ph.D. in October 2006. The higher study for which was carried out in the School of Chemistry, University of St Andrews between 2006 and 2010.

DATE **SIGNATURE OF CANDIDATE**

I hereby certify that the candidate has fulfilled the conditions of the Resolution and Regulations appropriate for the degree of Ph.D. in the University of St Andrews and that the candidate is qualified to submit this thesis in application for that degree.

DATE **SIGNATURE OF SUPERVISOR**

In submitting this thesis to the University of St Andrews I understand that I am giving permission for it to be made available for use in accordance with the regulations of the University Library for the time being in force, subject to any copyright vested in the work not being affected thereby. I also understand that the title and the abstract will be published, and that a copy of the work may be made and supplied to any bona fide library or research worker, that my thesis will be electronically accessible for personal or research use unless exempt by award of an embargo as requested below, and that the library has the right to migrate my thesis into new electronic forms as required to ensure continued access to the thesis. I have obtained any third-party copyright permissions that may be required in order to allow such access and migration, or have requested the appropriate embargo below.

The following is an agreed request by candidate and supervisor regarding the electronic publication of this thesis:

Access to all of printed copy but embargo of all of electronic publication of thesis for a period of one year on the following grounds of publication would preclude future publication.

DATE **SIGNATURE OF CANDIDATE**

SIGNATURE OF SUPERVISOR

Acknowledgements

First, I would like to express my deep and sincere gratitude to Prof. Neville Richardson for giving me the opportunity to pursue my doctor's study in his group. His encouragement, guidance and valuable suggestion from the initial stage to the final level enabled me to develop an understanding of the subject, and also provided a good basis for the work presented in this thesis. Thanks for the financial support from the EaStCHEM funding, which made my dream of studying here come true.

I wish to show my sincere thanks to my working colleagues, in particular Dr. Steve Francis for his generous technical support and valuable instructions throughout my PhD studies. And also Dr. Federico Grillo, he has given me lots of assistance in solving the problems I encountered and helpful suggestion in the performance of the experiments. I am very grateful to his patience in revising the English of my manuscript and the valuable discussions we had during my thesis writing. The thesis would not have been possible without their encouragements and support.

I awe my thanks to Dr. Marco Caffio for conducting the LT-STM experiments; Dr. Renald Schaub for use of his LT-STM instrument; and Dr. Herbert Fruchtl for his support in the theoretical calculation done in my work.

I wish to thanks all the warm-hearted colleagues working here for the friendly research environment they have created, which made my overseas research experience become more enjoyable and unforgettable. Especially great thanks to Dr. Bo Wang, Daniel Tee, Siddharth Jethwa, for their kind and in-time assistances during my work; Karen Wilson for the good time we spent together in gyms and playing badminton.

Lastly, I wish to express my thanks to my parents, for their moral support and encouragements whenever I am in difficulty and depression. Special to my husband, he is always standing by my side to share with me the happiness and bring me the courage and confidence in front of hard task.

Abstract

The adsorption of biologically active molecules, such as the DNA bases, amino acids, on solid surfaces has been the subject of a number of experimental and theoretical studies in the past years. The understanding of the self-assembly mechanism of bioactive molecules on surfaces not only is fundamentally important in the preparation of bioactive surfaces, but also provides us insight into the origins of life and homo-chirality in nature.

In this thesis, the adsorption behaviour of adenine and phenylglycine molecules on the Cu(110) surface has been investigated in order to understand the effect of experimental parameters like coverage, annealing temperature etc. on the molecular orientation and the ordering of the adlayer structures.

The thesis is organised in six parts:

- Chapter I gives an introduction to the relevance of surface sciences studies, describing the phenomena of surface chirality and molecular adsorption behaviours on surfaces.
- Chapter II gives an overview of the experimental techniques and introduces basic concepts of theoretical calculation.
- Chapter III investigates the effect of experimental parameters, *e.g.* surface coverage, annealing temperature and substrate temperature on molecular diffusion, molecular orientation and ordering of the adlayer structures. LT-STM examination of the contrast variations of adenine chains and isolated adsorbate as a function of the tip-sample bias voltage is also presented with the aim to understand the tunnelling mechanism.
- Chapter IV shows RAIR spectra studies of the evolution of phenylglycine molecular orientation as a function of surface coverage at room temperature. The adsorption geometry and binding nature of phenylglycine is discussed.
- Chapter V concerns with the adsorption behaviours of phenylglycine and adenine on Cu(110) surface pre-covered with oxygen.
- Chapter VI summarises the conclusions and describes the outlook of some future work.

List of Acronyms

UHV	Ultra-High Vacuum
STM	Scanning Tunnelling Microscopy
LEED	Low Energy Electron Diffraction
RAIRS	Reflection Absorption Infrared Spectroscopy
HREELS	High Resolution Electron Energy Loss Spectroscopy
NEXAFS	Near-edge X-ray Absorption Fine Structure
XPS	X-ray Photoelectron Spectroscopy
FCC	Face-Centred Cubic
HCP	Hexagonal Close Pack
BCC	Body-Centred Cubic
CCD	Charge-Couple Device
MCT	Mercury Cadmium Tellurium
DNA	Deoxyribonucleic Acid
RNA	Ribonucleic Acid
DFT	Density Function Theory
B3LYP	Becke, three-parameter, Lee-Yang-Parr
PBE	Perdew-Burke-Ernzerhof
GGA	Generalized Gradient Approximations
TSK	Terrace-Step-Link
2D or 1D	Two or one -dimensional
ML	Monolayer

Contents

Declaration i

Acknowledgements ii

Abstract iii

List of Acronyms vi

CHAPTER I Introduction

1.1 Background ……..... 1

1.2 Molecular and Surface Chirality ……... 5

1.2.1 Molecular chirality ……. 5

1.2.2 Surface chirality…….. 7

1.2.3 Chiral motif created via adsorption of prochiral molecules**……** 9

1.2.4 Chiral surface created via adsorption of chiral molecules……... 11

1.3 Molecular Adsorption at Surfaces……. 14

1.3.1 Molecular sticking coefficient……. 16

1.3.2 Physisorption and chemisorption…… 17

1.3.3 Molecular diffusion at surfaces……... 18

1.4 Single Crystal Surface…….... 22

1.4.1 Miller indices……... 22

1.4.2 Surface defects……. 25

1.5 Nucleobases and Amino Acids…… 26

1.5.1 Nucleobases……..... 26

1.5.2 Amino acids……. 27

1.6 References……. 29

CHAPTER II Experimental

2.1 Introduction……...……... 34

2.1.1 The system……...…… 34

2.2 The Ultra-High Vacuum System……. 35

2.2.1 Achieving and maintaining UHV……...……. 37

2.2.2 Sample and STM tip preparation……...…..... 38

2.2.2.1 Sample preparation……..……. 38

2.2.2.2 STM tip preparation……..…… 41

2.3 Scanning Tunneling Microscopy (STM)……..……. 43

2.3.1 Principle of electron tunneling……...……. 44

2.3.2 Scanning modes……..……..... 46

2.4 Low Energy Electron Loss Diffraction (LEED)……..……. 47

2.4.1 Basic principle of LEED…….……... 47

2.4.2 Experimental setup……..... 50

2.5 Reflection absorption Infrared Spectroscopy (RAIRS)…..…….……... 52

2.5.1 Surface dipole selection rule……...…… 53

2.5.2 UHV-RAIRS experimental setup…… 54

2.6 DFT Calculation ……...….. 55

2.7 Experimental Setup……..…….. 56

2.8 References……...…. 58

CHAPTER III

Adsorption of Adenine on Cu(110) Surfaces

3.1 Introduction……...….. 59

3.1.1 Adsorption of adenine on surfaces……...….. 59

3.1.2 Adenine molecule……..…. 64

3.2 Results and Discussions……..… 68

3.2.1 High coverage Adenine/Cu(110) ……..…….. 68

3.2.1.1 RAIRS studies……..… 69

3.2.1.2 STM and LEED studies…….…..… 75

3.2.1.3 Discussions…….…...… 79

3.2.2 Effect of annealing on Adenine/Cu(110) …….……...….. 80

3.2.2.1 STM studies……...…. 80
3.2.2.2 Discussions……...…… 84
3.2.3 Effect of substrate temperature on adenine self-organization…..….. **86**
3.2.3.1 STM studies…….…..... 87
3.2.3.2 Discussions…… 90
3.2.4 Effect of deposition rate on adenine adlayer structures……..... 94
3.2.4.1 STM studies…….….. 94
3.2.4.2 Discussions……..…..…… 102
3.2.5 Very low coverage adsorption on Cu(110) surfaces……....…..… 114
3.2.5.1 STM studies of very low coverage at 440 K…..…….....….. 115
3.2.5.2 Discussions……...…… 117
3.2.6 Contrast variations of adenine overlayer structures…… 119
3.2.6.1 Contrast changes at room temperature……...…..….. 120
3.2.6.2 Intermolecular contrast variations at 70 K……...… 123
3.2.6.3 Contrast variations of single adsorbed species…….…..... 127
3.3 Conclusions……...… **130**
3.4 References……...….. **133**

CHAPTER IV

(*R, S*)-phenylglycine on Cu(110) Surfaces

4.1 (*R, S*)-phenylglycine…….… **136**
4.2 Results and discussions…….…….… **140**
4.2.1 KBr spectrum and DFT calculations of phenylglycine ionic species.. 140
4.2.2 RAIR spectra of (*R, S*)-phenylglycine/Cu(110) …….……...…. 145
4.3 Conclusions……...… **157**
4.4 References…… **158**

CHAPTER V

Adsorption of (*R, S*)-phenylglycine and Adenine on p(2×1)O/Cu(110) Surfaces

5.1 Introduction…….. 160
5.2 Experimental……...…. 161

5.3 Results and Discussions……...… **162**
5.3.1 (*R*, *S*)-phenylglycine on Cu(110) surfaces…..……. 162
5.3.2 (*R*, *S*)-phenylglycine decorated added Cu-O rows……..…… 167
5.3.3 Adenine co-adsorbed on p(2 × 1)O/Cu(110) surfaces……...……. 169
5.4 Conclusions……...… **171**
5.5 References……...….. 172

CHAPTER VI

Conclusions and outlook

6.1 Conclusions……....….. 173
6.2 Outlook……...…….. 176
6.3 Papers under preparation……...…… 177

CHAPTER I

Introduction

1.1 Background

Studies of the behaviour of organic molecules in terms of their chemical structure, molecular orientation and bonding upon adsorption on solid surfaces, have been a subject of great interest in recent decades. It is believed that a good knowledge of the interactions between bioactive molecules, such as amino acids [1, 2] or nucleic acids [3-6], and solid surfaces is not only relevant to the preparation of biocompatible materials and biosensors [7-9], but also may contribute to explain the possible mechanism of prebiotic evolution before sophisticated organic molecules were formed [10-11]. In addition, adsorption of organic molecules with multifunctional groups is also one of the promising approaches to modifying surface properties by introducing additional functionalities, which gives rise to a wide range of applications in catalysis, molecular sensing and recognition, etc. [12-17].

Surface functionalization has been a very interesting and challenging aspect of the future development of new nanotechnological devices [12-17]. One promising approach to achieve this goal is through the adsorption of chemically reactive organic molecules, especially those containing multifunctional groups, such as carboxylic acids, amino acids, anhydrides and aromatic rings on target surfaces. After interacting with the surfaces, adsorbates can assemble into ordered two-dimensional superstructures where the molecular properties are preserved or slightly changed. At the same time the primary functionalities of the molecule can remain unchanged; by means of this method, therefore, surface functionalities can be tailored.

One well-known example of surface functionalization is the introduction of chirality onto an achiral surface through adsorption of chiral molecules. In heterogeneous catalysis [18-20], the creation of such surfaces with specific chirality offers the opportunity for the ultimate control over a chemical reaction by directing its enantioselectivity. Surface chirality is particularly attractive due to its potential applications in the pharmaceutical production, for an efficient separation of large

quantities of pure chiral product from its racemic mixture.

In order to obtain a well-functionalized surface using multifunctional organic molecules, the underlying driving force and mechanism responsible for the formation of ordered superstructures has to be well understood. Self-assembly of organic molecules on surfaces is defined as a spontaneous and reversible process in which molecules, mediated by a subtle interplay of various interactions existing between them, and that between adsorbates and substrates, assemble into ordered, stable, typically non-covalently bonded superstructures when an equilibrium state is reached [21]. In other words, the resulting superstructure observed on a surface, as regards the local molecular orientation, bonding and conformation, is an outcome of the delicate balance of varied complex intermolecular interactions, such as hydrogen bonding, van de Waals forces, π-π and other electrostatic interactions.

The behaviour of organic molecules on surfaces is not only influenced by the properties of the substrate, but also in large degree by the molecular chemical properties. The characteristics of the new system are a reflection of changes occuring in the molecular geometric and electronic structure upon adsorption, along with correlated alterations occurring in the substrate electronic properties. The understanding of the various substrate and lateral interactions that govern the ultimate orientation and two dimensional organization of an adsorbate at metal surfaces is the fundamental step toward controlling surface functional modification, in order to achieve the goal of developing new biomaterials or microelectronics.

Among the number of surface techniques widely used to study organic ultrathin films, scanning tunneling microscopy (STM) is the most popular and powerful tool due to its capability of providing us with a real space image of the adsorbed structure at a molecular level. Through a detailed analysis of the recorded images, information concerning the unit cell dimensions and geometries can be obtained. However, in practice STM cannot be used as a stand-alone technique able to give us sufficient information for a convincing structural determination. Hence, other surface sensitive spectroscopic techniques, such as reflection absorption infrared spectroscopy (RAIRS) and electron energy loss spectroscopy (EELS) are also employed, because of their unique capabilities in giving information on the molecular orientation, bonding natures and surface superstructure periodicity. These experimental techniques, in combination with the data simulations and theoretical calculations, allow us to model

the adsorbed species with respect to the chemical nature, bonding, and orientation more effectively.

In this thesis, the study of adenine on metal surfaces and its interactions with other adsorbates have been studied in detail, to improve an understanding of thin prototypical biomonolayer molecular adsorbates. Self-assembly of adenine (one of the DNA bases) on various surfaces under either liquid or ultra-high vacuum condition has been studied, using STM, low electron energy diffraction (LEED), and RAIRS. Previous research revealed that adenine formed a commensurate rectangular unit cell with two glide planes, containing four adenine molecules, on the graphite surface [22-26], which indicated a relatively strong molecule-substrate interaction. On the Cu(111) [27-32] adenine molecules assembled into one-dimensional chains and two-dimensional hexagonal networks at low temperature (70 K) [29], as a result of the intermolecular interactions, mainly originating from inter-molecular double hydrogen bonding. Recently, low temperature STM investigations (150 K) of the adsorption of adenine on the Au(111) surface [33, 34] under ultra-high vacuum conditions have been reported. Adenine was found to form two different honeycomb networks, upon deposition onto the surface at room temperature. One structure showed a hexagonal unit cell containing four adenine molecules, consistent with the hexagonal networks previously reported on a Ag-terminated Si(111) [35] surface; the other was a new superstructure which contains two molecules per primitive unit cell. Both structures were non-chiral and coexisted as neighboring domains on the same island. Increasing the annealing temperature led to the growth of one structure at the expense of the other.

In all these structures, adenine molecules are considered to be flat lying (or slightly tilted) with their molecular planes parallel to the surface at a considerable distance; the intermolecular hydrogen bonding is the dominating interaction responsible for the formation of the 2D networks. The common aspect of these experiments is that all STM measurements needed to be carried out at low temperature. This might be due to the low corrugation of the (111) surface which make the molecules highly diffusible over the surface, thus low temperature deposition is employed with the aim of reducing molecular diffusion upon scanning.

Room temperature STM investigations of the adsorption of adenine on Cu(110) surfaces have been conducted by Chen *et al.* [36], revealing that adenine could form

two reflection related domains after annealing the sample to 440 K. Each domain is composed of ordered and short adenine molecular dimer chains aligning along the (1, 2) and (-1, 2) directions, respectively. This serves as a model system for studying the molecular enantiomeric interactions on a solid surface. However, the problem with these chiral-related adenine dimer chains is that the domain sizes are very small, consisting of short chains with an average length distribution of 38 Å, which corresponds to five unit cells along the chain growing direction. One of the aims of this thesis is to determine how experimental parameters, such as temperature and coverage, affect the domain size, hoping to increase the length of these dimer chains. Bias dependent images of single adenine molecules adsorbed on the Cu(110) surface have also been collected in order to investigate the adenine molecular orbital contribution to the image as a function of the scanning bias applied.

Co-deposition of phenylglycine onto the adenine dimer chain pre-covered Cu(110) surface led to the formation of phenylglycine molecules of single chirality decorated chains [37]. This means (*S*)-phenylglycine molecules only interact with the chains aligning along the (1, 2) direction, while (*R*)-phenylglycine molecules connect only with the chains growing along the (-1, 2) direction. This finding is a particularly important example of chiral recognition at molecular level in adsorbed species. In addition, interactions of (*R, S*)-phenylglycine with Cu(110) in the absence of adenine have been investigated using LEED, EELS [38, 39]. In this case (*R, S*)- refers to a racemic mixture of (*R*)- and (*S*)- enantiomers. They showed the presence of ordered enantiomeric separated chiral overlayer structures, exhibiting commensurate unit cells with $\begin{pmatrix} 5 & -3 \\ 4 & 1 \end{pmatrix}$ and $\begin{pmatrix} 5 & 3 \\ 4 & -1 \end{pmatrix}$ periodicities, at saturation coverage upon annealing to 450 K. Another structure was formed upon annealing to 420 K, showing (3 × 2) periodicity. In this research, I will present vibrational spectroscopy studies of adsorbed phenylglycine on Cu(110) using RAIRS, in combination with DFT calculations of the vibrational frequencies of the free zwitterionic and anionic phenylglycine species, in order to probe the evolution of the molecular orientation as a function of coverage.

In addition, co-deposition of phenylglycine and adenine onto the Cu(110) surface pre-covered with (2 × 1) oxygen copper added rows was studied using STM; this revealed a different surface behaviour for these bio-active molecules even though

both contain the NH_2 group which was reported to show strong tendency to react with the oxygen rows formed on Cu(110) surface.

1. 2 Molecular and Surface Chirality

1.2.1 Molecular chirality

Chirality, meaning handedness in Greek, is simply a geometric property, and originally refers to any object the image of which is not superimposable on itself by any translation and rotation. In chemistry, the resulting two distinguishable mirror images are called enantiomers or optical isomers, and the absolute configuration of each enantiomer is labelled (*R*) or (*S*) as determined by the Cahn-Ingold-Prelog rules [40, 41]. According to the rules, each of the four different side substitutents surrounding the chiral center, often a carbon atom, is assigned a priority based on its atomic number. If the substitutent having the lowest priority group, based on the atomic number of the allocated atoms, is placed away from the viewer, then the priority of the remaining groups can decrease either clockwise or counter-clockwise: they are labelled (*R*) or (*S*), respectively, Figure 1.1. Chirality is an inherent property of many biologically active molecules, especially amino acids and sugars. It is found that all of these compounds in their naturally occuring form are of the same chirality: amino acids are (*L*) and sugars are (*D*), where (*D*) and (*L*) is the nomenclature system commonly used in biochemistry to express the chirality of the biologically active molecules.

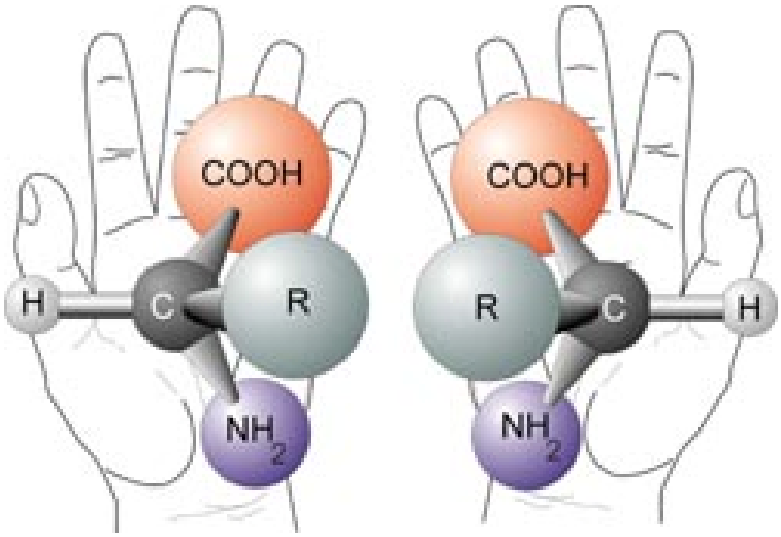

Fig. 1.1: Schematic representation of *S* (*L*) and *R* (*D*)-chirality of simple amino acid molecule, where *R* is the side chain referring to any functional group [42].

Beyond chemistry, a more popular and complete alternative, which could be applied widely in the determination of chirality existing generally in any object, is to determine whether an inversion centre or symmetry plane can be identified in the system. A chiral object always lacks these symmetry elements. This is also used to identify chirality at two-dimensional and inherent chiral surfaces.

Normally, enantiomers, regardless of being (*R*) or (*S*), behave identically, considering most of the chemical and spectroscopic properties, such as chemical reactivity, IR, NMR spectroscopy. A chiral molecule may smell differently to its enantiomer. A good example is the (*S*)-form of carvone, Figure 1.2, which smells like caraway, while its enantiomer has smell of spearmint [43]. The difference in smell is because the olefactory receptor of human beings has chirality that may respond differently to each of the enantiomers. One typical characteristic of enantiomers is their optical activities. It is discovered that enantiomers rotate the plane of the polarised light in opposite directions, either clockwise or counter-clockwise.

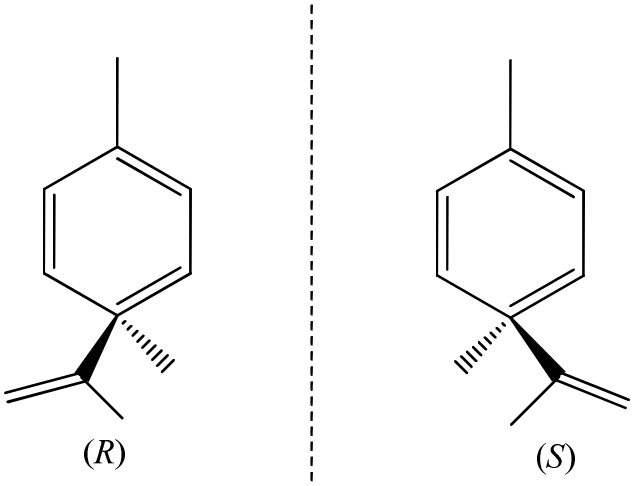

Fig. 1.2: Carvone is a molecule where the (*R*)-enantiomer (left) smells of spearmint, while its counterpart, (*S*)-form (right) has smell of caraway [43]. The olefactory receptor responds more strongly to one enantiomer than the other.

Purification of one specific enantiomer from its racemic mixture has attracted extensive attention, following realisation that each enantiomer displays a unique function in biological systems. It was found that in many cases, molecules of one enantiomeric form are helpful to the body while their enantiomeric counterparts might have side effects, even worse, show harmful effects [44]. Therefore, finding an effective synthesis of single enantiomer method to separate molecules of single chirality purposely from their naturally occurring racemic mixture has become a great challenge in pharmaceutical industry, because in the past almost all bio-active molecules are synthesized as a racemic mixture.

1.2.2 Surface chirality

A chiral surface is formed if there is no inversion or mirror plane symmetry present on the surface. Generally, there are two approaches widely used to bestow chirality on the surface. One way is via the adsorption of complex organic molecules, which provides a more sophisticated selectivity and asymmetrisation function to be introduced [45]. The alternative is via carefully cutting the crystal in such a way that chiral kinks and steps are exposed [46-48]; the Cahn-Ingold-Prelog analogy is used in

a similar way to determine the absolute stereochemistry of the kink site as (*R*) or (*S*) [47], Figure 1.3.

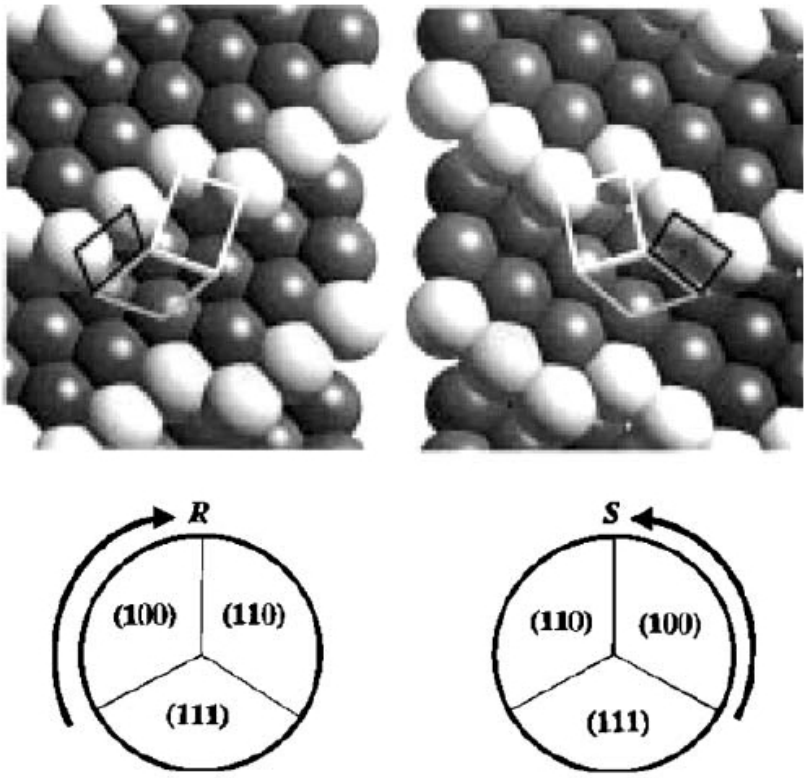

Fig. 1.3: Hard-sphere model of the chiral surfaces of Pt(6,4,3)^{R} and (6,4,3)^{S} . The three different facets, (110), (111), (100), composing the kink are indicated. The kink edges are highlighted. On the bottom, the Cahn-Ingold-Prelog analogy used to determine the absolute stereochemistry of the kink site as either (*S*) or (*R*) [46, 47].

As far as the former method is concerned, the creation of surface chirality includes two processes: the creation of local chiral motifs by single molecular adsorption onto a given substrate and the creation of chiral domains arising from the chiral arrangements of the individual motifs (*i.e.* organisational chirality or space group chirality) [49]. Chiral motifs can be created by adsorption of molecules of either inherent chirality or pro-chirality. Adsorption of inherently chiral molecules as the basic chiral building blocks onto the surface leads to the formation of a global chiral surface, because no mirror chiral motif can be conceived due to the inhibition of the formation of its mirror image. However, for the latter case, surface chirality is merely

limited to domains appearing at a local level over a restricted surface area, while chirality disappears at global level over the entire surface. No matter in which case, the creation of chirality requires the annihilation of the reflection symmetry that is originally perpendicular to the achiral surface of a given substrate via adsorption of organic molecules [49-51].

1.2.3 Chiral motifs created via adsorption of prochiral molecules

Prochiral molecules are a class of molecule widely employed to create chiral adsorbed motifs by means of adsorption. A prochiral molecule is an achiral molecule that becomes chiral due to the break of the symmetric elements in the single de-symmetrising step, which could arise from a physical interaction, or chemical reaction to a rigid adsorption [52]. In all these processes, the presence of molecules on surfaces leads to the removal of both molecular and surface reflection planes. Here, one example is the adsorption of a planar molecule onto the surface in such a way that breaks the molecular mirror plane symmetry. This is always the case for the molecular plane lying parallel to the substratre surface. The adsorption consequently leads to the formation of two enantiomers, which are not superimposable onto each other by any translation or rotation in the surface plane [49]. This phenomenon was well illustrated by 4-trans-2-(pyrid-4-yl-vinyl) benzoic acid (PVBA) adsorbing on Pd(110) [53, 54], where the two planar rings of PVBA could adsorb in either of the two orientations, Figure 1.4a. As a result, equal amounts of enantiomeric features were created due to the direct loss of the molecular mirror plane.

Another case is the adsorption of achiral molecules onto chemically active surfaces, where the strong interactions between more than one functional group and the substrate atoms can lead to the generation of highly defined adsorption geometry that causes the molecular mirror symmetry to be lost. This phenomenon was demonstrated by the adsorption of glycine, the simplest achiral amino acid, on a Cu(110) surface [55-58], Figure 1.4b, in which both the anionic carboxylate group and -NH_2 group interacted strongly with the copper atoms forcing its skeleton to align along the copper short bridge direction in two ways, either left-handed or right handed.

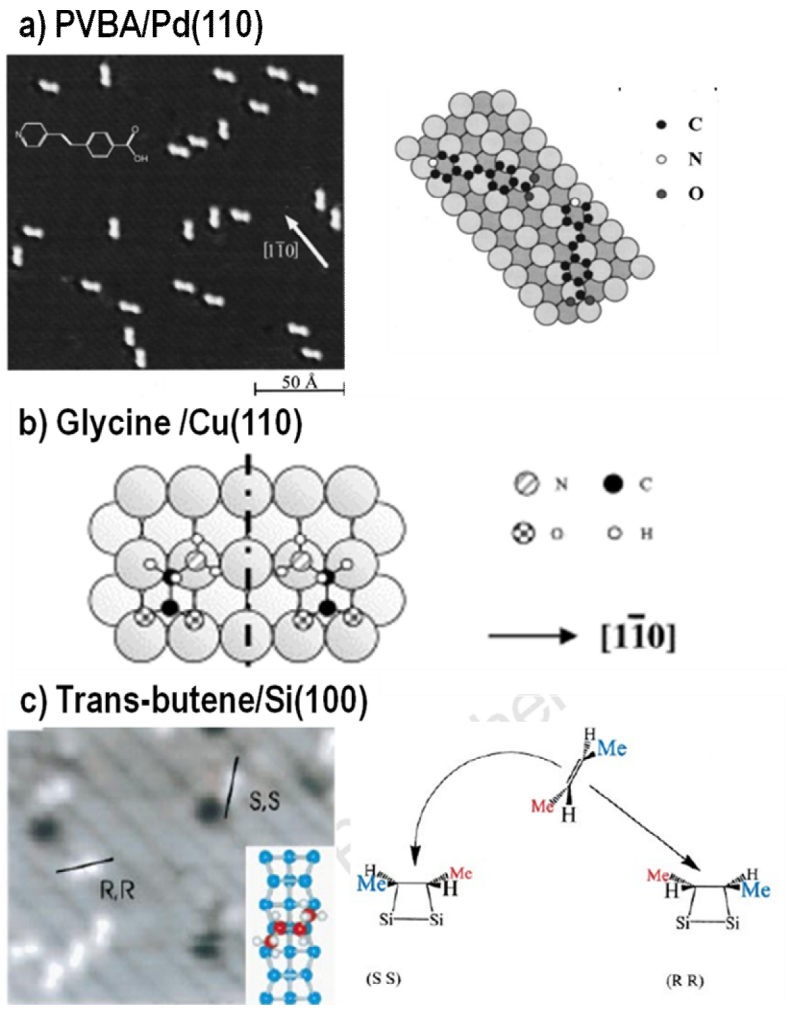

Fig. 1.4: Examples of local chiral motifs created via adsorption of prochiral molecules. a) STM image and model of the adsorption of PVBA on Pd(110) surface, showing the creation of mirror related chiral motifs through adsorption of planar prochiral molecules [54]. b) Schematic model of glycine adsorbed onto Cu(110), giving an example of chiral motifs created via rigid adsorption [49]. c) STM image and schematic showing the reaction of trans-butene on Si(100), which leads to the formation of (*S,S*) and (*R,R*) structures arising from the reaction of the silicon face with either faces of planar trans-2-butene molecule [59].

The last example is reaction induced chiral motifs. One example of this kind is the active adsorption of the trans-2-butene molecule at a Si(100) surface [59], leading to the production of (*R, R*) and (*S, S*) adsorption motifs in equal amounts, which were directly imaged by STM from the registry of the methyl groups with the underlying substrate, Figure 1.4c. In this adsorption system, the Si-Si dimers, which have σ and π bonds, *i.e.* some double bond character, are capable of interacting with the unsaturated double bonds of the butene molecule through the [2+2] cycloaddition reaction [60-

62]. This can re-hybridise the carbon atom from sp^2 to sp^3, leading to the creation of two chiral carbon centres upon adsorption.

The common characteristic of the chiral motifs created through adsorption of a prochiral molecule on surfaces is the production of enantiomeric motifs in equal amounts because they are energetically equivalent, and motifs with opposite chirality always have the same probability to be found on the surface. Chirality created in this way is limited to a local level. The organisation of these chiral motifs can lead to the formation of many forms of chiral ordering, ranging from chiral clusters to chiral chains to highly organized chiral domains. However, 2D chirality disappears over the entire surface area, making the overall surface achiral.

1.2.4 Chiral surface created via adsorption of chiral molecules

A truly chiral surface refers to a system possessing chirality in both a local and a global sense; this can only be achieved on an achiral substrate via the adsorption of an inherently chiral molecule. The phenomenon of globally organisational chirality was well determined by the adsorption of (*R, R*)- tartaric acid on Cu(110) surfaces [45, 59], Figure 1.5. This periodic chiral adlayer was composed entirely of the doubly dehydrogenated bitartrate species, bonded strongly to the surface via the four oxygen atoms of the carboxylate groups. The structural model determined from RAIRS, STM and LEED data showed that the individual motifs aggregate along the $<1\bar{1}4>$ direction, thus breaking the mirror symmetry of the Cu(110) surface. This organisational surface chirality was sustained at global level, and the switching of the surface chirality was achieved via the adsorption of the opposite enantiomer, the (*S, S*)-tartaric acid, where the mirror chiral adlayer consisted of long chains growing along the mirror $<\bar{1}14>$ direction. Similar phenomena of organisational chirality and chiral switching upon changing of enantiomer were also observed when (*S*)- and (*R*)-alanine were adsorbed on Cu(110) surfaces [60, 61]. The self-assembly of each original chiral species generates a truly globally handed organisation which is not superimposable on the mirror image created by its enantiomer. Coexistence of chiral separated domains occurs when the racemic mixture of chiral molecules are put on the surfaces. One

example that has been well-illustrated was the adsorption of phenylglycine on the Cu(110) surface [38]; the LEED patterns associated with each individual enantiomer were observed to coexist.

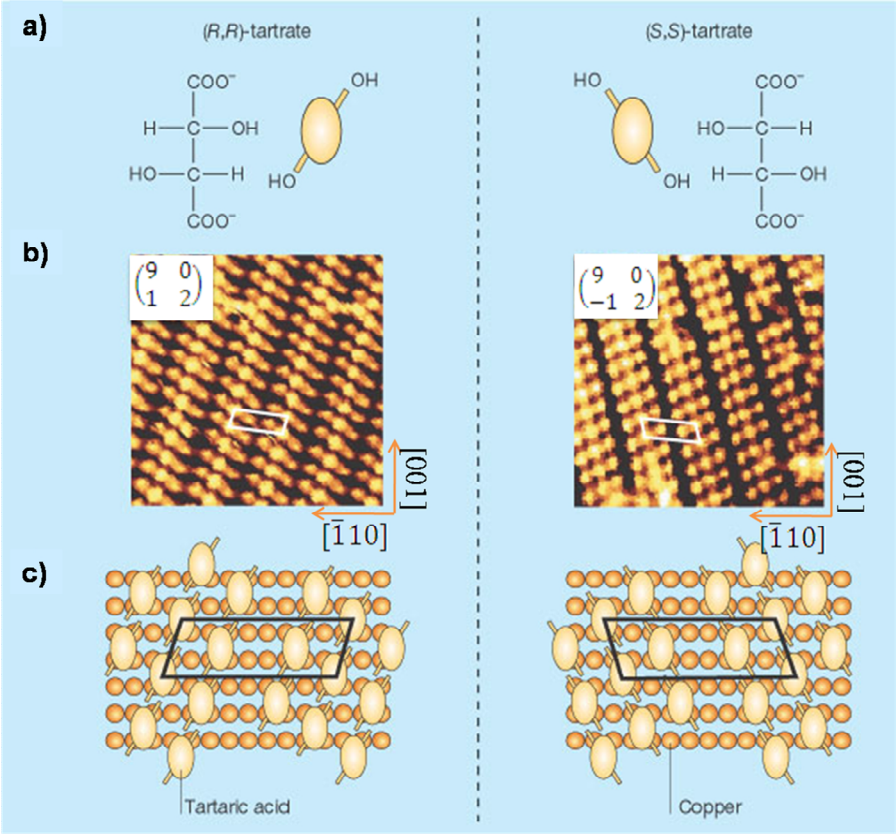

Fig. 1.5: a) Schematic of the dehydrogenated bitartrate species; b) STM images showing mirror chiral surfaces created by (*R*, *R*)- and (*S*, *S*)-tartaric acids on Cu(110); c) Structural models of the chiral domains constructed from RAIRS, STM and LEED data [adapted from Refs. [45, 59].

Self-assembly of chiral motifs, arising from either pro-chiral or chiral molecule, can yield highly organized and periodical arrays extended over large areas on the surface. Normally, several rotational and translational domains are formed over the entire surface because the driving forces, e.*g.* intermolecular hydrogen bond and van de Waals, contributing to the 2D ordering are short-range interactions. The symmetry of the unit cell in each chiral domain is assigned to one of the five surface space groups allowed at a chiral surface. Out of the 230 space groups existing in the three-

dimensional structures, only 17 are allowed for a two-dimensional structure at a surface because only those symmetry elements that are perpendicular to the surface can exist. The creation of chiral surfaces further requires the elimination of symmetry elements such as mirror planes and glide planes perpendicular to the surface, thus, only 5 space groups are left, described as C_1, C_2, C_3, C_4, and C_6 [62-65].

With a chiral surface, to ensure chirality extended at a global level, all the chiral domains formed must be equivalent and possess the same 'handedness'. Generally, only translational and rotational domains can be found on a global chiral surface [66]. Translational symmetry operations do not change the handedness of chiral organisations, thus, they are always allowed. For rotational domains, to ensure the preservation of the rotational symmetry of the original clean substrate, the number of rotational domains and the symmetry of the adlayer unit cell are constrained by the rule of surface symmetry conservation [46]. Take the chiral organisation formed on an fcc (110) surface for example: the presence of chiral adsorbates leads the surface symmetry to reduce from the original C_{2v} to C_2. If the adlayer unit cell has only C_1 symmetry, *e.g.* the 1D chiral chains, two rotational domains will be found on the same surface in order to recover the original surface C_2 symmetry. Only one domain is observed if the unit cell shows C_2 symmetry. Thus, the number of rotational domains decreases as the symmetry of the unit cell increases.

Reflectional domains are formed only on a local organisational chiral surface because this would lead to the coexistence of mirror-imaged domains, being necessarily not allowed on chiral surfaces extended at a global level. This phenomenon is observed on a chiral surface created via the adsorption of prochiral molecules, particularly, when the adsorbed chiral species of same 'handedness' aggregate along a direction aligning off the high symmetry axes of the underlying substrate, thus the symmetry planes of that surface are broken. Molecules of the opposite 'handedness' align along the mirror direction. In this case, two reflectional domains possessing local organisational chirality are formed with an equal probability, making the overall surface structures achiral. Each of the resulting chiral organisations is referred to as a homo-chiral domain, implying it is composed of molecules of a single chirality. In contrast, if both the vectors of the unit cell are aligned consistently with the symmetry axes of the substrates, hetero-chiral domains consisting of both enantiomers in equal amounts could exist.

The formation of chiral domains arising from the chiral organisations of individual chiral motifs is well-illustrated by the adsorption of amino acid bases and DNA bases on copper substrates. Most amino acids are inherently chiral molecules that adopt chiral adsorption geometries dictated by the strong substrate-adsorbate interactions, originating from the strong coordination of the $-NH_2$ group and deprotonated carboxylic group with the substrate atoms [38, 55-58]. The resulting chiral supramolecular assemblies are largely mediated by the intermolecular directional hydrogen bonds and the steric interactions. DNA bases are a class of prochiral molecules characterized by the heterocyclic structures that contain more than one electronegative nitrogen atom and electropositive CH group, which can participate in the formation of double hydrogen bonding. This type of intermolecular interaction is highly selective and directional; it plays a crucial role in directing and stabilizing the chiral organisations of adsorbed species [22-35].

However, since surface chirality is due only to removal of the mirror plane symmetry of the surface in the presence of a chiral adsorbate, the substrate electronic structure is not necessarily strongly perturbed. In other words, the chiral behaviour occurring to the underlying substrate electronic structure may be weak, likely because the molecule-substrate interaction is still not strong enough to cause significant change in the substrate electronic structure [67]. Therefore, the resultant surface is only bestowed with chirality physically rather than electronically.

1.3 Molecular Adsorption at Surfaces

Each unique superstructure appearing on the surface is in fact a macroscopic reflection of the various processes occurring at the atomistic scale. Figure 1.6 schematically illustrates the varied molecular behaviours occurring on a targeted surface [68]. As thermally vaporized molecules impinge on a given surface, under contamination free conditions, as in an ultra-high vacuum chamber, they may stick on a specific site by means of chemisorption or physisorption, depending on the strength of the interaction between adsorbates and substrate atoms. However, they can also undergo desorption, leaving the surface very soon after interaction; accordingly, there

is no adsorption eventually observed in this case. As for the molecules staying on the surface after impinging, some of them may diffuse across the surface seeking the most thermodynamically favorable states. Under the optimum condition, two or more of them can meet and stick together as dimers or nucleate in a specific way over large areas on the surface, leading to the observation of various supramolecular self-assembled structures.

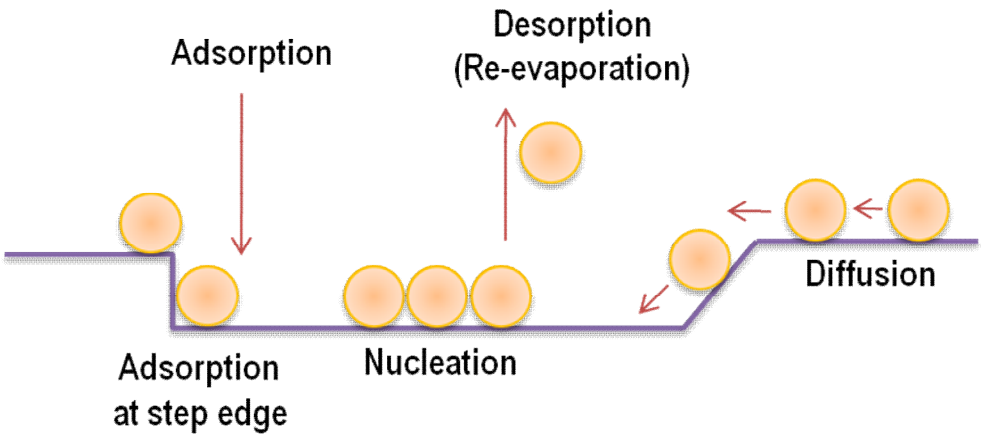

Fig. 1.6: Schematic representation of molecular behaviours upon impinging on the surface of interest (adapted from chapter 1 of Ref. 68).

In the adsorption process occurring at a surface, the primary mechanism underlying any molecular (also atomic) ordering is the migration of the adsorbed species, involving random hopping processes, on an atomistic scale [68, 69]. Theoretically, many factors can influence the degree of the ordering and assembly of the molecules, including the molecular sticking coefficient, the relative strength of various intermolecular and molecule-substrate interactions and the molecular diffusion rate. In experiments, the organization of the adsorbates at metal surfaces can be controlled through an appropriate choice of substrate geometry and optimization of the external experimental parameters, *e.g.* the temperature and the deposition flux rate.

1.3.1 Molecular sticking coefficient [69]

From a molecular kinetic point of view, the molecular adsorption rate is remarkably influenced by the molecular sticking coefficient, *S*, which is simply the probability of the particle sticking to the surface after impingement. It is described as the ratio between the number of the particles sticking on the surface per unit per time and that of those impinging, as given in the equation:

$$S = \frac{\text{the rate of sticking of molecule on the surface}}{\text{the rate of impinging of molecule with the surface}} = \frac{R_s}{z} \quad (1.1)$$

According to the Hertz-Knudsen equation, the molecule collision rate (*z*) with the surface is given as:

$$z = \frac{P}{(2m\pi kT)^{\frac{1}{2}}} \quad (1.2)$$

Where, *P* - Pressure (Pa)

T - Temperature (K)

m - Mass of the impinging species (kg)

k - Boltzmann's constant (1.38×10^{-23} J K^{-1})

R - Gas constant (8.31 J mol^{-1} K^{-1})

In ideal circumstances, if we assume that each adsorbed molecule occupies a single surface site, the coverage of surface is defined as:

$$\theta = \frac{\text{Number of surface sites occupied by adsorbate}}{\text{Total number of substrate adsorption sites}} = \frac{N_{ads}}{N_S} \quad (1.3)$$

Consequently, at a given pressure (*P)* and temperature (*T)*, the sticking coefficient *S* is in a linear relationship with the surface coverage, as indicated in the equation:

$$S = \frac{\sqrt{2\pi mkT}R_s(1-\theta)}{P} \quad (1.4)$$

Where $R_s=N_s/t$, *t* is the unit time.

As seen from the above equation, at a certain pressure and temperature the sticking coefficient is significantly affected by the surface coverage. As θ varies from 1.0 to 0,

where 1.0 indicates saturation coverage, the sticking coefficient *S* is in nearly linear relationship with the surface coverage.

Since the adsorption process always involves bond breaking and forming instantaneously, studies of the magnitude and variation of heat evolved as a function of coverage may reveal valuable information concerning the type of bonds between the substrate and the adsorbate, as well as the lateral interaction between adsorbates. Generally, the adsorption is favourable when the variation of free energy of the system is negative; in other words, adsorption is usually also accompanied by an entropy decrease, as the translational freedom of the gas molecule is reduced due to the adsorption equation. Hence, the variation of free energy (*G*) of the system has to be negative:

$$\Delta G = \Delta H - T\Delta S \qquad (1.5)$$

Where, ΔG - Variation of free energy (kJ mol^{-1})

ΔH - Variation of enthalpy (kJ mol^{-1})

T - Temperature (K)

ΔS - Variation of entropy (kJ mol^{-1} K^{-1})

According to the magnitude of their enthalpies of adsorption, the bonding between the substrate and adsorbate are classified into two types, physisorption and chemisorption.

1.3.2 Physisorption and chemisorption [69]

Physisorption is a long range but weak van der Waals-type interaction, hence, electron exchange between the substrate and adsorbate is usually negligible. This weak bonding is characterized by low adsorption energy $-\Delta H^0_{physisorption} < 35$ kJ mol^{-1}, and tends to be a reversible process. In contrast, chemisorptions is a strong interaction and easily distinguished from physisorption because of the magnitude of ΔH^0 ($\Delta H^0_{chemisorption} > 35$ kJ mol^{-1}). Depending on the nature of the electron exchange between adsorbate and substrate, the bonding can be discussed in terms of covalent,

ionic, and metallic bonds; and spectroscopic methods can be used to explore the nature of bonding involved in the adsorption. Surface coverage can cause the enthalpy of chemisorption to change dramatically as consequence of large intermolecular lateral interactions.

1.3.3 Molecular diffusion at surfaces

One crucial factor accounting for the appearance and the ultimate degree of order of the self-assembled structures is molecular diffusion since self-assembly is described as the spontaneous association of a supramolecular architecture from its constituents [70, 71], involving the free transport of the adsorbed species on the surface. Molecular diffusion is quantified by the mean square distance traveled per unit time *i.e.* diffusivity D, and is thermally activated obeying an Arrhenius type law. The ratio, D/F, between diffusivity D and the molecular deposition rate F, determines the average distance that an adsorbate has to travel before meeting another adsorbate. If D/F is small, the high deposition rate and limited diffusivity can cause the adsorbed species to be trapped in a kinetically limited state, leading to the formation of metastable self-organised structures, probably limited on the size of ordered region. On the other hand, if D/F is large, the adsorbed species are able to diffuse more freely on the surface and have more time to reach a minimum of energy configuration, resulting in the self-assembly of the thermodynamically favored, equilibrium structures [72, 73]. The difference between the self-assembly and self-organisationally limited structures is illustrated in Figure 1.7.

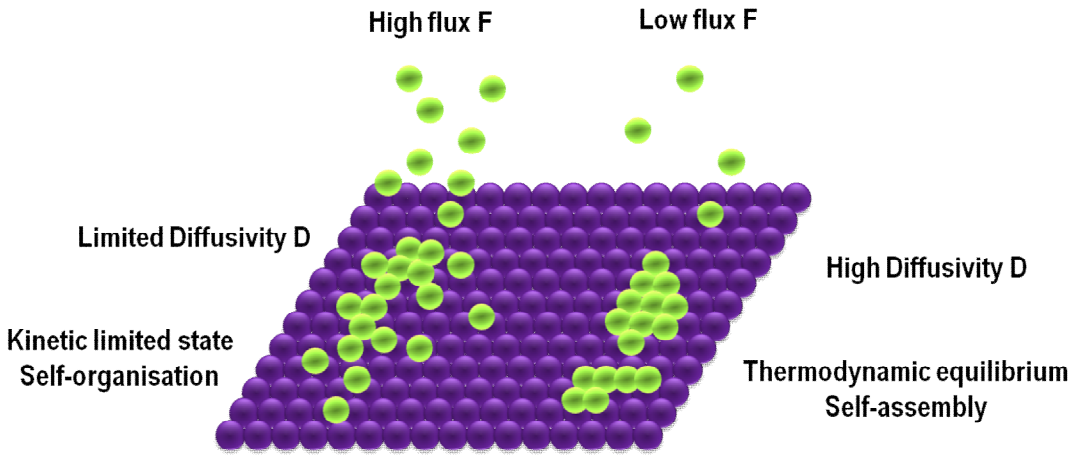

Fig. 1.7: Schematic illustration of the difference between self-organisation and self-assembly (adapted 69). The growth process is determined by the ration between diffusion rate D and deposition flux F. D/F. High flux F and low diffusivity D lead to the formation of kinetic limited state self-organisation structures. On the other hand, when the flux F is low and diffusivity is high, self-assembly structures are formed when the thermodynamic equilibrium state is reached (adapted from Ref. 73).

Molecular diffusion on surfaces can be controlled by variation of external parameters, *e.g.* substrate temperature and deposition flux rate. Increasing substrate temperature can provide the molecules with sufficient kinetic energy to overcome the diffusion barrier on the surface [73]. The magnitude of this energy, however, should not exceed the binding energy of the molecules on the surface to avoid molecular desorption. Additionally, to ensure the formation of a stable ordered structure, the intermolecular interaction energy should be only slightly larger than the kinetic energy; otherwise, irreversible molecular nucleation would occur if this local interaction were too strong, while adsorbates would not be able to reach the global equilibrium structures.

As well as the surface molecular diffusion, the order and arrangement of adsorbed species on the surface are an outcome of the delicate balance between the intermolecular interactions and molecule-substrate interactions. The molecule-substrate interactions involve metal-ligand σ bonds and π bonds, *etc.* Figure 1.8, metal-ligand σ bond interactions are common for the adsorption of alkanethiols on Au(111) surfaces [74], involving a covalent sulphur-gold bond, and the carboxylic

acids on copper surfaces [45, 75-77], where the strong coordination of the functional groups with the substrate atoms leads to the generation of chemisorbed species in both cases following adsorbate deprotonation. The diffusion barrier for chemisorption becomes very large, and the molecular assemblies, particularly formed at low coverage, on the surface are governed by this type of molecule-substrate interactions. Metal-molecule π interaction is a mere delocalized interaction and often occurs between the aromatic rings of the adsorbates and the substrate atoms. It is relatively weak and affected by the nature of the substrate atoms and the substitutents on the ring [78]. In smaller molecules, this interaction may give rise to a physisorbed species, this is often also linked to a low diffusion barrier. The resulting molecular assembly on the surface is the result of the interplay between directional intermolecular interactions and substrate-molecule interactions. As the surface coverage increases, lateral intermolecular interactions may start to gain influence over the molecule-substrate interactions, resulting in the creation of well-defined molecular structures.

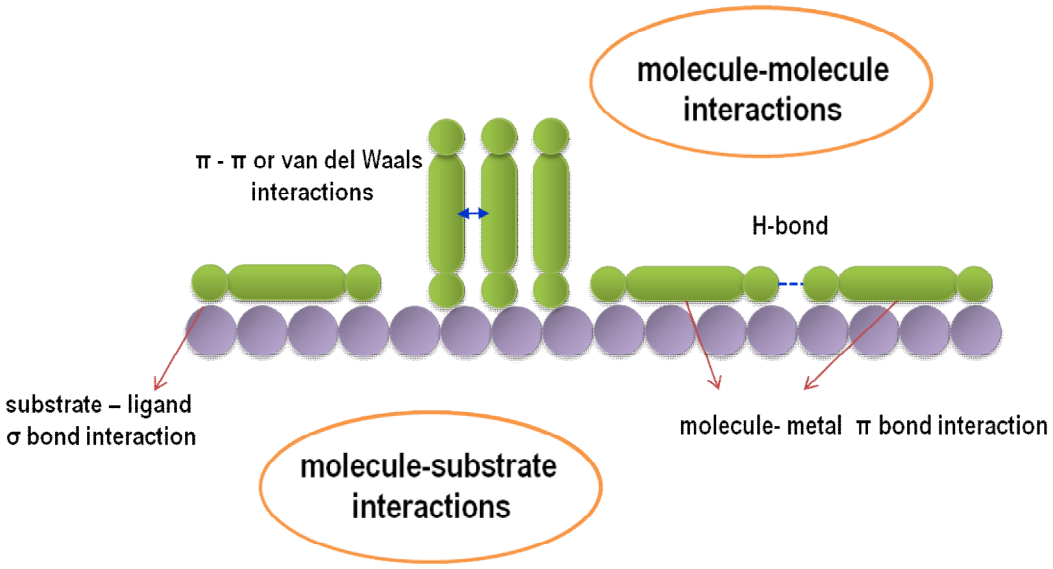

Fig. 1.8: Schematic illustration of the molecule-molecule (green) and molecule-substrate (purple) interactions that govern the formation of adlayer structures. The intermolecular interactions, including H-bond, π - π and van del Waals force may direct and stabilize the supramolecular assemblies. The molecule-substrate interactions *e.g.* metal-ligand σ bond, and molecule-metal π interactions are common for molecules containing carboxylate and thiol groups etc. and aromatic rings.

Among the basic types of intermolecular interactions considered for the molecular self-assembly, hydrogen bonds are the most important due to their high molecular selectivity and well-defined orientation. They are non-covalent attractive interactions occuring between an electronegative atom, *e.g.* N, O, and a hydrogen atom that is covalently bonded to another electronegative atom. The π-π stacking interactions have some similarity with the van de Waals interactions; they are less selective and comparatively weak in nature, but multiple weak couplings can result in a very stable network. This is the case for ordered networks formed by deposition of organic molecules containing aromatic rings [36] and long alkane chains [79, 80] onto surfaces. Some other intermolecular interactions include dipole-dipole and substrate-mediated interactions. Table I gives an overview of these interactions in terms of interaction strength, typical bonding length and nature.

Table 1: Classification of the typical intermolecular interactions with associated interaction energies, bonding length and nature

Interaction type	Strength	Bonding length	Nature
Hydrogen bonding	0.1 - 0.5 eV	2 - 3.5 Å	Selective, directional
Van der Waals	0.02 - 0.1 eV	5 - 10 Å	Nonselective
Dipole-dipole	0.1 - 0.5 eV	2 - 3 Å	Directional
Electrostatic	0.1 - 3 eV	Up to several nm	Non-selective
Metal mediated	0.1 - 1eV	Up to 70 Å	Oscillatory

The bonding energy, distance and nature can be very different depending on the interactions types. These can be utilized to for controlling molecular self-assembly [12, 73].

The adsorption of organic molecules is a complex process when studied at the molecular level. The design of ordered surface structures needs such parameters as the molecular mobility, the lateral interactions between the adsorbates and their bonding to the surface atomic lattices to be well tailored, all of which depend on the detailed

chemical nature of the adsorbates, substrate geometry and atomic environment [81-84]. Thus, these can be exploited to control the interplay of the lateral interactions and molecule-substrate interactions, with the aim to steer the supramolecular organization towards the desired structures. In addition, external experimental parameters, *e.g.* temperature and flux need to be controlled properly in order to satisfy the kinetic and thermodynamic requirements. However, in practice the complexity of the investigation into adsorbed system is further increased by some uncertain factors; for example, for thin films prepared from solution, solvent effects have to be taken into consideration.

1.4 Single Crystal Surface [68]

1.4.1 Miller indices

A single crystal metal surface is typically taken as the best candidate in Surface Science for studying molecular behaviour at the molecular level, because it can provide a well-defined surface to ensure reproducible experiments carried out at atomic scale. Most metallic crystal structures that have been widely examined are cubic, belonging to one of three kinds of lattices: the face centred cubic (FCC), body centred cubic (BCC) and the hexagonal close packed (HCP), Figure 1.10. In principle, flat crystal planes can be obtained by cutting a single crystal along any arbitrary direction, the given plane is conventionally denoted by using three integer numbers (x, y, z), so called Miller indices.

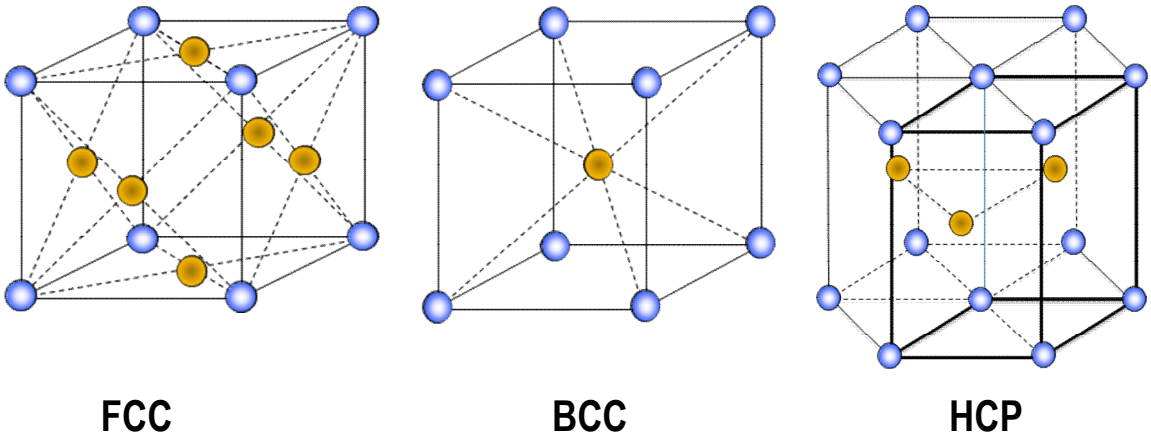

Fig. 1.10: A representation of FCC, BCC and HCP crystal structures.

In crystallography, the Miller index of a given plane can be determined in this way: first we decide the intercepts of the plane cutting the x, y, z-axes in multiples of the unit cell dimension, then calculate the reciprocals of these intercepts, and the resultant reciprocals are the Miller indices corresponding to the crystal plane. However, only the so-called low index surfaces, which mean the Miller index involves small integer, frequently only zero and one, are commonly studied due to thermodynamic reasons (minimisation of surface potential energy). Figure 1.11 identifies the low index crystal planes for an FCC crystal lattice structure using Miller index and sphere models with unit cell.

Each low index surface exhibits a unique surface geometry and surface atom coordination, therefore, giving rise to substantial differences in the surface reactivity and surface properties concerning catalytic activity and electronic properties. As shown in Figure 1.11b, taking the three low index copper surfaces for example, the surface energy decreases in the order of Cu(110) > Cu(100) > Cu(111), which reflects the increasing coordination of atoms in the given surface.

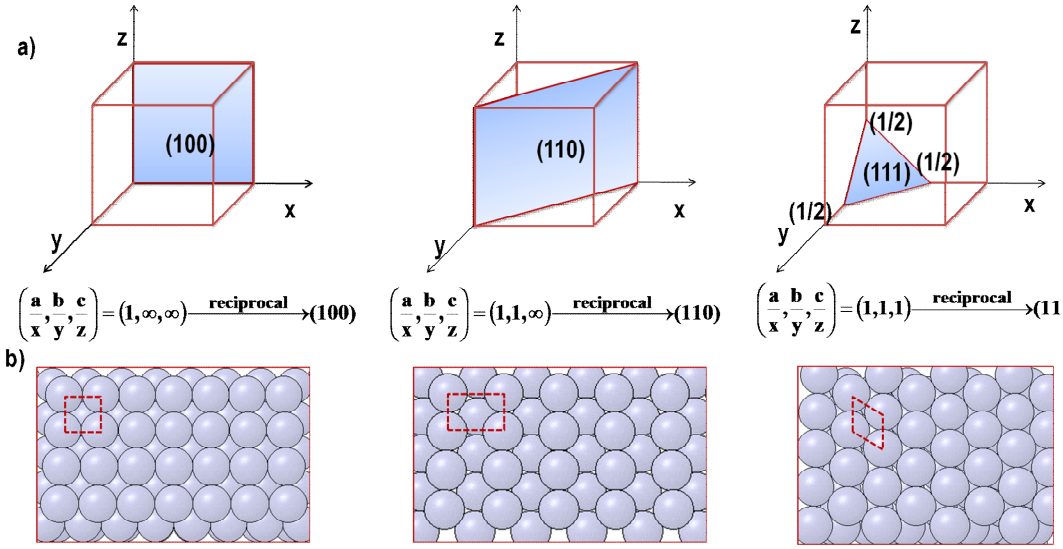

Fig. 1.11: Identification of the low-index crystal planes for an FCC crystal lattice using Miller indices. a) (100), (110) and (111) faces cut from a crystal b) Sphere model representation of the surfaces with the unit cell in red color (generated using the applet Surface Explorer [85]).

FCC(100) and FCC(111) are considered as smooth relatively dense surfaces with exposure of equivalent atoms only in the top layer, while for FCC(110), both the first and second atoms are exposed giving rise to an atomically rougher and more anisotropic surface. As far as the surface geometry and adsorption site of the low index faces are concerned, the FCC(110) surface has lowest symmetry of two fold rotation but exhibits three different 'high symmetry' adsorption sites, which are top site, short and long bridge site. This particular geometry of the FCC(110) surface makes it more commonly investigated by giving rise to a small number of rotational and reflectional domains besides a choice of adsorption sites.

Commercially purchased single crystals, manufactured through mechanical cutting and electrochemical polishing processes, can not be used directly for deposition. Cleaning procedures have to be carried out in order to get rid of the contamination sticking to the surface, and the unwanted impurities accumulated in the crystal bulk. Experimentally, different methods can be used to achieve a well-defined surface, depending on the properties of the substrate under investigation. A detailed description of these methods is given in Chapter II.

1.4.2 Surface defects

No matter which method is applied, it is impossible to obtain an ideal surface consisting of merely single flat layer atoms without any imperfection. Practically, various defects are unavoidably present on the surface. The Terrace-Step-Link (TSK) model of a surface shown in Figure 1.12, gives a clear illustration of the surface defects. The terrace is composed of flat layer atoms; large and atomically flat terraces are crucial because the majority of the surface reactions undergoing occurs on them. The step is located between two layers of atoms; it is approximately one or two atomic height separating terraces apart. The step itself may contain kinks defect orienting in different directions, mirror related kinks would give rise to a chiral surface. The existence of adatoms and missing atoms (vacancies) on each terrace are fairly common defects found on surfaces [86].

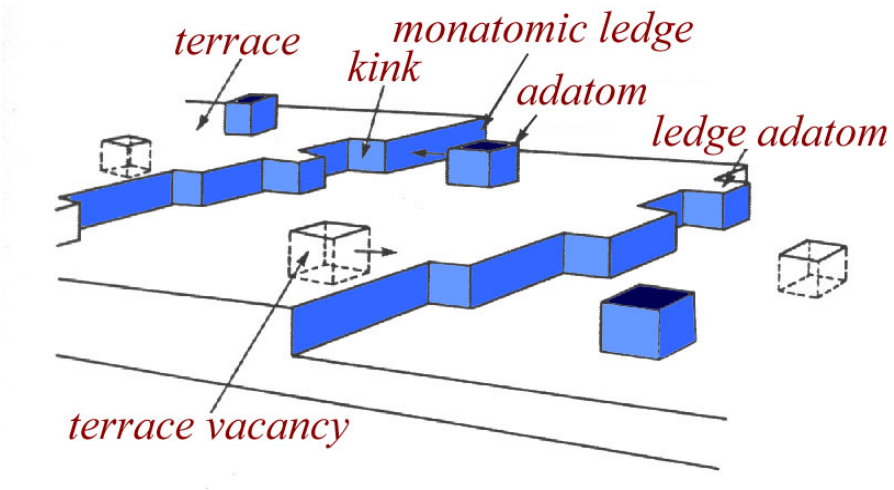

Fig. 1.12: The Terrace-Step-Kink shows the various defects existing on the solid surfaces [86].

Defects are able to cause noticeable effects on the surface reactivity since atoms in these sites are less strongly bound to the surface and accordingly show high activity during the adsorption. They are ordinarily referred as active sites with low surface barrier in favour of preferential molecular adsorption. However, it is generally considered that well-defined surfaces achieved experimentally contain a small ratio of defects and have atomically flat terraces of about 100 nm which would actually be good enough for providing us with reproducible substrates for experiments [68, 86].

1.5 Nucleobases and Amino Acids

1.5.1 Nucleobases

Nucleobases are the basic blocks in composing the double helix structures of DNA and RNA. The main ones are adenine, cytosine, thymine, guanine and uracil, abbreviated as A, C, T, G, and U, Figure 1.13a, respectively [87]. A, C, G. and T are called DNA bases because they are only found in DNA; while A, C. G and U are RNA bases in which uracil replaces thymine. Among the five bases, adenine and guanine belong to purines consisting of two hetrocyclic rings; the others are pyrimidines that are class of molecules composed of a single ring. One typical character of these bases is the tautomerism, arising from the shifting of one or two protons between different nitrogen atoms. In the two strands DNA structures, each type of base on one strand always connects with just one type of base on the other strand by double hydrogen bonds, forming base pairs, *i.e.* A-T and C-G pairs. However, mispairing may occur when one base is connected with a tautomeric form of the other bases, this is suspected to play an important role in spontaneous mutation in DNA replication [88].

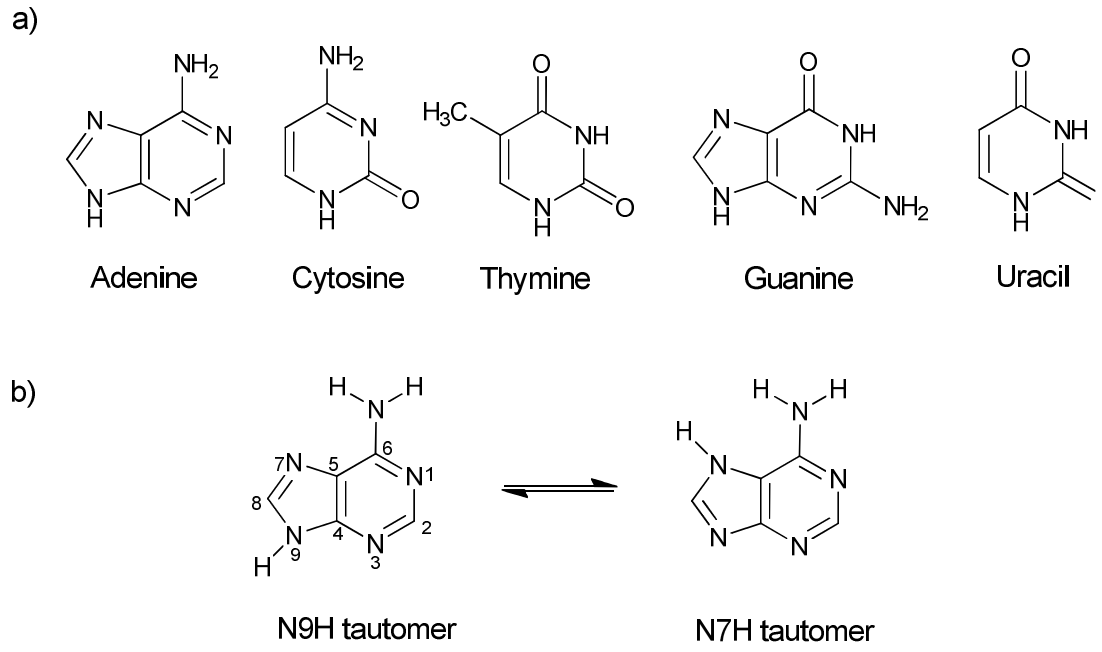

Fig. 1.13: a) General structures of nucleic acid bases. b) The atom numbering of adenine and two preferential tautomeric structures of adenine.

Adsorption of nucleobases on surfaces has been well studied in recent years because it has been hypothesized that self-assembly of nucleic acid bases on inorganic surfaces may have had a role in the emergence of terrestrial life [11, 89]. In particular, more attention has been paid to adenine adsorbed on various substrates [22-35] because the molecule plays an essential role in the DNA replication in all known living systems [90]. Interaction of adenine molecules with metals may be influenced by such characters as the tautomerism, acidity and hydrogen bonds. Adenine can exist in twelve tautomers of which two energetically preferred tautomeric forms are: N9H and N7H, Figure 1.13b, arising from the migration of an H atom between the N9 and the N7 atoms. Generalized gradient approximation of density functional theory (DFT) calculations predicts that the N9H tautomer is 8.0 kcal mol^{-1} lower in energy than the N7H tautomer [91]. In gas phase, only the N9H tautomer is suggested by available experimental data [92-95]; mixture of both tautomers can exist in solvents [96, 97]. As for the acidity of gas phase adenine, it is revealed by calculations that the site N9 is about 19.0 kcal mol^{-1} more acidic than the amino site [98]. In addition to pairing with thymine in DNA structures, adenine also has strong ability to form various double hydrogen bonded pairs between themselves. The relatively strong intermolecular interactions play an important role in the formation of ordered molecular assemblies on surfaces.

1.5.2 Amino acids

Amino acids are the basic building blocks of proteins. The general molecular formula of an α-amino acid is expressed as $H_2NCHRCOOH$; its chemical structure is shown in Figure 1.14a. The central carbon atom, usually referred as the α-carbon, is linked to three functional groups in addition to an H atom: an amino group, a carboxylic group, and the third group, R, which acts as side chain varying for size and composition and is responsible for giving each amino acid its specific properties. All amino acids with an exception are inherently chiral molecules in which the α-carbon, called chiral center, is linked with four different groups. The one exception is glycine [99], the simplest amino acid, where R=H, making it achiral in the gas phase. An amino acid can display different ionized structures: the neutral ionic amino acid, namely zwitterion, existing in solid and at isoelectric point in solution, the anionic

form in basic pH value due to deprotonation of the carboxylate group, and the cationic form resulted from the protonation of the amino group in acidic solution, Figure 1.14b. Each of the three forms can be interconverted by changing the solution pH value. Anionic amino acids were also found upon metal surfaces because of strong coordination of the oxygen atoms of the carboxylic group with the substrate atoms [38, 45, 55-58].

Amino acids are essential for the human body and play an important function in metabolism [100]. Due to their importance in biochemistry, they have found wide applications in the food technology as flavour enhancers [92] and the synthesis of drugs and cosmetics [101]. In addition, amino acids can be used as chiral starting materials in the enantioselective synthesis [102] in the pharmaceutical industry. The development of amino acid based biomaterials is other research area of interest. Depending on the amino acid composition and any further chemical modification, the chemical and mechanical properties of these materials can be tailored for wide applications [103].

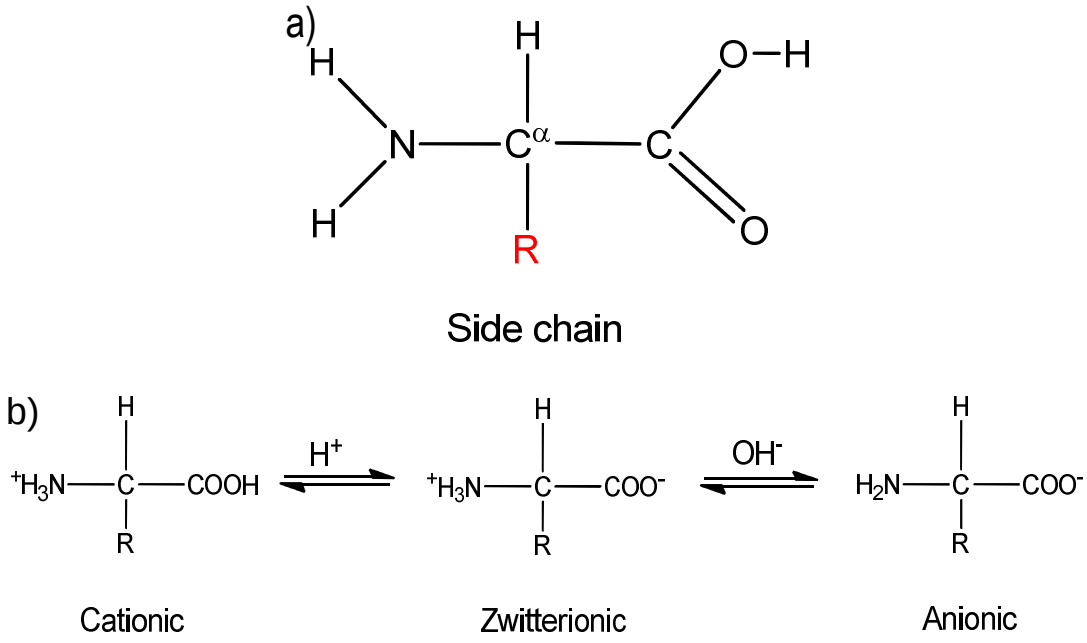

Fig. 1.14: a) General structure of an α-amino acid consisting of three functional groups: an amino group, an carboxylate group, and a side chain R in addition to a H atom. b) Three different forms of ionized amino acid, the interconversion of them can be realized by mediating the solution pH value.

1.6 References

1. B. Kasemo, *Curr. Opin. Solid State Mater. Sci*. 3, **1998**, 451.
2. O. I. Kiselyova and I. V. Yaminsky, *Coll. J*. 61, **1999**, 1.
3. Y. Maeda, T. Matsumoto and T. Kawai, *Appl. Surf. Sci.* 140, **1999**, 400.
4. T. Kanno, H. Tanaka, N. Miyoshi, M. Fukuda and T. Kawai, *Jpn. J. Appl. Phys*. Part I, 39, **2000**, 1892.
5. C. Hamai, H. Tanaka and T. Kawai, *J. Vac. Sci. Technol*. B, 17, **1999**, 1313.
6. C. Hamai, H. Tanaka and T. Kawai, *J. Phys. Chem.* B, 104, **2000**, 9894.
7. B. P. Nelson, T. E. Grimsrud, M. R. Liles, R. M. Goodman and R. M. Corn, A*nal. Chem.* 73, **2001**, 1.
8. R. M. Ostroff, D. Hopkins, A. B. Haeberli, W. Baouchi and B. Polisky, *Clin. Chem.* 45, **1999**, 1659.
9. S. Storri, T. Santoni, M. Minunni and M. Mascini, *Biosens. Bioelectron*. 13, **1998**, 347
10. S. J. Sowerby, W. M. Heckl and G. B. Petersen, *J. Mol. Evol*. 43, **1996**, 419.
11. S. J. Sowerby and W. M. Heckl, *Origins Life Evol. Biosphere* 28, **1998**, 283.
12. J. Barth, *Annu. Rev. Phys. Rev*. 58, **2007**, 375.
13. J. V. Barth, G. Costantini and K. Kern, *Nature* 437, **2005**, 671.
14. S. de Feyter and C. F. de Schryver, *Chem. Soc. Rev*. 32, **2003**, 139.
15. D. L. Keeling, N. S. Oxtoby, C. Wilson, M. J. Humphry, N. R. Champness and P. H. Beton, *Nano. Lett*. 3, **2003**, 9.
16. J. A. Theobald, N. S. Oxtoby, M. A. Phillips, N. R. Champness and P. H. Beton, *Nature* 424, **2003**, 1029.
17. S. De Feyter, A. Miura, S. Yao, Z. Chen, F. Würthner, P. Jonkheijm, A. P. H. J. Schenning, E. W. Meijer and C. F. De Schryver, *Nano. Lett*. 5, **2005**, 77.
18. S. Abramson, N. Bellocq and M. Lasperas, *Top. Catal*. 13, **2000**, 339.
19. X. H. Li, X. You, C. H. Liang, S. Z. Zhang, Z. B. Wei, X. Y. Li and C. Li, Chem. J. *Chin. Univ.: Chinese* 21, **2000**, 1900.
20. J. L. Margitfalvi, E. Talas and E. Tfirst, *Chim. Oggi-Chem. Today* 18, **2000**, 46.
21. G. M. Whitesides, J. P. Mathias and C. T. Seto, *Scienc*e 254, **1991**, 1312.
22. N. J. Tao and Z. Shi, *J. Phys. Chem*. 98, **1994**, 1464.
23. S. J. Sowerby, W. M. Heckl and G. B. Petersen, *J. Mol. Evol*. 43, **1996**, 419.

24. J. E. Freund, M. Edelwirth, P. Kröbel and W. M. Heckl, *Phys. Rev*. B 55, **1997**, 5394.
25. T. Uchihashi, T. Okada, Y. Sugawara, K. Yokoyama and S. Morita, *Phys. Rev*. B 60, **1999**, 8309.
26. W. Mamduh, M. Dong, R. E. A. Kelly, L. N. Kantorovich and F. Besenbacher, *J. Phys. Chem*. B 111, **2007**, 12048.
27. H. Tanaka, T. Nakagawa and T. Kawai, *Surf. Sci.* 364, ***1996***, L575.
28. T. Kawai, H. Tanaka and T. Nakagawa, *Surf. Sci*. 386, **1997**, 124.
29. M. Furukawa, H. Tanaka, K. Sugiura, Y. Sakata and T. Kawai, *Surf. Sci*. 392, **1997**, 33.
30. M. Furukawa, H. Tanaka, K. Sugiura, Y. Sakata and T. Kawai, *Surf. Sci*. 445, **2000**, L58.
31. M. Furukawa, H. Tanaka and T. Kawai, *Surf. Sci*. 445, **2000**, 1.
32. M. Furukawa, H. Tanaka and T. Kawai, *J. Chem. Phys*. 115, **2001**, 3419.
33. R. Otero and M. Schock, *private communication*.
34. R.E. A. Kelly, W. Xu, M. Lukas, R. Otero, M. Mura, Y. J. Lee, E. Lœgsgaard, I. Stensgaard, L. N. Kantorovich and F. Besenbacher, *Small* 4, **2008**, 1494.
35. L. M. A. Perdigão, P. A. Staniec, N. R. Champness, R. E. A. Kelly, L. N. Kantorovich and P. H. Beton, *Phys. Rev*. B 73**, 2006**, 195423.
36. Q. Chen, D. J. Frankel and N. V. Richardson, *Langmuir* 18, **2002**, 3219.
37. Q. Chen and N. V. Richardson, *Nat. Mater*. 2, **2003**, 324.
38. Q. Chen, L. C. W. Lee, D. J. Frankel and N. V. Richardson, *PhysChemComm*. 2, **1999**, 41.
39. Q. Chen, D. J. Frankel, C. W. Lee and N. V. Richardson, *Chem. Phys. Lett*. 349, **2001**, 67.
40. R. S. Cahn, C. K. Ingold and V. Prelog, *Angewandte Chemie International 5th Edition*, **1966**, 385.
41. R. S. Cahn, C. K. Ingold and V. Prelog, *Angewandte Chemie* 78, **1966**, 413.
42. http://en.wikipedia.org/wiki/Chirality_%28chemistry%29
43. T. J. Leitereg, D. G. Guadagni, J. Harris, T. R. Mon and R. Teranishi, *J. Agric. Food Chem*. 19, **1971**, 785.
44. E. J. Ariëns, *European Journal of Clinical Pharmacology* 26, **1984**, 663.
45. M. Ortega, C. J. Baddeley, C. Muryn and R. Raval, *Nature* 404**, 2000**, 376.
46. Q. Chen and N. V. Richardson, *Annu. Rep. Prog. Chem. Sect.* C 100, **2004**, 313.

47. A. Ahmadi, G. Attard, J. Feliu and A. Rodes, *Langmuir* 15, **1999**, 2420.
48. D. S. Sholl, A. Asthagiri and T. D. Power, *J. Phys. Chem.* B 105, **2001**, 4771.
49. R. Raval, *Current Opinion in Solid State and Materials Science* 7, **2003**, 67.
50. S. M. Barlow and R. Raval. *Surf. Sci. Rep.* 298, **2001**, 1.
51. S. M. Barlow and R. Raval, *Surf. Sci. Rep.* 50, **2003**, 201.
52. J. M. Murry. *Organic Chemistry 6th Edition*, Brooks/Cole. pp. 301–303.
53. J. Weckesser, J. V. Barth, C. Cai, B. Muller and K. Kern, *Sur. Sci.* 431, **1999**, 168.
54. J. Weckesser, J. V. Barth and K. Kern, *J. Chem. Phy.* 110, **1999**, 5351.
55. S. M. Barlow, K. J. Kitching, S. Haq and N. V. Richardson, *Sur. Sci.* 401, **1998**, 322.
56. J. Hasselstrom, O, Karis, M. Weinelt, N. Wassdahl, A, Nilsson, M, Nyberg, L. G. M. Pettersson, M. G. Samant and J. Stohr. *Sur. Sci.* 407, **1998**, 221.
57. M. Nyberg, J. Hasselstrom, O. Karis, N. Wassdahl, M. Weinelt, A. Nilsson and L. G. M. Pettersson, *J. Chem. Phys.* 112, **2000**, 5240.
58. N. A. Booth, D. P. Woodruff, O, Schaff, T. Giessel, R. Lindsay, P. Baumgartel and A. M. Bradshaw, *Sur. Sci*. 397, **1998**, 258.
59. M. Ortega Lorenzo, S. Haq, T. Bertrams, P. Murray, R. Raval and C. J. Baddeley, *J. Phys. Chem.* B 103, **1999**, 10661.
60. J. William, S. Haq and R. Raval, *Sci. Sci.* 368, **1996**, 303.
61. M. A. Filler and S. F. Bent, *Prog. Surf. Sci*. 73, **2003**, 1.
62. R. Raval, *Chem. Soc. Rev*. 38, **2009**, 707.
63. S. M. Barlow, S. Louafi, D. Le Roux, J. Williams, C. Muryn, S. Haq and R. Raval, *Surf. Sci*. 590, **2005**, 243.
64. Eds N. F. M. Henry and K.Lonsdale, *International Tables for X-ray Crystallography* Vol. 1, Kynoch, Birmingham, **1965**.
65. N. V. Richardson and N. Sheppard, *Normal modes at surfaces, in: Vibrational Spectroscopy of Molecules on Surfaces* (eds J. T. Jr. Yates, and T. E. Madey), Plenum, New York, **1987**, 1.
66. D. P. Woodruff and T. A. Delchar, *Modern Techniques of Surface Science*, Cambridge University Press, Cambridge, **1986**.
67. N. Bovet, N. McMillan, N, Gadegaard and M. Kadodwala, *J. Phys. Chem*. B 111, **2007**, 10005.
68. G. Attard and C. Barnes, *Surfaces*, Oxford Science Publications, **1998.**

69. D. A. King and D. P. Woodruff (Edt.), *the Chemical Physics of Solid Surfaces* Vol. 8, Elsevier, **1997**.
70. Z. Y. Zhang and M. G. Lagally, *Science* 276, **1997**, 377.
71. H. Brune, *Surf. Sci. Rep*. 31, **1998**, 121.
72. J. V. Barth, G. Costantini and K. Kern, *Nature* 437, **2005**, 671.
73. A. Kühnle, *Curr. Opin. Colloid Interface Sci*. 14, **2009**,157.
74. F. Schreiber, *Prog. Surf. Sci*. 65, **2000**, 151.
75. Q. Chen, D. J. Frankel and N. V. Richardson, *Langmuir* 17, **2001**, 8276.
76. B. G. Frederic, Q. Chen, F. M. Leibsle, M. B. Lee, J. J. Kitching and N. V. Richardson, *Sur. Sci*. 394, **1997**, 1.
77. Q. Chen, C. C. Perry, B. G. Frederick, P. W. Murray, S. Haq and N. V. Richardson, *Surf. Sci*. 446, **2000**, 63.
78. C. Seidel, H. Kopf and H. Fucks, *Phys. Rev.* B 60, **1999**, 14341.
79. J. C. Ma and D. A. Dougherty, *Chem. Rev.* 97, **1997**, 1303.
80. A. Ulman, *Chem. Rev*. 96, **1996**, 1533.
81. J. V. Barth, *Surf. Sci. Rep*. 40, **2000**, 75.
82. J. K. Gimzewski and C. Joachim, *Science* 283, **1999**, 1683.
83. F. Rosei, M. Schunack, Y. Naitoh, P. Jiang, A. Gourdon, E. laegsgaard, I. Stensgaard, C. Joachim and F. Besenbacher, *Prog. Surf. Sci*. 71, **2003**, 95.
84. J. V Barth, J. Weckesser, C. Cai, P. Gürgi, L, Bürgi, O. Jeandupeux and K. Kern, *Angew. Chem. Int. Ed. Engl*. 39, **2000**, 1230.
85. http://w3.rz-berlin.mpg.de/~rammer/surfexp_prod
86. P. W. Atkins, *Physical Chemistry 6th edition*, Oxford University Press, **1998.**
87. W. K. Purves, D. Sadava, G. H. Orians and H. G. Heller, *Life - the Science of Biology 7th Edition*, **2003**.
88. M. Topal and J. Fresco, *Nature* 263, **1976**, 285.
89. S. J. Sowerby, M. Edelwirth and W. M. Heckl, *J. Phys. Chem.* B 102, **1998**, 5914.
90. S. Robert, *Origins of Life and Evolution of Biospheres*, 25, Springer Netherlands publish, **1995**, 83.
91. C. Fonseca Guerra, F. M. Bickelhaupt, S. Saha and F. Wang, *J. Phys. Chem.* A 110, **2006**, 4012.
92. S. Peng, A. Padva and P. LeBreton, *Proc. Natl. Acad. Sci.* USA 73, **1976**, 2966.

93. J. Lin, S. Peng, I. Akiyama, K. Li, L. Kao Lee and P. LeBreton, *J. Am. Chem. Soc.* 102, **1980**, 4627.
94. R. Brown, P. Godfrey, D. McNaughton and A. Pierlot, *Chem. Phys. Lett.* 157, **1989**, 61.
95. M. Nowak, L. Lapinski and J. Kwiatkowshi, *Chem. Phys. Lett.* 157, **1989**, 14.
96. M. Schumacher and H. Gunther, *J. Am. Chem. Soc*. 104, **1982**, 4167.
97. K. Kanamori, N. Leonard and J. Roberts, *J. Am. Chem. Soc.* 105, **1983**, 2050.
98. S. Sharma and J. K. Lee, *J. Org. Chem.* 67, **2002**, 8360.
99. Creighton and H. Thomas, *Proteins: structures and molecular properties*, San Francisco: W. H. Freeman, **1993**, chapter 1.
100. W. Leuchtenberger, K. Huthmacher and K. Drauz, *Applied Microbiology and Biotechnology*, 69, **2005**, 1.
101. S. Garattini, *Journal of Nutrition*, 130, **2000**, 901s.
102. S. Hanessian, *Pure and Applied Chemistry*, 65, **1993**, 1189.
103. S. A. Guelcher and J. O, Hollinger (eds), *An Introduction to Biomaterials*, biomedical engineering series, CRC Press, Boca Raton, Fla., **2006**.

CHAPTER II
Experimental

2.1 Introduction

The aim of this chapter is to give a general overview on an Ultra-high Vacuum (UHV) system, a brief introduction of the experimental setup and some concepts underlying the techniques used in the experiments described in the thesis.

2.1.1 The system

Most of the UHV-STM experiments presented in this thesis were carried out on the Omicron VT-UHV system schematically shown in Figure 2.1. The system is divided into three parts: a preparation chamber, an STM measurement chamber and an infrared measurement chamber. The chambers are separated from each other by UHV gate-valves; samples can be easily transferred between chambers by a long horizontal magnetic transfer arm.

The preparation chamber is equipped with a mass spectrometer, an ion sputter gun and gas inlets, as well as LEED optics. Sample and tip can be exchanged in and out of the UHV system via a load lock attached to the preparation chamber without losing UHV conditions. Molecular deposition is carried out in either the preparation chamber or the infrared chamber via home-built evaporators that are separated from the chambers by gate valves. Samples can be moved in the three spatial directions through the manipulators to facilitate molecular deposition and sample transferring between the chambers.

The infrared chamber is coupled to a research grade Nicolet 760 Fourier Transform mid-IR spectrometer within the 800 - 4000 cm^{-1} range, which enables us to collect the vibrational spectra of the adsorbed species on the surfaces. KBr windows give access for the IR beam to the sample at a grazing incidence. A load lock, sputter gun and gas inlet are also installed in this chamber. Most molecular depositions during the experiments were carried out in this chamber so that RAIR spectra of the studied species could be collected before the sample was transferred to the STM chamber for measurement.

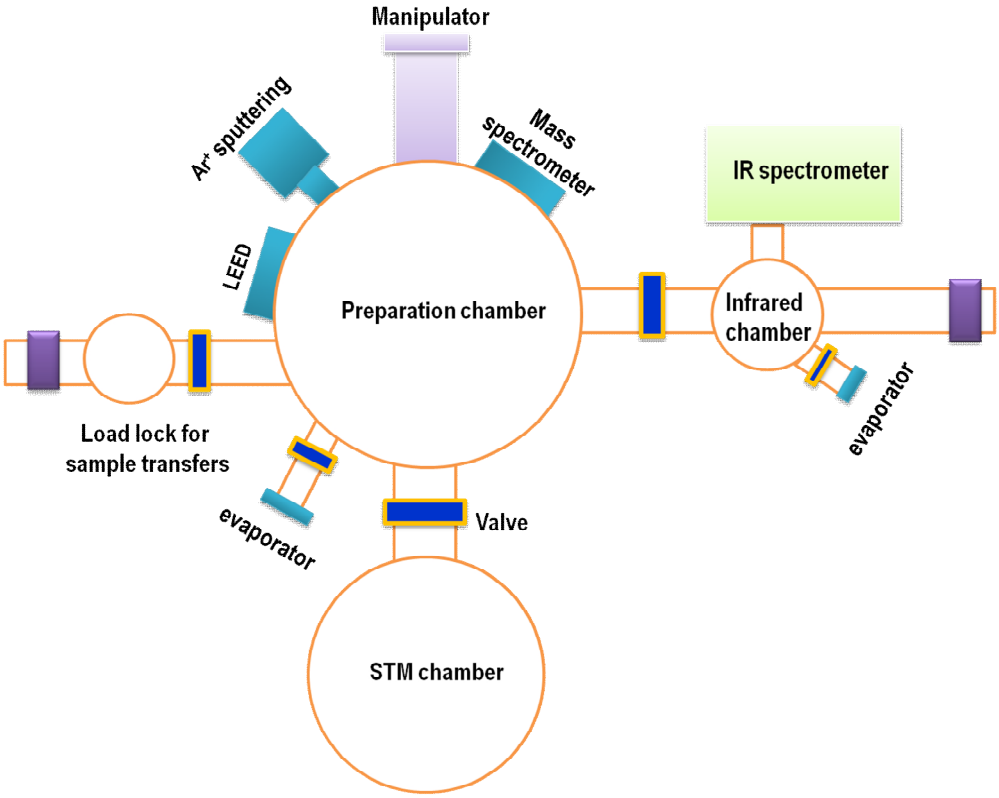

Fig. 2.1: Schematic of the VT-STM system used in our experiment.

The STM chamber is designed to permit only STM data acquisition. All three chambers are pumped with turbo pumps, sublimation pumps and ionization pumps working in combination; the pressure is measured by series of gauges such as ionization gauge and pirani gauges.

2.2 The Ultra-High Vacuum (UHV) System

The main reasons why an UHV system is necessary for surface science studies are: firstly, it provides an environment free of contamination so that reliable surface experiments can be carried out at an atomically clean surface over a given period of time. Secondly, it allows the use of the many surface sensitive techniques based on

electron scattering without the interference from gas phase scattering. Under UHV conditions, the mean free path for electrons, ions and photons is significantly increased; hence, the electrons emitted from surfaces being able to reach the analyser are maximized [1].

The behaviour of gas molecules under low pressure is explained in terms of molecular kinetic theory, so called the collision theory. Under the given gas pressure *P*, the number density of gas particle *n* is described by the equation:

$$n = P / kT \quad \text{(molecules m}^{-3}\text{)} \qquad (2.1)$$

Where: k - Boltzmann constant (1.38×10^{-23} JK^{-1}),

T - Absolute temperature (K),

P - Pressure (Pa)

A gas molecule is considered as a particle with a specific mass and velocity; it always keeps moving irregularly and colliding with the surrounding particles, as well as with the walls of the container. We define the average numbers of collision per second between particles as the collision rate *Z*,

$$Z = \frac{P}{(2\pi mkT)} \quad \text{(molecules m}^{-2}\text{s}^{-1}\text{)} \qquad (2.2)$$

and the mean free path of gas phase molecule λ is given by equation

$$\lambda = kT / 1.414\sigma P \qquad (2.3)$$

Where: m - Molecular mass (kg)

σ - Collision cross section (m^2)

As a result, under ultra-high vacuum condition with the pressure below 10^{-9} mbar, the collision rate of background gas particles with the surface is decreased greatly, hence the time for the surface to be completely covered by the residual gas can be of the order of hours; this provides sufficient time to allow typical surface experiments to be undertaken. In addition, the mean free path of the electrons and ions is considerably increased under this pressure, up to the order of meters. So, the interactions of the electrons with the surrounding residual gas can be considerably reduced, which is required by these spectroscopic techniques based on electron scattering to achieve a maximum efficiency because the loss of electrons emitted from surface encounter, before reaching the analyser, becomes as few as possible.

2.2.1 Achieving and maintaining the UHV

To achieve ultra-high vacuum conditions, system baking at temperature of about 120 ºC should be performed; this is a necessary first step to remove the adsorbed water and some other gases adsorbed on the internal walls of the chamber. The baking can take from several hours to even days depending on how poor the vacuum conditions were at the time of the experiment. Then degassing is operated before the system is allowed to cool down; it includes all the components like filaments, manipulators, and other equipment operating in the chamber. After degassing, the pressure of the vacuum chamber can reach to 10^{-8} mbar at least. Further pumping the system with varied kinds of pumps allows the background pressure to reduce below 10^{-10} mbar.

Vacuum pumps

The ultra-high vacuum system needs different pumps working together to achieve and maintain low pressure. The rotary vane pump acts as a backing pump and can achieve a rough pressure of 10^{-2} mbar. The turbomolecular pump works as the main pump and allows the vacuum to reach 10^{-9} mbar. Both pumps can start pumping from atmospheric pressure by physically removing the gas out of the chamber. The sublimation pump and ion pump belong to sorption pumps and are mainly used to maintain ultra-high vacuum by getting rid of the residual gas particles through trapping them in the walls of the chamber, either titanium coated surface or cathode. A combination of both of them allows pressure between 10^{-11} mbar and 10^{-12} mbar to be achieved.

Vacuum pressure measurement

The pressure is measured with two types of gauges in this UHV system. Pirani gauges are frequently used for monitoring the pressure above the rotary pump and work as a backing stage pressure indicator for the high vacuum pump. Pressure measurement by the Pirani gauge is sensitive to the nature of surrounding gas, and calibrated for nitrogen or air. The accuracy of a Pirani gauge is affected by its location in the chamber and therefore subject to some degree of systematic error. Ionisation

gauges are used in the high and ultra-high vacuum region. The pressure range measured by the ion gauge is down to 10^{-11} to 10^{-12} mbar. The ion gauge calibration is sensitive to the construction geometry and chemical composition of gas being measured.

Noise isolation

Vibration isolation has been a great concern in the process of designing a UHV system in order to obtain high quality STM images. Generally, two categories of noise have to be well isolated. Mechanical noise, arising from the external building vibration as well as acoustic waves in the range 1 to 100 Hz, can be effectively eliminated by hanging the STM scanner with spiral springs and suspending the whole system away from ground. Electrical noise is introduced by electromagnetic waves, and can be minimized by accurately grounding the system. Moreover, in order to achieve maximum stability during STM measurement, mechanical pumps and non-essential electrical devices are usually switched off.

2.2.2 Sample and STM tip preparation

2.2.2.1 Sample preparation

The Cu(110) surface

The copper single crystal has a face centred cubic structure with a lattice constant of a = 3.61 Å. In our experiments, the Cu(110) surface is chosen for several reasons: first, the {110} surface is relatively anisotropic with both the outermost and second layer atoms exposed; the corrugated surface is expected to limit the molecular diffusion at room temperature at least in one direction. Second, it is a low symmetry surface comprising varied adsorption sites, including on-top, two-fold hollow, short and long bridge sites. Moreover, the Cu(110) falls into the P2mm space group and limited numbers of rotational and reflectional domains might form in case of molecular adsorption. Figure 2.2a shows the clean Cu(110) surface, characterized by flat terraces larger than 100 Å, giving rise to a sharp (1 × 1) LEED pattern, b; the inset shows an atomic resolution image collected by scanning at 70 K.

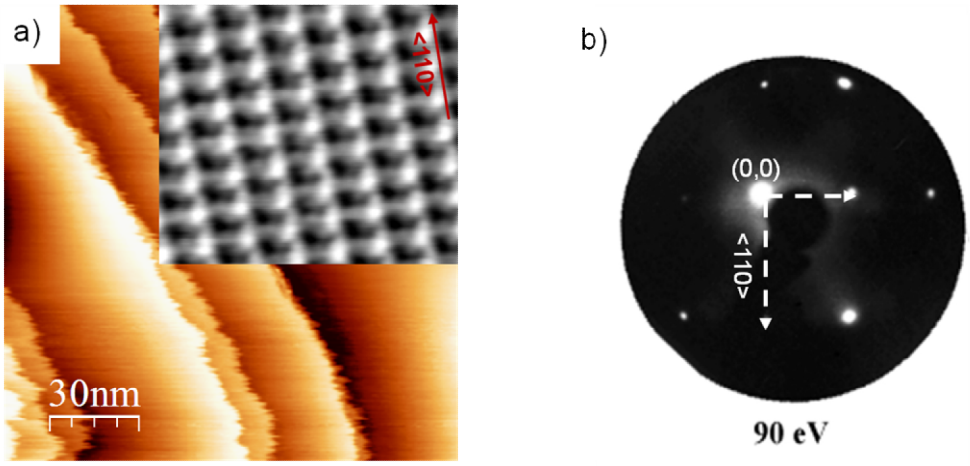

Fig. 2.2: a) STM image of the clean Cu(110) surface showing large flat terrace of larger than 100 Å (1.1 nA, -0.84 V, 151 × 151 nm^2), the inset shows atomic resolution by scanning at 70 K (1.3 nA, 0.27 V, 21 × 21 $Å^2$, Createc LT-STM). b) A sharp (1 × 1) LEED pattern of the clean Cu(110) surface recorded at 90 eV.

A Cu(110) single crystal substrate is typically cleaned by several cycles of argon ion bombardment following a relatively longer time annealing in UHV system. Within this method, the rough and unclean surface is sputtered with argon ion to remove the contamination, then, is annealed at a high temperature, in our case usually 500 ºC, to speed up diffusion and rearrangement of the atoms in order to create a flat surface in a short period of time. Commonly, a clean surface produced with this method is characterized by atomically flat terraces of at least 100 Å.

Sample mounting

We use a standard stainless steel sample plate provided by Omicron, shown schematically in Figure 2.3. A square shapes sample of 1.0 cm^2 is mounted on the flat sample plate of approx. 1.0 mm thick using spot welded metal clips. This avoids noise arising from sample vibrations. The eyehole at the top of sample place is designed for sample transfer with a wobble stick.

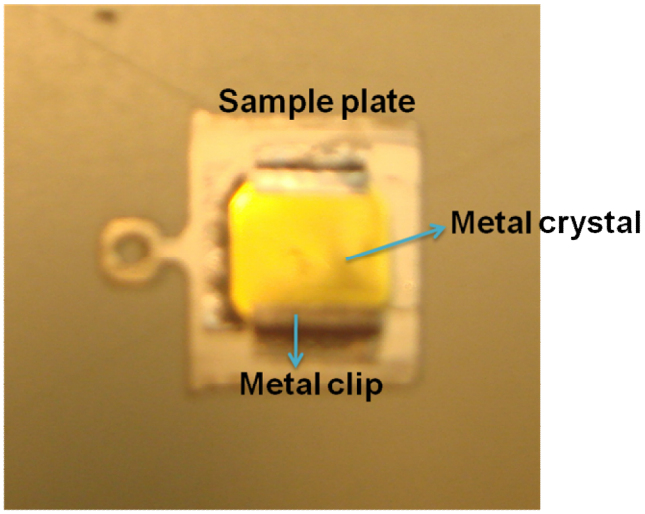

Fig. 2.3: Sample plate and sample mounting typically used in our STM experiment.

Evaporator

The evaporator used for molecular deposition is home built, schematically shown in Figure 2.4. Its design consists of a glass tube connected to a heating wire and a type K thermocouple used to measure the deposition temperature. The thin glass tube is used to contain the organic compounds of interest; chemical degassing by heating the tube to a temperature about 30 K lower than the deposition temperature is performed before deposition in order to remove the adsorbed gases.

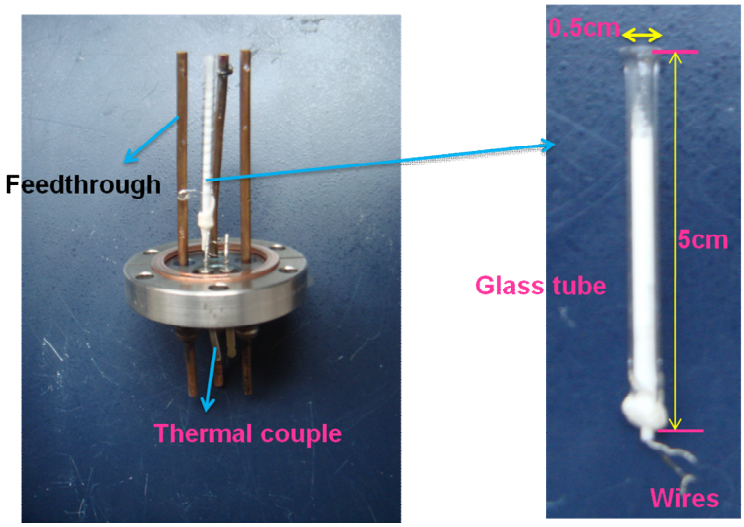

Fig. 2.4: Schematic illustration of the evaporator used in the experiments for thermal deposition.

Thin film preparation

In our experiments, we generally use thermal evaporation to deposit the molecules of interest onto a copper substrate via a home-built evaporator in UHV. In the thermal evaporation deposition, the chemical is vaporized by resistive heating [2]. This method commonly requires a UHV environment so that the adsorbate reaches the surface without interference of gaseous contamination. Thermal evaporation deposition is widely applicable in depositing small molecules with high vapour pressure. Molecules heated with higher vaporisation temperature might undergo decomposition during the heating process. With this method, surface coverage can be well controlled by appropriately adjusting the deposition temperature and the exposure time; moreover, side effects arising from solvents can also be effectively avoided.

2.2.2.2 STM tip preparation

In STM a very sharp tip, terminated with a single atom, is crucial in producing an atomic resolution image. A good tip is expected to have a small aspect ratio to reduce the mechanical vibration and to be capable of producing reliable and reproducible images. Two tip-forming approaches were adopted to make STM tips in most of the experiments.

The mechanical cutting is a straightforward procedure, widely employed in preparing tips used for STM in air due to its simplicity and convenience. Pt-Ir wire of 0.25 mm in diameter is the common material used in this method. A generally sharp tip can be yielded easily by cutting the wire held by a tweezers at an angle of 45º using a cutter or scissors. However, with this approach the quality of the tip can not be guaranteed [3].

Electrochemical etching is an effective procedure to produce a rather sharp tip, and consequently widely used to yield a tip used in STM applications in UHV. A tungsten wire, usually 0.40 mm in diameter is also a popular choice because tungsten is hard and very easily oxidized in the air but can resist for a long time in a clean environment such as the UHV chamber.

The experimental setup of the electrochemical etching is simple, shown in Figure 2.5a. It included a steel loop working as cathode, a tungsten wire and a tip holder

which is put tightly at the end of the tungsten wire, a DC voltage supply, and an electrolyte commonly NaOH or KOH solution with a concentration of 2M. During the process of electrochemical etching, the tungsten wire connected to the anode was placed vertically in the loop centre and held tightly by screws to ensure the tip to be produced having a proper length. Before the etching current was applied, the steel loop along with the wire was immersed into the electrolyte gently to form a uniform thin film inside the loop so that a closed circuit was built. The observable phenomenon when the etching starts was the appearance of gaseous bubbles around the loop and the solution particularly around the tungsten wire turned from clear to turbid. Shown in Figure 2.5b is a macro scale image of an ideal etched STM tip.

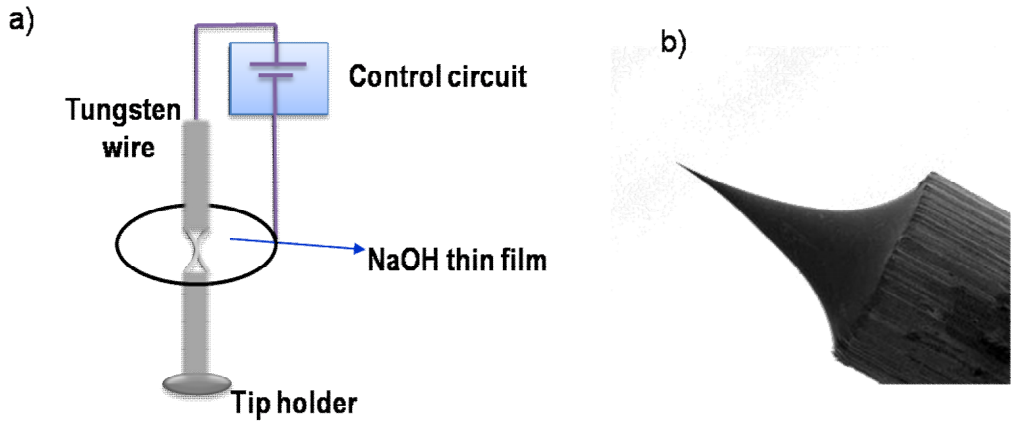

Fig. 2.5: a) Schematic illustration of the electrochemical experimental setup, b) Macro scale image of an ideal etched STM tip.

The general reaction is described as following [4]:

Anode: $W + 8OH^- = WO_4^{2-} + 4H_2O + 6e^-$,

Cathode: $6H^+ + 6e^- = 3H_2$

Total reaction: $W + 2H_2O + 2OH^- = WO_4^{2-} + 3H_2$

At the anode, the tungsten wire undergoes an oxidation reaction producing water soluble tungsten anions. This is accompanied by the production of gaseous hydrogen at the cathode. When the etching process is nearly finished, the tungsten wire will break by force of gravity and leave two tips where the wire breaks. Usually we only take the one held by the tip holder and wash it thoroughly using distilled water.

Newly prepared tips need further cleaning after being transferred into the STM chamber, because the surface is inevitably covered with some contaminants, which cannot be easily removed by rinsing with water. In practice, we commonly apply high bias voltage pulse of up to -7.0 eV for several times so that the contaminants can be removed leaving a clean and new sharp tip apex exposed. However, this approach is applicable only if the tip transferred to the chamber is already sharp.

Although many tip preparation methods have been introduced, generally it is taken as a tricky art more than a science to produce an ideal tip. Various factors might affect the quality of the yielded tip, such as the etching cut-off time, the applied voltage, the length of the tip exposed below the loop plane, the concentration of the electrolyte, etc. Hence, several tips are made as a bakcup and each of them is exposed to the optical microscope so that its sharpness can be checked. Then, the sharpest one is chosen for transferring to the STM chamber. Usually a sharp tip is characterised by a smooth surface with a very sharp end in the centre.

2.3 Scanning Tunneling Microscopy (STM)

STM has been considered as a powerful technique in surface analysis since it was first demonstrated by Binnig & Rohrer in 1982 [5, 6]. The reasons why the STM is so widely used in surface science come from two considerations. First, STM provides a straightforward view of the surface structure at an atomic scale with a lateral resolution of 1.0 Å and vertical resolution of 0.1 Å, provided that a sharp probe tip and extremely clean surface are available. Second, STM measurement can be performed under various conditions ranging from in air and various other liquid or gas environments to UHV conditions.

STM is a technique based on the principle of quantum tunneling, as schematically shown in Figure 2.6. According to the theory, when an atomically sharp tip approaches a conducting surface at a distance of a few Ångstroms, the overlap of the electronic wave functions of the electrons existing near the Fermi level (E_f) of these materials can tunnel across the narrow “barrier” between the tip and surface upon applying a potential of a few Volts. To record the image, the tip is moved laterally

across the surface with the aid of piezoelectric elements in the x, y directions, while the vertical movement is manipulated via a Z piezoelectric. In the constant current mode, where the tunneling current is kept constant, the tip and surface distance must be adjusted frequently using a feedback loop. Eventually a three dimensional mapping Z(x, y) of the surface is obtained since the vertical position Z of the tip is measured as a function of the lateral position (x, y). However, the obtained STM image does not simply reflect the topographic surface, but also the electronic structure of the surface; the tunneling current is actually function of the local density of states near the Fermi level of both the tip and the sample.

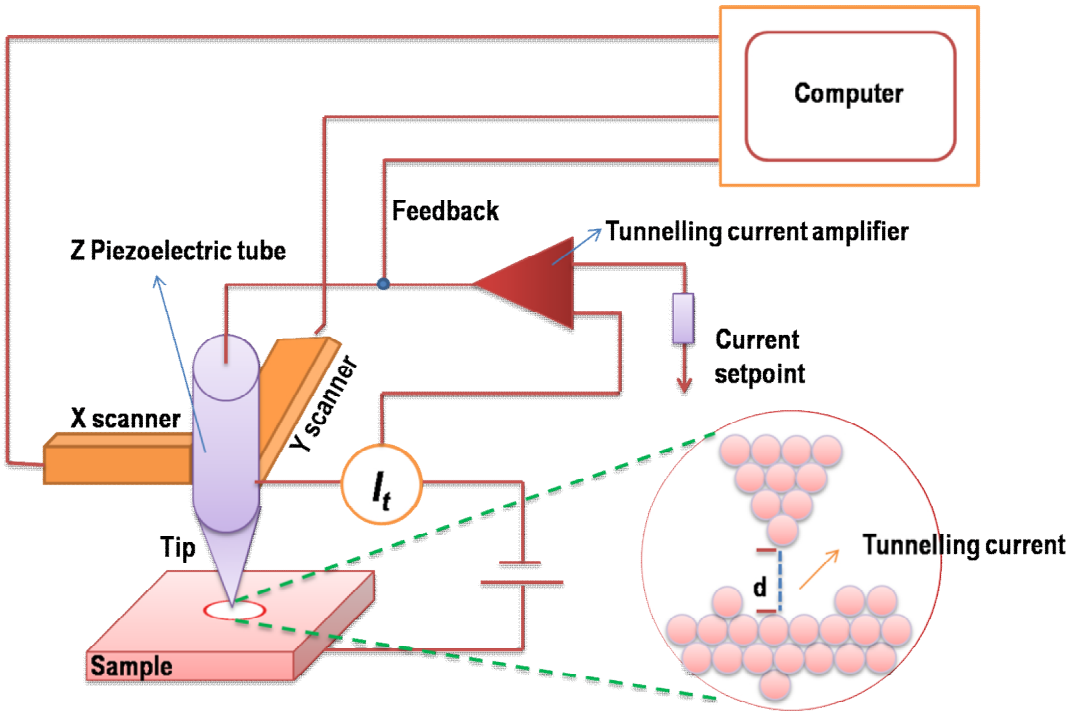

Fig. 2.6: Schematic illustration of the principle of STM.

2.3.1. Principle of electron tunneling

As schematically illustrated in Figure 2.7, electrons possess 'particle and wave duality'. As the tip is brought within the proximity of a planar surface and a small bias potential is applied, the overlap of the electronic wave functions of tip and surface leads electrons to penetrate into the vacuum gap between these two materials. This

gives rise to the so-called electron tunneling. The magnitude of the tunneling current I is the measure of the overlap of the two wavefunction, the current decays exponentially with the barrier width d, as given by

$$I_t \propto \exp^{-2kd} \qquad (2.4)$$

where k is related to the local work function by: $k = \frac{\sqrt{2m\Phi}}{\hbar}$

where m is the electron mass (9.11×10^{-31} kg), $\hbar$ is the reduced Planck's constant (1.05×10^{-34} J·s), and Φ is the average work function of tip and sample (eV). The tunneling current is very sensitive to sample-tip distance. A decrease in the sample-tip separation of 1.0 Å will increase the current by an order of magnitude. A vertical resolution of 0.1 Å is achieved if a single atom terminated tip is available.

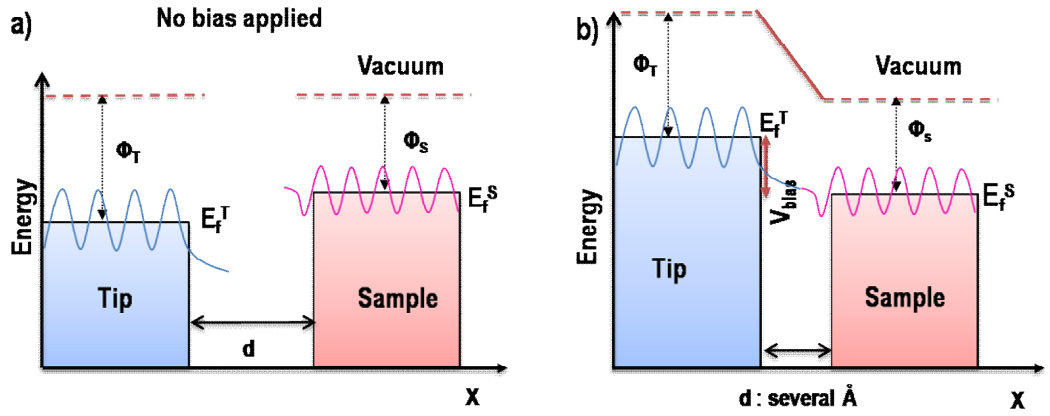

Fig. 2.7: a) Schematic representation of the energy levels of the tip and sample at large distance when no bias is applied. b) Schematic of the energy level diagram illustrating the overlap of the tip and sample wave functions in the tunnel region when a bias voltage V is applied, and the electrons tunnel from tip to sample. d is the barrier width, $E_f^{T/S}$ is the Fermi level of tip and sample respectively, while $\Phi_{T/S}$ are the wave function of the tip and sample respectively.

The electron tunneling direction is dependent on whether the surface is negatively or positively charged. A positively charged sample enables the electron to tunnel from tip to sample, thus the unfilled electronic state of the sample near the Fermi level is imaged. A negatively charged sample leads the electrons to flow in the opposite way and the resultant image reflects the filled electronic state of the sample.

2.3.2 Scanning modes

STM can be operated in two modes as shown in Figure 2.8: the constant current is the most common mode used to yield the 3D topographic image. In this mode, the tip position is adjusted continuously through a feedback loop to maintain a constant tip surface tunneling current when a constant bias is applied. The variation in vertical tip position, as the tip is scanned over the surface, represents the constant charge density contour of the surface. Changing the applied bias enables the contour of different charge density to be mapped. An alternative mode is the constant height mode, in which the tip height is maintained constant while scanning over the surface, hence current variation across the surface is imaged. We commonly use the former mode because it is ideal for rough surface area scanning, and a tip-surface crash can be effectively avoided. However, the drawback with this mode is that frequent alteration of the tip-surface distance will increase data acquisition time and limit the scan speed.

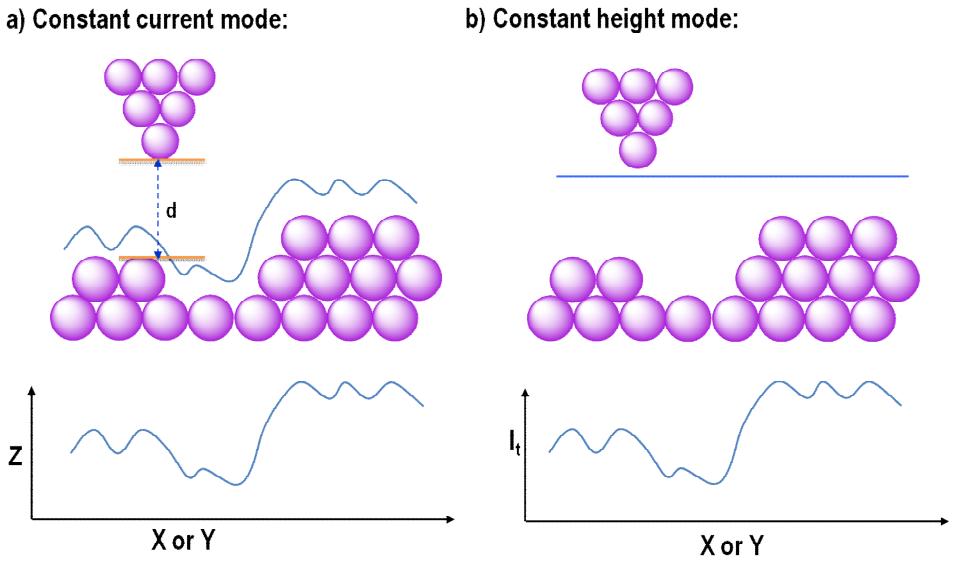

Fig. 2.8: Two scanning modes of STM: (a) constant current mode, (b) constant height mode.

STM reveals useful information concerning the electronic structure of the sample and the contrast shown in the STM image is directly related to the electron charge density profile of the studied surface. Therefore, if a series of bias dependent images are collected, the electronic charge density changes as a function of energy can be

investigated in detail. In constant current mode, this is achieved by simultaneously collecting images at various biases from positive to negative over the same scanning area; as a result, the interpretation of these voltage-dependent images reveals information concerning the empty and filled electronic states of the surface in great detail.

2.4 Low Energy Electron Diffraction (LEED)

The first LEED experiment was preformed by Davisson and Germer [7] in the late 1920's to observe the diffraction of electrons by nickel foil. However, the wide application of LEED in surface analysis did not start until the early 1960's. By then the development in UHV technology made it possible to monitor the directions and intensities of the diffracted electron beam. Furthermore, with the introduction of the post acceleration detection method, the scattered electrons were accelerated to high energy to produce a clear and visible diffraction pattern on a fluorescent screen.
Generally, the LEED is used in two ways:

1. Qualitatively, revealing useful information about the 2D periodicity and the size of the surface unit cell through analysis of the recorded spots position.
2. Quantitatively, determining the atomic position, bond lengths and angles by comparing the I - V curves, which refer to the intensities of the diffracted beams as a function of the incident electron beam energy, with theoretical curves.

2.4.1 Basic principle of LEED

LEED is based on the elastic scattering of low energy electrons incident normally onto a crystal surface [8]. Electrons in the energy range of 20 - 200 eV are excellent probes of surface structure because their inelastic mean free paths are between 5 - 20 Å, and can travel only a few atomic layers into the surface. According to the de Broglie hypothesis, electrons exhibit wave like behaviour and their wavelength is given by:

$$\lambda = \frac{h}{\sqrt{2mE}} \qquad (2.5)$$

Where: m - Electron mass (9.11×10^{-31} kg),

h - Planck constant (6.62×10^{-34} J·s),

E - Energy (eV),

λ - Wavelength (Å)

The dependence of λ on E can be obtained by

$$\lambda = \sqrt{\frac{150}{E(eV)}} \qquad (2.6)$$

Hence, for an electron beam with energy of 20 - 200 eV, the wavelength λ turns out to be 2.7 – 0.87 Å, which is of the same order of magnitude as the interatomic spacing of the atoms on the surface, making it ideal for a diffraction effect. The short mean free path of electrons means that only the topmost few atomic layers of a solid surface can be penetrated by the electron beam; as a consequence, contribution from the deeper atoms to the electron diffraction decreases progressively within this energy range and can be neglected in practice, which makes LEED a surface sensitive technique.

Electron backscattering in LEED can be explained by introducing a simplest 1D model. As illustrated in Figure 2.9, in which an electron beam impinges perpendicularly to a one-dimensional chain of atoms with interatomic separation of a. If we consider the backscattering of electrons from two adjacent atoms at a well defined angle θ with respect to the surface normal, then the radiation has to travel a path difference Δd to reach the detector. According to Bragg's law, for constructive interference to occur when the scattered beams eventually meet and interfere at the detector, this path difference must be equal to an integral number of wavelengths, which is expressed as:

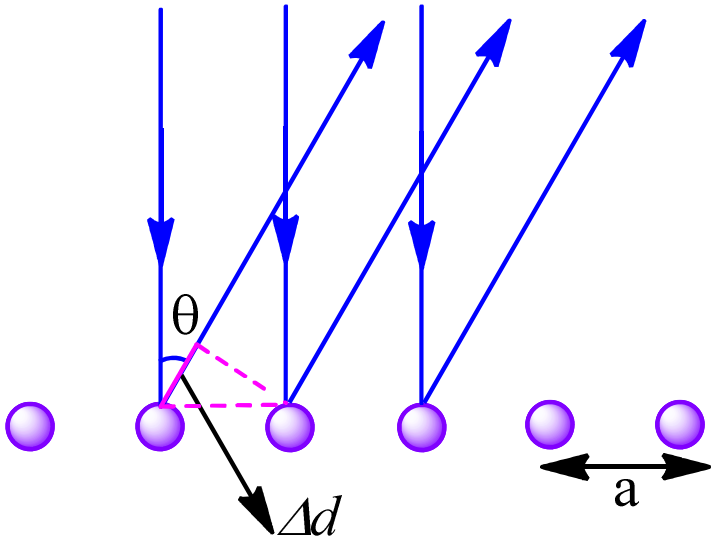

Fig. 2.9: Electron scattering on 1D atom arrays with separation of ***a***, *Δd* is the path difference the scattering beam travels before reaching detector.

$$\Delta d = a \sin\theta = n\lambda \qquad (2.6)$$

Where: λ – electron wavelength, and is constant for a given incident electron energy, *n* - integer (.., -1, 0, 1, 2, ..), and is known the order of diffraction

Rearranging the above equation yields,

$$\sin\theta = \frac{n\lambda}{a} \qquad (2.7)$$

Hence, the following information is derived:

1. *sin θ* is proportional to the *1/a*, thus as the inter-atomic distance gets bigger, the diffraction angle becomes smaller, which leads to narrowly spaced scattered beams.
2. *sin θ* is proportional to $1/\sqrt{E}$, so the diffraction angle decreases as the energy of the incident electrons increases, which results in more diffraction spots observable.

3. The resultant diffraction pattern is centrally symmetric since the diffraction has the same probability for n = 1 and n = -1.

Currently, the application of LEED focuses on the analysis of the spot positions to obtain information about symmetry and size of the adsorbate unit cell. The surface ordering and the size of the ordered array can influence the sharpness of the diffraction spots. However, a LEED pattern provides no information concerning the adsorption site of an atom, such as its bonding length and angle with respect to the surrounding surface atoms. Alternatively, information is revealed in the variation of diffracted beam intensities as function of the electron beam energy, known as *I(V)* curve. The disadvantage of this method is that there is no direct route to obtain surface geometries and an iterative process has to be adopted to find the best fit between experimental spectra and those of proposed structures, hence the application in practical work has been further restricted.

2.4.2 Experimental setup

LEED apparatus consists of three parts, as illustrated in Figure 2.10, an electron gun, a hemispherical concentric grids system and a fluorescent screen. The electron gun is composed of a negative potential cathode filament, usually a LaB_6 crystal, for generating a monochromatic electron beam to strike the sample. A series of grids are built to reject the inelastically scattered electrons from reaching the screen while accelerating the elastically scattered electrons in order for them to reach the screen. As a result, a pattern consisting of bright spots on a dark background is produced. The resultant LEED pattern is recorded typically by a CCD camera placed in front of the viewing window.

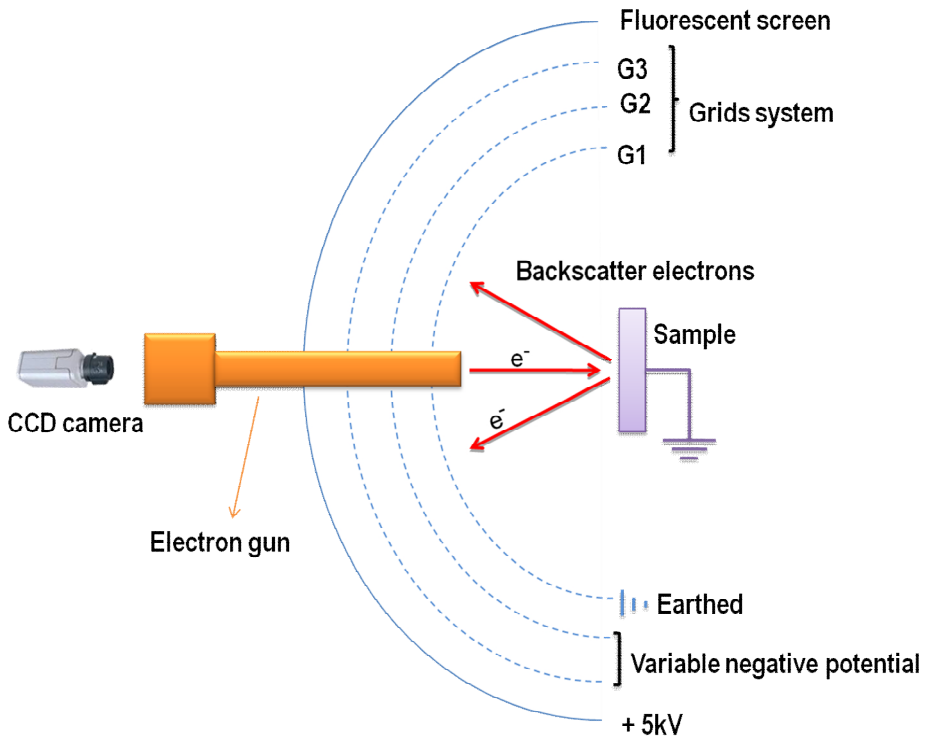

Fig. 2.10: Schematic representation of LEED apparatus setup

In our experiment, LEED was frequently used to check the surface geometry after argon sputtering and annealing, and monitor the superstructure changes occurring in the process of increasing adsorbate coverage and annealing. Generally, the appearance of sharp, bright spots is taken as evidence of a clean well-ordered surface good for deposition, while the appearance of the extra spots indicates the formation of new ordered superstructures upon changing the experimental parameters, such as annealing temperature and coverage. Since LEED is sensitive to an area of about 100 $Å^2$, a poorly ordered superstructure in small domains may not lead to any observable changes in the LEED pattern.

The LEED apparatus in this work is an Omicron Spectra LEED, which is installed in the preparation chamber allowing for collecting LEED pattern via a CCD camera.

2.5 Reflection Absorption Infrared Spectroscopy (RAIRS) [9]

RAIRS is a powerful surface specific tool for studying molecular orientation in the adsorbed layer formed at metal surfaces by utilising infrared beam to excite vibrations of molecules and atoms bonded to the surface during a single reflection near grazing angle with the surface. Incidence and reflection of IR beam in RAIRS is illustrated schematically in Figure 2.12, where the $\mathbf{E}_p$ refers to the parallel component of incident IR light electric field and $\mathbf{E}_s$ to the perpendicular component with respect to the plane of incidence. At the point where light contacts with the surface, the net amplitude of $\mathbf{E}_p$ component, oriented perpendicular to the surface plane, is twice of that of the incident light. Thus, it reaches to a maximum at high incident angle. The $\mathbf{E}_s$ component is effectively cancelled and the net amplitude is zero because the reflected beam undergoes an 180˚ phase-shift with respect to the incident beam. This means only the vibrations having a component of dynamic dipole moment perpendicular to the surface plane can be excited and observed in the RAIRS spectra. Generally, the sensitivity of RAIRS is strongly influenced by the following factors: the intensity of parallel component of incident IR beam, the incidence angle, usually at a grazing angle, together with the molecule with a large transition dipole moment arranged along the surface normal [9,10].

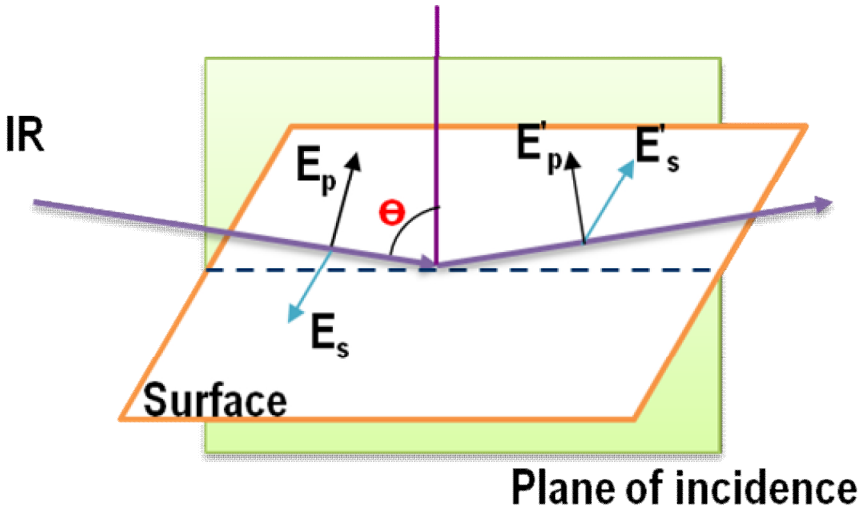

Fig. 2.12: Schematic illustration of parallel $\mathbf{E}_p$ and perpendicular component $\mathbf{E}_s$ of the IR beam electric field in RAIRS experiment [9, 10].

2.5.1 Surface dipole selection rule

In surface vibrational spectroscopy, the surface dipole selection rule is commonly applied to identify the peaks observed in the vibrational spectra. According to this rule, only molecular vibration modes having components of their dynamic dipole moments oriented perpendicular to the surface display observable peaks in the resultant spectra. This phenomenon is explained schematically in Figure 2.11. When molecules are adsorbed onto a metal surface, an image dipole moment will be induced on the surface due to the existence of metal conduction electrons. A perpendicular aligned dipole can induce an image dipole aligning in the same direction, consequently the resulting overall dipole amplitude is reinforced and gives rise to a measurable dipole. While a dipole aligned parallel with respect to surface plane induces an image dipole with opposite polarity, which leads to the cancellation of the overall dipole moment, yielding unobservable vibrational frequencies [10].

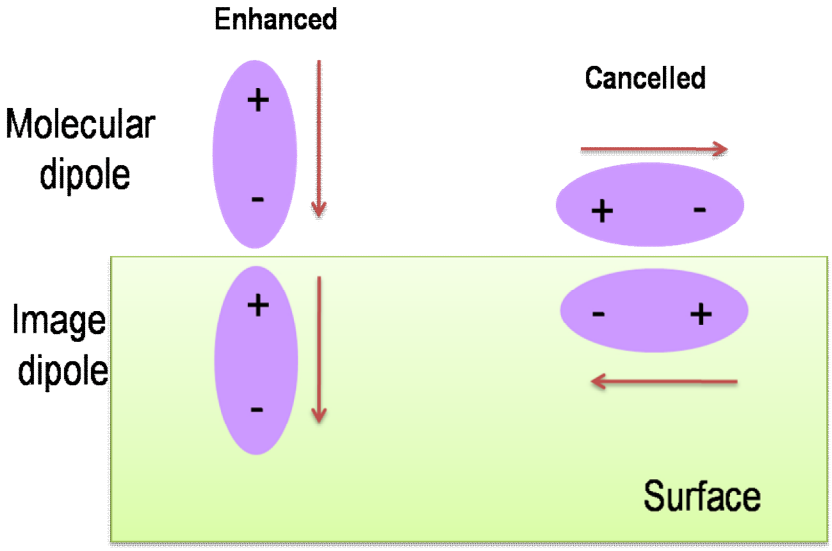

Fig. 2.11: Schematic representation of the two extremes of dipole orientation with respect to the surface plane and the corresponding orientation of image dipoles.

This surface selection rule is widely applied to determine the nature of the adsorption bond as well as the molecular orientation by evaluating the peak position and frequency intensity as a function of surface coverage and annealing temperature.

2.5.2 UHV-RAIRS experimental setup

A typical experimental layout for the UHV-RAIRS experiment is presented in Figure 2.13, the infrared radiation generated from the FT-IR spectrometer impinges on the sample at a grazing angle. After reflecting from the sample surface, the reflected beam is focused onto a MCT detector. Experimentally, dry nitrogen is used to purge the path of the IR beam in order to minimize the interference from gas phase water/CO_2 absorption; liquid nitrogen is used to cool the MCT detector. In RAIRS, with the use of a Fourier Transform IR spectrometer, the signal-noise ratio at any point in the spectrum as well as data acquisition speed is significantly increased.

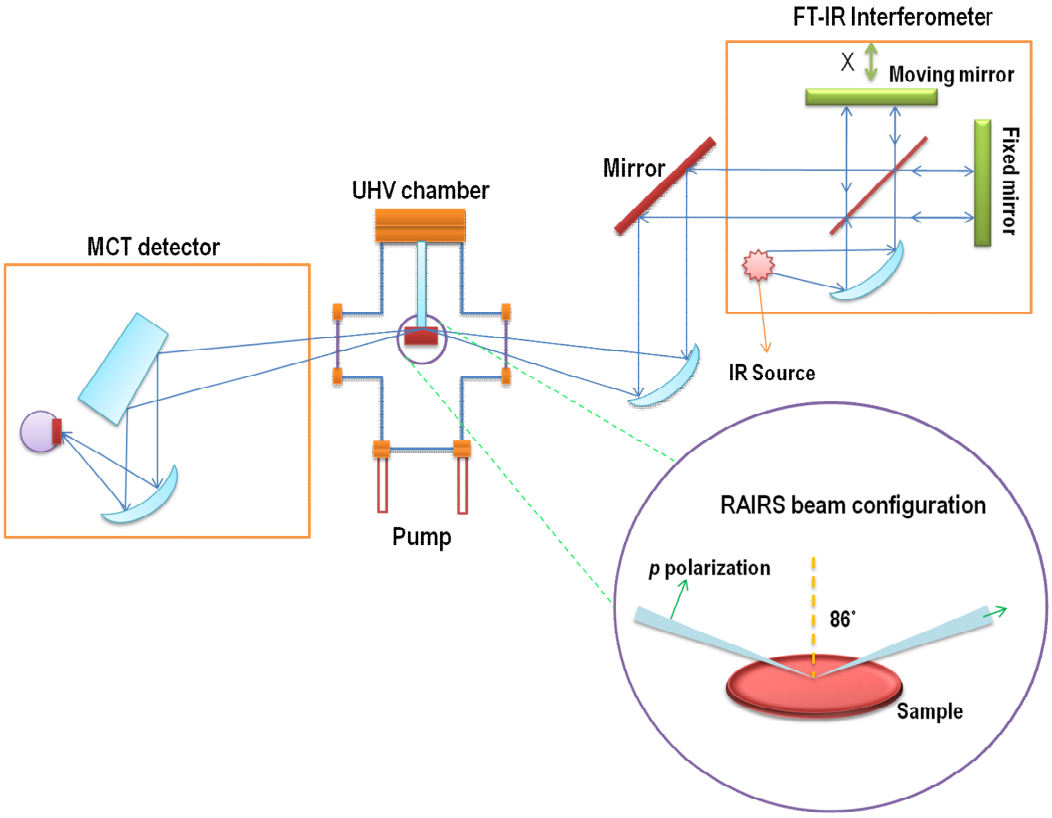

Fig. 2.13: Schematic diagram of the UHV-RAIRS experimental configuration, the grazing incident angle is about 86° [10, 11].

Due to the better resolution at which the spectra can be acquired, RAIRS is widely employed in the study of thin molecular films deposited onto metal surfaces; it can provide information concerning the intrinsic vibrations of the adsorbed species in a range of 800 - 4000cm^{-1}. Thus, it helps us to infer the nature of the bonding at the

surface and to identify the molecular orientation of the adsorbed molecules. In RAIRS, the peak FWHM is determined entirely by the heterogeneity of the surface and the nature of the surface-molecule interaction; the relative peak intensity grows approximately linearly with increasing coverage providing that no molecular reorientation occurs. However, the drawback with this technique is that the frequency below 800 cm^{-1}, which is commonly associated with the adsorbate-substrate bond vibrations, is generally unobservable.

2.6 DFT Calculation

For a better understanding of the orientation, the chemical binding of the adsorbed species and the driving forces for the observed superstructures, the experimental results obtained by vibrational spectroscopy and STM are supplemented by theoretical calculations. With reference to the calculated data concerning the molecular orbital, local electron density and the vibration frequency of the given molecular configuration under investigation, it is possible to construct the most likely adsorption model and compare it with the STM image.

Theoretical investigations aim to find the system ground state energy and the corresponding molecular geometry, vibrational spectrum, as well as other properties, such as dipole moment, electron potential, etc. Two *ab-initio* approaches are used to treat the many-electron system, one is called Hartree-Fock (HF) method and the other is Density Functional Theory (DFT) [12].

For the calculations of the vibrational frequencies, the ground state energy and the corresponding molecular geometry and orbitals, the Gaussian 03 software package has been used [13]. Here the DFT approach and the B3LYP (Becke, three-parameter, Lee-Yang-Paar) [14, 15] functionals are chosen to optimize the isolated molecular species of interest. Vibrational frequencies of isolated adenine and phenylglycine molecules were calculated using the 6-31G basis set with the addition of a diffuse function. The calculated results in combination with solid state KBr spectra were used to provide a reference for the RAIR spectra of adsorbed species. Thus, they enable a good interpretation of molecular orientations and binding natures in the self-

assembled structures. Also, the stabilization energy of selected adenine dimers, as well as the trimers, was calculated using the 6-31G basis set, which is believed to yield good results for hydrogen bonding. With reference to the molecular properties such as the molecular orbitals, bonding lengths and molecular optimized geometries, provided by the calculation, some reasonable structural models have been suggested and were proven to give a good explanation for the features observed in STM images. For visualization of the results obtained with Gaussian 03, Gaussview was used [13].

2.7 Experimental Setup

All room temperature experiments described in this section were performed in the Omicron VT-UHV system described in the Chapter II. A clean Cu(110) crystal surface was obtained by cycles of argon sputtering (typically 800 V, 1.5×10^{-5} mbar, 20 μA) followed by annealing at 800 K; it was assessed by the appearance of a sharp (1 × 1) LEED pattern with low dispersed background intensity. The low temperature STM measurements were carried out on a SPS-Createc LT-STM.

The RAIRS measurements were carried out on a research grade Nicolet 760 Fourier Transform Mid-IR spectrometer within the 800 - 4000 cm^{-1} range. All spectra were recorded with a liquid nitrogen-cooled, narrow-band MCT detector and collected with spectra resolution of 4 cm^{-1}; each spectrum consists of 1024 scans. Reprocessing against a clean surface background and standard water subtraction were performed in order to reduce the signals arising from water vapour in the light path. A continuous flow of a dry nitrogen purge was required during the whole operation in order to minimize the background signal arising from the H_2O, CO_2 in the spectrometer, light paths and the detector chamber.

LEED patterns were recorded via a CCD camera and a frame grabber card (Falcon PCI3) installed on a computer. The room temperature STM data was recorded in constant current mode via the *Scala pro.5.0* program and processed using the WSxM program [14]. The lattice of the real space unit cell is described conveniently in Wood notation (x × y), where each integer represents one of the real space unit cell lattice vectors. Conventionally, the first integer, x, refers to the <110> direction of the copper surface, in unit of the interatomic spacing 2.55 Å, and the second integer, y, refers to the <100> direction with unit of 3.61 Å.

The adenine (Aldrich, 99% purity) crystalline solid was deposited onto the Cu(110) surfaces by thermal evaporation. The compound was contained in a glass tube mounted on a feedthrough that is separated from the main chamber via a gate valve, and was pumped and degassed overnight at 370 K prior to deposition. The deposition temperature was maintained constant during deposition, and well controlled via a thermocouple sensor to ensure reproducibility. The background pressure in the chamber was typically below 1×10^{-10} mbar and rose to 1×10^{-9} mbar during the depositions.

The racemic mixture of phenylglycine (Aldrich 99 % purity) was dosed onto the Cu(110) surface via a home-built evaporator separated from the chamber by a gate valve. Before evaporation, the phenylglycine was out-gassed overnight at 310 K and heated to 320 K, before exposing to the copper single crystal. The pressure increased from 1×10^{-10} mbar to 1×10^{-9} mbar during evaporation. The coverage was controlled by the exposure time.

All theoretical calculations were performed using the Gaussian 03 software package [12] with 6-31G basis set using the hybrid density functional theory (DFT) with the non-local, Becke's three parameter functional (B3LYP) [15, 16] to describe the exchange and correlation energy. The structure of an isolated phenylglycine molecule in anionic and zwitterionic form was fully geometrically optimized and followed by a calculation of the vibrational frequencies.

2.8 References

1. A. Chambers, R. K. Fitch and B. S. Halliday, *Basic Vacuum Technology 2nd Edition*, IOP publishing, **1998**.
2. J. Küther, M. bartz, R. Seshadri, G. B. M. Vaughan and W. Tremel, *Mater. Chem.* 11, **2001**, 503.
3. I. Ekvall, E. Wahlström, D. Claesson, H. Olin, and E. Olsson, *Meas. Sci. Technol*. 10, **1999**, 11.
4. J. P. Ibe, P. P. Bey Jr, S. L. Brandow, R. A. Brizzolara, N. A. Burnham, D. P. DiLella, K. P. Lee, C. R. K. Marrian and R. J. Cotton, *J. Vac. Sci. Tech.* A 8(4), **1990**, 3571.
5. G. Binnig and H. Rohrer, *Scientific American* 253, **1985**, 40.
6. G. Binning and H. Rohrer, *Helvetica Physic Acta.* 55, **1982**, 726.
7. C. Davisson and L.H. Germer, *Nature* 119, **1927**, 558.
8. *Spectra LEED Optics and Electron Gun, User's Guide*, Version 4.1, Omicron Vakuumphysik GmbH, Germany, **2002**
9. J. C. Vickerman and I. Gilmore, *Surface Analysis: the Principal Techniques 2nd Edition*, Wiley publisher, **2009**.
10. B. L. Frey, R. M. Corn and S. C. Weibel, *Polarization-modulation Approaches to Reflection-Absorption Spectroscopy*, John Wiley & Sons Ltd, **2002**.
11. P. Gardner, S. LeVent and M. J. Pilling, *Surf. Sci.* 559, **2004**, 186.
12. R. Dreizler and E. Gross, *Density Functional Theory*, Plenum Press, New York, **1995**.
13. M. J. Frisch, *et al. Gaussian 03*, Gaussian Inc., Pittsburgh, **2003**.
14. I, Horcas, R. Fernández, J. M. Gómez Rodríguez, J. Colchero, J. Gómez. Herrero and A. M. Baro, *Review of Scientific Instruments*, 78, **2007**, 013705.
15. C. Lee, W. Yang and R. G. Parr, *Phys. Rev.* B 37, **1998**, 785.
16. A. D. Becke, *Phys. Rev.* A 38, **1998**, 3098.

CHAPTER III
Adsorption of Adenine on Cu(110) Surfaces

3.1 Introduction

3.1.1 Adsorption of adenine on surfaces

The adsorption of adenine molecules on solid surfaces has been the subject of a number of experimental and theoretical studies in the past years. The ability of adenine to self-assemble into one- or two-dimensional nano-scale structures upon deposition onto various surfaces, stabilised by inter-molecular hydrogen bonds, makes it a model system for the investigation of the bonding nature between DNA base molecules and metal surfaces, and two-dimensional chiral assemblies [1]. The understanding of the self-assembly mechanism of bioactive molecules on surfaces is not only fundamentally important in the preparation of bioactive surfaces [2-4], but also provides insight into the origins of life [5-8] and homo-chirality in nature [9].

We generally focus on three aspects when examining the adsorption behaviour of adenine at a well-defined metal surface: the molecular orientation, the bonding nature of the adsorbate and the driving forces accounting for the formation of various ordered layers. The particular molecular arrangement in the self-assembled structures depends on the surface that the molecules are deposited onto, the deposition rate and the temperature [10]. In ultra-high vacuum conditions, adenine molecules form one-dimensional chains on the Cu(110) [1, 9] and (111) [10-14] surfaces, and two-dimensional hexagonal networks on Cu(111) [15] and Au(111) [16, 17] surfaces similar to those observed previously on other surfaces, such as molybdenite [5], and graphite [18, 19]. Double-chain structures coexisting with hexagonal networks have also been revealed on the Cu(111) surface [15] upon depositing at a low deposition rate. A phase transition from one type of honeycomb monolayer structure composed of parallel arranged hexagons to a new phase of super-structures in which the hexagonal units are tilted with respect to each other, upon annealing the Au(111) sample from 150 K to 370 K was reported recently [16, 17]. The former molecular network is consistent with that reported on the Ag-terminated Si(111) [20] surface. In most cases, adenine was suggested to adsorb with its molecular ring lying flat (or

slightly tilted) at a considerable distance from the surface [1, 12, 18]. The lateral intermolecular double hydrogen bonds, dominating over the molecule-substrate interactions are the primary driving force for the formation of various overlayer structures.

Among these studies, adsorption of adenine on Cu(110) surfaces concerning the molecular orientation and nature of bonding have attracted extensive research interests. Infrared spectroscopic investigation on the molecular adsorption geometry of adenine on the Cu(110) surface has been reported by McNutt *et al.* [21]. A substantially tilted molecular orientation was suggested in which the molecule bonds with the substrate via the N9 and N3 atoms, Figure 3.1, while leaving the two hydrogen atoms of the amino group at an equivalent distance from the surface. This conclusion is reached based on the detailed analysis of the intensity variation in the peak associated with the NH_2 scissor vibration, along with the in-plane ring stretch modes, as a function of coverage and temperature. Phase transition of the adlayer from heterogeneity to well ordered was also predicted from the subtle shifts of the NH_2 scissoring and stretching vibrations due to the formation of one type of dominating H-bonds upon annealing. In the final ordered molecular assemblies, the existence of bent hydrogen bonds, arising from a compromise between the strong molecule-substrate interactions and weak intermolecular lateral hydrogen bonds are suggested; this weak lateral interaction accounts for the 2-D molecular organisation.

In conflict with the upright standing geometry, a flat-lying or only slightly tilted adsorption geometry has been suggested by several other research groups using a combination of several surface sensitive techniques. Chen *et al.* studied the adsorption of adenine on Cu(110) surface after annealing at 430 K by STM, LEED, and HREELS [1], and came to the conclusion that in chiral related molecular chains, both the purine and NH_2 planes are aligned almost parallel to the surface while the C-NH_2 bond is tilted away from the plane. The binding occurs exclusively between the amino group nitrogen atom and the copper atom; a clear re-hybridization of N atom in the NH_2 groups from sp^2 to sp^3 was also confirmed by DFT calculations, predicting a Cu-N length of 2.2 Å.

Based on the same assumption made by Chen *et al.* [1], a detailed analysis of the bonding between the amino group and Cu(110) by means of first principles calculation was carried out by Preuss *et al.* [22]. The computational results show that

the molecule binds via the N atom of the amino group with the substrate and the molecular plane is slightly tilted; the amino group is bent by 17.7° and the purine ring by 26.4° with respect to the surface plane, giving the amino group nitrogen atoms sp^3 hybridized character. The Cu-N distance is 2.32 Å; this is consistent with the bond length calculated by Chen *et al.* [1] and in other organometallic complexes. The strong adsorbate-substrate interaction leads to a slight structural change in the amino group and to local charge transfer; the electrostatic interaction arising from the mutual polarization between the substrate and the adsorbate is responsible for the bonding. Furthermore, this group also examined the mechanism of adenine adsorption and dimer chain formation of adenine deposited on the Cu(110) surface from the aspects of bonding, geometry, and energy. A three-step reaction pathway for the formation of molecular network is proposed; it consists of the dimer formation, the registry of the pair to the substrate, and the connection of neighbouring pairs via hydrogen bonds. In this process, the hydrogen bonds are, on one side, responsible for the connection of two isolated molecules to form the dimer, on the other side, link together these dimers giving rise to the one dimensional chains.

A similar parallel molecular orientation is also indicated by the vibrational spectroscopic investigation on the adsorption of adenine on Cu(110) by Yamada *et al.* [23] using IRAS, and the surface coverage is quantitatively determined using the carbon Auger signal. At coverage less than one monolayer, the flat-lying molecular orientation is suggested and is determined from the absence of the vibrational frequencies associated with the NH_2 scissor mode and the in-plane ring vibrations. As the coverage increases to over 1.0 ML, the observation of a prominent peak, assigned to the NH_2 scissoring vibration, along with these in-plane modes shows a strong evidence for the appearance of strongly tilted adsorbates. Hence, it is concluded that the molecular orientation changed as the coverage increased.

Calculation of the adsorption of a single adenine molecule on Cu(110) surface was carried out by Rauls *et al*. [24]. Two different configurations were studied in terms of adsorption geometries, binding energy, strain and dispersion interactions, as well as electrostatic effects, shown in Figure 3.1. In one orientation, the molecules bind only via the amino group, resulting in the purine ring being slightly further tilted to 26°; in the other one, the molecule interacts via two nitrogen atoms, namely the amino N atom and N7 atom, with the substrate, giving rise to a more planar adsorption

configuration on the surface with a tilting angle of 15°. The more planar adsorption configuration favours stronger covalent molecule-substrate interactions and local charge transfer, hence, it is a more energetically favourable adsorption configuration for adenine deposited on the Cu(110) surfaces.

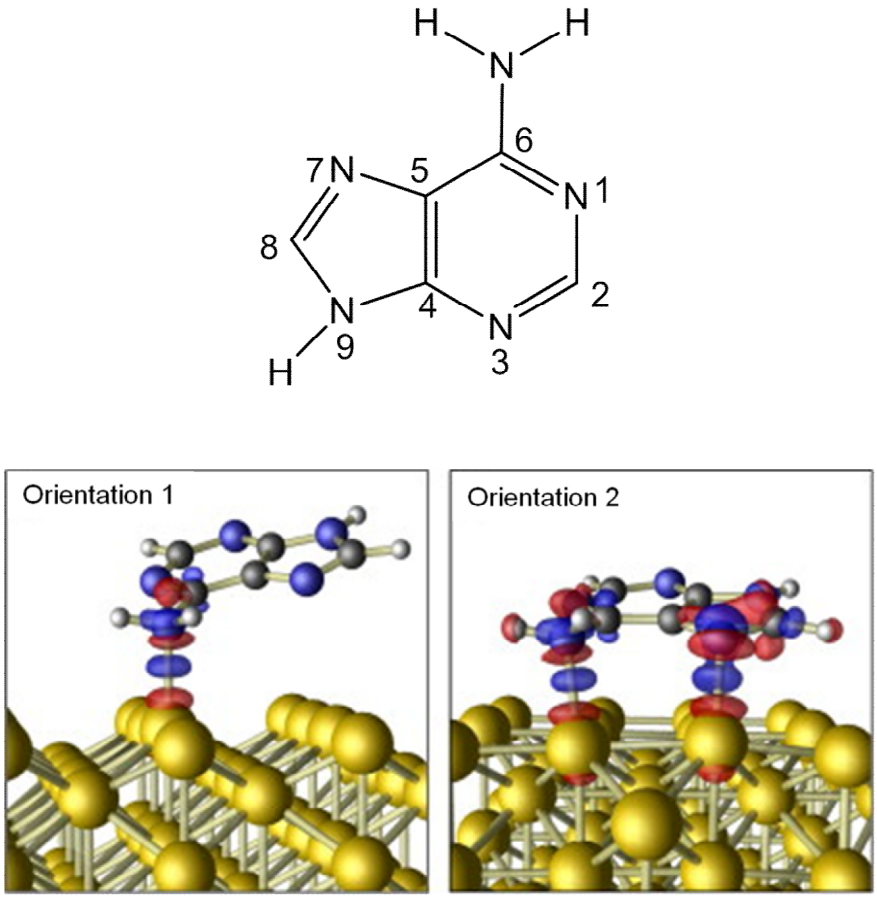

Fig. 3.1: Atom numbering of adenine (on the top), and the induced charge density for adenine on the Cu(110) surface in orientation 1 and 2. Orientation 1 bonds via only the amino group nitrogen atom; orientation 2 interacts via both the amino N atom and N7 imino atom, giving rise to more planar adsorption configuration. Along the molecule-substrate, blue and red regions denote the electron accumulation and depletion [24].

Very recently Feyer *et al.* [25] conducted a spectroscopic investigation of adenine/Cu(110) using angular Near-edge X-ray Fine Structure (NEXAFS), X-ray Photoelectron Spectroscopy (XPS) and DFT calculations, they revealed a coverage dependent molecular reorientation after examining the relaxed geometry of adenine at different coverage on Cu(110) surfaces. At coverage ≤ 0.167 ML, the molecule

prefers to lie flat on the surface with a small tilting angle of 28° with respect to the surface; the binding takes place through the N7 imino atoms and to a lesser extent, through the NH_2 amino group. As coverage is increased to between 0.2 - 0.33 ML, the molecules undergo orientation changes, and the molecular plane is oriented at a steep angle greater than 55° with respect to the surface. Finally, the tilting angle of the adenine plane to the surface increases to 89.75° when the coverage reaches to 0.33 ML *i.e.* saturation coverage. At high coverage, the molecule binds with the substrate via the N1 imino atom and partially via the amino group. The molecular re-orientation and bonding nature is confirmed by the changes in the angular dependent Near-edge X-ray Absorption Fine Structure (NEXAFS) spectra and the chemical shift associated with the N1s core-level XPS spectrum. In this study, the conclusion concerning the almost parallel molecular adsorption geometry is in good agreement with the study of Furukawa *et al.* [26] by NEXAFS and XPS at low coverage, while the tilted geometry is consistent with the vibrational spectroscopy data of McNutt *et al*. [21].

Among these studies, vibrational studies reported very different intensities for the same frequency, the NH_2 scissor vibration, giving rise to conflicting conclusions for the molecular orientation, either almost flat-lying or up-right, because of a failure to determine the coverage. Theoretical calculations, along with NEXAFS and XPS results, agree well with the STM observations on the almost flat-lying orientation of adenine at low coverage. However, there is still not a consensus on the nature of bonding of adenine to copper, particularly concerning the bonding strength, the bonding sites of adenine, which to some extent, depends on the accuracy of different computational methods and the starting model for the calculations.

In this work, we will present detailed STM investigations of the effect of experimental parameters, *e.g.* substrate annealing temperature, surface coverage and deposition rate, on super-structures formed by adenine upon deposition onto the Cu (110) surface; some new superstructures will be described in this chapter. Additionally, low temperature (70 K) STM examination of the adenine dimer chains and monomers as a function of bias voltage has also been carried out.

For all the adenine molecular networks on the Cu(110) surface presented in this thesis, we construct the corresponding adenine molecular structural models in the following way. Firstly, because of the high ability of adenine to form double hydrogen bonding pairs, all the possible adenine pairs are considered, including the

ones that are not energetically favourable in the gas phase, but that might become favourable building blocks in the presence of a substrate. Secondly, we select as the most probable pairs those exhibiting apparent similarity in shapes and dimensions with the molecular features imaged via STM. Finally, we construct some gas-phase structural models that resemble the observed networks by properly connecting these possible pairs together via hydrogen bonds, and then select the ones having high stabilization energies and lattice parameters that match well with the experimental results.

Despite the great success that scanning tunnelling microscopy has achieved as a powerful tool to identify molecular networks on surfaces, it is not easy to obtain atomic resolution of the molecular assemblies involving small planar organic molecules, particularly DNA bases, due to the small corrugation of the local density of states at the Fermi level [17]. In addition, since the corrugation height mapped by STM is merely a direct reflection of the electronic structure of the tunnelling state, it is not a measure of the real geometrical height of the adsorbed species. Hence, other methods have to be employed in combination with STM in order to study the super-structures in detail.

In our experiments, high sensitivity RAIRS was used as a useful tool for the identification of the bonding and chemical nature of the adsorbates with respect to the surfaces, and monitoring the evolution of the molecular orientation as a function of the experimental parameters, like surface coverage and annealing temperature. In addition, LEED was used to follow the degree of ordering of the adlayer structures and the corresponding changes in the surface periodicity upon annealing. Finally, theoretical calculations using DFT methods are adopted as complementary methods enabling us to construct possible structural models that match well with the observed features mapped via STM, thus, helping to provide models to interpret the experimental results.

3.1.2 Adenine molecule

DFT calculations show that in the gas phase, the adenine molecule, a DNA base, is an almost planar molecule consisting of five and six membered ring with an amino group $–NH_2$ connected to it via a sp^3 hybridization; this results in the two hydrogen

atoms slightly tilted out of the plane at a shallow angle of 14° according to our DFT calculation. Displayed in Figure 3.2 is the configuration of a single molecule in top view, denoted as **A**; **Ā** is its enantiomeric motif, obtained by reflecting **A** in mirror plane perpendicular to the page. Because of the nearly planar configuration, the adenine molecule is considered as prochiral and belongs to a C_s point group. Two mirror-related adsorbed species, resulting from the two modes of adsorption by either face-up or face down [1], can be generated upon adsorption on surfaces.

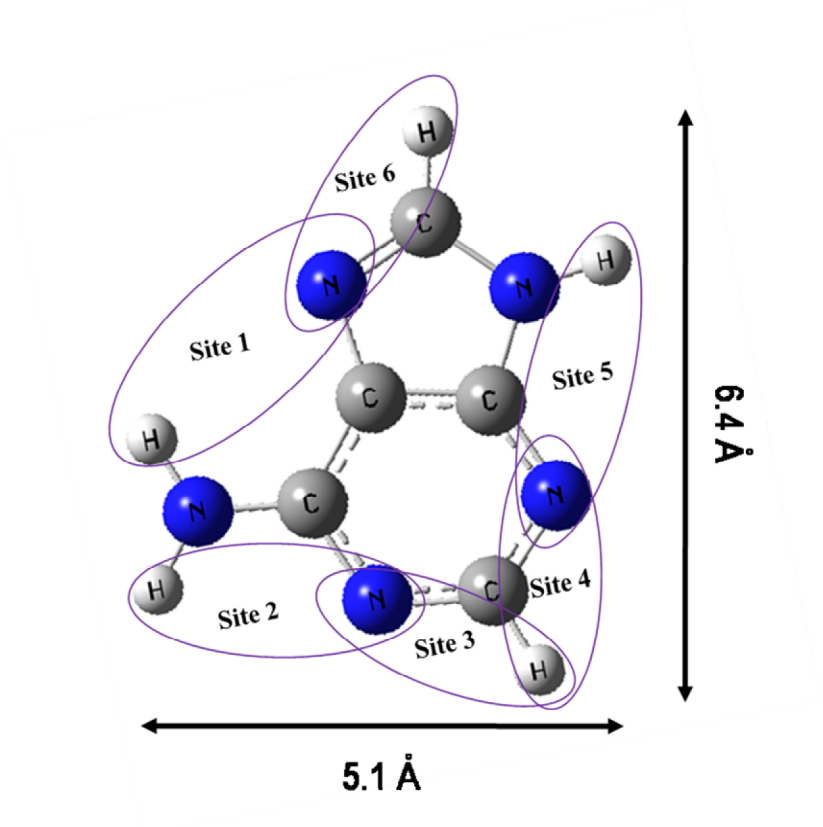

Fig. 3.2: Adenine molecule in configuration **A**, **Ā** is obtained by reflecting **A** in a mirror plane perpendicular to the page. The six possible adenine pairs of nearest N and H atoms, referred as bonding site, that can participate in the formation of two adjacent hydrogen bonds between the two molecules are indicated [27]; the approximate dimension of an adenine molecule is also indicated, it is about 6.4 Å in length and 5.1 Å in width.

Adenine is capable of forming hydrogen bonded pairs arising from the existence of the N atoms and CH or NH groups; generally, a stable molecular dimer is characterised by at least one pair of double hydrogen bonds [28, 29]. Based on this principle, six pairs of adenine hydrogen bonding sites are identified in the adenine

molecule [10, 27], as described in Figure 3.2. Each bonding site refers to the neighbouring hydrogen bond donor, CH or NH groups, and acceptors, N atoms, and is capable of connecting with the site from another molecule in the formation of double hydrogen bonds. Hence, a total of 21 adenine dimers can be obtained; nine pairs are hetero-chiral, **A$\bar{\mathbf{A}}$**, where one of the molecules should be flipped to facilitate the formation of double hydrogen bonds between two corresponding sites, and twelve are homo-chiral, *i.e.* **AA** or $\bar{\mathbf{A}}\bar{\mathbf{A}}$. The corresponding double hydrogen bond connected dimer is denoted as $\mathbf{A_nA_m}$ or $\mathbf{A_n\bar{A}_m}$, where n, m refers to the hydrogen bonding sites involved. The chirality of each adenine dimer is determined by considering the individual chirality of the two molecules composing the dimer. Among these dimers, six $\mathbf{A_nA_n}$ possess C_2 symmetry where double hydrogen bonding forms between the same binding sites, and the large dipole moment is cancelled in these cases [1]. As a result, stable centro-symmetric pairs are usually adopted as the most common pairs in the construction of gas-phase overlayer networks.

Here, we present the relaxed geometries of the six centro-symmetric adenine pairs, in order of stability from high to low, Figure 3.3. All the relaxed pairs exhibit very near-planar geometries; the dimer, denoted as $\mathbf{A_5A_5}$, has the highest stabilization energy, it is connected with other less energetically favourable dimers in the construction of adenine dimer chains observed on the Cu(110) surface [1]. Here, the structure of each pair is optimized using DFT methods with the B3LYP functional and the 6-31G basis set. It is assumed that the B3LYP functional gives a better description of the system containing hydrogen bond [30].

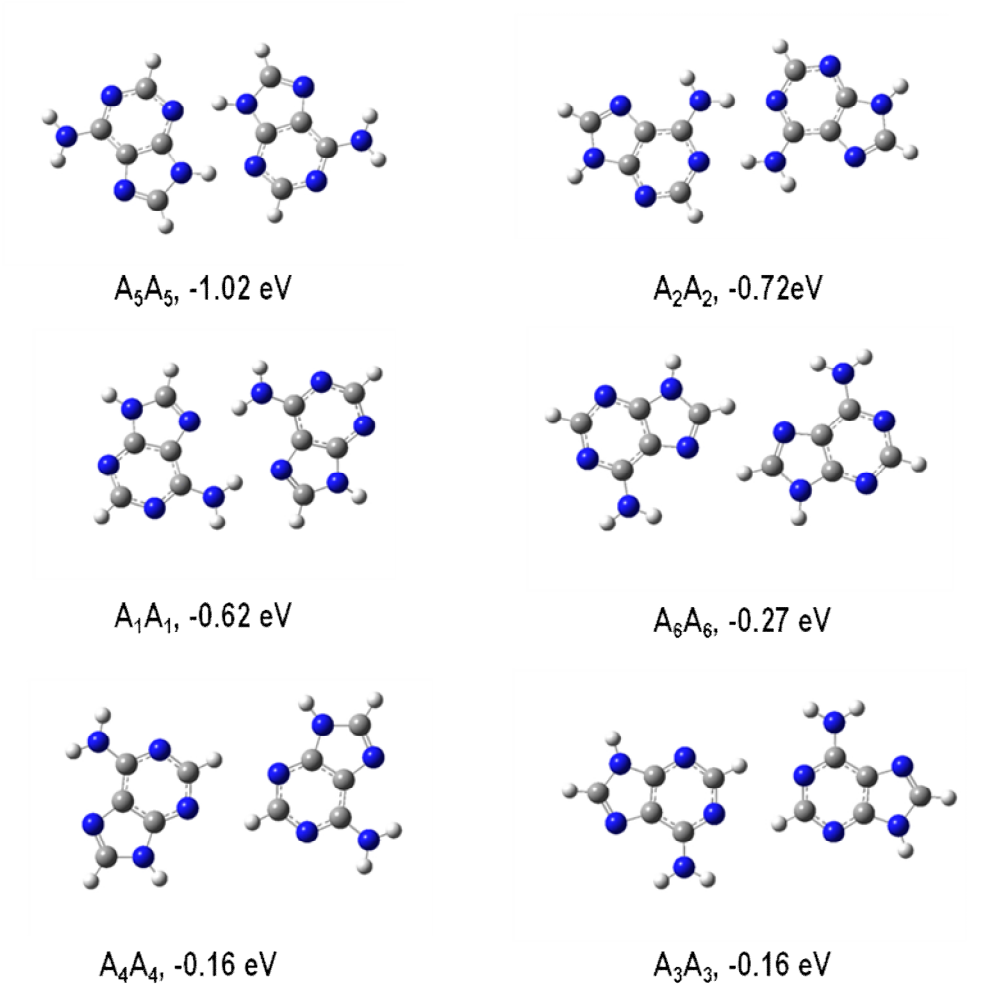

Fig. 3.3: Six centro-symmetric adenine pairs and the corresponding stabilization energies are given. Each molecule of the pair denotes the same hydrogen binding sites. The structures are optimized using DFT methods B3LYP functional with 6-31G basis sets. The adenine pair is denoted as $\mathbf{A_nA_m}$, where n and m indicate explicitly the hydrogen bonding sites of the two molecules engaged in each pair.

There have been different calculation results reported concerning the stabilization energies of the six centro-symmetric pairs, which might be due to the different functions used in the geometric optimization. However, all pairs are in the same energetic order and show the same almost planar geometries [1, 27]. The stabilization energies of all 21 gas-phase adenine pairs have been calculated by Kelly, *et al.* using the PBE and the B3LYP GGA functionals [27], the corresponding relaxed geometries are presented. According to their results, the $E_{stab,}$ which is defined as the total energy of the relaxed dimer minus the total energy of the individual monomers relaxed separately for all the dimers, is in the range of -0.03 eV to -0.86 eV [10]; the

deformation energies are small, indicating that the atomic relaxation in each dimer is not significant, hence, it can be neglected to give a good approximation during adsorption. Dimers involving the electronegative nitrogen atoms are expected to be more energetically favourable than those including the less electronegative carbon atoms. In addition, the strength of the hydrogen bonds can be approximately evaluated by considering the corresponding hydrogen bond length and the angle between the two molecules. Stable dimers are supposed to have shorter hydrogen bond lengths and an angle of nearly 180º [10].

As we come to build up the structural models for the observed STM structure, several factors must be taken into consideration. Firstly, the geometry of the adenine pair chosen should match well the molecular features imaged in STM. Secondly, the relative stability of each adenine pair involved in the suggested building blocks has to be accounted for. This can be evaluated theoretically by the corresponding stabilization energy, referred as E_{stab} [31]; hence, a stable dimer always has negative stabilization energy. Lastly, in order to satisfy all the necessary links between the molecules comprising the networks with the presence of the substrate, both the favourable and less favourable pairs need to be considered [16].

3.2 Results and Discussions

3.2.1 High coverage Adenine/Cu (110)

RAIRS investigations on the molecular orientation and intermolecular interactions of adenine on the Cu(110) surfaces have been previously reported by Raval, *et al*. [21]; they derived an upright standing molecular orientation at sub-monolayer coverage by examining the intensity variations associated with the NH_2 scissor vibration. However, this conclusion is controversial with other relevant studies because RAIRS fails to detect the coverage quantitatively. Here we present our RAIR spectra and related STM studies of the adenine adsorbed on the Cu(110) surface.

3.2.1.1 RAIRS studies

Figure 3.4 shows a comparison between the experimental spectrum of the solid adenine and the calculated frequencies of a single molecule derived by DFT calculations. The experimental IR spectrum is dominated by a series of low to medium intensity bands in the range of 800 - 1700 cm^{-1}, associated with the molecular in-plane skeleton stretches and ring C-H and N-H twist vibrational modes. The vibrational frequencies found at 1675 and 1604 cm^{-1} are attributed to the $-NH_2$ scissoring mode; this is the most intense vibration in the IR spectrum. The preservation of this band with high intensity for adsorbed adenine molecule provides information for the identification of the molecular bonding nature and orientation. Most vibrational frequencies below 800 cm^{-1} are unobservable in the KBr spectrum; these vibrations are assigned to the ring C-H and N-H out-of plane vibrational modes. The assignments of the experimental vibrational frequencies for the solid adenine, those obtained by theoretical calculations on the free adenine and those of the adsorbed species are listed in Table 1. Most of the calculated vibrational frequencies for the isolated adenine molecule are in good agreement with those experimentally observed.

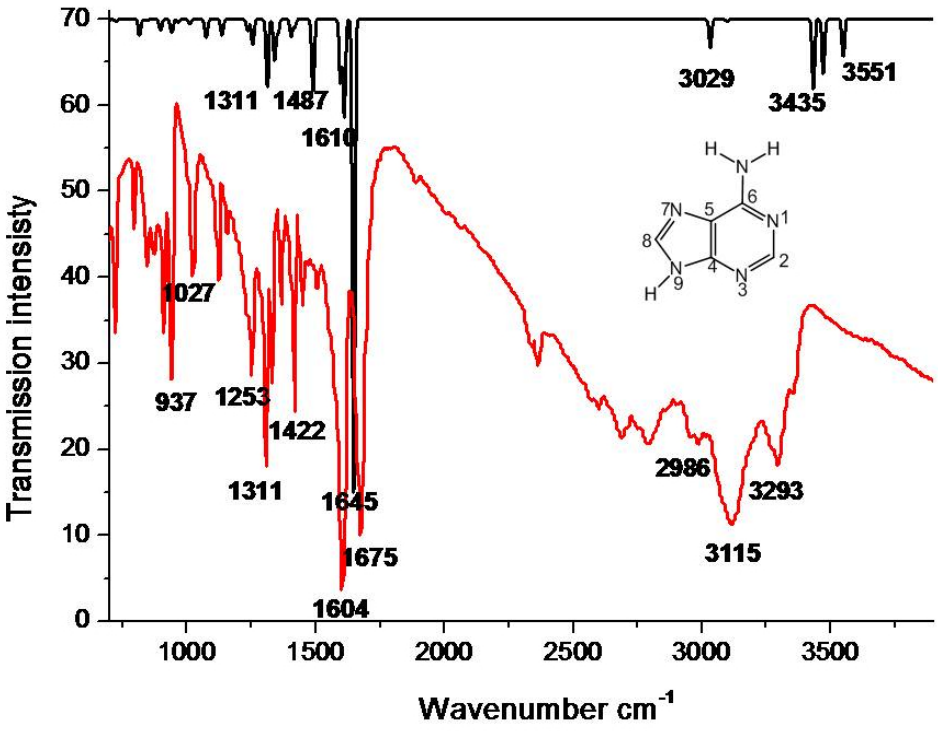

Fig. 3.4: Transmission IR spectrum of KBr solid adenine (*red*) and the calculated vibration frequencies of the isolated adenine molecule using DFT *(black).*

Table 1. Comparison of the experimental frequencies of characteristic vibrational modes of adsorbed adenine and adenine in gas phase with calculated frequencies of adenine using DFT calculations

Adenine/Cu (110)	Adenine (KBr)	Theory DFT(B3LYP)/6-31G(d)	
υ (cm^{-1})	υ (cm^{-1})	υ (cm^{-1})	Assignments
	3293	3551	ν_{asym} NH_2
	3115	3435	ν_{sym} NH_2
	2986	3029	ν C8H, ν C2H
1653	1675	1645	δNH_2, νC6N10, νC5C6
1648	1604	1610	δNH_2, νC4C5
1456	1422	1487	νN1C6,νN7C8, νC6N10, νC2N3, βC8H, βN9H, βC2H, βN10H
1363	1365	1407	νN1C2, νC5N7, βC2H βN9H
	1334	1346	νC2N3, νC5C6, νC5N7, νN1C2, β C2H
1295	1311	1311	νN1C2, νN7C8, βC8H, βN9H
	1253	1247	βC2H, βC8H, βNH_2 rock, νC4N9, νC6N10, νC5N7, δ $N3C4C5^{sym}$
	1118, 1027	1131, 1075	νC8N9, β C8H, βN9H
	937	940	βr
	910	898	βR
	848	812	γC8H

Description of the symbols: ν-stretch, δ-scissor, β-bend, γ-wag, βr-five memebered ring deformations, βR-six membered ring deformations. Abbreviations: sym - symmetric, asym - asymmetric.

Figure 3.5 a-d shows the spectra of adenine adsorbed on Cu(110) as a function of increasing coverage. As the coverage increases at room temperature, a number of subtle variations are identified in the spectra. At low coverage, the spectra are dominated by a single broad band at around 1634 cm^{-1}, which is assigned to the in-plane scissoring mode of the -NH_2 vibration. The observation of this band with high

intensity indicates the -NH_2 group is not lying parallel to the surface, according to the surface dipole selection rule. There is no observation of other peaks associated with this group; the NH_2 stretching vibrations are anticipated at around 3551 cm^{-1} and 3435 cm^{-1}, respectively; they are the asymmetric and symmetric NH_2 stretching vibrations, respectively. At higher coverage, a number of relatively low intensity bands are found at 1456, 1363, and 1295 cm^{-1}; they are attributed to ring in-plane vibrational modes. The observation of these vibrations in the RAIRS provides evidence that the molecular plane is tilted away from the surface plane in this phase. However, it is impossible to quantitatively determine the molecular orientation because most of the out-plane vibration modes lie below 800 cm^{-1} which is out of the detector range. There are no obvious changes occuring to the spectra when increasing the coverage gradually up to saturation coverage, except that the continuous growth in the intensity of the band associated with the -NH_2 scissoring mode. Additionally, the overall pattern of the band remains similar, indicating that the molecular bonding and orientation remain unchanged.

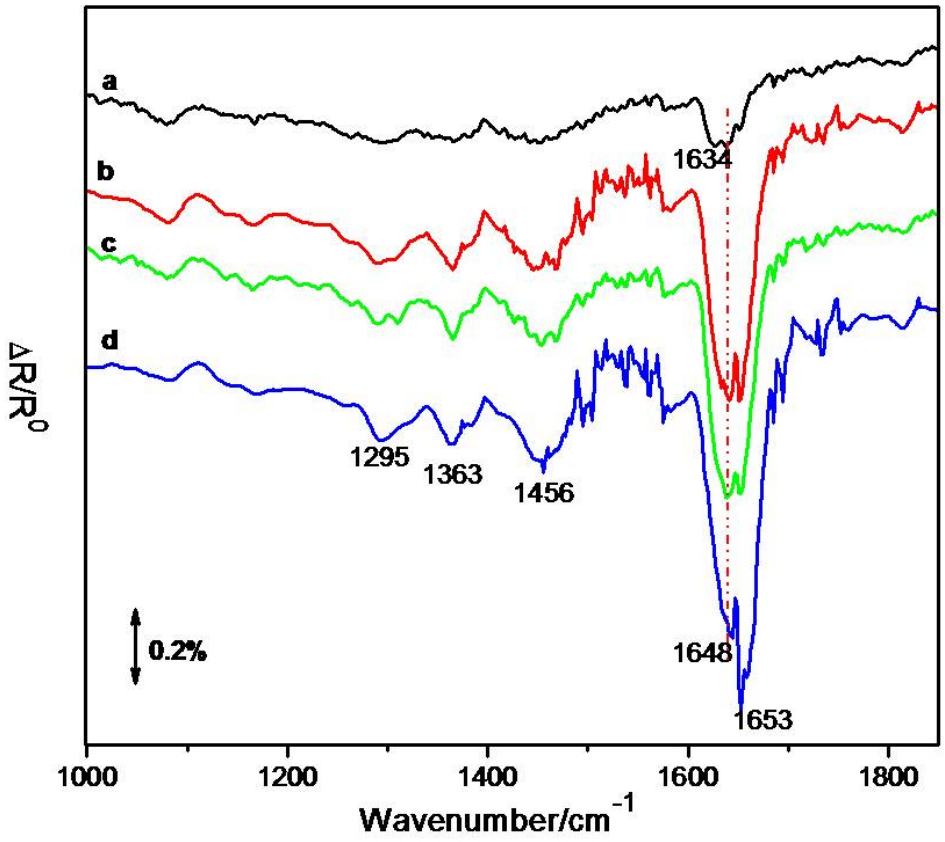

Fig. 3.5: RAIRS spectra of adenine adlayer on the Cu (110) surface showing the evolution of the vibrations as a function of the coverage at room temperature, (a) 0.2 L; (b) 0.5 L; (c) 0.6 L (d) 0.9 L; blue-shift of the frequency of the $-NH_2$ scissor mode is marked by dash line at 1646 cm^{-1}

However, some variations, associated with the characteristic vibrational frequencies and their relative intensity, in particular NH_2 scissoring vibrations, were revealed when examining the high coverage spectra in more detail. The noticeable changes are considered as the result of the formation of hydrogen bonds among adsorbed molecules at the higher coverage. The formation of hydrogen bond leads the vibrations, especially those associated with the N-H or C-H stretch modes, to shift towards low frequency and become broad; this trend is also accompanied by an increase in intensity. Moreover, the deformation of the N-H vibration tends to shift towards higher frequency but show no substantial intensity change or band broadening [21]. This is consistent with the trend of the vibration related with the $-NH_2$ scissoring which is shifted to 1653 cm^{-1} in the high coverage spectrum, Figure

3.5d. This blue shift provides evidence of the aggregation of the monomers to form dimers and multimers in the adenine adlayer.

The RAIR spectra shown in Figure 3.6 were obtained upon subsequently annealing a saturation coverage deposited at room temperature to 330, 380 and 420 K. The general pattern of the most characteristic bands of the adsorbed species remains largely similar upon annealing; this indicates that there are no changes in the molecular orientation occuring during this process. The exception is that the vibrations found at 1153, 1291, 1376, 1446 cm^{-1}, arising from the ring in-plane stretch vibrational modes, show a significant sharpening. This phenomenon is particularly evident with the band found at 1653 cm^{-1}, associated with the $-NH_2$ scissoring vibrational mode. The broad band, seen at room temperature, is replaced by a fairly sharp and intense narrow one after annealing to 380 K. This behaviour displayed by the $-NH_2$ scissor mode is attributed to the disordered adsorbed layer is converted into a more ordered self-assembled adlayer, in which one type of hydrogen bonds become the predominant interactions, leading to the formation of more ordered structures. A sudden drop in the intensity of this vibrational mode upon further annealing to 420 K, indicates that desorption of the ad-layer might have occured. High desorption temperature also suggests strong bonding between adenine molecules and copper atoms.

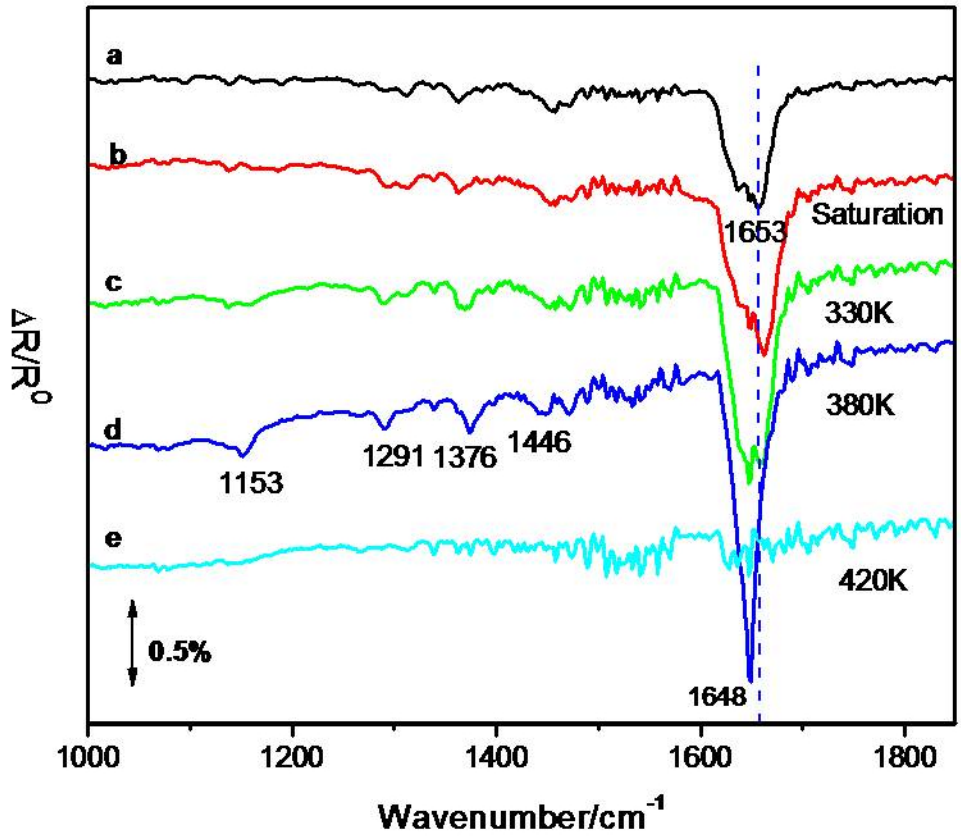

Fig. 3.6: RAIR spectra of adenine adlayer on the Cu(110) surface showing the effect of annealing; the red dash line indicates the position of the -NH_2 scissoring mode, showing an obvious sharpening and red shift upon annealing as a result of the formation of more ordered layer. (a) 1.0 L; (b) 1.1 L.

Adenine is taken as an essentially planar molecule even though both the amino hydrogen atoms are aligned slightly out of the molecular plane at a dihedral angle between 11 and 22º [32]. Thus, we can suggest that the existence of intense -NH_2 scissoring vibration, along with most of the in-plane vibrations observed in all the spectra, might indicate that the molecular plane is more likely to be tilted rather than oriented parallel to surface plane. This conclusion is in disagreement with the conclusions derived from previous STM studies carried out at other metal surfaces, such as the Au(111) [16, 17], Cu(111) [10-15], Cu(110) [1]. However, our RAIRS investigation agrees well with the results published by Raval *et al*. [21]. In their study, adenine was proposed to interact with the copper atoms via the imino nitrogen atoms of the rings. In this adsorption geometry, the molecular plane is highly tilted away

from the surface plane; the two amino hydrogen atoms are placed at equidistance from the surface, making some in-plane vibrations dipole active including the NH_2 scissoring mode. Considering the molecular orientation and binding nature suggested by STM at the Cu(110) surface, the discrepancy is believed to be caused by the fact that the absolute coverage is not identified certainly in the RAIRS. The observation of the -NH_2 scissoring vibrational mode could result from multilayer adsorption or the highest monolayer coverage. At the higher coverage, the adenine molecular plane is forced to tilt up due to the steric repulsion between the molecular rings; this can make the –NH_2 RAIRS dipole active.

3.2.1.2 STM and LEED studies

As aforementioned, the observation of the intense -NH_2 scissor vibration in the RAIR spectra, upon depositing adenine onto the Cu(110) surface, might result from the multilayer or high dense monolayer adsorption. Here we present experimental evidence showing higher coverage adsorption obtained via STM and LEED.

Shown in Figure 3.7 are STM images of the adenine multilayer adsorption upon annealing the sample to 440 K; several different superstructures have been observed. In Figure 3.7a, the bright chain features on the top layer are clearly distinguishable from those on the underlying layer that appear as slightly darker features. Within the top layer, short arrays of bright spots are identified; they mainly grow along two directions, but neither of them aligns along the high symmetry directions of the substrate, as indicated by the blue solid arrows. Similar chain features, indicated by dash arrows, are also observed in the underlying layer. The growth directions of these short chains in both layers are the same, but it seems that the adenine molecular arrangements on the underlying layer have little influence over the inter-molecular interactions on the top layer. This is indicated by the fact that the dark adenine chains growing along one direction are surrounded by the arrays of bright protrusions aligning along the other direction. The measured dimensions of these features, in terms of chain width (8.0 Å), and the separations of adjacent rows (16.1 Å), together with the growth directions with respect to the high symmetry directions of the Cu(110) substrate, are found to match well with those of chiral-related adenine chains

reported by Chen *et al.* [1]. Hence, it is believed that adenine molecules are arranged in the same way as that in those dimer chains.

As the coverage is further increased, ordered single adenine chains growing along the <110> direction of the substrate are formed. The length of the chains is slightly longer (>100 Å) than that of adenine dimer chains, as shown in Figure 3.7b, c, d. The corresponding LEED patterns showed a clear (1 × 2) periodicity for the self-assembled structures shown in c and d. Conventionally, the first number refers to the <110> direction of the copper substrate, in unit of the inter-atomic spacing of 2.55 Å, and the second refers to the <001> direction in the unit of 3.61 Å. Thus, the size of the unit cell is approximately 18.41 $Å^2$, which is much smaller than the dimension of a single adenine flat lying on the substrate, for which the maximum size is about 32.64 $Å^2$. This finding may further suggest that the observation of the intense peak of the -NH_2 scissoring in RAIR spectra is resulted from a multilayer or dense monolayer adsorption in which the molecular plane of adenine is tilted away from the surface, where the standing up molecular rings give rise to a smaller “footprint” on the surface.

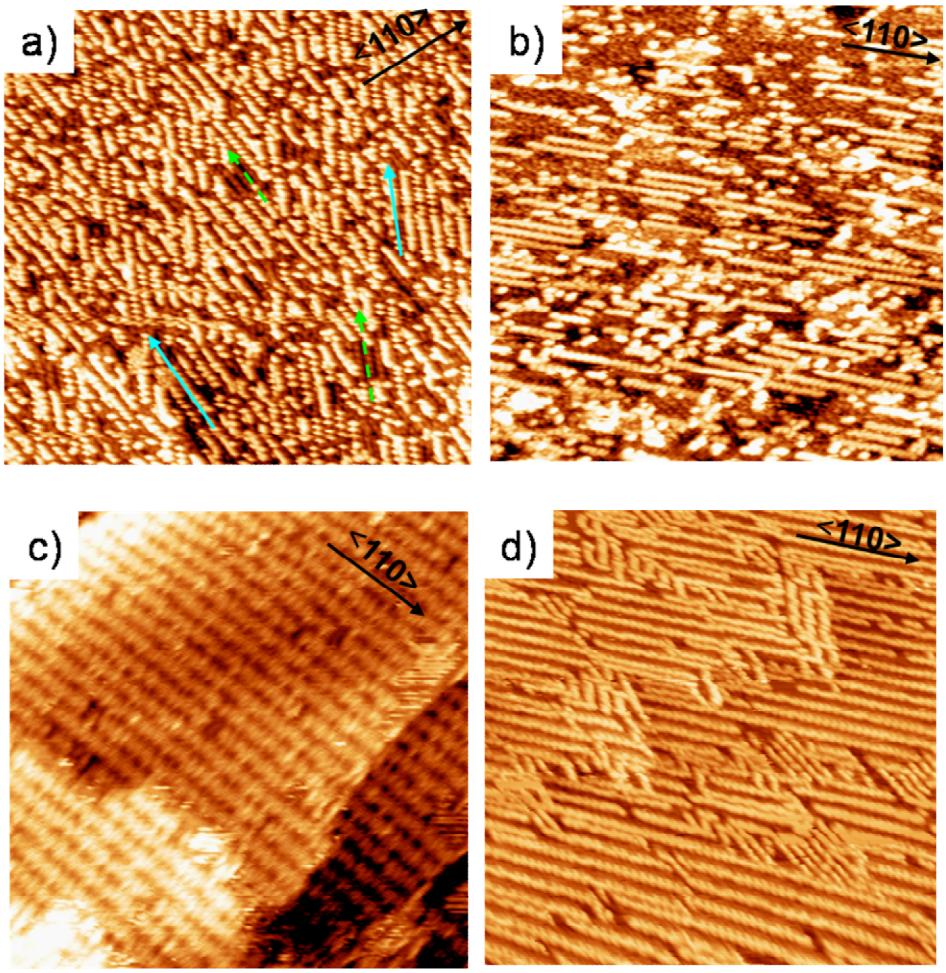

Fig. 3.7: STM images of adenine adsorbed on Cu(110) at higher coverage showing the evolution of the superstructures with increasing coverage upon annealing the sample to 440 K. a) adenine chains growing along the (1, 2) and (-1, 2) directions of the substrate, the top layer and under layer chains are indicated with solid and dash line respectively. (0.21 nA, -1.07 V, 70 × 70 nm^2) b) and c) ordered adenine rows aligning along the <110> direction, (0.44 nA, -1.39 V, 42 × 42 nm^2, 0.9 nA, -0.52 V, 41 × 41 nm^2); d) large adenine domains along the <110> direction (1.01 nA, 0.70 V, 52 × 52 nm^2).

In Figure 3.8, LEED patterns of adenine high coverage adsorption on Cu(110) surfaces, recorded at 32 eV (a) and 128 eV (b), respectively, are presented along with the corresponding STM images. The first order spots of the clean copper substrate are indicated with circles and the one in the middle refers to the position of the (0, 0) beam. In Figure 3.8a, half order spots are clearly seen and both lattice vectors of the overlayer structures are aligned along the high symmetry directions of the substrate, so the real space unit cell of the overlayer structures is described as (1 × 2). The

vector along the <100> direction is 7.22 Å, which is slightly larger than the maximum length of a single adenine molecule, 6.4 Å. From the corresponding STM images, Figure 3.8c, we can see that adenine molecules arrange themselves in a close packed way with their long dimension parallel to each other in the rows; each of the narrow features might correspond to a single adenine molecule having its long dimension aligning along the <001> direction. This high coverage adlayer structure is well ordered along the <110> direction; the average width of each chain measured from the line profile is 13.6 ± 0.3 Å, and the average distance between neighbouring chains is approximately 17.5 ± 0.3 Å. These values seem to disagree with the periodicity determined from the corresponding LEED pattern; they are more likely to result in a (1 × 4) pattern. The surface corresponding to Figure 3.7d and 3.8d, has similar but faint (1 × 2) LEED pattern; the measured width of each row is about 10.0 ± 0.3 Å, and the separation of neighbouring rows is about 16.0 ± 0.3 Å. The unit cell along the <110> direction is composed of two narrow features of slightly different contrast; the short length of the narrow feature lying in the middle of the chain is only 3.3 ± 0.2 Å and the longer length is about 6.8 ± 0.2 Å. The short dimension of the feature is narrower than the width of a flat-lying individual adenine, *ca.* 5.3 Å, hence, adenine is more likely to orient with its aromatic ring tilted away from the surface plane in order to reduce the space the adsorbed adenine takes up at multilayer coverage. It is still difficult to explain why these structures give rise to a (1 × 2) pattern; this does not agree with the physical dimension of the corresponding features measured on the topographic STM images.

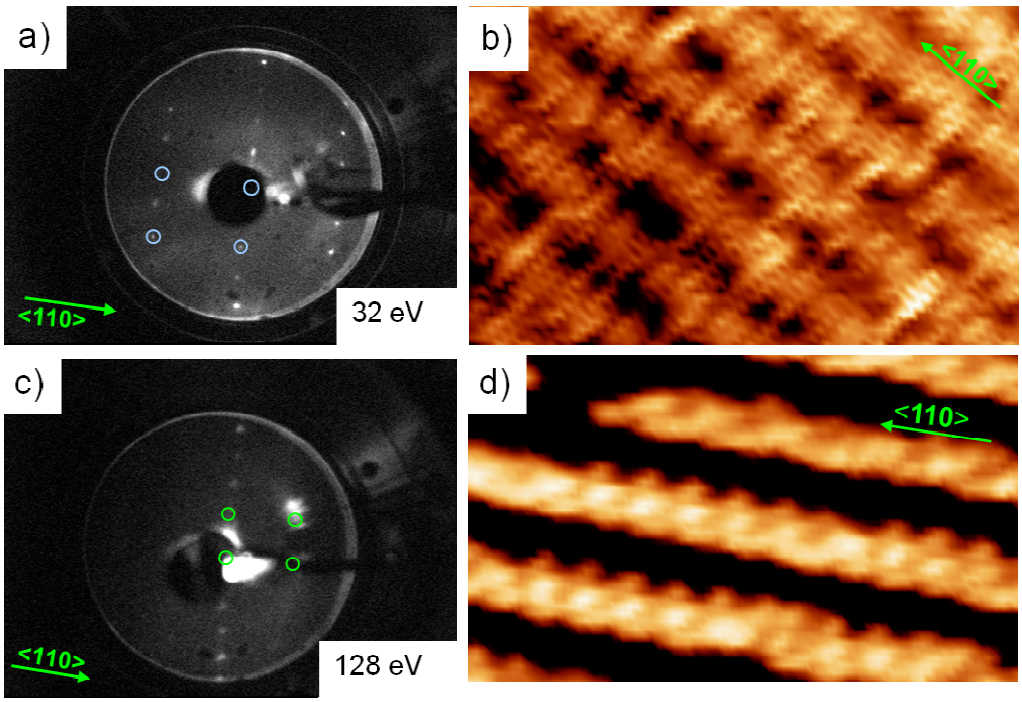

Fig. 3.8: The (1 × 2) LEED patterns of adenine on Cu(110) surface in dense monolayer recorded at 32 eV and 128 eV. High symmetry directions and the first order substrate spots are indicated. On the right side are the magnified STM images of the overlayer features shown in Figure 3.7c (15 × 8 nm^2) and d (8 × 5 nm^2), respectively.

3.2.1.3 Discussions

Based on the analysis of these features observed in our STM images, we can see that adenine undergoes orientation changes upon increasing the coverage from sub-monolayer to much higher coverages (*e*.g. dense monolayer or multilayer). It is suggested that, in this process, adenine molecules adopt a flat lying orientation in the sub-monolayer regime; at increased coverage, adenine molecules are forced to tilt up and propagate in a parallel fashion along one direction as a result of the weaker lateral hydrogen bonding and π-π stacking interaction of the aromatic rings. The coverage difference is the main reason for the formation of different two-dimensional architectures.

From the STM investigation of the adlayer structures at high coverage, we can see that the preservation of intense -NH_2 scissoring vibrations in the RAIR spectra is an

indication of high coverage adsorption. In the high coverage structures, the molecular plane of the adenine molecule is forced to tilt with respect to the surface, making the dipole moment of the -NH_2 scissoring mode strongly active in the spectra. Moreover, the sudden drop in the intensity of the scissoring mode of the amino group cannot be taken as convincing evidence of molecular desorption; the changes in molecular orientation from standing up to flat-lying can also make the frequencies related with the in-plane and -NH_2 scissoring vibrations disappear.

3.2.2 Effect of annealing on Adenine/Cu(110)

Previous research suggested that the formation of ordered adenine dimer chains on the Cu (110) surface is a coverage driven process; strong attractive intermolecular interactions, along the (±1, 2) directions, between the adsorbed species are responsible for the formation of ordered domains at high coverage upon annealing to 430 K [1]. Here I present STM investigations of the evolution of the overlayer superstructures as a function of the annealing temperature. A surface coverage of 75% of saturation (0.75 ML) (Figure 3.9a, b) was achieved by controlling the exposure time. Here, the saturation coverage refers to the surface that is fully covered by a monolayer of adsorbates. The actual coverage is directly measured by counting the number of individual molecular features on the corresponding STM images.

3.2.2.1 STM studies

A series of STM images of adenine deposited on Cu(110) surfaces, representing an overview of the evolution of varied superstructures as a function of the annealing temperature, are shown in Figure 3.9. At room temperature, Figure 3.9a, adenine molecules aggregate into small islands and short molecular arrays on the copper terraces. Within the overlayer island structures, molecules connect with their surrounding counterparts in a disordered manner. The molecular features within the short arrays show different contrast with respect to the substrate and islands of molecules; these depressed features are considered to be a result of molecular etching

during adsorption. It is a direct evidence of the strong adsorbate-substrate interaction occuring even at room temperature, originating from the strong interaction of the nitrogen atom of the amino group with the copper atoms [33].

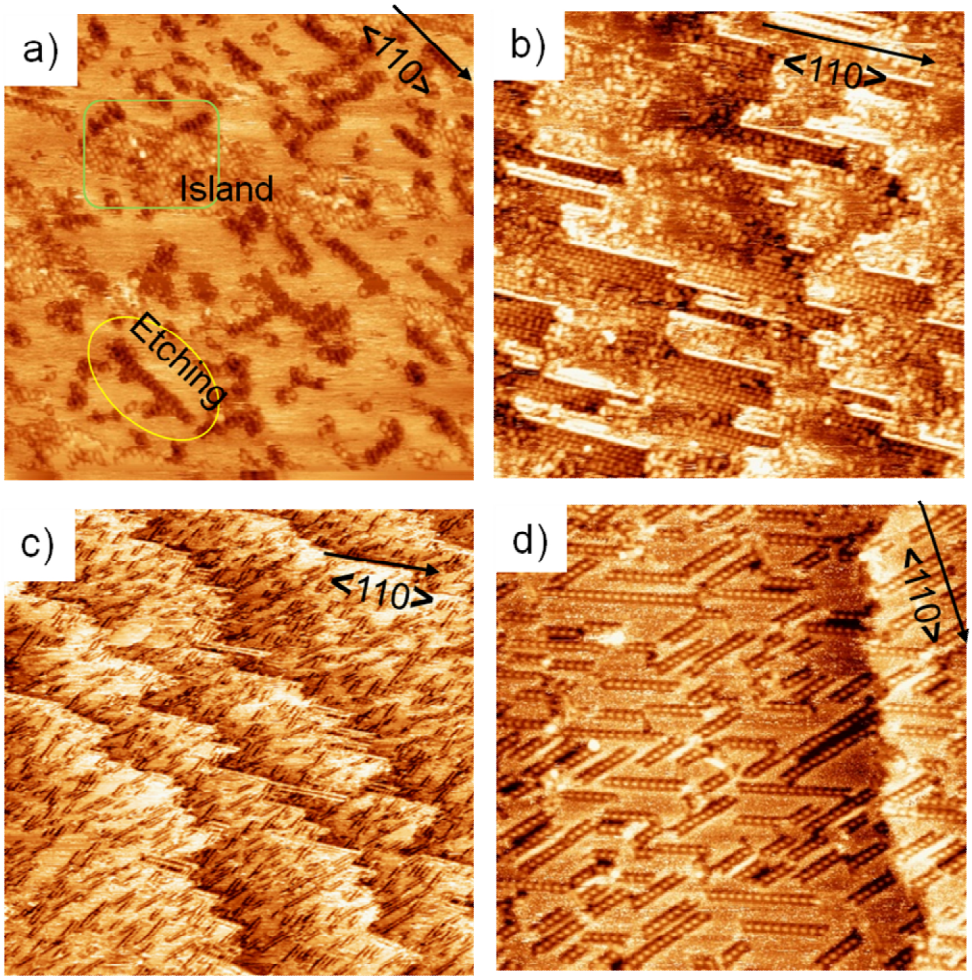

Fig 3.9: STM images of adenine adsorbed on Cu (110) surfaces showing the evolution of the superstructures as a function of the annealing temperature. a) Room temperature (0.314 nA, -1.2 V, 60 × 60 nm^2), b) annealing to 420 K (0.76 nA, -0.97 V, 66 × 66 nm^2); c) annealing to 450 K (1.321 nA, -0.80 V, 90 × 90 nm^2); d) annealing to 480 K (0.51 nA, -1.15 V, 44 × 44 nm^2).

Relatively ordered superstructures appeared on the surface after annealing to 420 K, Figure 3.9b. A significant aggregation of the adsorbates occurs at the step edges; this is linked to adsorbate induced surface etching. In this new phase, the step edges of the substrate are decorated with adsorbed molecules organising along the <110> direction. On the terraces, upon annealing, a large population of adenine molecules self-

assemble into ordered arrays of circular shaped spots with some randomly distributed molecules in the surrounding areas. This molecular network seems more likely to form close to the step edges and each small domain is separated from its neighbouring one by some bright line-shape features which are an extension of an upper terrace. These line features are aligned along the <110> direction and are observed frequently when the adenine pre-covered surface is annealed to 420 K.

The well-defined step edges and molecular arrays were substituted by randomly distributed short chains when the annealing temperature was raised to 450 K, Figure 3.9c. In this process, adenine molecules are suggested to undergo diffusion over the surface; as a result, they are likely to self-assemble into ordered short chains covering more evenly the overall surface. The surface features shown in Figure 3.9c are determined as an initial ordered phase; this is followed by the formation of more ordered and longer adenine chains aligning along (±1, 2) directions, after the surface was annealed to higher temperature (490 K). The so-formed adenine chains, Figure 3.9d, have higher thermal stability. STM images revealed that molecular desorption occurred only as the annealing temperature was raised to 520 K. This high desorption temperature provides evidence of the strong interaction existing between adenine molecules and the copper atoms.

It is found that the annealing temperature is the main factor accounting for the ordering of the various molecular arrangements. High annealing temperature is required to overcome the energy barrier for molecular self-assembly to occur. However, annealing for long time at a constant temperature did not lead to the growth of longer adenine rows. This means that this adsorption system is thermodynamically but not kinetically limited.

Shown in Figure 3.10 is an STM image of the surface annealed to 420 K in which molecularly decorated step edges and molecular arrays are clearly identified. The step edges are characterized by straight molecular chains aligning along the <110> direction of the substrate. The appearance of well-defined step edges is considered as the result of the surface faceting induced by the presence of the adsorbates. Surface faceting is a phenomenon taking place on surfaces with high anisotropic surface free energies [32, 33]. In this process, the initial clean surface breaks up into a number of adjacent steps in regular arrangements as a consequence of mass transportation that involves diffusion of both substrate atoms and adsorbates. Therefore, surface faceting

usually requires high temperature annealing to overcome the diffusion barrier and to provide sufficient mass transportation. In our case, formation of well-defined step edges induced by adenine adsorption is a thermally mediated process; the preferential alignment of the resultant step edges along the <110> direction suggests relatively strong attractive intermolecular interactions, largely due to the double hydrogen bond, mediated by the substrate atoms along this direction. It is suggested that the diffusion energy barrier for the adsorbate is much higher than that of the substrate atoms; annealing the surface to higher temperature leads to higher molecular diffusion across the overall surface, eventually new overlayer structures of high stability are achieved.

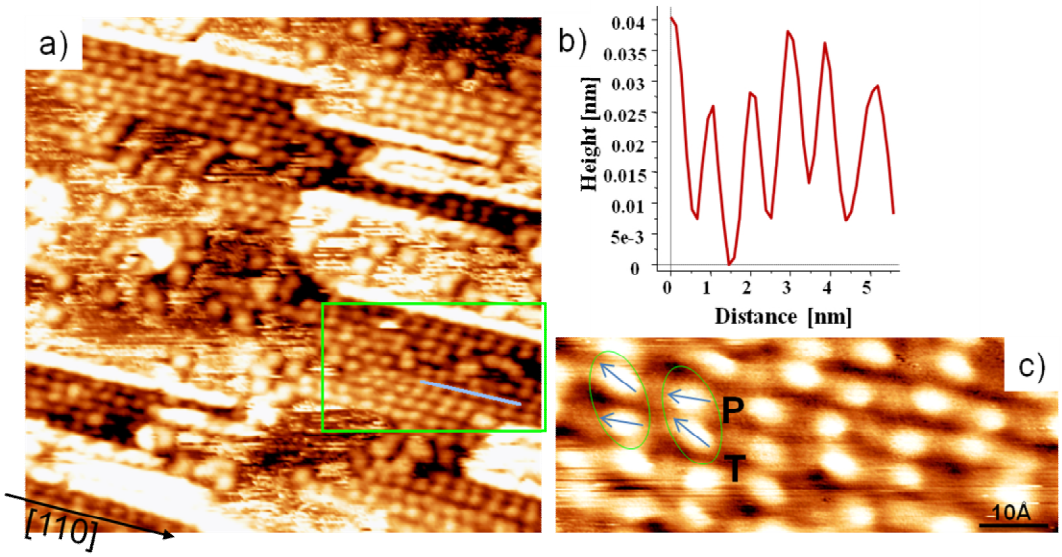

Fig. 3.10: STM image of adenine adlayer structures at the Cu (110) surface, obtained upon annealing to 420 K (0.76 nA, -0.97 V, 28 × 28 nm^2). a) Adsorbate induced surface reconstruction and small areas of molecular arrays near step edges. b) Line profile of the molecular arrays along the <110> direction in selected area. c) Close-up image of the molecular features identified in molecular arrays, indicated with T is the elongated and tilted molecular feature, and P is the circular shaped feature, they appear in pairs (0.14 nA, 0.97 V, 7.0 × 2.5 nm^2).

Within the molecular arrays, according to the line profile shown in Figure 3.10b, the average distance between two neighbouring bright spots along the <110> direction is 10.0 ± 0.3 Å; the average width of the bright circular feature is about 7.0 ± 0.3 Å; this is quite close to the size of the long dimension of the isolated adenine molecule. For a single adenine, the approximate dimension is about 5.1 Å in width and 6.4 Å in length. In addition, the distance between neighbouring chains is 8.0 ± 0.3 Å; this value

suggests that molecules align with their short axis parallel to the <100> direction. Hence, we may assume that each of the bright circular shape features accounts for a single adenine adsorbed species. The large molecular footprint suggests that the adenine is flat lying on the surface. The longer intermolecular distance, about 10 Å along the <110> direction, rules out the formation of hydrogen bonds along this direction.

Furthermore, if we take a close look at these bright features, two different molecular orientations are identified; they are labelled as feature T and P in Figure 3.10c. Feature T is in a slightly elongated shape with its long dimension tilted away from the <110> direction by a small angle. Feature P presents a circular shape and is positioned often paired with the elongated feature T. However, no clear periodicity could be identified within these molecular arrays; this might be because these adenine pairs are still arranged in a relatively disordered and random manner. The phase of small molecular arrays is considered as a kinetically limited state, and might result from the high coverage and deposition rate, leading to a large population of molecules trapped in specific sites. Further annealing the preparation to high temperatures led to the transition of this self-organised phase to a new well-ordered adlayer structure, showing high thermodynamic stability.

3.2.2.2 Discussions

Based on the above analysis, we proposed the structural models for the two different features, T and P, as shown in Figure 3.11; two adenine molecules of opposite chirality are connected by one type of double hydrogen bond. The corresponding dimer TP is denoted as $\mathbf{A_2\bar{A}_1}$, meaning that the hydrogen bond site 1 of one adenine, referring to feature P, is connected to the hydrogen bond site 2 of the other adenine molecule, feature T. The longer dimension of the adenine molecule that gives rise to the elongated feature T is slightly rotated with respect to the <110> direction of the substrate, in order to facilitate the formation of a double hydrogen bond. The adenine molecule accounting for the observed feature P participates in the hydrogen bond with site 1; in this case, no molecular rotation is required, P is aligned with its long axis along <110> azimuth. Since the two molecules in each dimer have

opposite chirality, we denote the dimer as heterochiral. However, the resultant dimer is chiral because it is not an $\mathbf{A_n\bar{A}_n}$ dimer, $\mathbf{A_2\bar{A}_1}$ has no mirror plane and hence, is chiral; its mirror image is $\mathbf{\bar{A}_2A_1}$. Furthermore, this dimer is also energetically favourable as determined from its stabilization energy of -0.54 eV [27].

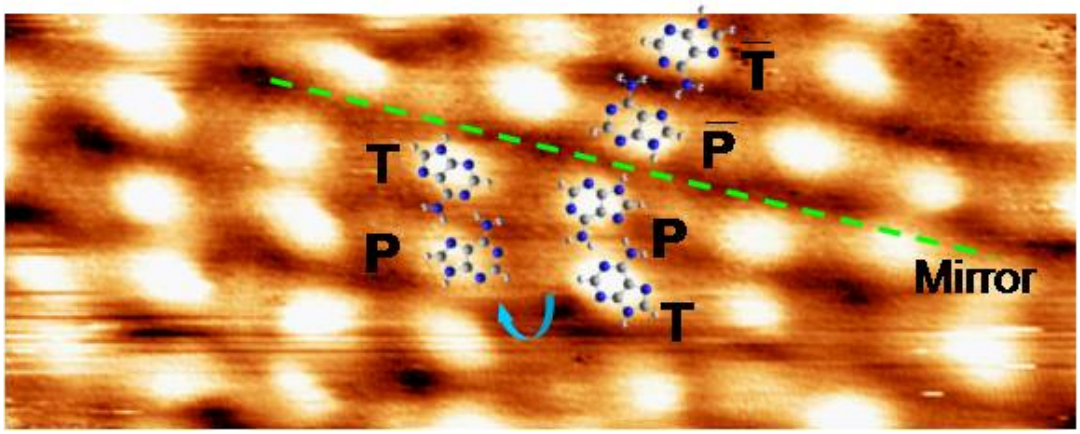

Fig. 3.11: STM image showing adenine arrays superimposed with suggested structural dimer models (0.14 nA, 0.97 V, 7.0 × 2.5 nm^2). T and P refer to the different observed features. Molecular arrangement of TP ($\mathbf{A_2\bar{A}_1}$) is related with PT by 2-fold rotation, while TP and $\overline{\text{TP}}$ ($\mathbf{\bar{A}_2A_1}$) dimers are enantiomeric image of each other. The double hydrogen bond between T and P is denoted as $\mathbf{A_2\bar{A}_1}$, referring to the hydrogen-bonding site 2 from one molecule is connected with site 1 of its mirror counterpart.

Hence, with the suggested dimer as the basic building unit, we are able to account for the observed molecular arrays by simply manipulating the dimers via rotational and reflectional symmetry operations. The building block is referred as TP ($\mathbf{A_2\bar{A}_1}$) for convenience of description; the unit PT is obtained by rotating the TP by 180°, which matches well with the experimental finding that both dimer features have equal chance to be found in the paired rows. The unit $\overline{\text{TP}}$ ($\mathbf{\bar{A}_2A_1}$), obtained by reflecting the unit TP along a mirror plane, can explain properly the disagreement in alignments of the paired spots on either side of the dash line, Figure 3.11. All suggested structural units fit well with the features mapped in the STM image. The intermolecular distance in the dimer is about 8.0 Å, and the maximum length of adenine is nearly 6.4 Å according to distance measured from the full geometrically optimized structures of the adenine pair. The theoretical parameters are in good agreement with the measured

ones. The long distance between neighbouring spots in each row does not favour the formation of hydrogen bonds in adjacent molecules.

In summary, the ordering of the adenine adlayer structures evolves as a function of the annealing temperature. The evolution is believed to be a thermally mediated process in which the annealing temperature, rather than the annealing time, is the main factor accounting for the transformation of less ordered structures to the well ordered and thermally stable adlayers. Structural models consisting of adenine dimers related by reflectional and rotational operations have been suggested to explain the dynamically limited structures obtained at 420 K. The observation of this metastable phase is believed to be caused by the high coverage obtained with a relatively high deposition rate.

3.2.3 Effect of substrate temperature on adenine self-organization

Different overlayer structures have been observed by depositing adenine onto the Cu (110) surface at room temperature upon annealing at elevated temperature. It was found that the annealing temperature played a major role in the formation of ordered and thermodynamically stable overlayer structures. However, increasing the annealing temperature and the annealing time did not lead to any obvious growth in the domain size and the length of the adenine chains. Here adenine was evaporated onto the Cu (110) surfaces kept above 370 K and then the sample was annealed to the temperature at which we were able to produce the ordered overlayer chiral chains structures. The effect of the substrate temperature on the domain size and structural properties is investigated using STM.

3.2.3.1 STM studies

STM images of adenine on the Cu (110) surface deposited at substrate temperature maintained at 400 K, 450 K, and 490 K, respectively, are shown in Figure 3.12, the usual annealing temperatures at which we expected to observe these relatively ordered overlayer structures. Although there is a large population of disordered molecules found at the surface maintained at 450 K, Figure 3.12b, the growth in the length of the adenine chains is more apparent compared to the surface deposited at 400 K, Figure 3.12a. The formation of longer chains is considered as an outcome of increasing coverage and temperature. The similar chiral related chains have been observed by Chen *et al.* on the Cu(110) upon annealing the sample at 430 K, they are mirror related and align along the (1, 2) and (-1, 2) directions of the substrate [1].

Two distinct isolated domains, domain I and II, composed of ordered adenine rows were observed when adenine was deposited onto the substrate kept at 490 K, as shown in Figure 3.12c; this image was obtained by rotating the fast scanning direction by an angle of 60° anti-clockwise in the attempt to achieve a better resolution. The size of domain I is much larger than that of domain II; they are separated by largely rough surface areas. On the domain boundaries, some disordered molecules were found; there is no molecular adsorption identified in the surrounding areas. The discrepancy in the aligning directions of the substrate high symmetry axis in these images is due to the slight sample rotation with respect to the fast scanning direction in different experiments.

Since adsorption of prochiral molecules on surfaces usually produce chiral adsorbed species of opposite chirality in an equal amount, and there is segregation of the two enantiomers, they will form mirror related domains with none of the unit vectors of the formed structures aligning along the high symmetry direction of the substrate. Hence, the two domains, Figure 3.12c, are identified as reflection related; each domain consists of adenine molecules of single chirality. In this case, the angle between the chain growing directions in the two domains is about 70º, as indicated with green arrows; the <110> axis of the substrate, indicated with yellow arrow, is aligned along the bisector of the domains, orienting 55º with respect to each domain.

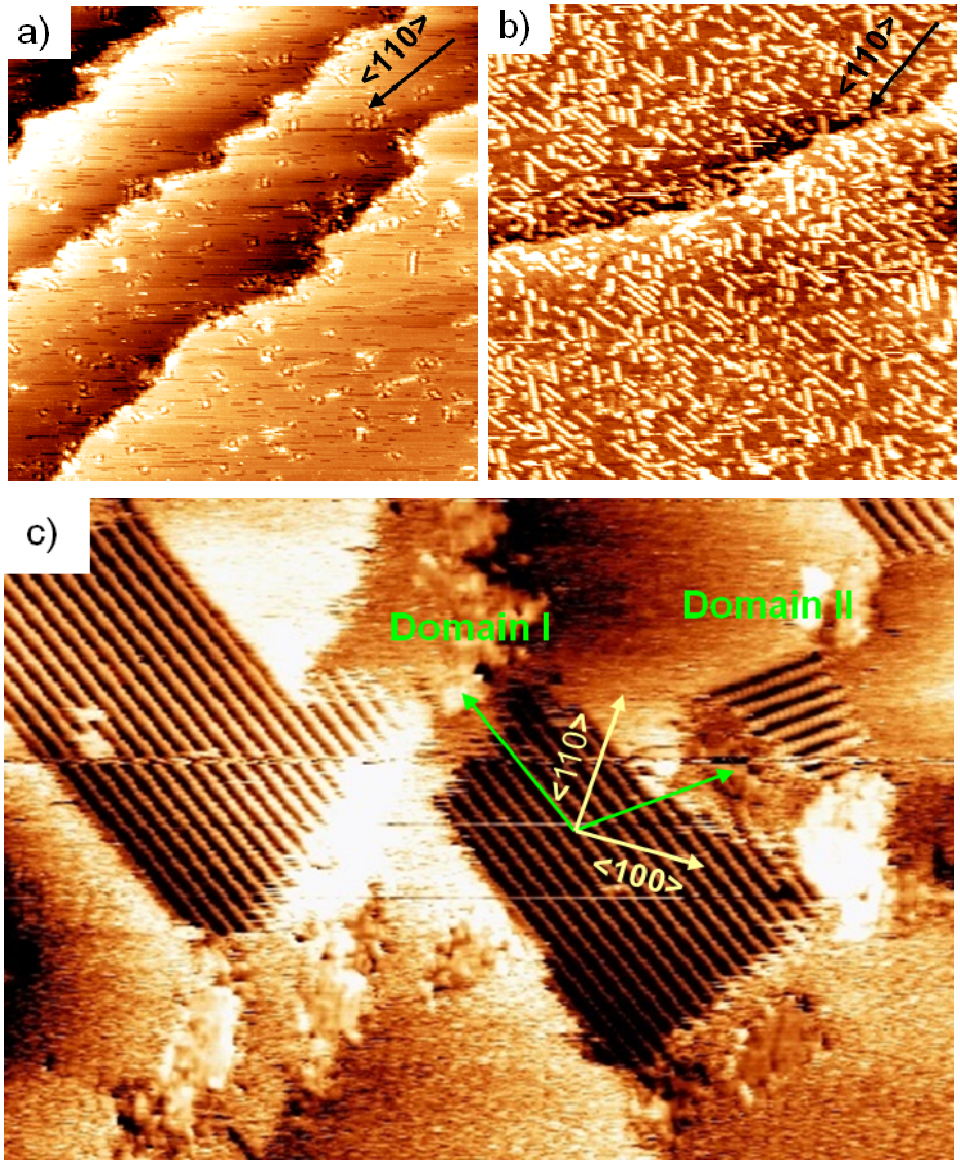

Fig. 3.12: STM images of adenine deposited onto the substrate maintained at different temperatures. a) 400 K (0.17 nA, -1.20 V, 77 × 77 nm^2), b) 450 K (0.12 nA, -1.20 V, 42 × 42 nm^2), c) 490 K (0.61 nA, -1.20 V, 65 × 47 nm^2), this image is obtained by rotating the fast scanning direction by an angle of 60º anti-clockwise.

A high resolution STM image of the overlayer structures in domain I is presented in Figure 3.13. The unit cell vectors are marked with arrows; the average angle between the two unit cell vectors is 70 ± 2º. In the unit cell, only one type feature is identified, which appears of elliptical shape. The features are arranged with their longer axis parallel to the unit cell short vector **b**. The dimension of the feature is about 4.4 Å in

width and 7.2 Å in length; this size approximately matches the 'footprint' of a single flat lying or slightly tilted adenine molecule. Hence, we assign each of the elongated features observed in the domain to a single adsorbed species. In addition, the size of the unit cell in domain I is **a** = 6.4 ± 0.3 Å, **b** =11.2 ± 0.3 Å. Both vectors of each unit cell are not aligned along the high symmetry directions of the substrate and the C_2 symmetry is assigned to the unit cell; this finding is consistent with the observation of two mirror related domains. The rhombic shape unit cell and periodicities of the overlayer structures are also confirmed by the 2D Fourier transform spectrum of the corresponding STM image, shown in Figure 3.13b, where the reciprocal unit cell is marked. The relatively strong intensity of the patterns indicates a high overlayer ordering.

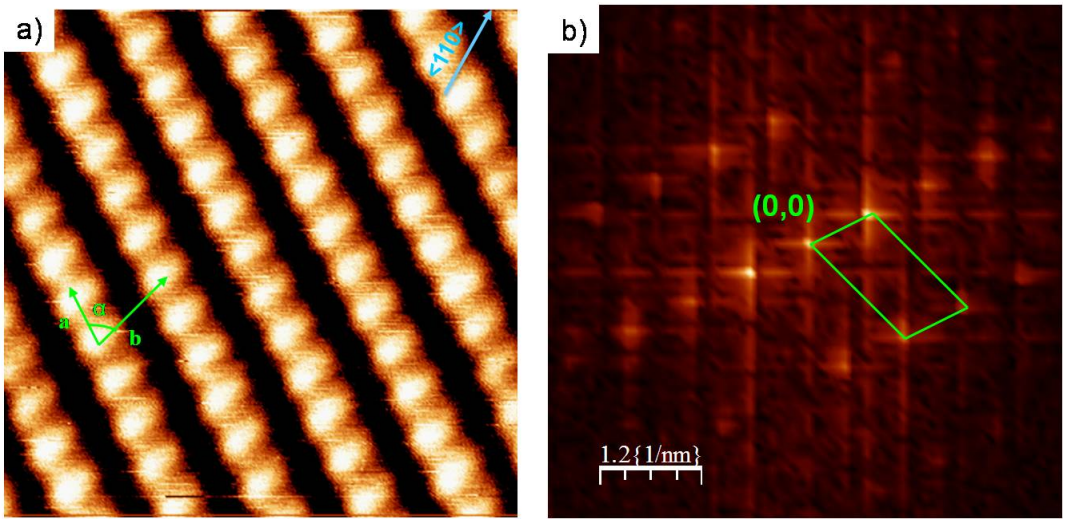

Fig. 3.13: STM images of the overlayer structures in the domain I and its corresponding 2D-FFT spectrum. a) Constant current STM image of the assembled structures in the domains, the overlayer unit cell vectors are marked, the angle α is about 70° (0.68 nA, -1.1 V, 77 × 77 Å^2). b)The corresponding 2D FFT spectra of the raw data, exhibiting the periodicity of the overlayer structures.

3.2.3.2 Discussions

Based on the above analysis, we proposed structural models of the molecular features observed in the STM image. For the sample prepared at room temperature

upon annealing to 430 K, adenine molecules were suggested to interact relatively strongly with the Cu(110) surface through the mutual polarization and Coulomb interaction, originating from the nitrogen atom of the amino group and the copper atoms [33]. Generally, adenine is considered to physisorb on most of the surfaces, such as Cu(111) [10-14] and Au(111) [16, 17], previously studied. However, in this case, we assume that increasing the substrate temperature provides adenine molecules with sufficient activation energy to overcome the chemisorption barrier, leading to the formation of chemisorbed species. The resulting ordered molecular arrays are not only governed by the intermolecular H-bond interactions, but also by the strong substrate-adsorbate binding induced by the chemisorption [34].

The coordination sites for adenine in the copper (II) complex have been well studied using the X-ray methods. It was revealed that adenine might bind with the metal ions via one or two of the four basic nitrogen atoms, N(1), N(3), N(7), N(9), as indicated in Figure 3.1. For example, in complexes of Cu(Ade)(GlyGly)(H_2O) [35], and cis-[Cu(Ade)$_2$Br$_2$]·Br_2 [36], [Cu(AdenineH)$_2$Cl$_2$]$^{2+}$ [37], adenine is coordinated with the copper ions by the N(9) site. In the bridging bidentate complexes: [Cu$_2$(Ade)$_4$·(H_2O)]$_2$]·(ClO_4)$_4$·H_2O [38], Cu$_2$(Ade)$_4$Cl$_4$·3H_2O [39], Cu(Ade$^-$)$_2$·(H_2O)$_4$ [40], and Cu$_3$(AdeH$^+$)$_2$Cl$_8$·4H_2) [36], both the N(3) and N(9), due to the tautomerization of the imidazole hydrogen atom between the N(7) and N(9) atoms, bind with the copper ions. The coordination of adenine to copper through the N(7) atom has also been reported in the complexes of [Cu(acac)$_2$(Adenine) [41], and the N-substitute iminodiacetato-copper (II) chelates [42]. In addition, XPS studies of the bonding of adenine on Cu(110) surfaces has revealed that at low coverage adenine interacts via the imino N7 atom and to a less extent via the NH_2 group [25] with the copper atoms. Here, we suggest that the chemisorbed adenine species are coordinated with the copper atoms through the imino N(7) atom with contribution from the interaction between the nitrogen atom of the amino group and the copper substrate [1, 33], upon depositing the adenine onto the substrate kept at 490 K. This binding nature enables the hydrogen atoms attached to the N(9) and the N(3) atoms to be available for the formation of a double hydrogen bond with another molecule, resulting in the formation of the most stable dimer A_5A_5.

Therefore, in the proposed structural model, adenine species are arranged to facilitate the binding of the N(7) atoms and the interaction of the nitrogen atom of the

amino group with the copper atoms. Figure 3.14 shows the electron density map of the ordered structure in the domain I superimposed with the suggested structural model. Along the adenine row growth direction, the chains are developed with alternation of different hydrogen bonded adenine pairs, denoted as $\mathbf{A_5A_5}$ and $\mathbf{A_2A_2}$. Both pairs are composed of adenine molecules of the same chirality, thus, the resulting adenine rows are homochiral. In the model, constrained by the hydrogen bond, the periodicity along the adenine rows, according to the DFT geometry optimization using 6-31G basis set, is 12.29 Å, thus the adjacent intermolecular distance is about 6.14 Å; this is consistent with the vector **a** determined from the unit cell of the adlayer structures in the two domains. In each row, adjacent molecules are stabilized by intermolecular hydrogen bonds that direct the growth direction of the adenine rows; the suggested molecular orientations fit well with the protrusions observed in the image. Additionally, because of the relatively larger inter-row separation, the interaction of molecules in adjacent rows via H-bond is excluded. Hence, the periodicity along the vector **b** is more likely to arise from the strong substrate-adsorbate interactions. Given the suggested model, the imino N(7) atoms are oriented outside the chains, which might favour the coordination of the N atoms with the copper atoms; this binding, along with the amino N-Cu interactions, accounts for the ordering along this direction. The vector **b** is about 11.6 Å; this distance is approximately equal to the four copper units cells along the <110> direction, which also makes the N-Cu interaction favorable.

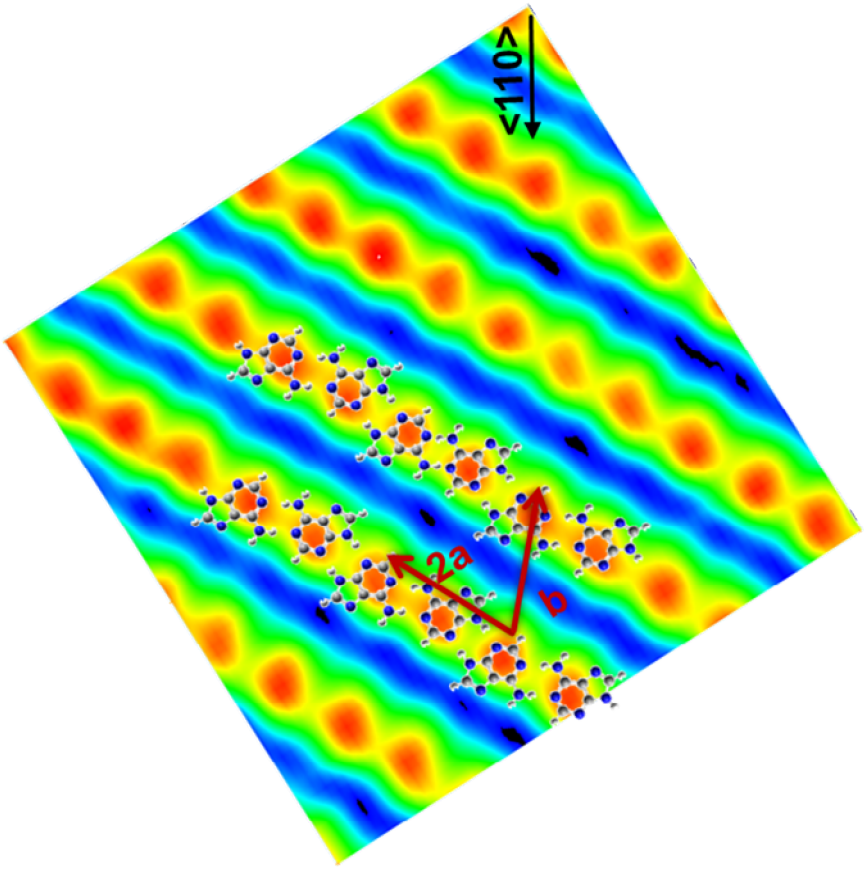

Fig. 3.14: The electron density map of the corresponding STM image of the domain I superimposed with the proposed structural model (50 × 50 Å^2). Along the adenine rows growth direction, double hydrogen connected adenine pairs, denoted as **A_5A_5**, **A_2A_2**, are arranged alternately. Each adenine molecule binds with the copper substrate via the amino N and imino N(7) atoms. The geometry of the gas phase structural model (one unit cell) is optimized with DFT methods, using the 6-31G basis set. The electron density map is obtained using the SPIP program.

Furthermore, according to the stabilization energies of the dimers composed of the chains, both are good candidates for the construction of energetically favorable structures. The stabilization energy of the dimer A_5A_5 is about -1.02 eV; it is the most stable pair, and is the basic unit employed to constitute the structural models for most of the observed adenine adlayer structures. The dimer A_2A_2 has stabilization energy of -0.72 eV; it is slightly less stable than the dimer A_5A_5. Both dimers have the nitrogen atoms participating in the formation of hydrogen bonds, therefore, the suggested gas-phase models are considered as energetically favorable in the construction of a model that fits well with the features observed in the STM images.

To further prove the suggested model, we consider the registry of the model on the Cu(110) lattice. The geometry of the adenine trimer unit that is formed by connecting three molecules together via the hydrogen bonding site 5 and 2 is optimized using DFT methods with the B3LYP functional and the 6-31G basis set. As shown in Figure 3.15, within the suggested molecular alignments, the adsorption of the adenine molecules breaks the mirror plane symmetry of the free adenine molecules; as a result, two mirror related domains are induced with each of them consisting of adsorbed species of the same chirality. The growth direction of each adenine row is closely related to its chirality; molecules of opposite chiralities are arranged in an angle of 55° with respect to the <110> direction of the copper substrate; this is consistent with the experimental results mentioned before. In the suggested registry, both the amine N(7) atoms and the nitrogen atoms of the amino groups are placed close to the top-site, thus, the molecular orientations in the suggested models facilitate the binding of the N(7) atoms and the interactions of the nitrogen atoms of the amino group with the copper substrate. With the suggested model, each chiral row is aligned 55° with respect to the <110> direction of the substrate and the distance between neighbouring chains is about 10.8 Å, in agreement with the experimental values measured from the STM image.

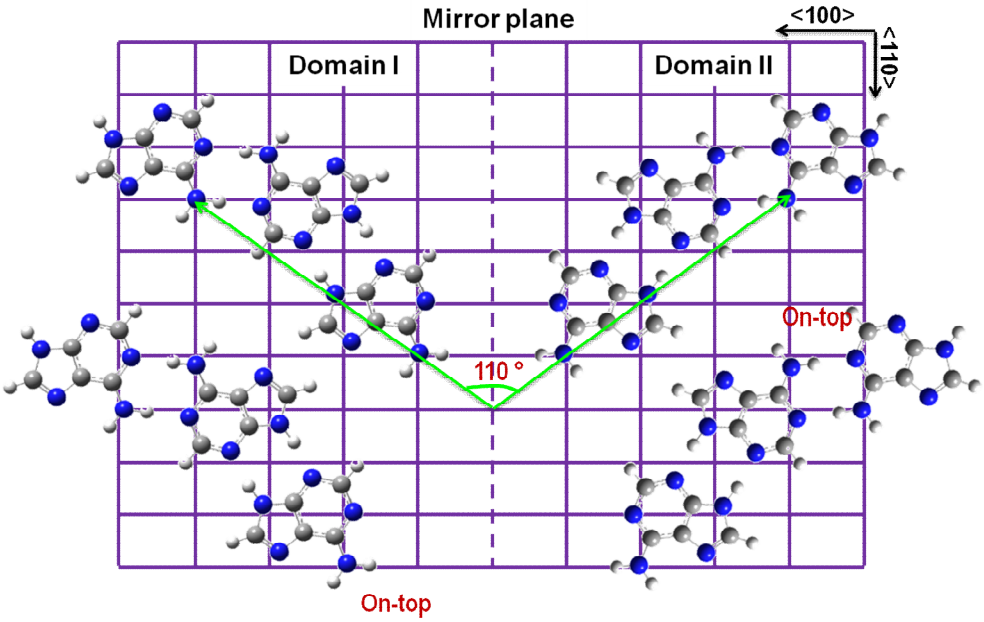

Fig. 3.15: The proposed registry of the adenine dimer chains on the Cu(110) mesh. Domain I and II have opposite chirality and are related by the mirror aligning along the <110> direction of the substrate. In the suggested model, all the amino N atoms and the imino N(7) atoms are placed closely to the on-top sites, in favour of the N-Cu interaction.

3.2.4 Effect of deposition rate on adenine adlayer structures

Adenine was observed to form ordered one-dimensional chains and two-dimensional hexagonal networks on the Cu(111) at 70 K using scanning tunnelling microscopy [13]; the behaviour of adenine is however strongly influenced by the deposition rate and the coverage. At low coverage and low deposition rate, adenine molecules have sufficient time to diffuse across the surface; this favours the formation of ordered hexagonal structures and one-dimensional parallel chains. However, at high coverage and high deposition rate, molecular aggregation occurs, leading to the formation of only disordered one-dimensional chains. The dependence of the self-assembled structures on the deposition rate and coverage provides evidence that the dynamic process also plays an important role in the formation of various superstructures [13].

Here, we present our investigation of the effect of deposition rate on the adenine overlayer structures on the Cu(110) surface at high coverage upon annealing. In comparison with the Cu(111) surface, which has lower electron density corrugation [43], allowing easier molecular diffusion at low temperature, the Cu(110) surface tends to anchor the molecular assembly because of the strong interaction between adenine and the copper atoms [1]. Hence, a different self-assembly mechanism is expected upon depositing adenine onto the Cu(110) surfaces at low deposition rate to achieve a high coverage, $\theta \approx 0.70$ ML. In this experiment, the deposition rate is about half that, which was adopted to obtain the surface covered merely with one-dimensional adenine chiral chains aligning along the (±1, 2) directions [1]. The deposition rate is evaluated approximately by the deposition time it takes to obtain a similar coverage; the monolayer coverage refers to the surface fully covered by a monolayer of adsorbates.

3.2.4.1 STM studies

Shown in Figure 3.16 are the STM images of the surface obtained at medium coverage with lower deposition rate, displaying the effect of annealing temperature on the molecular ordering on the Cu(110) surfaces. At room temperature, adenine molecules aggregate to form large heterogeneous islands on the flat terrace areas.

Within the islands, the molecules appear as bright circular features and arrange themselves in disordered manner. On the island boundaries and along the step edges, some depressions are found; this is likely to be caused by adsorbate induced surface etching. After annealing the surface to 430 K, ordered double chains consisting of circular shaped spots aligned along the <110> direction were observed. In addition, a large number of disordered molecules were found distributed across the terraces and appear as dark features. This phase is considered as a kinetically limited state and was replaced with highly ordered, new adlayer structures after the sample was annealed to 490 K, Figure 3.16c, resulting from the high degree of molecular diffusion.

As shown in Figure 3.16c, three types of chain structures are distinguished and are considered as a thermally stable phase. Type I is the adenine chiral related rows commonly observed on the surface that was prepared at a normal deposition rate upon annealing to 490 K. These structures are well ordered and consist of ordered dimer rows aligning along (±1, 2) directions [1]. Both the new structures, II and III, were observed for the first time, and were uniquely formed at Cu(110) surfaces prepared at a deposition rate which is half the normal rate. These new chains grow along one of the high symmetry directions of the substrate, the <110> azimuth, and mainly align adjacent to each other. The new adlayer structures usually display apparently bright contrast with respect to the rest of the surface, and particularly in comparison with the chiral chains.

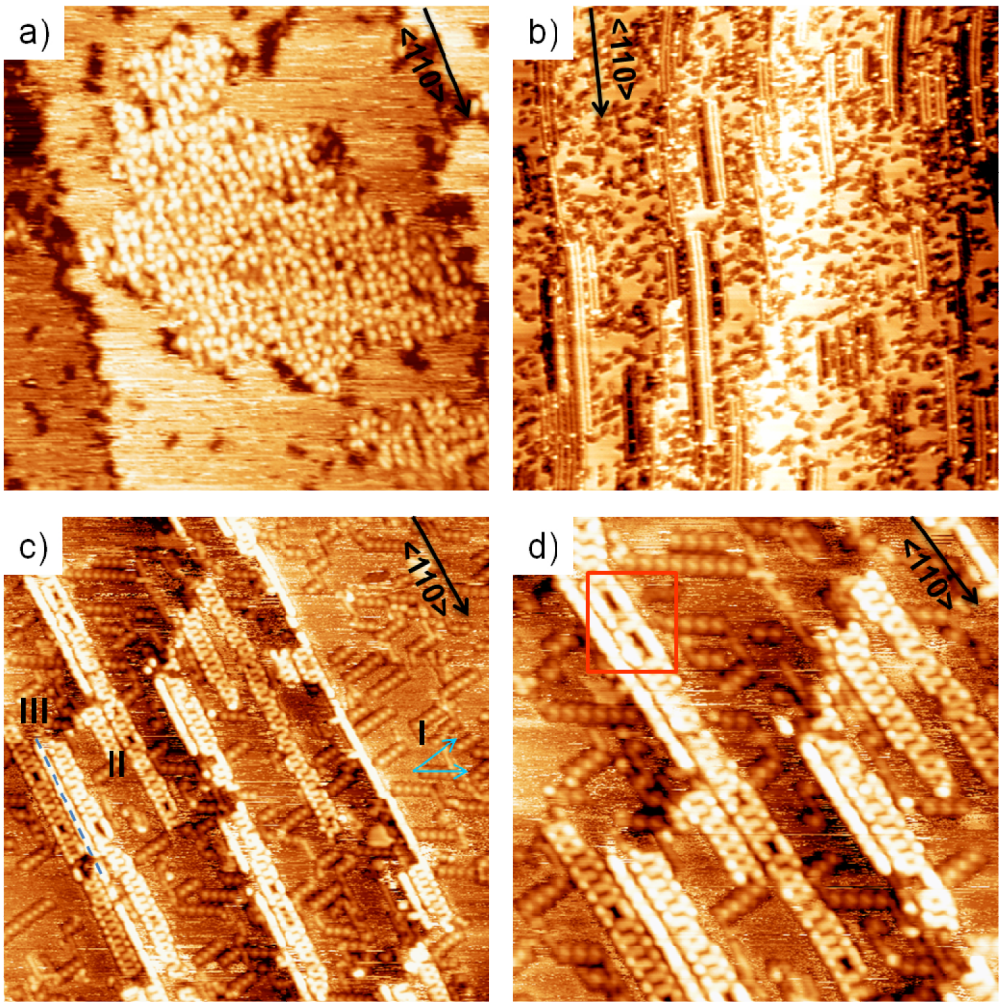

Fig. 3.16: STM images of adenine adlayer structures on the Cu(110) at high coverage and lower deposition rate after annealing at different temperatures. a) At room temperature (0.18 nA, -0.95 V, 41 × 41nm^2); b) Annealing to 430 K (0.10 nA, -1.2 V, 94 × 94 nm^2); c) and d) Annealing to 490 K (0.19 nA, -1.07 V, 37 × 47 nm^2, 0.19 nA, -1.14 V, 21 × 21 nm^2).

Figure 3.16d shows the STM image of the new chain structures clearly at high resolution. The type II structure looks like a ladder in which adenine molecules mainly arrange themselves into parallel chains with cross-linking rungs. The average dimension of each elongated feature along the <110> axis is 7.0 ± 0.3 Å, and the width along <100> is 5.0 ± 0.3 Å; these values match well with the 'footprint' of an individual flat-lying adenine molecule, indicating that adenine is likely to adsorb in a flat-lying or slightly tilted orientation. In this structure, each adenine is connected to neighbouring molecules via hydrogen bonds. The length of most of these ladder chains along the <110> direction are over 80 Å and is longer than that of chiral chains

along (±1, 2) directions. This may suggest that hydrogen bonds accounting for the growth of these chains are stronger than those governing the chiral chains. However, this structure is not well ordered and uniform with the rungs of the ladder occasionally missing, as indicated by the selected rectangular area in Figure 3.16d.

The type III structures are bright linear chains aligning adjacent in parallel to the ladder chains, type II, along the <110> azimuth, as indicated by the dash lines in Figure 3.16c. Within this structure, individual features comprising of the chains are not so easily distinguished in the STM image. The apparent width of this molecular chain is 7.0 ± 0.3 Å, which is close to the long dimension of a free adenine molecule; it suggests that adenine may orient with its short dimension aligning along the <110> direction. The chain width is approximately 2.0 Å wider than the parallel molecular rows consisting of the ladder chains; this indicates that the molecular orientation with respect to the substrate in this chain is different from that in the parallel chains of the ladder structure. In this case, adenine molecules are believed to arrange neighbouring to each other with the long dimension aligning along the <110> direction.

The appearance of the linear chains and the ladder structure have some similarities, considering the chains width and lateral dimension of each individual feature comprising the chain, with the hexagonal structures and parallel chains observed on the Cu(111) surface, when adenine was deposited at low deposition rate and low coverage [13]. In that work, since the interaction between the adenine and the substrate is weak at room temperature, the low deposition rate provides molecules with enough time to diffuse freely across the surface; this favours the formation of self-assembled hexagonal networks and other chain structures, mediated via the strong attractive intermolecular hydrogen bonds. In our cases, due to the relatively strong adsorbate-substrate interaction, high temperature annealing is required to provide sufficient energy to overcome the diffusion barrier. This leads to the formation of a variety of different overlayer structures, *e.g.* the kinetically limited parallel chains upon annealing to 430 K; the thermally stable chain structures upon annealing to 490 K. In addition, it is also believed that the formation of ladder chains and linear chains along the <110> direction might be influenced by the large molecular aggregation on the terraces observed at room temperature. Hence, both the deposition rate and the annealing temperature, as well as the coverage, are important factors influencing the self-organization of adenine depositing onto Cu(110) surfaces.

Topographic line profiles of the adenine adlayer structures are presented in Figure 3.17; profiles A and B demonstrate the height difference between the ladder structures, II, the copper substrate and the adenine chiral chains, I. The bright ladder chain feature has an apparent height of 1.6 Å with respect to the copper surface; this distance is in reasonable agreement with the calculation of weakly bound π-systems lying flat on metal surfaces [44, 13, 16], while the apparent height difference between the chiral chain and the copper surface is about 0.8 Å. The small height difference rules out the possibility that the new structures result from a second layer adsorption. Theoretical calculations have revealed that in the adenine chiral chains, adenine is adsorbed with its molecular ring nearly flat lying on the Cu(110) surface and interacts strongly with copper atoms through the hybridized nitrogen atom of the amino group [1, 9]. Therefore, we suggest that the adenine molecular plane might be tilted at a shallow angle in these new structures, giving rise to a bright topographic feature.

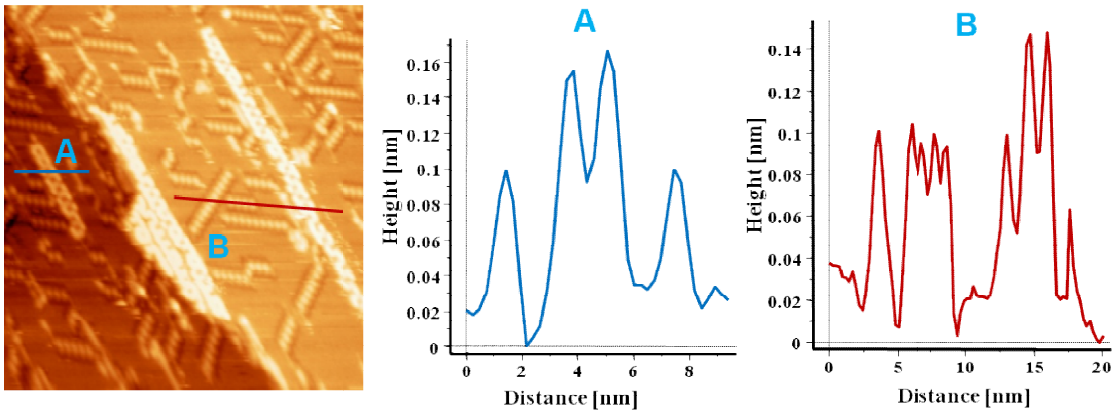

Fig. 3.17: STM image of adenine overlayer structures obtained at low deposition rate and high coverage (θ ≈ 0.70 ML) (0.13 nA, -1.07 V, 51 × 47 nm^2). Indicated with A and B are the line profiles associated with the bright features and chiral rows formed on the surfaces, representing the topographic height difference between the features of different contrast.

An STM image of the ladder structures, type II, with molecular resolution, and the topographic line profiles of the corresponding features are shown in Figure 3.18. From the STM image, Figure 3.18a, two molecular arrangements are identified, and are marked with A and B. Along the <100> direction of the substrate, chain A is 16.3 ± 0.3 Å in width and is slightly wider than the chain B, which is 14.5 ± 0.3 Å. The periodicity along the parallel rows in the ladder chain A is 10.1 ± 0.3 Å,

corresponding to the line profiles I, II and III, in Figure 3.18b. This distance is nearly equal to four copper unit cells along the <110> direction, suggesting that this ladder chain is commensurate with the substrate. It is also slightly larger than the longest inter-molecular distance, *ca.* 7.0 Å, between two double H-bond connected adenine molecules, which indicates the two neighbouring molecules along the <110> direction might not be connected by H-bonds. The periodicity of structure B along the <110> direction is 9.0 ± 0.3 Å, indicated by the line profile Figure 3.19b IV, which is *ca.* 1.0 Å smaller than the corresponding measured distance in structure A. A close examination of these two structures A and B reveals that molecular arrangements in the parallel rows of the ladder are fairly similar to each other, except that the tilted alignment of the features in the rung position. However, the little discrepancy in the periodicities may arise from the alterations in the molecular orientation, making the features in the structure B more closely packed than those in structure A. Even though both structures A and B coexist along the same ladder chain, the A is considered more favourable structures than B, which is evident from the bigger areas they are observed.

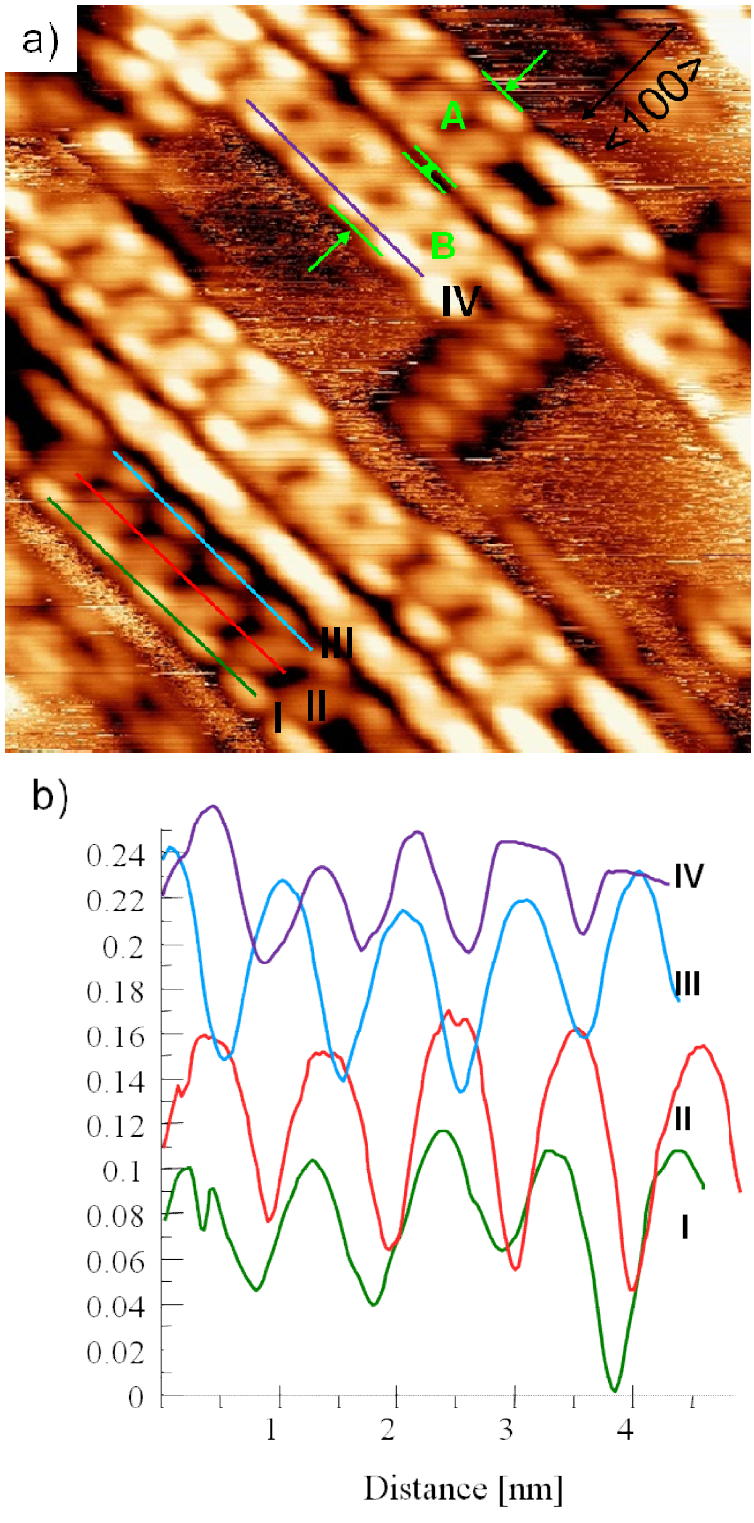

Fig. 3.18: a) STM image of adenine ladder chain structure, II, with molecular resolution (0.15 nA, -1.14 V, 11 × 11 nm^2). b) The corresponding line profiles of each adenine rows along the chain. The two different molecular arrangements are marked with A and B. I, II, III are topographic line profiles associated with the three parallel adenine rows in structure A, and IV is the line profile of the row in structure B, demonstrating the periodicities along the rows.

Now we take a close look at the more favourable structure A. In the wider ladder structure A, Figure 3.19, three types of features are recognized and indicated with α, β, γ respectively. α are β are 'T' shape units; they are identified as 2-fold rotation related trimers, which is indicated by the tilt angle of the middle feature with respect to its two neighbouring molecules lying on the shoulder. This is clearly evident from the corresponding electron density maps of the two T shape units, α and β, inset in Figure 3.19. Feature γ commonly appears in pair with α or β, and is separated with its neighbouring molecules by dark gaps. The width of the T shape trimer along the <100> direction is 9.0 ± 0.5 Å; it is nearly twice the minimum dimension of adenine, indicating the adjacent molecules might have their long axis aligned close to the <110> direction. The elongated feature γ displays as an individual separated feature; however, it is unlikely that an isolated adenine molecule occurs, *i.e.* unconnected to other molecules, due to its strong ability to form double hydrogen bonding with the neighbouring molecules. Thus, we suggest that the slighter dark narrow gap separating the trimer from the elongated γ feature is associated with the different molecular orientation with respect to its neighbouring molecules, *e.g.* the rotation of its long axis; this might give rise to its unique appearance in comparison with its surrounding trimers.

Extension of this ladder chain can be achieved via repeating the T shaped units side-by-side, or face to face, along the chain growth direction, as schematically illustrated with solid and dash line circles in Figure 3.19b, then the γ species are placed between the adjacent rungs on the edges, as indicated by the yellow dotted line circles. Due to the random arrangements of these units, the ladder chains can end up with different defects, such as the missing of rungs in the middle or the γ features on the edges.

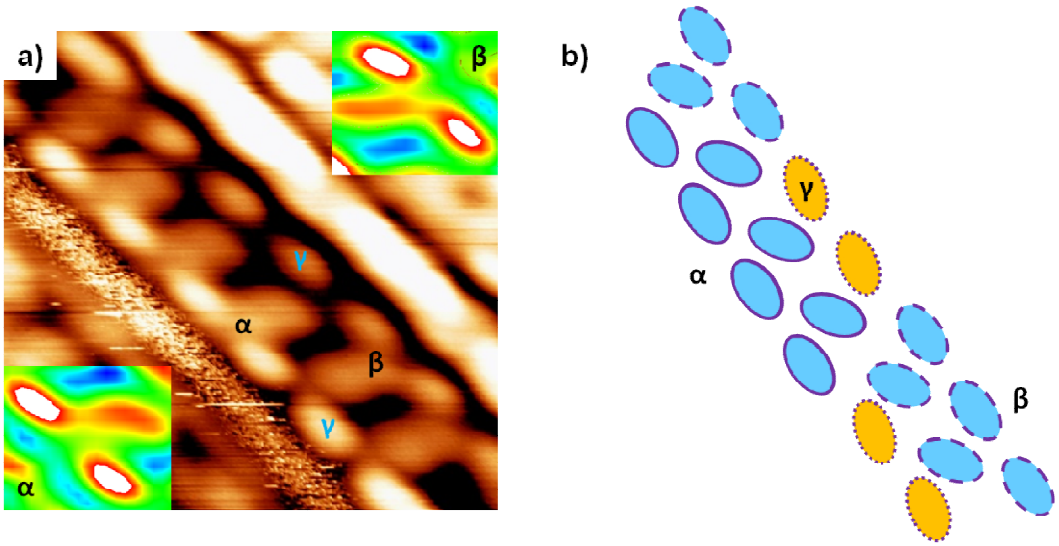

Fig. 3.19: a) Magnified STM image of the ladder structure A (0.19 nA, -1.14 V, 5.4 × 5.4 nm^2), insets are the electron density maps of the T shaped units α and β, which are C_2 related. γ is the isolated feature, indicating a different molecular orientation. b)Schematic illustration of the formation of ladder chains via randomly repeating the suggested units α, β and γ along the chain growth direction, in which each elongated circles represents one adenine molecule, α and β are indicated with solid and dash line circles in blue respectively, and γ is illustrated with dotted line circle in yellow.

3.2.4.2 Discussions

In order to gain a further insight into these observed overlayer structures, in particular the ladder chains II, we shall propose gas phase adenine structural models the geometries of which resemble the structural dimensions and features observed experimentally. As discussed above, the ladder chains can be formed by arranging these trimer features, α and β, and the elongated feature γ, in different ways. Hence, we shall start with constructing reasonable trimer structural models, then repeat these units, along the chain growth direction, the <110> axis, to reproduce the observed ladder structures. Since Kelly, *et al*. have calculated the optimized geometries of 21 possible adenine pairs and the corresponding stabilization energies using DFT methods [27], the stabilization energy of gas-phase structural models can be approximately estimated as a sum of the stabilization energy of each isolated dimer consisting the model. Here, we take the geometries of all adenine pairs into consideration, then select the most suitable dimers the geometries of which reproduce the features observed experimentally and have high stabilization energy. When

reasonable adenine pairs are selected, we can connect these pairs with another molecule to construct the trimer units, α and β, as well as the four-molecule units that can be built up by connecting the trimer with the fourth molecule that accounts for the elongated feature γ. In this work, the geometries of these constructed units were optimized by means of DFT methods with the B3LYP functional using the 6-31G basis; the associated intermolecular distances in the trimer along the chain growth direction and the approximate width of the four-molecule units are then compared to the experimentally measured parameters.

We have mentioned in the introduction section (chapter 3.1.2) that there is a total of 21 hydrogen bonded adenine pairs; each of them displays a distinct configuration. From these, the two H-bonded dimers, $\mathbf{A_5A_5}$, and $\mathbf{A_3A_3}$, as shown in Figure 3.20a, have been selected, to build the trimer units. Both are energetically favourable pairs where the N atoms are involved in hydrogen bonds [27]. The stabilization energies of them are -1.02 eV and -0.16 eV, respectively, according to our DFT calculations; this makes them good candidates in the construction of the trimer model and account for the observed C_2 related trimer features, α and β.

In the suggested trimer model, indicated on the right side of Figure 3.20a, the middle molecule is connected with its two adjacent molecules on the shoulder by H-bond sites 5 and 3, such that the upper pair corresponds to a $\mathbf{A_3A_3}$ dimer and the lower pair to a $\mathbf{A_5A_5}$. Each individual molecule is oriented with its longest axis tilted slightly away from the chain growth direction, but this orientation seems to be in good agreement with our experimental findings in which the short dimension of each elongated feature along the <100> direction is close to the short dimension of a free adenine molecule. This model is composed of adenine molecules of the same chirality; hence, it is a homochiral structure. The intermolecular distance, measured from the optimized geometry of the trimer, between the two molecules, upper and lower of Figure 3.20a, is 10.16 Å; resembles closely the value measured from STM images, which is about 10.1 ± 0.3 Å. In addition, this model and its C_2 related counterpart also fit well with the observed trimer features α and β, making them suitable models for the trimer units of the ladder chains.

Now we can start building the four-molecule units by adding the fourth molecule to the suggested trimer model. As shown in Figure 3.20b, when the structure of the trimer is set, there are only two possible orientations for the fourth molecule, γ,

according to the requirement of STM results that the long axis of the feature γ is aligned nearly along the <110> direction. In the first case A, the fourth molecule is connected with the H-bond site 1 of the molecule lying in the middle of the trimer by site 5, the resultant dimer is denoted as $\mathbf{A_1A_5}$. In order to facilitate the H-bonding interaction, the long axis of this molecule is rotated slightly with respect to the others, which makes its long axis align nearly parallel to the chain growth direction, the <110> direction. However, in the second case, the H-bond site 1 of the fourth molecule, γ, can also form a double H-bond with the same molecule in the trimer by site 1, the corresponding double H-bond linked pair is referred as $\mathbf{A_1A_1}$. This generates a similar four-molecule unit, referred to as unit B. In this model, the long axis of each molecule involved in the formation of double H-bonds is oriented almost in parallel, which results in a parallel feature γ. The approximate calculated width of the unit A is 15.1 Å; it is about 0.7 Å wider than that of the unit B, which is 14.4 Å. These values, including the small width difference between them, are consistent with the corresponding experimental values.

The stabilization energies of the dimers, $\mathbf{A_1A_5}$ and $\mathbf{A_1A_1}$, are -0.66 eV and -0.47 eV [27], respectively. Both are anticipated to yield energetically favourable structures upon adsorption on Cu(110) surfaces. However, the slightly higher stabilization energy of the dimer $\mathbf{A_1A_5}$ seems to suggest that the four-molecule unit A is a preferred model for the wide ladder chain A. The slight rotation of the long axis of the fourth molecule in unit A with respect to that of its neighbouring molecules might give rise to the isolated feature γ observed in the wider ladder chain A. While the less energetically favourable unit B consisting of dimer $\mathbf{A_1A_1}$ is likely to account for the narrow ladder chain B. The parallel orientation of the molecules in this unit B might give rise to the elongated features aligning on both sides of the cross-linking rungs of similar appearance. In both structural models, the fourth molecule has the same chirality as the molecules composing of the trimers, therefore, these proposed four-molecule units are homochiral.

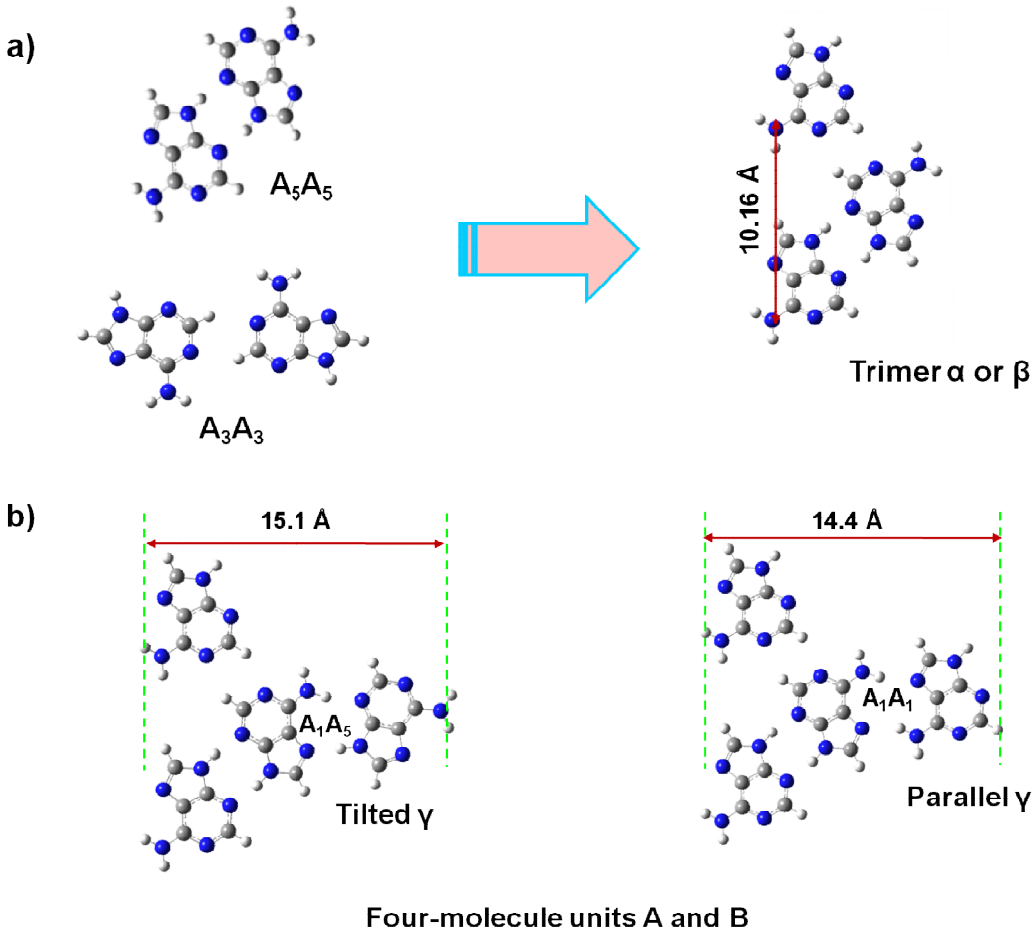

Fig. 3.20: a) Selected H-bonded adenine pairs, $\mathbf{A_5A_5}$ and $\mathbf{A_3A_3}$, and the trimer structural model, constructed with the selected pairs the geometry of which resembles closely that of the trimer, α or β. The intermolecular distance along the chain growth direction is 10.16 Å. b) The two possible four-molecule units, A and B, built up by connecting the trimer with the fourth molecule accounting for the feature γ. The unit A is about 15.1 Å in width and is formed by connecting the trimer with the fourth molecules by H-bond sites 1 and 5, denoted as $\mathbf{A_1A_5}$, in which the long axis of the fourth molecule is slightly rotated with respect to that of other molecules. The unit B is about 14.4 Å in width, in which the fourth molecule is connected with the trimer by site 1, indicated as $\mathbf{A_1A_1}$; all the long axes of the molecules involved are aligned in parallel.

Figure 3.21 shows the magnified STM image of the ladder chains II superimposed with the proposed structural models of α and β, and the four-molecular units A and B. The proposed four-molecule units fit well with the associated features observed in the ladder chain structures, particularly for the unit B for which both the width and

intermolecular distance are in good agreement with the observed features. In the model A, the slight rotation of the long axis of the fourth molecule with respect to that of its neighbouring molecules might give rise to the isolated feature γ observed in the wider ladder chains. The width of the suggested unit A is calculated to be 15.4 Å; it is about 1.0 Å narrower than the corresponding measured value, *ca*. 16.3 Å, however, this small difference might be induced by structural relaxation upon adsorption due to the strong substrate-adsorbate interaction. It is suggested that the presence of the substrate can result in an increase in the intermolecular distance with respect to the values in the gas-phase model by up to ~0.5 Å [22]. Arranging either the trimer α or β side by side along the chain growth direction can give rise to short comb chain structures, missing the γ features in the ladder chains, with reproducible periodicities. However, when the trimers α and β are arranged face to face, there is no hydrogen bond that can be formed between the molecules lying in the rung positions. So this arrangement might be mediated mainly by the strong interaction between the copper atoms and the adsorbates.

It is also found that the suggested homochiral trimer models, α and β, can only fit with the observed ladder-chains, while their counterparts of opposite chirality do not fit the structure at all. The main discrepancy of the suggested models of opposite chirality with the observed feature is related to the orientation of the elongated feature lying in the rung position of the ladder, as indicated in Figure 3.21. Since the trimers, α and β, are C_2 related, and ladder chains of opposite chirality co-exist, also, they must be aligned along the high symmetry <110> direction. However, it is difficult to distinguish the opposite chiral ladder chains from the large area STM image because molecules of either chirality in the rung position were observed to appear as circular features and arranged in parallel, although, in fact, the rung of opposite chirality must slope in the mirror direction. Additionally, the orientation of the fourth molecule in the structural model B is different; it has the same experimental parameters, *e.g.* periodicity and dimension of each elongated feature, with the model A. However, the different appearance of the narrow chains B with that of A might be caused by the slightly more closely packed molecules mediated by the substrate-adsorbate interactions, or due to the tilting of the molecular ring away from the surface, which gives rise to smaller molecular footprint on the surface.

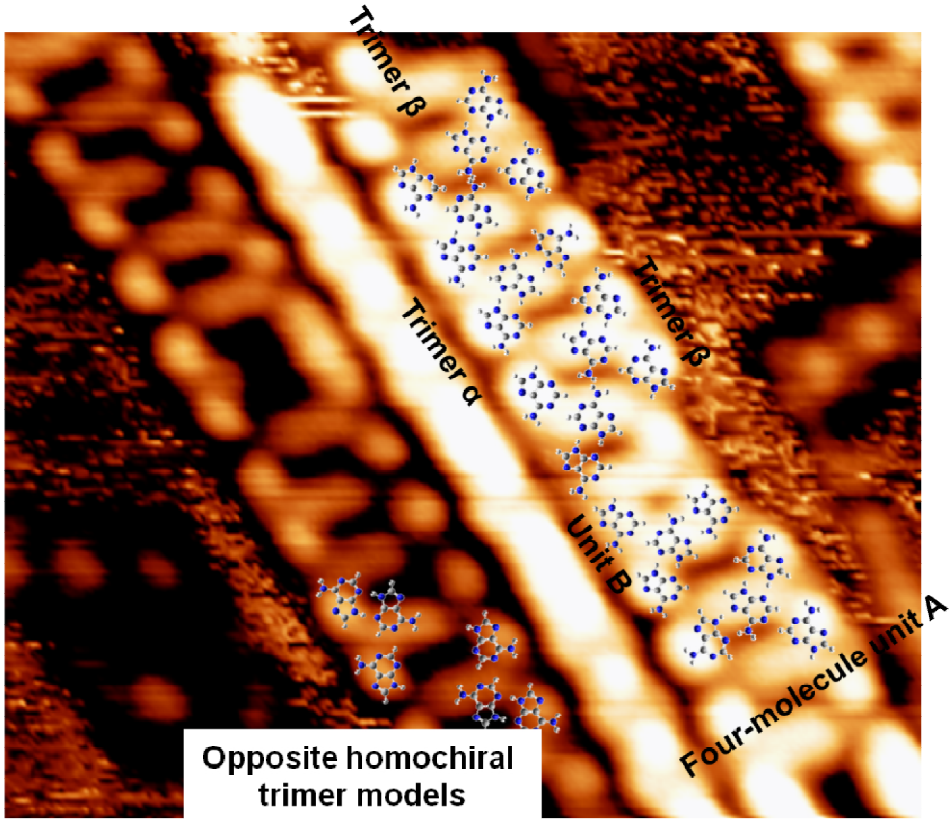

Fig. 3.21: Magnified STM image of the ladder chains superimposed with the suggested structural models α and β. as well as the units A and B (13 × 10 nm^2, 0.15 nA, -1.0 V). Opposite homochiral trimer models are also presented, the orientation of the molecule in the rung position of the ladder does not fit with the corresponding features.

Repeating each four-molecule units, A and B, along the <110> direction of the substrate can give rise to the ladder chains observed. These structures are merely observed on the Cu(110) surface, it is suggested they are influenced by the deposition rate and coverage. Extending these units in 2D will give rise to a number of hexagonal networks, similar to those observed on the Au(111) [16, 17] and Ag-terminated Si(111) [20] surfaces. The smooth potential energy surface of these substrates favours the formation of 2D periodical structures as result of less constrained molecular self-assembly. However, in our case, the strong interaction between the nitrogen atoms of the amino group and the copper atoms may increase the diffusion barrier, which inhibits the formation of long range ordered structures. In addition, the rectangular

lattice of the Cu(110) substrate might have a significant impact on the way the adsorbed species organize. As a result, only short range ordered one-dimensional chains are observed on the surfaces. In all the networks reported previously, the centro-symmetric $\mathbf{A_5A_5}$ unit, commonly used in the construction of most gas-phase networks, is connected in combination with other less energetically favourable adenine pairs, leading to the formation of various self-assembled structures observed experimentally.

One dimensional adenine linear chains showing similar width have been observed previously on the Cu(111) surface [13], and the corresponding gas-phase structural model has been suggested, as illustrated in Figure 3.22 C1. In this model, the dimers, $\mathbf{A_5A_5}$, are connected to the neighbouring dimer by H-bond site 1, and the corresponding link is denoted as $\mathbf{A_1A_1}$. This leads to the formation of one-dimensional chains having a width of 6.5 Å. The short dimension of the molecules is aligned almost in parallel along the chain growth direction, which is in agreement with our STM observation that the width of the chain is nearly equal to the long dimension of the free adenine molecule. However, in addition to this model, there is also the other possibility that the dimer $\mathbf{A_5A_5}$ can connect with another dimer via the site 2, yielding adenine chains having a similar dimension of 6.3 Å, as illustrated in Figure 3.22 C2. In this chain, the short dimension of the adenine molecules is only slightly rotated away from the chains growth direction. This model is also considered as a possible candidate for the one-dimensional chains observed by us for adenine on Cu(110). The stabilization energy for the pair $\mathbf{A_1A_1}$ is -0.72 eV, while that for the pair $\mathbf{A_2A_2}$ is -0.62 eV; both are likely to give rise to energetically favourable gas-phase structural models, making it difficult to select one model over another.

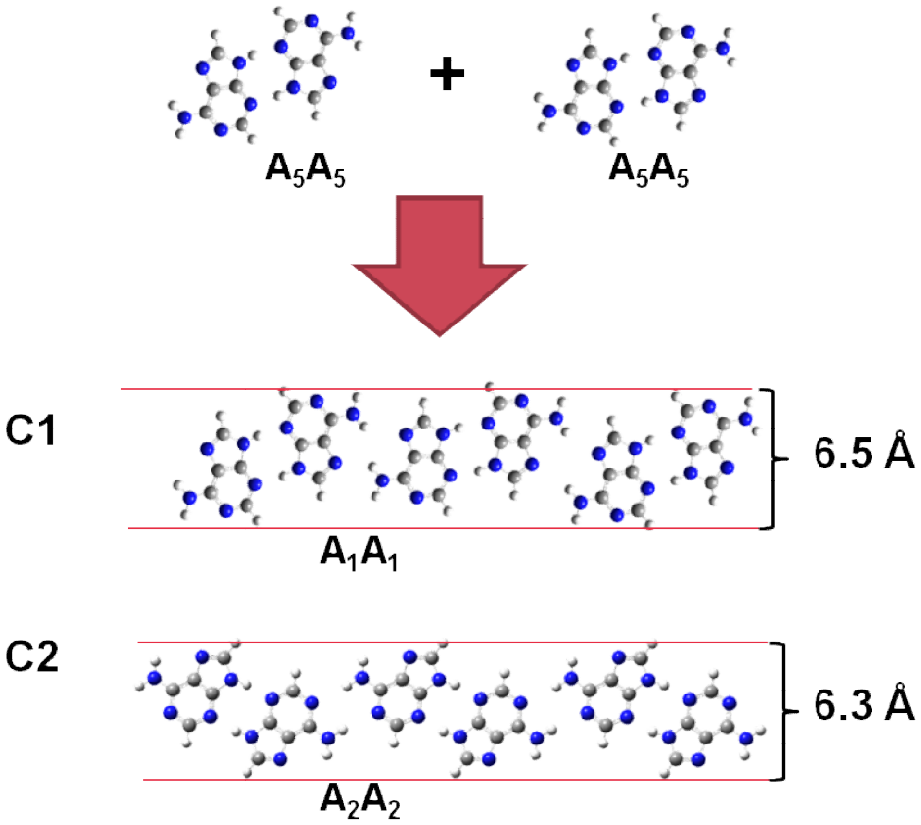

Fig. 3.22: One-dimensional chains constructed by connecting dimers $\mathbf{A_5A_5}$ by two other types of double H-bonds. a) 1D chain formed by connecting two adjacent dimers, $\mathbf{A_5A_5}$, via H-bond site 1, the corresponding dimer is denoted as $\mathbf{A_1A_1}$, and is evaluated to be 6.5 Å in width. b) 1D chain formed by connecting dimers via site 2, the resultant dimer is referred as $\mathbf{A_2A_2}$ having a width of 6.3 Å approximately.

To further establish the validity of the proposed gas-phase structural models for ladder chains, II and the 1D chains, III, we shall take the registry sites of adenine molecules on the Cu(110) mesh into consideration. Previous studies of chiral chains on the Cu(110) surface suggested that adenine prefers to interact with the substrate via the N atom of the amino group, and all the amino nitrogen atoms are accommodated on the preferential on-top positions [1]. As shown in Figure 3.23, for four-molecule units suggested for the ladder chain A and B, since the periodicity along the <110> direction is 10.16 Å, both the amino N atoms can be placed perfectly at the on-top

positions; this also leaves the rest of the amino N atoms allocating closely to the on-top positions. Consequently, the N-Cu interaction is significantly facilitated for the suggested molecular orientation, which makes them very reasonable models for the observed structures. As for the one dimensional chains, in the model C1, when the amino N atoms of the first dimer $\mathbf{A_5A_5}$ are accommodated at the on-top sites, those of the second dimer are more likely to be placed on the short bridge site, arising from the requirement of the corresponding double hydrogen bond length in the $\mathbf{A_1A_1}$ dimer. However, in the model C2, all the amino N atoms of the molecules are accommodated close to the on-top sites. Hence, considering the requirement of the adsorption site, we tend to prefer C2 as the more suitable model that accounts for the observed one-dimensional linear chains. Furthermore, the relative orientation of dimer $\mathbf{A_5A_5}$ with respect to the substrate lattice in the model C2 is similar to that in the ladder chains. Thus, by slight re-orientation of the long axis of each dimer, $\mathbf{A_5A_5}$, in the chain, clockwise, accompanied by the breaking of H-bonds in dimer $\mathbf{A_1A_1}$ and the formation of new H-bonds as $\mathbf{A_3A_3}$, we are able to obtain the comb like structure that can be produced by arranging the trimer units in a side by side manner.

Based on the analysis of the registry of adenine molecules in the proposed models on the Cu(110) mesh, it is quite likely that the adsorbate-substrate interaction plays an important role in anchoring the orientation of the stable dimer $\mathbf{A_5A_5}$. This initial orientation might govern the specific direction along which the second dimer will interact with it via a double hydrogen bond. Accordingly, the orientation of the dimer with respect to the substrate, along with the directional double H-bonds, determines the growth direction of the chains. From the STM images, the chiral related chains along the (1, 2) direction are the most dominant overlayer structures, while the other two types of structures, in particular the ladder chains, have some defects, arising from a missing molecule in the rung position or the fourth molecule, γ, appearing linked to the trimers. This might imply the N atoms of the amino groups of some adenine molecules in the new chains are not perfectly located at the on-top sites like these in the chiral related chains; as a result, these new adlayer structures might be less favourable structures which could be formed only at a low deposition rate.

For the ladder chains, arranging the four-molecule models along the <110> direction via either face to face by C_2 rotation or shoulder to shoulder, as schematically indicated by circles, Figure 3.23A, can yield long chains commensurate

with the substrate. However, when the trimers α and β are arranged in a face to face way, as shown on the top of Figure 3.23A, it seems that the molecule lying on the position where the fourth molecule γ is supposed to be placed might interact with the middle molecule in α by a single H-bond. Moreover, slight molecular reorientation might occur to facilitate the formation of less favourable double H-bonds. The formation of ladder chains via arranging these molecular units along one of the symmetry direction of the substrate, rather than two dimensional hexagonal networks, suggests that the copper-adenine interactions on the Cu(110) are much stronger than the Cu(111) surface. This strong interaction, mediated by the H-bond, can govern the molecular assemblies upon annealing, thus, leading to the formation of various chain structures.

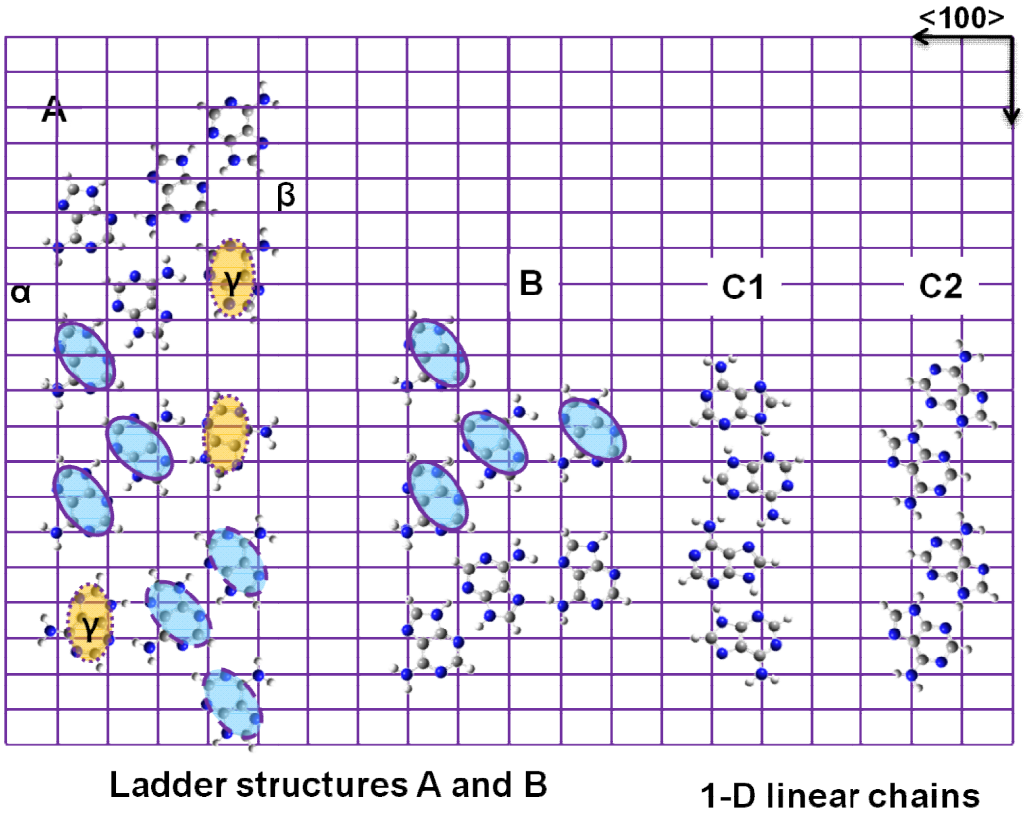

Fig. 3.23: The proposed registry of the ladder chains, A and B, and the one-dimensional linear chains C1, C2, on the Cu(110) mesh. Structural models A and B are commensurate with the substrate along the <110> direction and all the amino N atoms are accommodated at or close to on-top sites. Both C1 and C2 are energetically favourable structural models for the linear chains. In C1, only the amino N atoms of the first dimer $\mathbf{A_5A_5}$ are placed at the on-top sites while these of the other are close to short-bridge sites. In C2, all the amino N atoms are accommodated closely to on-top sites, making it more probable model for the linear chains.

Now we consider all the structures, the chiral chains along the (±1, 2) directions, the ladder chains, II, and the one-dimensional linear chains, III, aligning along the <110> direction together, in the attempt to find out the possible formation mechanism of these overlayer structures. Schematically illustrated in Figure 3.24, is the possible molecular self-assembly mechanism we presented for the different overlayer structures obtained at a low deposition rate and high coverage. Upon depositing adenine onto the Cu(110) substrate at room temperature to high coverage (0.70 ML), adenine molecules aggregate into small molecular islands in which molecules interact with each other via various double hydrogen bonds in a disordered manner. Upon annealing to relatively low temperature, 430 K, significant molecular diffusion occurs, which leads to the formation of ordered double chains and disordered small molecular clusters that are formed by connecting molecules in the surrounding areas via various double H-bonds. Since the diffusion barrier for the molecular clusters is higher than that for the individual adsorbate, further annealing the sample to 490 K is required to enable these clusters to diffuse freely across the surface in the attempt to meet each other. This is accompanied by the re-orientation of the molecules of the double chains. However, at high coverage, it is believed that adenine molecules are more likely to form the most stable dimer $\mathbf{A_5A_5}$ first upon annealing. When this dimer is formed, there are only four H-bond sites, 1, 2, 3, and 6, available for further connection via H-bonds. Due to limited free space left for molecular diffusion, the other molecules can approach the dimer $\mathbf{A_5A_5}$ in different ways. Thus, when two dimers of the same chirality are connected via the H-bond 6, the chiral chain along the (±1, 2) is formed. Meanwhile, the dimers can also connect with each other via site 2 or 1, which can give rise to the one-dimensional chains. Finally, the connection of dimers $\mathbf{A_5A_5}$ via the H-bond site 3 would result in these ladder chains.

Along the chain growth direction, since the strength of the double H-bonds, which is estimated approximately according to the stabilization energy of the corresponding dimer, decreases in the order of $\mathbf{A_1A_1}$>$\mathbf{A_2A_2}$>$\mathbf{A_6A_6}$≥$\mathbf{A_3A_3}$, thus, the connection of dimers, $\mathbf{A_5A_5}$, by site 1 or 2 is expected to lead to formation of longer chains. This is true for the dimer chains along the (±1, 2) directions in which the double H-bonds governing the chain growth direction are weaker, thus the length of these chains is shorter than that of the others. While for the ladder chains, the weak H-bond between

dimer $\mathbf{A_3A_3}$, might account for the observation of these trimers units, or short chains formed by arranging these trimer side by side.

In addition to the intermolecular hydrogen bonds, the substrate-adsorbate interaction also plays a very important role in the molecular organization, particularly upon increasing the annealing temperature. As shown in the Figure 3.23 and 3.24, the growth of each chain along a specific direction is determined by the orientation of the dimer, $\mathbf{A_5A_5}$, with respect to the substrate high symmetry directions. In other words, the adenine dimer, $\mathbf{A_5A_5}$, forming the chiral chains along the (1, 2) direction is oriented differently from those forming the one-dimensional linear chains and the ladder chains along the <110> direction. Therefore, it is suggested that the substrate-adsorbate interactions may direct the orientation of the stable dimer $\mathbf{A_5A_5}$, *i.e.* the registry of the molecules with the substrate. Then the second type of double-hydrogen bonding determines the growth direction of the chains, mediated by the subtle substrate-adsorbate interactions. The different orientations of the dimer $\mathbf{A_5A_5}$ with respect to the substrate are believed to be associated with the aggregation of molecules upon deposition at room temperature. The relatively disordered molecular islands obtained by dosing adenine at low deposition rate might favour the formation of the stable dimer $\mathbf{A_5A_5}$ upon annealing; connection of these dimers which may have different registries on the substrate along different directions, leads to the formation of the various observed adlayer chain structures.

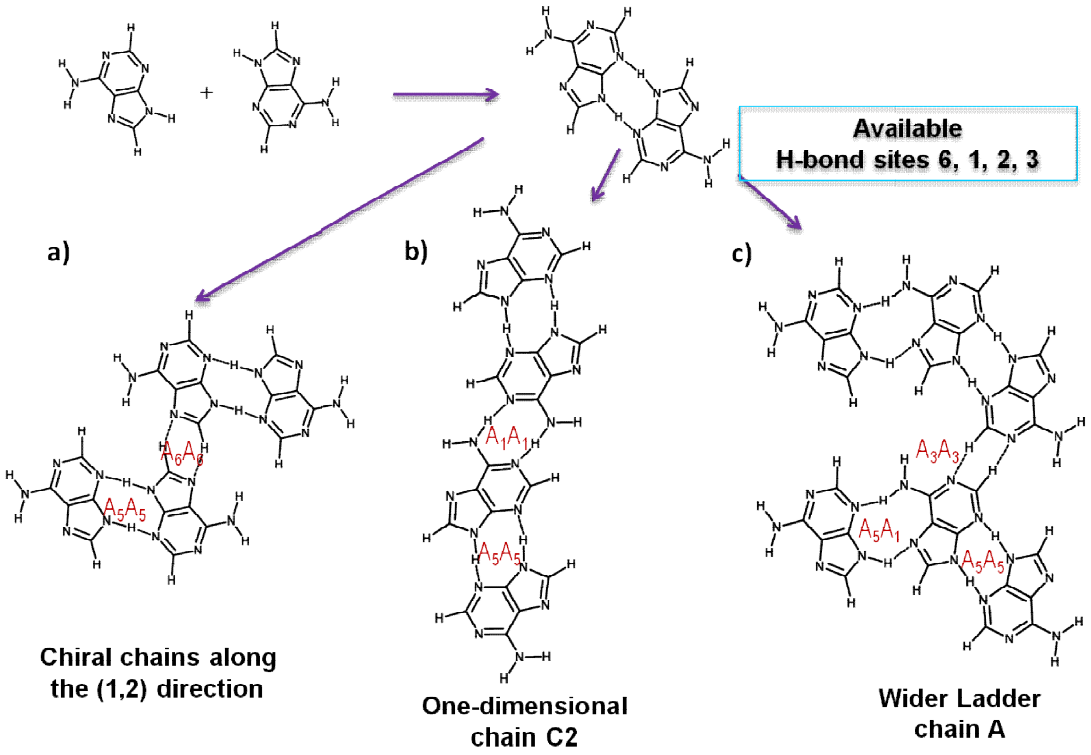

Fig. 3.24: Suggested formation mechanism of the chiral chains along the (±1, 2) directions, the ladder chains II, and the 1D linear chains, III, along the <110> directions at the Cu(110) surfaces at low deposition rate. Adenine molecules diffuse to form the most stable dimer, $\mathbf{A_5A_5}$, upon annealing. a) Adenine chiral chains formed by connecting the dimers by one of the available H-bond site 6, indicated as $\mathbf{A_6A_6}$. b) Formation of 1D linear chain via connecting the dimers by site 2, indicated as $\mathbf{A_2A_2}$. c) The wider ladder chains formed by connecting the dimer by site 3, then the middle molecule is connected to the site 5 of another molecule by third H-bond site 1, denoted as $\mathbf{A_5A_1}$.

3.2.5 Very low coverage adsorption onto the Cu(110) surfaces

Previous STM studies of the adsorption of adenine on Cu(110) surfaces [1] mainly focused on the medium to high coverage regime at which it is believed that the lateral intermolecular hydrogen bonds, more than the adsorbate-substrate interactions, account for the well ordered self-assembled structures. However, at low coverage the adsorbate-substrate interaction might become the dominant driving force directing the formation of the ordered structures experimentally observed. Hence, investigation into

the molecular behaviour at low coverage might help us to understand the formation mechanism of ordered adenine superstructures obtained at high coverage.

3.2.5.1 STM studies of very low coverage at 440 K

Very low coverage STM images of ordered adenine overlayer domains were obtained after dosing a small amount of molecules onto the Cu(110) surface and annealing to 440 K. As shown in Figure 3.25a, in addition to the short adenine dimer chains, consisting of two or four dimers, some elliptical and triangular features were also observed. These features look quite like adenine dimer and trimer units from their appearance in comparison with the dimer chains; they were replaced with short and well-ordered dimer rows upon annealing the sample to 490 K, the common temperature we are able to obtain the ordered adenine chiral chains. This finding suggests the existence of strong adenine-copper interactions at low coverage, thus, high temperature annealing is required to overcome the activation energy barrier for molecular diffusion to occur, in particular for the dimers and trimers, this leads to the formation of well-ordered chains.

Close-up STM images of some selected elliptical features, D1 and D2, and triangular features, T1 and T2, are shown in Figure 3.25c, along with a cross-sectional line profile of the dimer, indicated with arrows. Feature D1 and D2 have great similarities in terms of the appearance and cross-sectional dimension. Both of them are composed of two centro-symmetric depressed lobes separated by a small protrusion. The lateral dimension of this elliptical feature is 12.1 ± 0.4 Å in length along the long axis, indicated with arrows, and 7.2 ± 0.4 Å in width. These parameters resemble closely to the corresponding dimensions of adenine dimer, $\mathbf{A_5A_5}$, which is 11.3 Å in length and 6.4 Å in width, Figure 3.25b. This dimer is centro-symmetric and is the most stable adenine pair; it is usually considered as the basic unit in the construction of gas-phase adenine chains. Hence, we tend to assign these elliptical features as adenine homochiral dimers.

In addition to the similarities mentioned above, the long axis of these elliptical dimer features, D1 and D2, are oriented clearly in two different directions with respect to the <110> direction of the substrate, Figure 3.25b. The angle between the

long axis of feature and the <110> azimuth is approximately 50°; this indicates that these features are mirror related along the high symmetry directions of the substrate; each feature is homochiral and has C_2 symmetry. This finding reveals the tendency of adenine molecules to form stable chiral dimers at the initial stage of the formation of dimer chains upon annealing. However, it is still impossible to assign the orientation of the individual molecule with respect to the substrate lattice due to the poor STM resolution of the internal molecular feature. From the images, we can only suggest that each depression in the elliptical feature is associated with the aromatic ring of adenine, while the protrusion in the middle might refer to the double H-bond.

Now we take a close look at these triangular features, T1 and T2, Figure 3.25c, in which four features oriented differently are distinguished. The width of these features, indicated by the arrows, is very close to that of D1 and D2, 11.8 ± 0.4 Å; however, it is 15.5 ± 0.4 Å along the direction perpendicular to the arrows. This wider dimension suggests that another molecule must be connected to the dimer, $\mathbf{A_5A_5}$, by a double hydrogen bond; this leads to the formation of adenine trimers. According to the appearance of these triangular trimer features and their orientations with respect to the substrate, the two trimers in T1 and T3, respectively, are considered mirror related; while the two trimers in T1 are related to those in T2 by the C_2 rotational operation. Therefore, the observation of the four different adenine trimers seems to disagree with the previously suggested formation mechanism of ordered adenine chains at the Cu(110) surfaces. Rather than connections of adenine stable dimers to form the longer chains, driven by annealing, individual adenine is more likely to connect with its neighbouring counterpart forming the stable dimer first at low coverage upon annealing to 440 K. When one stable dimer is formed, its motion on the surface is restricted due to the relatively strong interactions between adenine and copper atoms; as a result, another molecule of the same chirality can approach this dimer in two directions, giving rise to the variety of trimers we observed at this stage. Therefore, at low coverage, the substrate-adsorbate interaction plays an important role in the molecular assemblies.

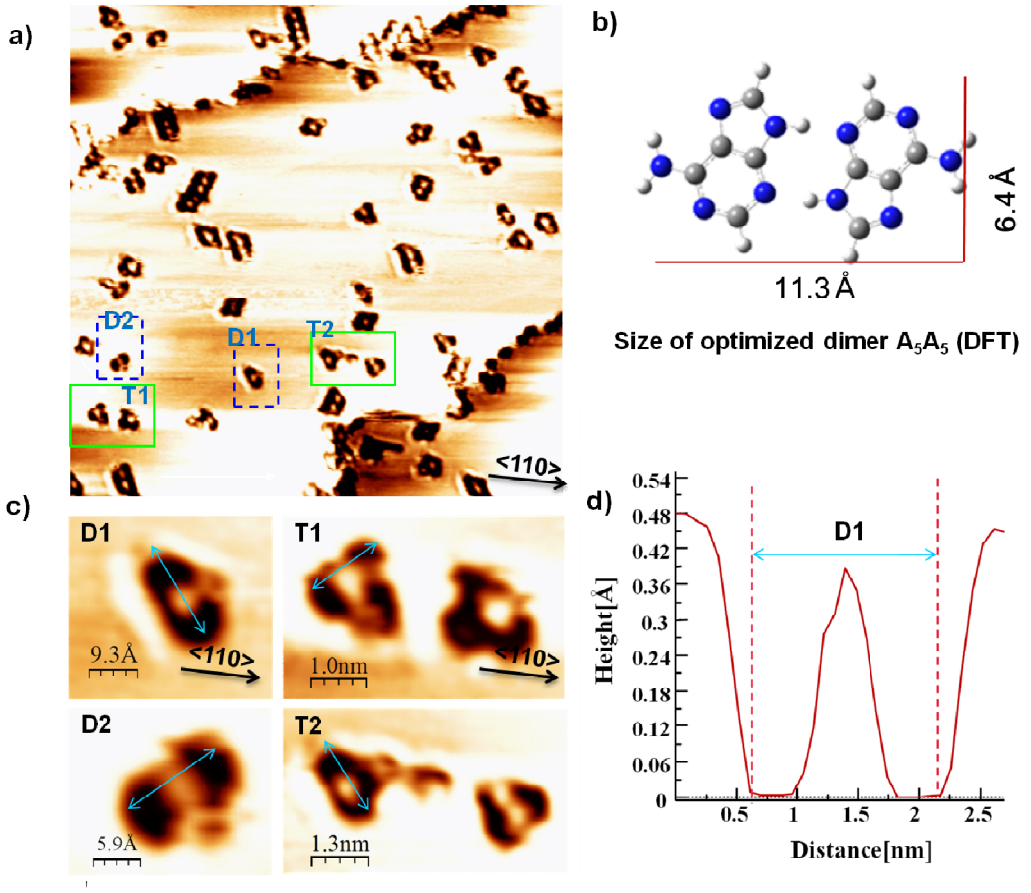

Fig. 3.25: a) STM image of ordered adenine arrays obtained upon annealing to 440 K (1.17 nA, -0.64 V, 39 × 39 nm^2); Indicated D1, D2, and T1, T2 are the elliptical and triangular features. b) Size of the optimized dimer $\mathbf{A_5A_5}$ using DFT method with B3LYP functional and 6-31G basis set; c) Close-up STM images of the D1, D2, and T1, T2 features; d) The line profiles of the long axis of the elliptical features in D1; the orientations of the long axis these features are indicated with arrows.

3.2.5.2 Discussions

In reference to the structural models suggested for the ordered adenine dimer chains [1], here, we suggest the most probable formation mechanism for the formation of the adenine dimers and trimers observed at low coverage. As schematically illustrated in Figure 3.26, upon annealing, one adenine interacts with another neighbouring molecule of the same chirality by H-bonds, which leads to the formation of the most stable centro-symmetric homochiral dimers, $\mathbf{A_5A_5}$ and $\mathbf{\bar{A}_5\bar{A}_5}$. When an individual adsorbed dimer species is formed, its diffusion across the large free surface existing at

low coverage is restricted as a result of the stronger interaction between adenine and copper atoms and the increasing in size of the diffusing species [45]. Thus, the single adsorbate of the same chirality which can diffuse more easily at this stage is likely to approach the homochiral dimers in either of two possible directions, in the attempt to connect with them via the H-bond site 6. This gives rise to the C_2 rotation related trimers, denoted as $\mathbf{A_5A_5}$ and $\mathbf{A_6A_6}$. Since adsorption of prochiral molecules always yields an equal amount of enantiomers, the connection of the opposite homochiral dimer, $\mathbf{\bar{A}_5\bar{A}_5}$, with another adsorbate of the same chirality leads to the formation of another pair of trimers, i.e. $\mathbf{\bar{A}_5\bar{A}_5}$ and $\mathbf{\bar{A}_6\bar{A}_6}$. Each pair of C_2 related trimers are reflectional images of each other. Thus, we are able to observe the various small molecular arrays at low coverage upon annealing to 440 K.

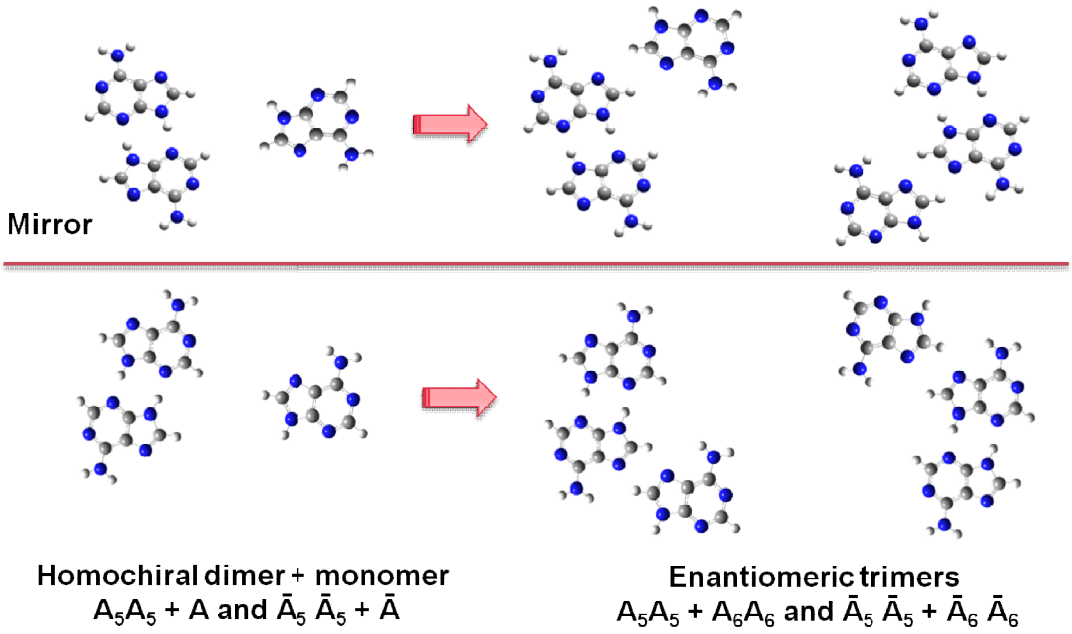

Fig. 3.26: Schematic illustration of the proposed formation mechanism for adenine dimers, $\mathbf{A_5A_5}$ and $\mathbf{\bar{A}_5\bar{A}_5}$, and trimers formed by connecting the dimer with another pair of the same chirality by the H-bond 6; **A** represents an individual adenine molecule. On the left, two homochiral dimers, $\mathbf{A_5A_5}$ and $\mathbf{\bar{A}_5\bar{A}_5}$, are formed at first, then each dimer is connected to another molecule of the same chirality, **A** and $\bar{\mathbf{A}}$, in two directions, giving rise to two C_2 rotational related trimers on the right; thus totally, four trimers are constructed including their mirror reflectional enantiomers.

In this experiment, the observation of dimers and trimers at low coverage is more likely to suggest a different formation mechanism for the ordered adenine chains from that proposed by the theoretical calculations. The calculated results for the adenine adsorbed on the Cu(110) substrate suggest a three-step formation mechanism that involves the formation of dimers, $\mathbf{A_5A_5}$ and $\mathbf{\bar{A}_5\bar{A}_5}$, then the registry of the dimer on the substrate, and the connection of these dimers to yield the ordered chains [22]. This mechanism is in agreement with that suggested for the various superstructures of adenine adsorbed on other low corrugation surfaces, *e.g.* Cu(111) [10-15], Au(111) [16, 17]. However, our finding indicates the formation of short adenine chains at low coverage upon annealing to 490 K results from the diffusion and connection of these dimer and trimer units, driven by the high temperature annealing.

The mechanism at low coverage is described in this way. Firstly, upon annealing, adenine molecules were able to overcome the diffusion barrier and formed dimers having high stabilization energy. Secondly, rather than connecting the adenine pairs of the same chirality via the second type of hydrogen bond, $\mathbf{A_6A_6}$, all the surrounding single adsorbates of the same chirality have equal possibility to interact with the dimer, thus, different trimers were formed. Lastly, after further annealing, these small molecular clusters diffused again, which led to the formation of short ordered chains stabilized via both the intermolecular H-bonds and the substrate-adsorbate interactions. This phenomenon suggests not only the formation of adenine chains is mainly a thermally driven process, but also the important role that the substrate-adsorbate interaction plays in the adenine self-assembly on the Cu(110) substrate. However, the suggested formation mechanism might be only true for low coverage because it is still unclear why we did not observe other trimers since the third molecule might also approach the dimer, $\mathbf{A_5A_5}$, in other different directions, which might lead to the formation of various trimers oriented differently.

3.2.6 Contrast variations of adenine overlayer structures

The intramolecular contrast of adsorbates in topographic STM images reflects the density of states near the Fermi energy [46]; it can be influenced by several other factors: the tip-surface separation, the tip apex structure and the applied bias voltage.

For example, changes of the distance between the tip and the surface can generally alter the force between them; a strong force can even result in deformations and displacement of the adsorbate, as a result, it strongly affects the STM contrast [47-49]. The influence of the tip apex structure on the internal contrast of adsorbates is more likely unintentional and less controllable. Random modification of tip apex structures, due to atomic diffusion at the tip apex or atomic or adsorbates transfer to the tip, can result in sudden changes in the appearance and amplitude of the corrugation images of the adsorbates [50].

In most experiments, since STM measurements are carried out at low bias range and the tip apex structure is well characterized, experimental observations of variations in the contrast of adsorbates are mostly presented by changing the applied bias voltage. Bias-dependent images have been reported for many studies of molecular adsorbates on highly oriented pyrolytic graphite (HOPG) [51-55] and other surfaces [56-60]. The contrast changes of the imaged patterns reflect the variations of electronic structures of the MOs of the adsorbate, the tunnelling process could involve a resonance of several MOs of the adsorbates with the Fermi level of the tip and surface. It is suggested that the molecular orbitals of the adsorbates at energy levels away from the Fermi level can even participate in the electron tunnelling via tails of resonance or orbital mixing [51, 52, 59, 60].

In this section, we present the experimental observations of contrast variations in the STM images of adenine dimer chains at room temperature and 70 K. The dependence of the image contrast of the adlayer structures and isolated adsorbates on the tip-sample bias voltage has also been studied; several tunnelling mechanisms, which might account for the observed contrast variations of adenine molecules adsorbed on Cu (110) surfaces are suggested.

3.2.6.1 Contrast changes at room temperature

Shown in Figure 3.27 are the STM images of ordered adenine chiral chains along the (1, 2) and (-1, 2) directions obtained after annealing the sample at 490 K. These chains are in good agreement with the previous experimental findings revealed by Chen *et al.* [1] except that they show better intramolecular contrast of the individual

features. As seen from the image, Figure 3.27a, individual elongated features of the row along the (-1, 2) direction seem to be more clearly resolved than those along the (1, 2) direction. Since the tip apex structure and tip-sample bias voltage are maintained constant during scanning, we attribute the internal contrast difference in both chains to the effect of different scanning direction with respect to the molecular orientations rather than to the asymmetry of tip structures. In order to achieve molecular resolution of both chains, the tip has to be rotated at an angle with respect to the scanning direction.

In Figure 3.27b, a sudden change in the contrast of the adsorbates is observed, it corresponds to the variations in the electronic conductivity of the tunnelling junction. We suggest that this phenomenon is due to the variation of the tip condition during scanning; for example, an adenine molecule can be adsorbed on the STM tip, which can modify the contrast of the same features within the same image. With an adenine adsorbed on the W tip, the tunnelling junction will become Cu-adenine-adenine-W rather than Cu-adenine-W. In this new junction, a higher resistance could be responsible for the depressed molecular features in the image [1]. Hence, we should emphasize that this depression is due to an electronic effect rather than a height effect.

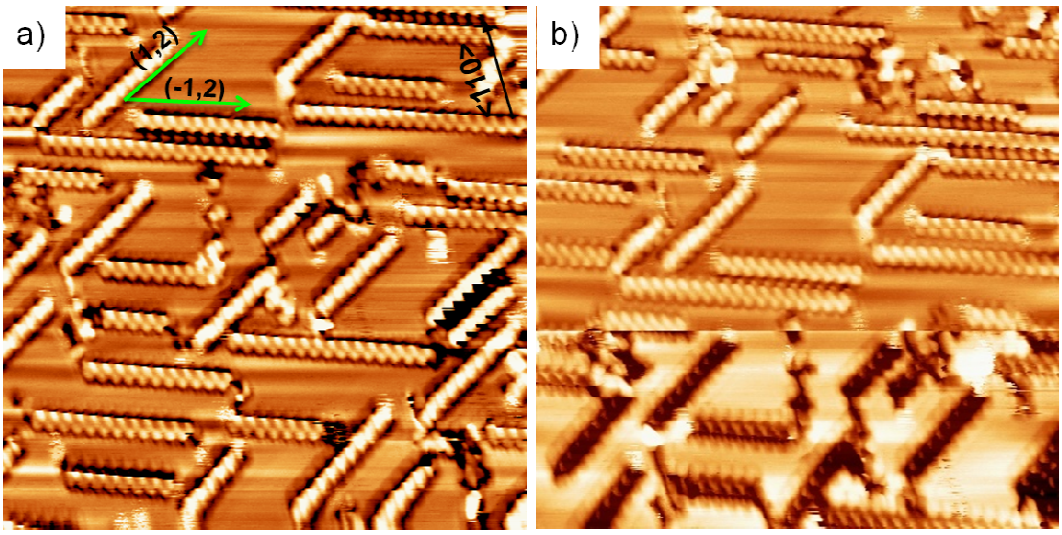

Fig. 3.27: STM images of adenine dimer chains with different contrast at medium coverage (0.20 nA, -0.96 V, 33 × 33 nm^2, 0.20 nA, -0.86 V, 33 × 33 nm^2). a) The contrast of the chains along the (1, 2) direction is different from that along (-1, 2) direction. b) The sudden change in the contrast of the molecular rows with respect to the substrate indicates a variation in the tunnelling junction.

A molecular resolution STM image of the dimer chains aligning along (1, 2) and (-1, 2) directions is shown in Figure 3.28; the slight contrast difference of the imaged molecular features between the two chains is identified. The chains along the (1, 2) direction formed by two parallel rows of circular shape spots arranged side by side, while the molecular features appear of elongated shape in the chains along the (-1, 2) direction. Even though the observation of contrast difference between the adsorbate features, the periodicities of the unit cell in both chains are very close. The unit cell is about 7.5 Å in length and has C_2 symmetry. Since the coexisting molecular chains are mirror related and each is homochiral, the observation of slight contrast discrepancy of the adsorbate features could result from a scanning drift or the effect of the fast scanning direction with respect to the specific molecular orientation in both domains. Note that the contrast difference of the individual molecular features forming the mirror related chains is not distinguished in STM when scanning across surface areas of over 400 Å; only arrays of bright and elongated features are observed in both chains.

Corresponding structural models, denoted $\mathbf{A_5A_5}$, $\mathbf{A_6A_6}$ and $\mathbf{\bar{A}_5\bar{A}_5}$, $\mathbf{\bar{A}_6\bar{A}_6}$, are presented in Figure 3.28, following the structural model suggested by Chen *et al.* [1]. In the superimposed model, the dimer, $\mathbf{A_5A_5}$ or $\mathbf{\bar{A}_5\bar{A}_5}$, is connected with dimers of the same chirality by the second type H-bond site 6 along the chain growth direction. Along each chain, only molecules of the same chirality are included and the chain growth direction is strictly related to the specific molecular chirality. The molecular planes are oriented nearly parallel to the surface and all the amino nitrogen atoms are allocated at preferential on-top sites.

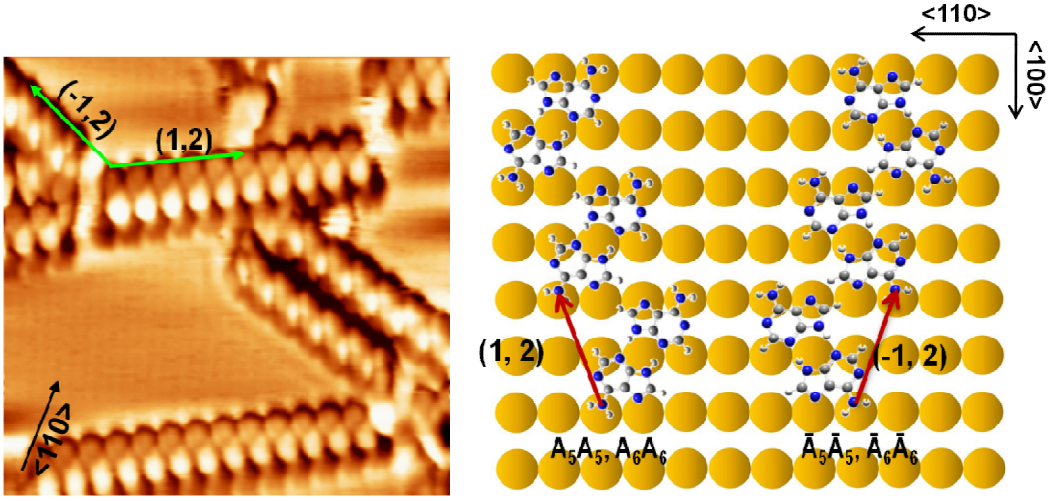

Fig. 3.28: Molecular resolution STM image of ordered adenine chains at medium coverage and the proposed structural models and registry of adsorbates on the Cu(110) mesh [1] (0.65 nA, -1.12 V, 14 × 14 nm^2). Each adenine row is composed of adenine dimers of same chirality, $\mathbf{A_5A_5}$ or $\bar{\mathbf{A}}_5\bar{\mathbf{A}}_5$, connecting along the chain growth direction by the H-bond site 6; all the amino N atoms bind with the copper substrate at on-top sites.

3.2.6.2 Intermolecular contrast variations at 70 K

Shown in Figure 3.29 are the STM images of an adenine chain aligning along the (1, 2) direction obtained at 70 K; the magnified STM image at the bottom is superimposed with the suggested structural model for the chain along the (1, 2) direction. Clearly observed from the images, two types of image contrast are identified upon changing the magnitude and polarity of the bias voltage. Worthy of notice, in this LT-STM, the tip is grounded, hence, changes in the electron density of the unfilled state of the adsorbates are mapped upon scanning at positive bias, and contrast variations of the observed features might reflect the corresponding electronic structure of the adsorbates. At positive bias voltages between 1.416 V and 0.492 V, the chain is characterised by arrays of small bumps surrounded by depressed elongated features and stripes, Figure 3.29a and b. A contrast change occurs when the tip-sample bias is reduced to 0.19 V, seen from the STM image shown in Figure 3.29c. Some rhombic shaped features, interspaced between the adjacent bumps, are found; four distinct sub-molecular features are resolved in the chain now. At negative bias, images obtained at -1.416 V and -0.19 V show great similarity with these obtained at

equivalent positive bias. The changes of feature contrast are induced, therefore, by changing the magnitude of the applied tip-sample bias rather than the polarity. However, changing the polarity of the bias voltage at 0.49 V can also affect the image contrast, as shown in Figure 3.29b and e. In the image at the bottom, the proposed structural model for the adenine dimer chains along the (1, 2) direction is presented, the two molecules in the dimer $\mathbf{A_5A_5}$ fit well with the two elongated feature arranged in parallel. At room temperature STM experiment, the sample is grounded, images of adsorbates at positive tip bias, which corresponds to the tunnelling from the HOMO orbitals of the adsorbates to the tip, are generally unstable and short lived, however, at 70 K, high resolution images are obtained at negative polarity.

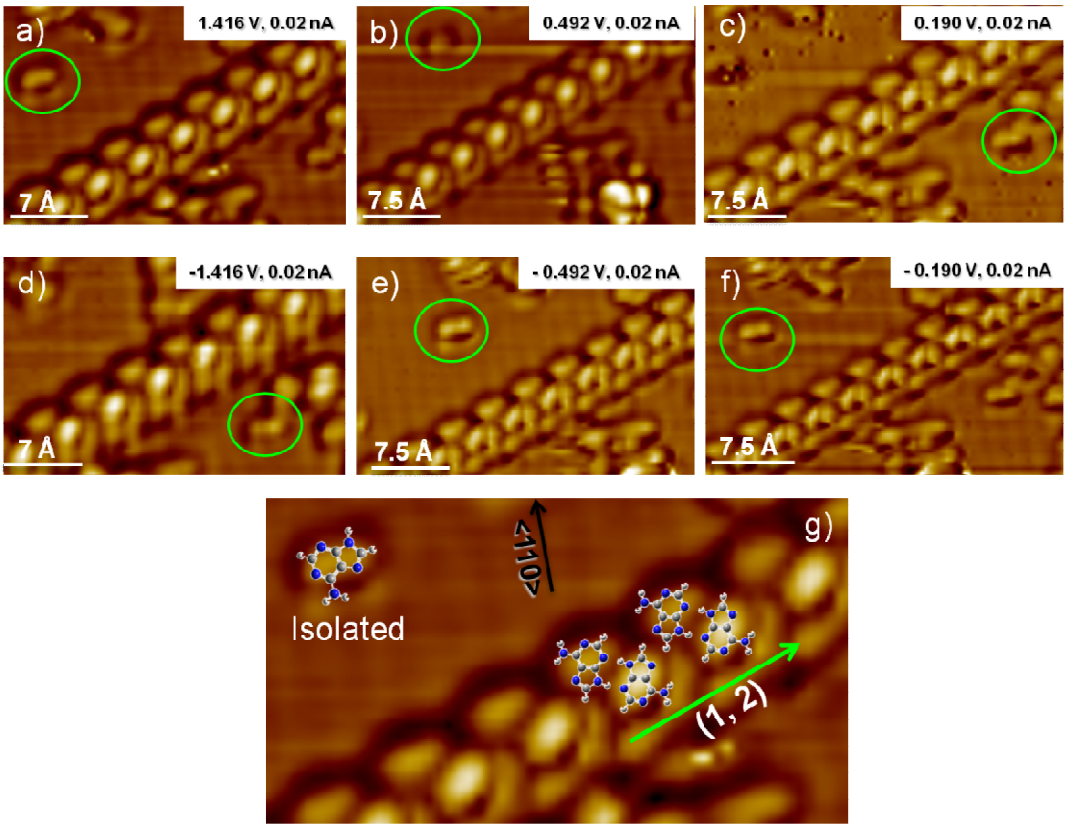

Fig. 3.29: STM images of adenine chain aligning along the (1, 2) direction obtained at 70 K and different bias voltages. In the circles, isolated adsorbate species in lamella shape (b) and peanut shape (e) are indicated. At bottom, g) is the magnified adenine chain superimposed with the chiral structural model and the isolated feature with a single adenine molecule. The orientation of the isolated molecule is different with those composing of the chain. Images are processed using SPIP 5.08.

Similar contrast changes are also observed for the *isolated* adsorbates, as indicated by the circles in Figure 3.29. Features observed in the neighbouring areas of the ordered chain also exhibit two types of contrast. One looks like a lamella and is imaged at 0.492 V; the other is characterized by two lobes in a peanut shape; it is clearly resolved at a voltage range from -0.190 V to -1.416 V. The isolated species show similar bias-dependent behaviour with the contrast of adsorbates in the chains. In comparison with the features resolved in the ordered chains, the isolated adsorbate pattern resembles none of the sub-molecular features that presented in the chains in terms of the internal appearance and the orientation of its long dimension with respect to the substrate. The difference in the internal contrast of an adsorbate molecule might arise from the fact that the interference effect between adsorbates is enhanced in the chains; the final image contrast more likely results from the interference of several electron tunnel paths [56].

The short cross-section of the isolated species is 3.0 ± 0.3 Å, the long axis aligned nearly along the <100> direction is 6.6 ± 0.3 Å; thus, it is assigned to a single adsorbed adenine molecule. The orientation of its long dimension with respect to the substrate lattice can be estimated by analyzing the STM image at -0.492 V, where the substrate lattice is weakly observed. The elongated feature only occupies two unit cells of the lattice, identified clearly from the magnified STM image shown at the bottom of Figure 3.29. At 70 K, the molecular mobility is limited, which enables the single diffusing molecules to be imaged. The observation of the individually adsorbed species and the accumulated molecular clusters coexisting with the ordered adenine rows, upon annealing to 470 K, also indicates a high diffusion barrier for a single adenine molecule adsorbed on the Cu(110) surface.

As far as the adenine rows growing along the (-1, 2) direction is concerned, Figure 3.30, similar contrast variations are observed when the bias voltage is changed at 0.492 V from positive to negative. However, the internal contrast of the adsorbates is different from the molecular structure along the (1, 2) direction; this chain is characterized by two bright spots aligning in parallel. The inter-spots distance along the chains growth direction is 7.5 ± 0.2Å and the chain width is about 9.5 ± 0.2 Å; both are consistent with the corresponding values of its mirror chains in Figure 3.29. Furthermore, these clearly distinguishable spots aligned in parallel imaged at 70 K resemble closely the individual features composed of the chains resolved at room

temperature, Figure 3.28, however, these chains are aligned along the (1, 2) direction. The merely common aspect of these chains in the two images at different temperature is that both of them, regardless of the chirality, are oriented almost in parallel with the scanning direction. This is also true for the chains along the (1, 2) direction scanned at 70 K and the opposite chiral chain along the (-1, 2) direction resolved at room temperature; where both of them are composed of elongated features arranged side by side and are imaged at a certain angle with respect to the fast scanning direction. Hence, we tend to attribute the contrast difference of the imaged patterns in the mirror related chains to the effect of the molecular orientation with respect to the fast scanning direction. It has been suggested that the electric field, generated by the potential difference between the tip and sample, can interact with the cyclic hydrogen bond between adjacent adenine molecules in an angle dependent fashion. Zundel *et al*. [60, 61] have suggested that the proton polarization within the π-electron stabilized cyclic hydrogen bonds is highly anisotropic, and the induced in-plane dipole moment scanned across the hydrogen bond in both chains is different with respect to the scanning direction; this might account for the contrast difference observed in this experiment.

In the magnified image shown at the bottom of Figure 3.30, the structural model composed of adenine dimers of opposite chirality, $\bar{\mathbf{A}}_5\bar{\mathbf{A}}_5$ and $\bar{\mathbf{A}}_6\bar{\mathbf{A}}_6$, and a single adenine molecule, $\bar{\mathbf{A}}$, are superimposed onto the observed circular features. In the chain, only one molecule of each dimer, $\bar{\mathbf{A}}_5\bar{\mathbf{A}}_5$, can fit with the protrusion, while the other accounts for the depression between the less bright circular protrusions along the chain. A single adenine molecule of the same chirality fits well with the observed isolated feature; however, it shows a different orientation from those molecules forming the chains. The discrepancy between the isolated adsorbate and the adsorbates in the chains implies molecular re-orientation is required upon forming the chains in order to facilitate the formation of H-bonds and favour the substrate-adsorbate interaction. It is believed that both the interactions work in combination to yield chains growing along a specific direction.

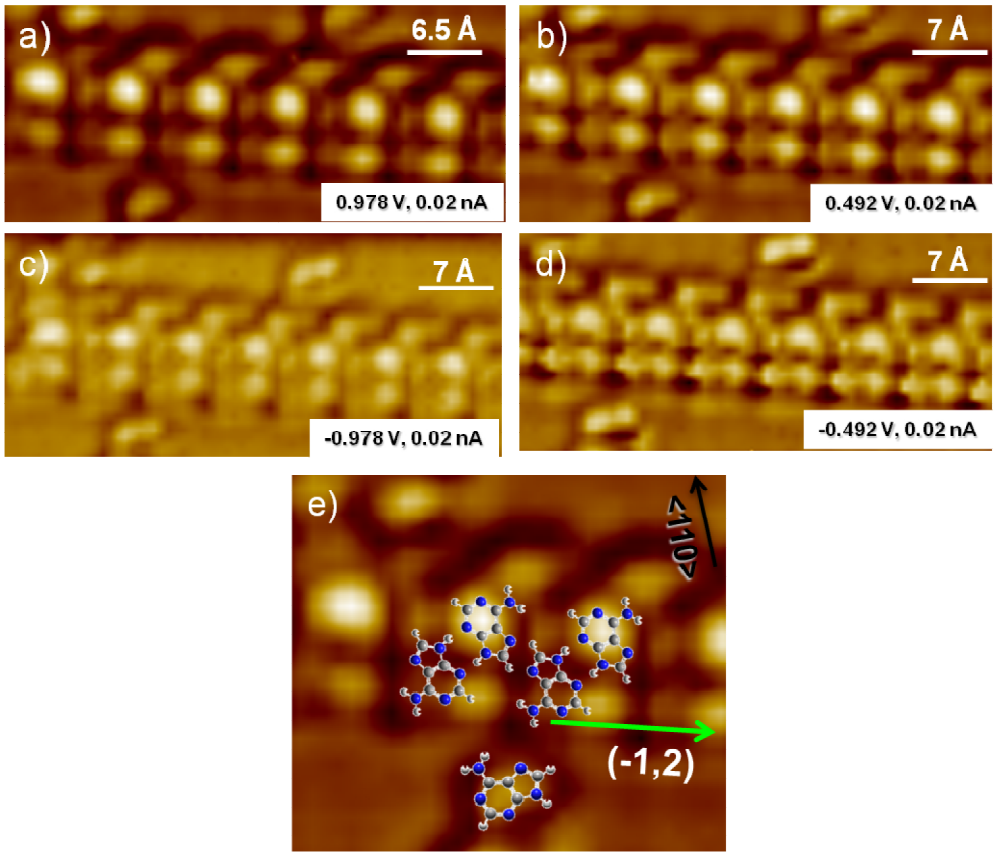

Fig. 3.30: High resolution STM images of adenine rows aligning along the (-1, 2) direction obtained at 70 K. In the magnified image e) at the bottom, the proposed structural model [1] and isolated adsorbate of the same chirality are superimposed, demonstrating the different orientations between the adenine molecules composed of the chains and the isolated adsorbate. Images are processed using SPIP 5.08.

3.2.6.3 Contrast variations of single adsorbed species

In order to understand further the contrast changes of the observed patterns in the ordered chains, a series of STM images of adenine monomers were acquired as a function of the applied bias voltage at 70 K. In Figure 3.31a and b, two characteristic types of contrast are presented at positive bias, corresponding to the electron density states of the LUMOs of the adsorbate. A third type is observed at negative bias, which may reflect the electronic structures of HOMOs, Figure 3.31c and d. The contrast shown in Figure 3.31a can be imaged at a bias range from 2.276 V to 0.978 V; it resembles the bright spot features forming the chains obtained at room temperature.

On reducing the bias further, only the second type of contrast, in S-shape, is obtained; this suggests that changes in electron channels might occur due to the bias variation. The molecular contrast obtained at negative bias, shown in Figure 3.31c and d, consists of two elongated protrusions arranged with their long dimensions in parallel; it seems not to be bias-dependent since its appearance does not change upon changing the tip-sample bias from -2.267 V to -0.275 V. Both the latter two contrasts are observed for the first time for adenine adsorbed on the Cu(110) surfaces.

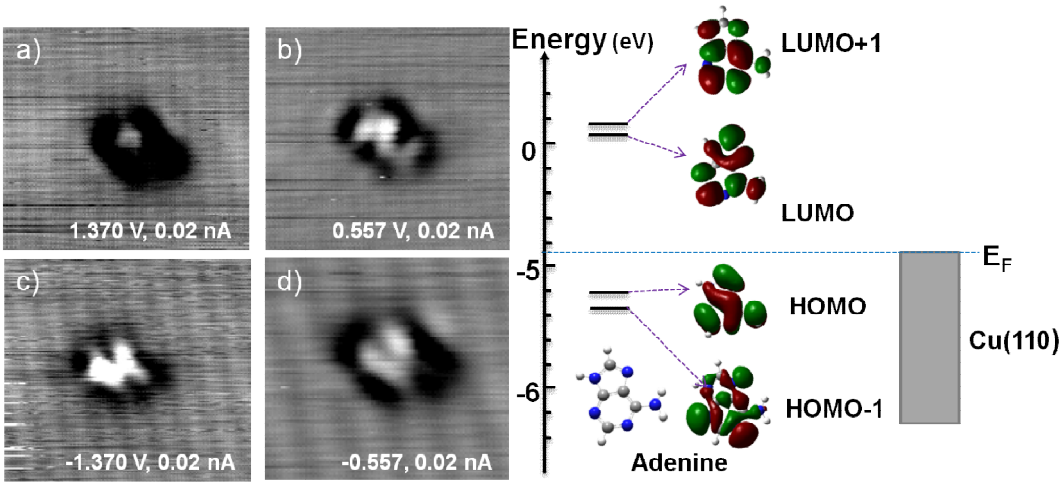

Fig. 3.31: Three types of contrast features of the single adsorbed species, obtained by changing the magnitude and polarity of the tip-sample bias, are presented. On the right are the energy diagram of adenine and the Fermi level of the Cu(110) substrate, and selected molecular orbitals of optimized configuration of adenine, four frontier orbitals, HOMO, HOMO-1, LUMO and LUMO+1 are shown.

Shown on the right side in Figure 3.31 is the energy level diagram of the HOMOs and LUMOs of the adenine molecule relative to the Fermi level of the Cu(110) substrate. The selected contrast patterns of the single adsorbed species acquired at different tip-sample bias voltages are compared to the electronic contour of the frontier orbitals of the free adenine molecule optimized using DFT. However, none of the listed contours seems to resemble the observed adsorbate contrast. The diagram indicates that the HOMO (-6.05 eV) is lower than the Fermi level of Cu(110) substrate (-4.48 eV) by 1.57 eV; while the LUMO is situated at -0.62 eV below the vacuum level, it is about 3.86 eV above than the Fermi level of the substrate. Hence,

the HOMO is closer to the Fermi level and the energy gap between them might be overcome by changing the bias-voltage. The energy difference between the adjacent HOMO and HOMO-1 is less than 0.8 eV and that for the first two unoccupied MOs is 0.54 eV, so the energy gap between the two immediate orbitals seems to be big enough for the STM to probe them individually. This might account for the observations of several contrast features of the adsorbate as the bias voltage is changed.

The observation shows more than one contrast for adenine monomers as a function of the tip-sample bias voltage, yet the poor correlation of the image with the shape of the molecular orbitals suggests that electron tunnelling might occur through a resonance tunnelling mechanism. In this process, orbitals lying in far energy away from the Fermi level might make a significant contribution to the electron tunnelling via resonance, thus, a number of orbitals rather than only the HOMO or LUMO of the adsorbate needs to be considered in order to describe the contrast variation accurately. The strength of the contribution of orbitals to the tunnel current is affected not only by the energy separation from the Fermi level, but also by the strength of the electron coupling of the molecular orbital with the surface and with the tip; both factors can influence the image contrast [59, 60, 62]. The interaction of the tip with orbitals having fewer nodal planes perpendicular to the surface is favourable, therefore, the contributions of the orbital to the tunnelling is stronger even though they may be located away from the Fermi level.

In the case of adenine adsorption on the Cu(110) surface, the mutual polarization results in charge redistribution in the molecular plane, this might modify the alignment of frontier orbital energies and broaden the discrete molecule levels into resonances [56]. Previous studies have proposed the resonant tunnelling as the dominant tunnelling mechanism for a number of systems [63, 64]. One example is the adsorption of DNA on gold surfaces [65] where the strong interaction between the electronic energy levels of the adsorbate and those of the substrate may mediate the electron tunnelling between tip and surface.

3.3 Conclusions

In this chapter, the effect of experimental parameters, *e.g.* surface coverage, annealing temperature, and substrate temperature, on the adenine self-assembled structures on Cu(110) surfaces has been studied in details using STM and RAIRS. At high dense monolayer coverage, adenine tends to form ordered 2D chains aligning along the <110> direction. Within the adlayer structures, the adenine molecule is suggested to have its molecular plane tilted towards the surface normal. This molecular orientation also accounts for the observation of the $-NH_2$ scissoring vibration in the RAIR spectra.

At high coverage, the ordering of adenine adlayer structures is strongly influenced by the annealing temperature; this is considered as the main driving force responsible for the significant molecular diffusion occuring on the surface. At room temperature, adenine molecules aggregate to form disordered islands on the terraces. Upon annealing to 440 K, relatively ordered chains grow along the <110> direction are formed; this phase is only kinetically stable and was replaced by well ordered dimer chains after the sample was annealed to 490 K. The evolution of several adlayer structures, increasing in order as a function of the annealing temperature suggests that the diffusion barrier of adenine on the Cu(110) surface is relatively high.

New phase of chiral related domains were observed after depositing adenine onto the substrate maintained at 490 K. Within the domains, adenine molecules are believed to be chemisorbed on the surfaces and bind with the copper atoms via the ring imino N(7) atoms, along with partial contribution from the interactions between the amino N atoms and copper atoms. Hence, it is suggested that the strong adsorbate-substrate interaction and the directional intermolecular double hydrogen bond are responsible for the formation of 2D chirally related molecular arrays. In the proposed structural models, two types of hydrogen bonded pairs, referred as $\mathbf{A_5A_5}$ and $\mathbf{A_2A_2}$, are involved; the corresponding molecular orientations in the models are not only in favour of the formation of the most stable adenine pair, $\mathbf{A_5A_5}$, but also facilitate the interaction of amino N7 atoms with the underlying substrate atoms.

At a low deposition rate, new adlayer structures were formed when the adenine molecules were deposited on Cu(110) surfaces upon annealing to 490 K. Alongside the chirally related dimer chains reported previously [1], ladder chains and one-

dimensional linear chains growing along the <110> high symmetry direction of the substrate were revealed in the experiment. After detailed analysis of the STM images of these new structures, we presented the gas-phase homo-chiral structure models composed of three types of H-bonded dimers for the ladder chains; the corresponding pairs are denoted as $\mathbf{A_5A_5}$ and $\mathbf{A_3A_3}$, and $\mathbf{A_1A_5}$ or $\mathbf{A_1A_1}$. The one-dimensional chain is suggested to consist of the dimers $\mathbf{A_5A_5}$ that are connected by the H-bond site 1 along the chain growth direction. For all the structural models, the amino N atom is allocated to either the on-top site or close to the on-top site in order to facilitate the N-Cu interaction. The inter-molecular H-bonds and strong-substrate interactions are the driving forces for the formation of various structures.

At very low coverage, chirally related adenine dimers and trimers were observed on the Cu(110) surface upon annealing to 440 K. The coexistence of both dimers and trimer species suggests a new formation mechanism for the adenine chains. At low coverage, adenine molecules prefer to form the stable dimer, $\mathbf{A_5A_5}$, upon low temperature annealing. When the dimer is formed, its diffusion across the free surface is restricted due to the increase in the diffusion barrier. Hence, rather than the connection of the dimers, other single molecules of the same chirality can diffuse to interact with each dimer in two directions via the third type of H-bond, site 6; this leads to the formation of the different trimers observed on the surface. After further annealing to higher temperature, these small molecular clusters diffuse again to form the ordered chain structures.

STM investigations of the intramolecular contrast of the adenine adsorbate in the ordered chains and monomers at room temperature and 70 K have been conducted. It revealed that both the relative orientation of each chiral chain with respect to the fast scanning direction and the magnitude and polarity of the tip-sample bias voltage could influence the contrast appearance of the adsorbates. At both room temperature and 70 K, adenine chiral chains oriented almost along the fast scanning direction, regardless of the respective chirality, are characterized by two bright circular spots arranged side by side, while the chiral chains aligned at a certain angle with respect to the fast scanning direction are composed of two elongated features oriented in parallel. Different submolecular contrasts of the adsorbates in the chains were also observed upon changing the magnitude and polarity of the applied bias. Comparison of the contrast of the single adsorbate with the shape of molecular HOMOs and LUMOs

implies that the tunnelling of adenine on Cu(110) surfaces occurs via a resonance mechanism, arising from the coupling of the molecular orbitals with the tip and sample Fermi levels.

3.4 References

1. Q. Chen, D. J. Frankel and N. V. Richardson, *Langmuir*, 18, **2002**, 3219.
2. B. P. Nelson, T. E. Grimsrud, M. R. Liles, R. M. Goodman and R. M. Corn, *Anal. Chem.* 73, **2001**, 1.
3. R. M. Ostroff, D. Hopkins, A. B. Haeberli, W. Baouchi and B. Polisky, *Clin. Chem.* 45, **1999**, 1659.
4. S. Storri, T. Santoni, M. Minunni and M. Mascini, *Biosens. Bioelectron*. 13, **1998**, 347.
5. S. J. Sowerby, W. M. Heckl and G. B. Petersen, *J. Mol. Evol*. 43, **199**6, 419.
6. S. J. Sowerby and W. M. Heckl, *Origins Life Evol. Biosphere*, 28, **1998**, 283.
7. S. J. Sowerby, P. A. Stockwell, W. M. Heckl and G. B. Peterson, *Origins Life Evol. Biosphere*, 30, **2000**, 81.
8. S. J. Sowerby, N. G. Holm and G. B. Peterson, *Biosystems*, 61, **2001**, 69.
9. Q. Chen and N. V. Richardson, *Nat. Matter*. 2, **2003**, 324.
10. R. E. A. Kelly and L. N. Kantorovich, *Surf. Sci*. 589, 2005, 139.
11. H. Tanaka, T. Nakagawa and T. Kawai, *Surf. Sci*. 364, **1996**, L575.
12. T. Kawai, H. Tanaka and T. Nakagawa, *Surf. Sci*. 386, **1997**, 124.
13. M. Furukawa, H. Tanaka and T. Kawai, *Surf. Sci*. 392, **1997**, L33.
14. M. Furukawa, H. Tanaka, K. Sugiuva, Y. Sakata and T. Kawai, *Surf. Sci*. 445, **2000**, L58.
15. M. Furukawa, H. Tanaka and T. Kawai, *J. Chem. Phys*. 115, **2001**, 3419.
16. M. Lukas, R. E. A. Kelly, L. N. Kantorvich, R. Qtero, W. Xu, E. Lœgsgaard, I. Stensgaard and F. Basenbacher, *Jour. Chem. Phys*. 130, **2009**, 024705.
17. R. E. A. Kelly, W. Xu, M. Lukas, R. Otero, M. Mura, Y. J. Lee, E. Lœgsgaard, I. Stensgaard, L. N. Kantorovich and F. Basenbacher, *Small*, 4, **2008**, 1494.
18. J. E. Freund, M. Edelwirth, P. Kröbel and W. M. Heckl, *Phys. Rev.* B 55, **1997**, 5394.
19. M. Edelwirth, J. Freund, S. J. Woerby and W. M. Heckl, *Surf. Sci*. 471, **1998**, 201.
20. L. M. A. Perdigão, P. A. Staniec. N. R. Champness, R. E. A. Kelly, L. N. Kantrovich and P. H. Beton, *Phys. Rev*. B 73, **2006**, 195423.
21. A. McNutt, S. Haq and R. Raval, *Surf. Sci*. 531, **2003**, 131.
22. M. Preuss, W. G. Schmidt and F. Bechstedt, *Phys. Rev. Lett*. 94, **2005**, 236102.
23. T. Yamada, K. Shirasaka, A. Takano and M. Kawai, *Surf. Sci.* 561, **2004**, 233.

24. E. Rauls, S. Blankeburg and W. Schmidt, S*urf. Sci*. 602, **2008**, 2170.
25. V. Feyer, O. Plekan, K. Prince, F. Šutara, T. Skála, V. Cháb, V. Matolín, G. Steniut and P. Umari, *Phys. Rev*. B 79, **2009**, 155432.
26. M. Furukawa, T. Yamada, S. Katano, M. Kawai, H. Osegawara and A. Nillson, *Surf. Sci*. 601, **2007**, 5433.
27. R. E. A. Kelly, Y. J. Lee and L. N. Kantorovich, *J. Phys. Chem.* B, 109, **2005**, 11933.
28. J. D. Watson and F. H. C. Crick, *Nature*, 171, **1953**, 737.
29. W. Sanger, *Principles of Nucleic Acid Structure*; Spinger: New York, **1984**.
30. M. D. Segall, *J. Phys.: Condes. Matt.* 14, **2002**, 2957.
31. J. Sponer, J. Leszczynski and P. Hobza, *Biopolymers*, 61, **2001**, 3.
32. Q. Chen and N. V. Richardson, *Progress in Surface Science*, 73, **2003**, 59.
33. F. Ortman, W. G. Schmidt, and F. Bechstedt, *Phys. Rev. Lett*. 95, **2005**, 186101.
34. E. D. Williams and N. C. Bartelt, *Science*, 251, **1991**, 393.
35. K. Tomita, T. Izuno and T. Fujiwara, *Biochem. Biophys. Res. Commun*. 54, **1973**, 96.
36. P. deMeester and A.C. Skapski, *J. Chem. Soc. Dalton Trans*. **1973**, 424.
37. D. B. Brown, J. W. Hall, H. M. Helies, E. G. Walton, D. J. Hodgson and W. E. Halfield, *Inorg. Chem*. 16, **1977**, 2675.
38. A. Terzis, A. Beauchamp and P. Rivest, *Inorg. Chem*. 12, **1973**, 1166.
39. P. DeMeester and A. Skapski, *J. Chem. Soc*. A, **197**1, 2167.
40. E. Sletten, *Acta Crystallogr*. B 25, **1969**, 1480.
41. M. J. Zaworotko, H. H. Hammud, A. Kabbani, G. J. McManus, A. M. Ghannoum and M. S. Masoud, *J. Chem. Crystallogr*. 39, **2009**, 853.
42. T. Nakamor, H. Abe, T. Kanamori and S. Shibata, *Jap. J. Appl. Phys*. 27, **1899**, 1265.
43. S. J. Stranick, M. M. Kamma and P. S. Weiss, *Surf. Sci*. 338**, 1995**, 41.
44. A. Kühnle, *Current Opinion in Colloid & Interface Science*, 14, **2009**, 157.
45. B. G. Briner, M. Doering, H. P. Rust and A. M. Bradshaw, *Science*, 278, **1997**, 257.
46. J. Tersoff and D. R. Hamann, *Phys. Rev*. B, 31, **1985**, 805.
47. M. M. Ramos, A. M. Stoncham, A. P. Sutton and J. B. Pcthica, *J. Phys.: Condens. Matter*. 2, **1990**, 5913.

48. M. M. D. Ramos, A. P. Sutton and A. M. Stoneham, *J. Phys.:Condens. Matter*. 2, **1991**, S127.
49. P. Zeppenfeld, *New Sci*. 20, **1991**, 1757.
50. P.Sautet, *Chem. Rev*. 97, **1997**, 1097.
51. H. S. Lee, S. Iyengar and I. H. Musselman, *Langmuir*, 14, **1998**, 7475.
52. D. Cyr, B. Venkataraman, G. W. Flynn, A. Black and G. M. Whiesides, *J. Phys. Chem*. 100, **1996**, 13747.
53. C. L. Claypool, C. L. F. Faglioni, W. A. Goddard, H. B. III. Gray, N. S. Lewis and R. A. Marcus, *J. Phys. Chem.* B, 101, **1997**, 5978.
54. L. Giancarlo, D. Cyr. K. Muyskenes and G. W. Flynn, *Langmuir*, 14, **1998**, 1465.
55. J. Fisher and P. E. Blöchl, *Phys. Rev. Lett*. 70, **1993**, 3263.
56. P. Sautet and C. Joachim, *Chem. Phys. Lett*. 185, **1991**, 23.
57. T. Schimizu and M. Tsukada, *Solid State Commun*. 87, **1993**, 193.
58. D. F. Padowitz and R. J. Hamers, *J. Phys. Chem.* B, 102, **1998**, 8541.
59. T. Schimizu and M. Tsukada, *J. Vac. Sci. Technol*. B, 12, **1994**, 2200.
60. D. Zundel, A. Müller, H. Ratajczak, W. Junge and E. Diemann, *Studies in Physical and Theoretical Chemistry*, 78, **1992**, 313.
61. S. J. Sowerby, M. Edelwirth, M. Reiter and W. M. Heckl, *Langmuir*, 14, **1998**, 5195.
62. D. M. Cyr, B. Venkataraman and G. W. Flynn, *Chem. Mater*. 8, **1996**, 1600.
63. N. J. Tao, Phys. *Rev. Lett.* 76, **1996**, 4066.
64. L. Giancarlo, D. Cyr, K. Muyskens and G. W. Flynn, *Langmuir,* 14, **1998**, 1465.
65. E. Shaper, J. Yi, H. Cohen, A. B. Kotlyar, G. Cuniberti and D. Porath, *J. Phys. Chem.* B 109, **2005**, 14270.

CHAPTER IV

(*R, S*)-phenylglycine on Cu(110) Surfaces

4.1 (*R, S*)-phenylglycine

Phenylglycine is an aromatic amino acid in which one of the α-carbon hydrogen atoms of glycine, NH_2CH_2COOH, is replaced with a phenyl ring, making it an inherently chiral molecule. Like all the other amino acids, phenylglycine can take on various chemical structures. In the solid state, it is a white polycrystalline solid and exists in zwitterionic form, $NH_3^+CHPhCOO^-$. In solution, it has forms ranging from cationic through zwitterionic to anionic as the acidity of the solution decreases [1]. Different forms of phenylglycine salts, *e.g.* $NH_2CHPhCOOK$ [2], are expected in solution containing metal ions. Non-ionic forms can only be obtained in gas phase or matrix conditions [3].

In Figure 4.1, the structural configurations of the (*S)*- and (*R*)-phenylglycine in the gas phase and the conversions of phenylglycine species in different forms are shown. The inter-conversion between different phenylglycine species can be achieved via changing the pH value of the solution. Non-ionic phenylglycine consists of three functional groups, the phenyl ring, amino group and carboxylic group; each of them is capable of giving rise to a series of characteristic peaks in the infrared spectra, which is of great help in the determination of its bonding geometry and molecular orientation at metal surfaces.

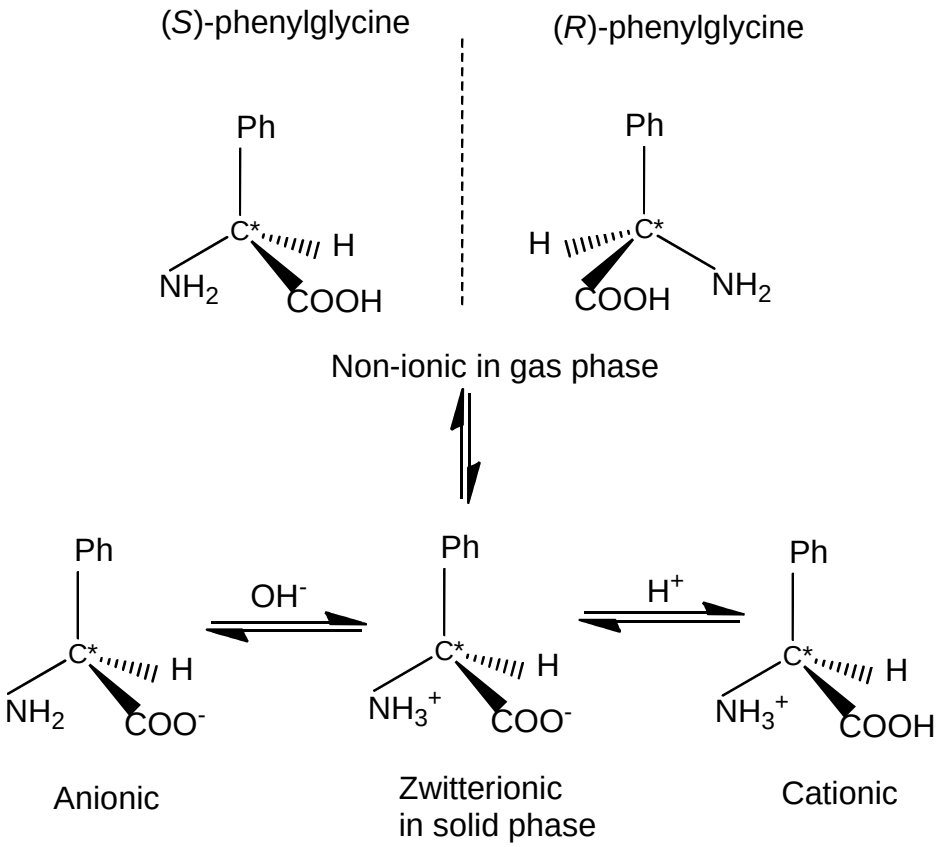

Fig. 4.1: The structure of (*R*)- and (*S*)-enantiomers of phenylglycine molecule, and the conversions of phenylglycine species between different forms.

Interactions of amino acids, especially glycine [4-6], alanine [7-10], the simple amino acids, on metal surfaces have been studied extensively using scanning tunnelling microscopy (STM), infrared spectroscopic methods and other surface sensitive techniques [4-10]. So far, a large number of different ordered enantiomeric overlayer structures have been reported upon adsorption of amino acids on copper substrates. These structures are the result of relatively strong adsorbate-substrate interactions and extensive intermolecular hydrogen bonding, originating from the hydrogen atoms of the amino group and the oxygen atoms of the carboxylate group. The chiral nature of amino acids and the existence of multi-functional groups, with each being capable of coordinating with the copper atoms in a strong manner, upon adsorption can not only bestow unique chirality to a surface, but also provide the possibility to tailor the surface

properties. Therefore, a good knowledge of the behaviour of amino acids at metal surfaces is of great significance in the preparation of biosensor and biocompatible materials [11] and heterogeneous catalysis for enantioselective reactions [12].

Phenylglycine is an appropriate model for studying the aromatic ring-interaction and cation-π (aromatic) interactions widely present in biological systems [2]. Additionally, the intrinsic chiral nature of phenylglycine makes it capable of forming chirally separated domains, when a racemic mixture of (*R*)- and (*S*)-phenylglycine is deposited onto the Cu(110) surface. LEED analysis suggests phase separation of the two enantiomers on the Cu(110) surface is mediated by the strong substrate-adsorbate interactions, the steric limitations arising from the aromatic rings and the requirements of the unique configurations possessed by the (*S*)- and (*R*)-enantiomers of phenylglycine [13]. Spectroscopic studies of the bonding of (*R*)-phenylglycine on Cu(110), using impact scattering EELS [14], indicate an almost on-top adsorption for both the oxygen and nitrogen atoms with the phenyl ring plane tilted close to the surface normal, Figure 4.2 a. This geometry was derived from a saturation coverage followed by annealing to 450 K. Additionally, investigation of the interaction of phenylglycine with colloidal silver in solution, using Raman Spectroscopy and Surface Enhanced Raman Spectroscopy (SERS), has revealed a slightly different adsorption geometry. In this case, the anionic phenylglycine coordinates with the metal atoms via both its amino and carboxylic functional groups, but with the carboxylate binding through a single oxygen atom in a unidentate manner, and with its phenyl ring being oriented nearly perpendicular to the surface [1], Figure 4.2 b.

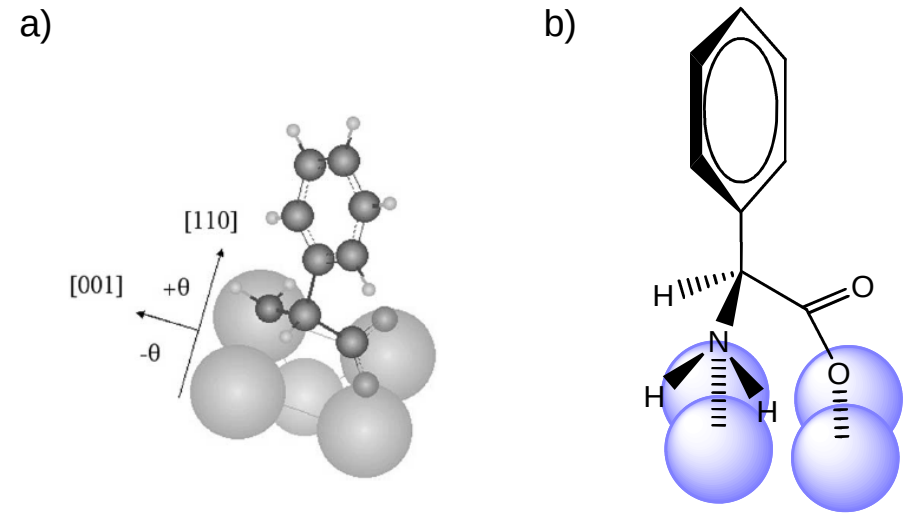

Fig. 4.2: a) Proposed structural model of (*R*)-phenylglycine anion adsorbed on the Cu(110) surface [14], b) Proposed adsorption geometry of α-phenylglycine anion adsorbed on colloidal silver [1].

Here we present RAIR spectra of (*R, S*)-phenylglycine vacuum deposited on Cu(110) surfaces as a function of coverage, with the aim of studying the chemical state and bonding manner which phenylglycine adopts when it bonds to metal surfaces at room temperature. Vibrational studies of amino acids on metal surfaces are quite complex, given that the interaction can take place through one or two functional groups or even through the additional functional group in its α-position, *e.g.* the aromatic ring of phenylglycine. RAIRS is particularly suitable for studying this adsorption system because of its strong ability in distinguishing different functional groups. By applying the surface selection rule, it can help us to confirm the molecular orientation with respect to the surface, previously suggested by EELS [14]. According to this rule, only the vibration having a significant component of its dipole moment perpendicular to the surface contributes to the observed vibrations.

4.2 Results and Discussions

In order to interpret the RAIR spectra of phenylglycine adsorbed on the Cu(110) surface and determine the bonding nature of the adsorbed species to the substrate, it is helpful to consider the vibrational assignments of the phenylglycine in various structures. Each form can be distinguished via the examination of the characteristic bands associated with the main functional groups present in the respective species. The main difference is expected to correspond to these vibrations arising from the carbonyl (C=O) and $-NH_2$ group in non-ionic form in comparison with the carboxylate ($-COO^-$) and $-NH_3^+$ groups in the ionized form.

4.2.1 KBr spectrum and DFT calculations of phenylglycine ionic species

Table 1 lists the proposed assignments of the characteristic vibrational frequencies of the solid-state phenylglycine spectrum with comparison to the DFT calculations of the anionic and zwitterionic forms. The vibrational assignments were done based on the experimental IR spectra of potassium (*R, S*)-phenylglycinate [2], Table 1. Note that unambiguous assignments of the vibrational modes to localized functional groups are very difficult due to the extensive intermixing of the vibrational modes below 1600 cm^{-1}. These modes mainly arise from deformation vibrations of in plane C-H modes and C-C stretching which arise from the aromatic ring and the chiral C atom, superimposed with deformation vibrations associated with $-NH_2$ or $-NH_3^+$. However, the asymmetric (-1600 cm^{-1}) and symmetric (-1400 cm^{-1}) carboxylate stretches of the carboxylate functionality, $-COO^-$, should be clearly distinguishable from the carbonyl (C=O) stretch (1720 cm^{-1}) of the acid group, -COOH. Thus, a detailed analysis of the changes in vibrational modes associated with carboxyl and amino group will enable us to estimate the bonding nature of phenylglycine with metal atoms, accordingly, its molecular orientation with respect to the surface plane.

Table1. Comparison of the experimental frequencies (cm^{-1}) of the characteristic bands of phenylglycine with those calculated for phenylglycine anion, and sodium phenylglycinate using GAUSSIAN 03 DFT method and the B3LYP functional with the 6-31G*(d) basis set

Assignment	Experimental spectra		Calculated spectra Corrected as n/p = 1.0087-0.0000167*p [15]	
	$NH_3^+CHPhCOO^-$ (solid KBr)	$NH_2CHPhCOOK$ [2]	$NH_2CHPhCOO^-$ (*Calculated*) (Intensity)	$NH_3^+CHPhCOONa$
ω CH(out-if ring), $\nu C^*\text{-}CO_2$	737(m), 694(s)	892(w), 838(s)	845(33) 827(176)	756(48), 710(36)
ω NH_2, νC^*N	917(m),844(w)	911(s)	948(176)	891(42)
ρ_t CH(out- ring)		984(vw), 930(w)	971(12), 959(7)	944(10),913(28)
$\rho_t NH_2$, $\rho_r CH$, C^*H bending,	1267(w) 1201(m) 1127(w)	1327(m), 1254(w), 1197(w)	1304(60), 1280(60), 1155(55)	1365(29), 1272(20), 1199(20)
$\nu_s OCO^-$, $\rho_t NH_2$	1350(m)	1355(s)	1321(212)	1375(213)
$def_s NH_3^+$	1400(s)			1439(336)
$\nu_{ring}C=C$, ρ_r CH, C*H bending	1513(vs), 1449(m)	1495(m),1452(m)	1505(12), 1371(11)	1475(10)
$\nu_{ring}C=C$, δNH_2	1553(m)	1540(s)	1613(70)	1620 (1), 1606(1.9)
δNH_2 or $def_{as}NH_3^+$	1579(m)		1621(199),	1662(30), 1625(22)
δNH_2, ν_{asym} OCO^-	1612(s)	1608(vs)	1686(299),	1676(317)
νNH^+	2935(w)			2941(300)
νC^*H	2988(w)	2954(vw)	2923(42)	3006(4)
$\nu_{ring}CH$	3067(w)	3063(w)	3050(36), 3039(68)	3073(8), 3036(5)
$\nu_s NH_2$		3302(vw)	3247(61)	3287(65)
$\nu_{as}NH_2$		3378(m)	3351(6)	3350(76)

Description of the symbols: ν-stretching, ρ_r-rocking, ρ_t-twisting, ω-wagging, δ-scissoring, def-deformation. Abbreviations: s-symmetric, as-asymmetric, Very strong-vs, Strong-s, Very weak-vw, Weak-w, Medium-m.

A comparison between the experimental infrared spectrum of solid-state phenylglycine and the vibrational frequencies of zwitterionic phenylglycine obtained from theoretical calculation is given in Figure 4.3a and b. From the spectra we can see a slight downward shift associated with the carboxylate group vibrations in the Infrared spectrum of solid phenylglycine in comparison with these obtained from the theoretical calculation of zwitterionic form. In the high frequencies region, we tend to assign the broad band found at 2935 cm^{-1} with medium intensity to the NH stretching vibrations of the ionized NH_3^+ instead of the C^*-H stretching mode, even though they tend to appear in a similar region, around 3000 cm^{-1}. According to the theoretical spectrum, the N-H stretching appears to be a very strong band in the lower frequency region in comparison with the weak peak attributed to the ring C-H stretching, which is found at 3067 cm^{-1} in the experimental spectrum. Besides, the apparent broadening and downward shift associated with the N-H stretching also indicates the presence of extensive intermolecular hydrogen bonding in the phenylglycine crystalline.

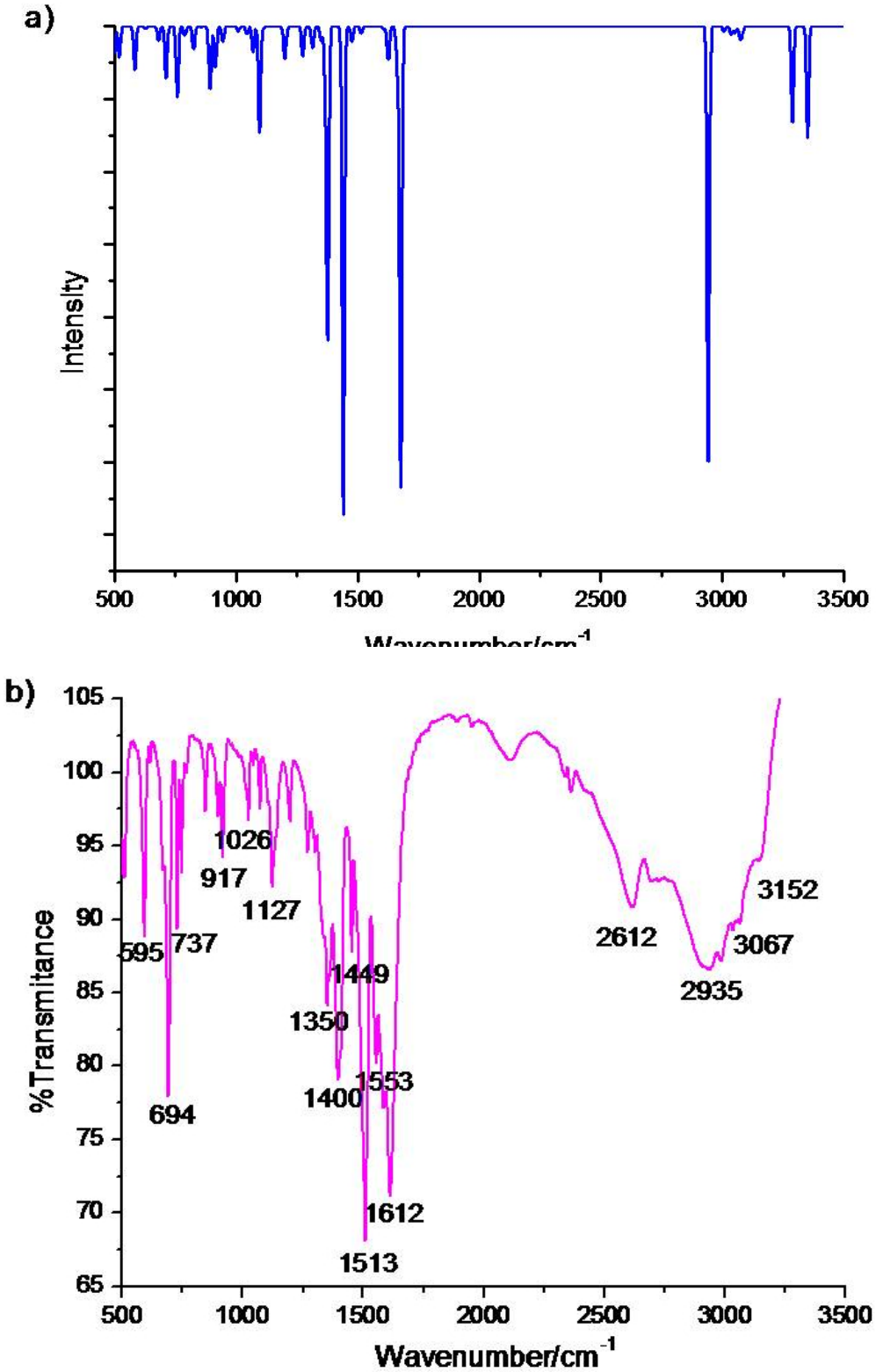

Fig. 4.3: The comparison of the theoretical IR spectrum of sodium phenylglycinate, $NH_3^+CHPhCOONa$, calculated using DFT method **a),** and the experimental IR spectrum of crystalline phenylglycine **b)**.

In the frequency region below 1700 cm^{-1}, several high to medium intensity bands are observed. The band at 1612 cm^{-1} with high intensity is assigned to the asymmetric stretching of the OCO^- group, superimposed with the NH_2 scissoring mode or more exactly the NH_3^+ asymmetric deformation mode. The neighbouring vibration, found at 1400 cm^{-1}, is accordingly assigned to the symmetric deformation of the NH_3^+ group, based on the assignments of the phenylglycine in zwitterionic form. It is difficult to assign the vibrations associated with the $-NH_2$ group and ionized NH_3^+ due to the similar region where the vibrations usually appear. The observation of a strong peak at 1350 cm^{-1}, originating mainly from a symmetric OCO^- stretch with partial contribution from a NH_2 twisting or a NH_3^+ deformation vibrational mode, is considered as strong evidence of the existence of COO^-, carboxylate group, rather than the carboxyl acid uniquely belonging to the non-ionic amino acids. There is a large amount of intermixing between the vibrational modes related to the NH_2 twisting or the NH_3^+ asymmetric deformation, the phenyl ring C-H in-plane and the C*-H bending modes, including partial contributions from the C*-N stretching mode. These frequencies are relatively weak and are supposed to be observed between 1400 cm^{-1} and 1100 cm^{-1}, according to the calculated IR vibrational frequencies. Here we assign the peak appearing around 1267 cm^{-1}, 1201 cm^{-1} and 1127 cm^{-1} to the in-plane C-H twisting intermixing with the vibrations related to C*-H bending and C-C*-C stretching modes. The medium intense vibration at 917 cm^{-1} is assigned to the NH_3^+ wagging mode including the contribution of the ionized amino group and the C*-N stretching. There is a band at around 694 cm^{-1} with high intensity which is mainly associated with the phenyl ring C-H out-of plane wagging, with a contribution from the C*-CO_2 stretching along with the OCO^- wagging modes; the out-of-plane vibrational modes are accounting for the low intensity bands observed in the neighbouring region. The observation of vibrations associated with the asymmetric and symmetric stretch of the carboxylic group provides convincing evidence of the existence of phenylglycine in ionic form.

Due to the limitation of the infrared detector and beam splitter, vibrations below 600 cm^{-1} are not detected. The assignments of most of the vibrations are in good agreement with the results of the experimental infrared spectra corresponding to the ionic phenylglycine. Distinguishing between the phenylglycine anion and zwitterion merely from the infrared spectra is not experimentally applicable due to the fact that the $-NH_2$ and NH_3^+ vibrations appear in a similar region; in addition, the considerable

intermixing with the phenyl ring skeletal deformations also complicates the spectrum. From the corresponding theoretical calculation results, two characteristic vibrations of high intensity, associated with NH_3^+ stretching and deformations, are expected to be observed at 2941 cm^{-1} and 1439 cm^{-1}. From the experimental spectra, we can see that the frequency associated with the carboxylate group tends to shift downward *ca*. 25-50 cm^{-1} in comparison to the calculated frequencies for the isolated phenylglycine species, as result of the massive intermolecular hydrogen bonding involved in the solid phase.

4.2.2 RAIR spectra of (*R, S*)-phenylglycine/Cu(110)

Infrared spectroscopy is taken as a useful method to determine the way in which the carboxylate ions bond to a metal atom or atoms by examining the vibrational frequencies related with the carboxylate group [16, 17]. It is demonstrated that the oxygen atoms of the carboxylate group can usually coordinate with the metal surface in one of the following ways, Figure 4.4 [4]:

The unidentate mode **I** where only one oxygen atom binds to the metal with the other directing away from surface; the bidentate **II** where both oxygen atoms bind to a single metal atom, and the bridging **III** where two oxygen atoms bind to two neighbouring metal atoms at equidistance. In the first case, the coordination of the oxygen atom with the metal in a unidentate manner causes the asymmetric stretching of the carboxylate group to shift towards higher frequency while the symmetric stretching move to lower frequency [18, 19], appearing in the range of 1400 - 1620 cm^{-1}. As a result, a large separation between them, *i.e.* $\Delta\nu(OCO) = \nu_{as} - \nu_s$, is anticipated in the spectra. Previous studies of vibrational spectra of the metal (Cu, Zn) amino acids compounds [19], such as glycine [20], α-alanine [21], show that this separation is about 220 cm^{-1} [19]. The wavenumber difference becomes smaller for the bidentate coordinated carboxylate complexes; it amounts to about 180 cm^{-1} in the copper acetate complex [19], and is about 140 cm^{-1} in the spectra of alkaline carboxylate salts [1]. The last binding mode is rarely discussed in the adsorption systems; however, the separation between the asymmetric and symmetric vibrations of the carboxylate group is found too close to be that for the free carboxylate ion. Therefore, by comparing the wavenumber difference of the asymmetric and symmetric stretching vibrations of the carboxylate ion for the

metal complex with that for the adsorbed anion, we are able to estimate approximately the binding mode in the adsorption systems.

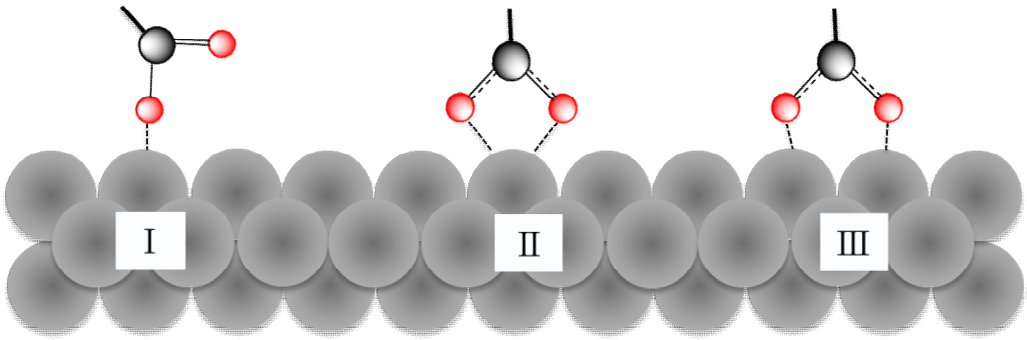

Fig. 4.4: The three binding modes that the carboxylate group coordinates to the metal atoms: I: the unidentate, II: the bidendate, III: the bridge sites

The rules mentioned above can only be used as rough guide in determining the molecular binding geometry of amino acids on the metal surfaces. In the RAIR spectra, a more general way to determine the molecular orientation and binding nature is by applying the dipole selection rule. Here, the dipole moments of the most characteristic vibrations of anionic phenylglycine are schematically illustrated in Figure 4.5. The dynamic dipole moments of the symmetric (Z) and asymmetric stretches (X) of the carboxylate group are orthogonal to each other, thus the surface selection rule can be applied to determine the orientation of the O···O axis of the carboxylate group with respect to the surface, through the comparison of the relative intensity of both vibrational modes. In the bidentate and bridge adsorption geometry where the O···O axis of the OCO^- plane is oriented parallel to surface, thus, only the symmetric stretching mode of the carboxylate group is dipole active. The intensity of this symmetric vibration decreases as the plane of the carboxylate group is tilted away from the surface normal. Both the symmetric and asymmetric stretching vibrations become observable as the carboxylate group changes to coordinate with the substrate atoms in way. In this case, the intensity of the asymmetric frequency increases as the tilt angle of the O··O axis of the carboxylate group with respect to the surface rises. The transition

of these adsorption phases can be easily determined from an apparent increase in intensity of the OCO^- asymmetric stretching vibration, which is commonly observed at around 1600 cm^{-1}; while only small intensity changes are observed for the symmetric vibration when the oxygen atoms of the carboxylate group are aligned at an inequivalent distance from the surface.

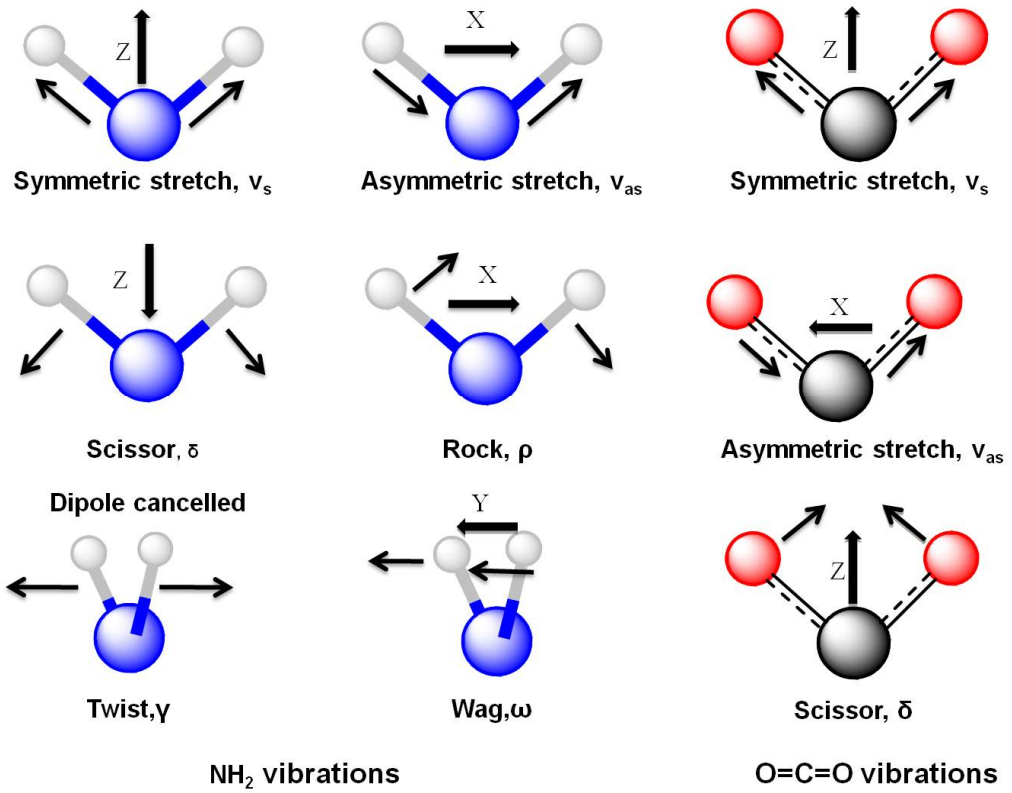

Fig. 4.5: Schematic illustration of the principal localized vibrations and the local dipole moments associated with the $-NH_2$ and $-COO^-$ functional group of phenylglycine anion.

A similar method can also be applied to determine the orientation of the amino group with respect to the surface through the investigation of the intensity associated with the $-NH_2$ scissoring mode, appearing in the range of 1500 cm^{-1}, and the wagging mode at *ca.* 1000 cm^{-1}, which have dipole moments (Z, Y) perpendicular to each other. Upon adsorption onto the surface, the scissoring mode is only observable in the IR spectra if the plane of the amino group is oriented perpendicular to the surface, which gives rise to a perpendicular dipole moment while leaves the dipole moment of the wagging mode aligning parallel to the surface. Otherwise, both vibrational modes might be observed when the plane of the amino group is aligned at a specific angle with respect to the

surface; in this case, components of both dipole moments of the scissoring and wagging modes can contribute to the IR frequencies.

Additionally, the binding nature of the amino group with the substrate can be predicted by a detailed examination of the phenyl ring in-plane and out-of-plane vibrational modes, as well as the vibrational frequency shifts related to the amino group. On the one hand, the nearly standing up orientation of a phenyl ring with respect to the surface requires the plane of the $-NH_2$ group being aligned perpendicular to the surface as a result of rigid molecular geometry; this can give rise to an enhancement of the intensity of the $-NH_2$ scissor vibration. On the other hand, the binding of the nitrogen atom of the amino group to metal atoms can produce a downward shift in frequency due to a large charge transfer from the metal to ligand, which can soften the N-H and C^*-N bonds [20].

The series of RAIR spectra shown in Figure 4.6 represent the evolution of the characteristic vibrational modes of adsorbed phenylglycine with increasing exposure time at 300 K. With increasing exposure, the saturation coverage was achieved when the intensities of all these observed frequencies stopped growing. The adsorption geometry of (*R*)-phenylglycine on Cu(110) at saturation coverage after annealing at 450 K has been studied in details using low impact scattering of EELS [14]. This revealed that phenylglycine adopts an on-top adsorption of both oxygen atoms and nitrogen atom.

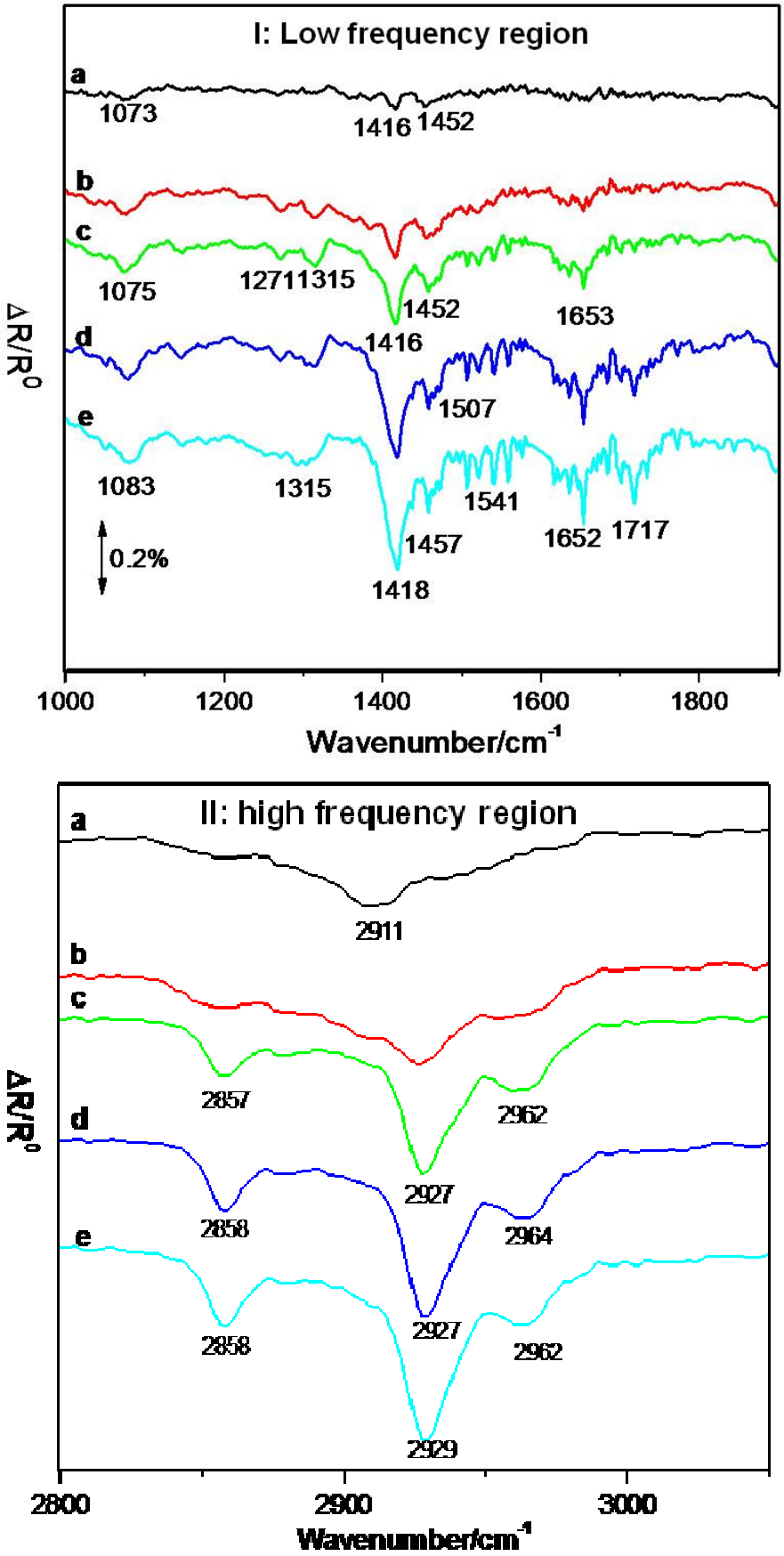

Fig. 4.6: RAIRS spectra of phenylglycine on Cu(110) surface representing evolution of the vibrational modes with increasing coverage. The overall spectra are divided into two regions: I) the lower frequencies region, namely finger print region, and II) the C-H region appearing around 3000 cm^{-1}. Coverage: (a) 0.2 L; (b) 0.4 L; (c) 0.6 L; (d) 0.8 L; (e) 1.0 L.

The proposed assignments of the infrared frequencies observed at room temperature for the low coverage, medium and saturation coverage of phenylglycine are listed in Table 2, with reference to the suggested assignments from the SER spectra of phenylglycine adsorbed on silver colloid particles at pH7 [1]. The observation of the vibrations related to the carboxylate stretching rather than carboxylic stretch provides strong evidence that phenylglycine adsorbs on the Cu(110) surface in an ionic form; this finding is in good agreement with that revealed for other amino acid molecules, such as glycine [4-6] and alanine [7-10]; upon adsorption on metal substrates at sub-monolayer coverage.

Table 2. Proposed assignments of characteristic vibrations of (*R, S*)-phenylglycine adsorbed on clean Cu(110) surface at 300K, in comparison with SERS data of phenylglycine adsorbed on colloid silver surface [1]

Assignment	Low coverage	Medium coverage	Saturation coverage	SERS
ν_{ring} CH	-	2962	2962	3066
ν C*H	2911	2927	2927	2928
ν C=O(COOH)	-	-	1717	-
ν_{as} OCO^-	-	1653	1652	1640
δNH_2, νC=C	-	1636	1636	1614
νC=C, ν_{ring}CH, C*H in-plane bending	1452	1452,1507, 1541	1452,1507, 1541	1454, 1580
ν_s OCO^-, ρNH_2	1416	1418	1418	1408
ν_{ring} CH, C*H bending	-	1271,1315	1315	1253, 1209
ωNH_2	1075	1075	1083	-

Description of the symbols: ν-stretching, ω-wagging, δ-scissoring, ρ-twisting, s-symmetric, as-asymmetric

At low coverage, Figure 4.6II a, only one low intensity broad band appeared at around 2911 cm^{-1} in the high frequency region, which is mainly assigned to the C^{*}-H stretching mode. Bands at higher frequency assignable to N-H or O-H stretching are not observed, indicating the deprotonation of the -COOH group. This frequency is shifted downward by about 11 cm^{-1} with reference to the calculated frequency of phenylglycine in anionic form. This shift can be accounted by charge transfer during the chemisorption; a similar effect have been observed with the adsorption of glycine on Cu(110), where the downshift associated with CH_2 stretching is *ca.* 11 cm^{-1}[4]. The observation of the C*-H stretching mode suggests that this group is directed away from surface to generate a component of the dipole moment perpendicular to surface. The broad appearance of this feature may be attributed to the overlapping in-plane C-H and C*-H stretching modes, in this case, the phenyl ring must be tilted slightly to generate a weak dipole moment component along the surface normal.

In the low frequency region, Figure 4.6I a, the frequency at 1416 cm^{-1} is assigned to the symmetric vibration of a carboxylate functionality; the neighbouring weak band at 1452 cm^{-1} is interpreted as a contribution from the ring skeletal C=C stretch modes and C*-H bending. The absence of an intense C=O stretch vibration at 1720 cm^{-1} and the bands associated with O-H stretching indicates the adsorbed species exists as $-COO^{-}$, carboxylate group, rather than the –COOH, acid group. Furthermore, the absence of the asymmetric stretching mode of the OCO^{-} group around 1600 cm^{-1} suggests that the O···O axis of the carboxylic group is parallel to the surface with both the carboxylate oxygen atoms placed equidistantly from the metal substrate, seen from the dipole moments related to the OCO^{-}stretching modes in Figure 4.5. The weak intensity of the band associated to the symmetric $O\text{-}C\text{-}O^{-}$ stretching indicates that the plane of the carboxylate group must be tilted slightly away from the surface normal so that only a significant component of the dipole moment associated with this vibration is aligned perpendicular to the surface. This proposed adsorption geometry is consistent with the observations of the weak frequencies associated with the phenyl ring in-plane vibrational modes; the tilting of the carboxylate plane with respect to the surface normal leads to an adsorption configuration in which the plane of the phenyl ring is aligned tilted slightly away from surface.

This suggested geometry is very similar to that adopted by carboxylic acid molecules, such as formate and acetate, exposed to copper and other metals [22-26]. The plane of the carboxylic group of these adsorbed species is perpendicular to the surface with the oxygen atoms binding on-top of adjacent copper atoms along the close packed direction, the <110> direction in the case of Cu(110) surface. In this process, the acid proton leaves as H_2 or transfers to convert $-NH_2$ to $-NH_3^+$. The former suggestion of anionic adsorbed species, is more popular, considering the adsorption of amino acids onto the copper crystal. It is quite difficult to determine the nature of the $-NH_2$ group by means of IR alone, however, XPS data of (*S*)-alanine adsorbed on Cu(110) surfaces at room temperature, at the monolayer coverage, has confirmed the existence of neutral amino group [9]. The observation of frequencies associated with ring in-plane skeleton deformations, coupled with the C^*-H bending modes, indicates that the phenyl ring has to be tilted up slightly from the surface in order to produce a small dipole activity for the in-plane vibration modes.

Another weak low frequency peak is found around 1075 cm^{-1}; it is associated with the $-NH_2$ wagging vibrations and includes partial contribution from the C*-COO bending and the out of plane CH bending modes. In the suggested model, the nearly perpendicular orientation of the OCO^- plane with respect to the surface indicates the ring C-H in-plane bending modes and the $-NH_2$ scissoring vibrations will be weak since the dynamic dipole moments of these vibrations is nearly parallel to surface plane. This is also true for the C*-N stretching mode. On the other hand, given the orientation we suggested, the $-NH_2$ wagging and C^*-C bending vibration are expected to be observed because their dipole moment components are more aligned along the surface normal, although the C*-C bending mode is not intrinsically intense. It is difficult to assign this band unambiguously because of the large intermixing of these C-H bending modes with C*-N and C-C* stretches.

The adsorption geometry of the adsorbed species is proposed based on the above analysis of the observable frequencies at low coverage. As shown in Figure 4.7, phenylglycine is adsorbed in anionic form and binds with the copper atoms via the two oxygen atoms of the carboxylate group along the <110> direction. The plane of the OCO^- group is inclined towards the surface; this leads to the phenyl ring being oriented at a shallow angle from the surface plane; this molecular orientation can account for the observations of the weak frequencies arising from the in-plane vibrational modes.

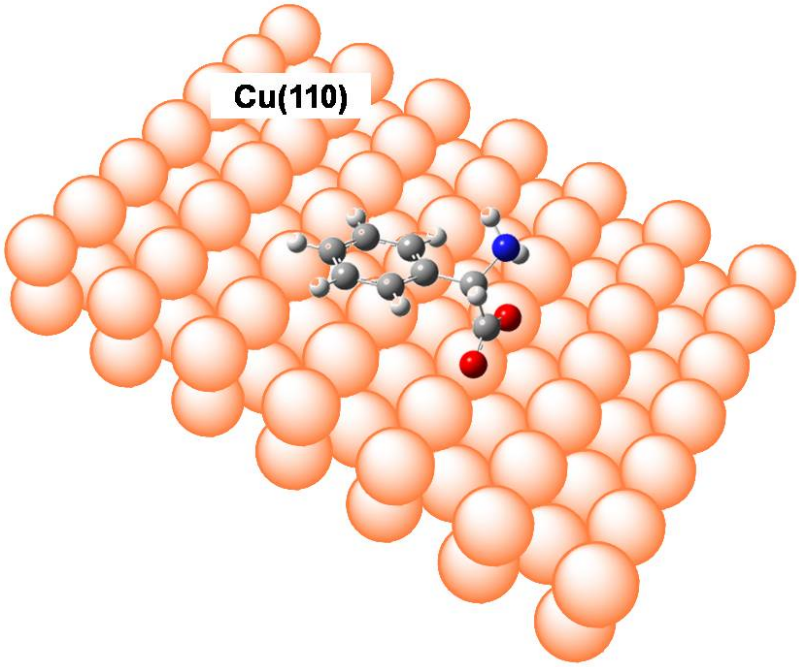

Fig. 4.7: Proposed orientation and bonding nature for phenylglycinate species on the Cu(110) surface at low coverage, where phenylglycine anion binds with the Cu atoms via both the oxygen atoms of the carboxylate group, whilst the phenyl ring is nearly parallel to the surface. The geometry of phenylglycine anion is optimized via DFT, the B3YLP function with the 6-31G*(d) basis set.

As the coverage continues to increase, Figure 4.6I b and c, some new peaks are observed and they are accompanied by an evident increase in the intensity of the frequencies already present. The most noticeable changes are the dramatic growth in the intensity of the band related to the OCO^- symmetric stretch mode. Increasing exposure leads to the symmetric (OCO^-) stretch mode becoming the dominant peak in the spectra as expected. On the other hand, a new type of adsorbed species is introduced; this is evident from the observation of a new band found at 1653 cm^{-1}, which can be easily attributed to the OCO^- asymmetric stretch mode of the carboxylate group. These observations indicate that the two oxygen atoms of the carboxylate group are placed at inequivalent distance to the copper atoms; therefore, the axis of O···O of the carboxylate group is tilted away from the surface plane. This geometry allows both

asymmetric and symmetric dipole moments of the OCO^- stretching vibrations to become active.

The wavenumber difference for the asymmetric and symmetric vibrations of OCO^-, $\Delta\nu_{(OCO^-)} = \nu_{as} - \nu_s$ amounts to 237 cm^{-1}, this value is very close to 232 cm^{-1} obtained from SERS of phenylglycine adsorbed on colloidal silver [1]. Additionally, it is also corresponds approximately to the separation measured from the spectra of glycine [4] and (*R*)-alanine [7] adsorbed in a unidentate manner on the Cu(110) surface. Such a value suggests that the coordination of the carboxylate group to the metal is unidentate with one oxygen atom tilted away from the surface to adopt a pseudoester structure R-C(=O)-O-M [27] .

This change in molecular orientation is evident with the observations of some new weak bands found at 1315 cm^{-1} and 1217 cm^{-1}. These are mainly attributed to the intermixing of the C-H in-plane rocking mode with scissoring modes and C*-H bending vibrations, following the assignments in the anionic form. These are essentially weak vibrational modes according to the theoretical frequency calculation of both anionic and zwitterionic phenylglycine, as is indicated by the slow intensity growth of this mode upon increasing coverage. The vibrations associated with the amino group also change in this process. The intensity of the $-NH_2$ wagging mode, at 1075 cm^{-1}, remains dipole active and becomes stronger, exhibiting a similar intensity to the in-plane ring vibrations, upon increasing exposure. In addition, the $-NH_2$ scissoring vibration, superimposed with the ring C=C stretching modes, is now allowed, and it is shown by the observation of the characteristic vibrations in the region of 1450 -1640 cm^{-1}. Based on this analysis, we can suggest that the plane of the $-NH_2$ group is now largely perpendicular to the surface, giving rise to a significant component of the dipole moment along the surface normal. The conclusion drawn from the investigation of the vibrations arising from the $-NH_2$ scissoring and wagging modes provides further evidence for the orientation changes of the phenyl ring, which is directed close to the surface normal upon increasing exposure.

In the high frequency region, Figure 4.6II b and c, the broad band found at 2911 cm^{-1} at low coverage, exhibits considerable broadening and upward shifting, *ca* 16 cm^{-1}, upon further deposition, and is also accompanied by evident growth in its intensity. Finally, two low intense bands are observed as shoulders to this band, found at 2927 cm^{-1} with relatively high intensity. The higher frequency band at 2962 cm^{-1} displaying weakest intensity is attributed to the ring in-plane CH stretch mode; even though each CH

stretch vibration is weak, in combination they may give rise to enhanced intensity in the spectra. The bands, found at 2927 cm^{-1}, are assigned to the C^{*}-H stretch modes; this is an intrinsically weak mode and further changes in the molecular orientation leads to its dipole moment being directed further towards the surface normal, thus enhancing its dipole activity. The lowest frequency band, found at 2858 cm^{-1}, is too low to be assigned to the CH vibrations; it might be caused by the combination of some other low frequencies below 1500 cm^{-1}.

It is suggested that further adsorption leads to significant changes in the binding nature of the adsorbed phenylglycine species. This is revealed by the observation of the asymmetric stretch mode of the carboxylate group and the $-NH_2$ scissor mode, the evident enhancements in the intensity of these bands associated with phenyl ring in-plane modes. The proposed adsorption geometry in this phase is shown in Figure 4.8, in which the phenylglycinate anion binds to the copper atoms via the nitrogen atom of the amino group and only one oxygen atom of the carboxylate group, whilst the phenyl ring is placed nearly perpendicular to the surface.

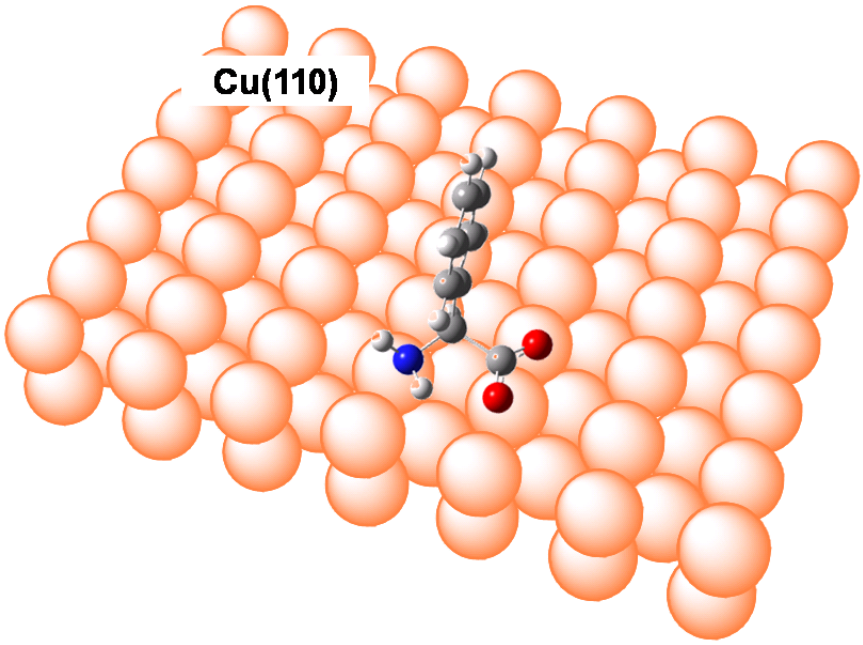

Fig. 4.8: Proposed orientation and bonding nature for phenylglycinate species adsorbed on the Cu(110) surface at medium coverage. Phenylglycine adsorbs in anionic form with the carboxylate group coordinated with the copper atoms in side-way and the nitrogen atom of the amino group placed at the on-top site.

Unlike the behaviour of glycine adsorbed on the Cu(110) surface which results in only the formation of monolayer coverage on a substrate kept at room temperature, multilayer coverage may be obtained by dosing the molecules onto the surface kept below 290 K [4]. However, in our case with phenylglycine, Figure 4.6I d and e, the saturation coverage ends with the appearance of a vibrational band found around 1717 cm^{-1}, which is related with the C=O stretch mode, a characteristic vibration of the carboxylic group from the non-ionic form of phenylglycine. There is no significant change in the general pattern of these bands already existing upon increasing the coverage successively, with the exception of a continuous increase of their intensities. The saturation coverage is reached when the intensities associated with the vibrations of the anionic adsorbed species stop growing. Further exposure of the surface to phenylglycine only lead to an increase in the intensity of the C=O stretching band.

The observation of the characteristic frequency of the C=O stretch mode can only suggest the presence of the carboxylic group in this phase; this means the phenylglycine molecule stays at the surface as a neutral molecule. However, it does not necessarily indicate the formation of multilayer adsorption in which phenylglycine is expected to exist in zwitterionic form as it is preferred in solid phase; this will give rise to some vibrations attributed to NH_3^+, especially the NH stretching mode, which is supposed to contribute with a strong peak at around 1500 cm^{-1}. Additionally, there is no evidence of large intermolecular hydrogen bonding interactions, which are expected to be observed in the region around 3000 cm^{-1}, showing a large band broadening.

The creation of two differently oriented phenylglycine species on Cu(110) surfaces is apparently influenced by the exposure time. At the low coverage, the anionic phenylglycine species is only coordinated with the oxygen atoms of the carboxylate group with its phenyl ring tilting towards the surface; this is facilitated by the availability of large free surface space. As the coverage is increased, the steric repulsion arising from the crowding in the adlayer would force the phenyl ring to be directed away from the surface. This new adsorption geometry favours interaction of the nitrogen lone pair with the surface and can reduce the footprint of the adsorbed species. The third binding geometry was revealed after annealing the surface to 450 K [13]. A detailed investigation using impact scattering in EELS reveals that phenylglycine is bonded to the surface in an anionic form via the two oxygen atoms of the carboxylic group and the nitrogen atoms, with its molecular ring aligning nearly parallel with the surface normal. Hence, we can predict that annealing to 450 K might cause desorption

of non-ionic phenylglycine, the adsorbed species remaining on the surface to rearrange and yield ordered superstructures.

4.3 Conclusions

In summary, detailed investigation of the behaviour of (*S, R*)-phenylglycine adsorption on Cu(110) surfaces has been carried out using reflection absorption infrared spectroscopy (RAIRS) at room temperature. It is revealed that both the coverage and the annealing temperature can influence the molecular orientation on the surface. At low coverage, phenylglycine is bonded via both the oxygen atoms at equidistance along the <110> direction of the Cu(110) substrate. At higher coverage, a new type of adsorption geometry is suggested in which the nitrogen atom of the amino group and only one of the oxygen atoms of the carboxylate group are participating in binding with the substrate. This binding nature is consistent with these suggested for glycine [4] and alanine [7], upon adsorption on the Cu(110) surfaces under vacuum conditions. Finally, annealing the high coverage surface leads to new molecular orientations, based on the adsorption model proposed by previous work [14].

4.4 References

1. J. J. Castro, M. R. López Ramírez, I. López Tocón and J. C. Otero, *Journal of Colloid and Interface Science* 263, **2003**, 357.
2. M. M. IIczyszyn, T. Lis, M. Wierzejewska and M. Zatajska, *Journal of Molecular Structure* 919, **2009**, 303.
3. M. E. Sanz, V. Cortijo, W. Caminati, J. C. López and J. L. Alonso, *Chem. Eur. J.* 12, **2006**, 2564.
4. S. M. Barlow, K. J. Kitching, S. Haq and N. V. Richardson, *Surf. Sci.* 401, **1998**, 322.
5. J. Hasselstrom, O. Karis, M. Weinelt, N. Wassdahl, A. Nilsson, M. Nyberg, L. G. M. Pettersson, M. G. Samant and J. Stohr, *Surf. Sci*. 401, **1998**, 221.
6. N. A. Booth, D. P. Woodruff, O. Schaff, T. Giessel, R. Lindsay, P. Baumgartel and A. M. Bradshaw, *Surf. Sci*. 397, **1998**, 258.
7. J. Williams, S. Haq and R. Raval, *Surf. Sci*. 368, **1996**, 303.
8. S. M. Barlow, S. Louafi, D. Le Roux, J. Williams, C. Muryn, S. Haq and R. Raval, *Langmuir* 20, **2004**, 7171.
9. S. M. Barlow, S. Louafi, D. Le Roux, J. Williams, C. Muryn, S. Haq and R. Raval, *Surf. Sc*i. 590, **2005**, 243.
10. D. I. Sayago, M. Polcik, G. Nisbet, C. L. A. Lamont and D. P. Woodruff, *Surf. Sci*. 590, **2005**, 76.
11. B. Kasemo, *Curr. Opin. Solid State Mater. Sci.* 3, **1998**, 451.
12. Y. Izumi, *Adv. Catal*. 32, **1983**, 315.
13. Q. Chen, C. W. Lee, D. J. Frankel and N. V. Richardson, *PhysChemComm*. 9, **1999**, 05986
14. Q. Chen, D. J. Frankel, C. W. Lee and N. V. Richardson, *Chemical Physical Letters*, 349, **2001**, 167.
15. T. Kasahara, H. Shinihara, Y. Oshima, K. Kadokura, Y. Uriu, C. Ohe and K. Itoh, *Surf. Sci.* 558, **2004**, 65.
16. K. Nakamoto, *Infrard and Raman Spectra of Inorganic and Coordination Compounds*, 4th edn, Wiley, New York, **1986**.
17. G. B. Deacon and R. J. Phillips, *Coord. Chem. Rev*. 33, **1980**, 227.
18. E. G. Palacios, G. Juárez-López and A. J. Monhemius, *Hydrometallurgy*, 72, **2004**, 139.

19. K. Nakamoto, Y. Morimoto and A. E. Martell, *Am. Chem. Soc*. 83, **1961**,4528.
20. G. C. Percy, *Spectrochim. Acta*. 32A, **1976,** 1287.
21. G. C. Percy and H. Stretton, *J. Chem. Soc.* Dalton, Trans. **1976**, 2429.
22. K. U. Weiss, R. Dippel, K. M. Schindler, P. Gardner, V. Fritzsche, A. M. Bradshaw, A. L. D. Kilcoyne and D. P. Woodruff, *Phys. Rev. Lett.* 69, **1992**, 3196.
23. D. P. Woodruff, C. F. McConville, A. L. D. Kilcoyne, T. Lindner, J. Somers, M. Surman, G. Paolucci and A. M. Bradshaw, *Surf. Sci*. 201, **1988**, 228.
24. M. Bowker and R. J. Madix, *Appl. Surf. Sci.* 8, **1981**, 229.
25. M. Bowker and R. J. Madix, *Vacuum*, 31, **1981**, 711.
26. S. Bao, G. Liu and D. P. Woodruff, *Surf. Sci.* 203, **1988**, 89.
27. G. B. Deacon and J. Phillips, *Coord. Chem. Rev*. 33, **1980**, 227.

CHAPTER V

Adsorption of (*R*, *S*)-phenylglycine and Adenine on the p(2 × 1) O/Cu(110) Surfaces

5.1 Introduction

Interactions of (*R, S*)-phenylglycine molecules with the Cu(110) substrate have been studied in details using EELS and LEED methods [1, 2]. It was revealed that at saturation coverage, phenylglycine could form ordered enantiomerically separated domains displaying $\begin{pmatrix} 5 & -3 \\ 4 & 1 \end{pmatrix}$ and $\begin{pmatrix} 5 & 3 \\ 4 & -1 \end{pmatrix}$periodicities, respectively, upon annealing at 450 K. The adsorbed species bind with the copper atoms via both the oxygen atoms of the carboxylate group and the nitrogen atom of the amino group, whilst the phenyl ring is directed nearly along the surface normal. In our studies using RAIRS, it is suggested that the adsorption geometry of phenylglycine evolves as a function of the exposure time. At low coverage, phenylglycine is more likely to interact with the substrate directly through its carboxylate group. At this coverage, the phenyl ring is, however, oriented nearly parallel to the surface plane. This adsorption geometry will generate a large footprint and facilitate the π-metal interactions through the aromatic ring. Hence, we may expect to see a new phase of overlayer structures upon low exposure time.

It has been reported that each enantiomer of phenylglycine exhibited unique preference to decorate adenine chains of specific chirality upon co-deposition on a Cu(110) surface pre-covered with ordered mirror-related adenine dimer chains [3]. This enantiomeric self-recognition achieved at molecular level can be well understood in terms of hydrogen bonds, substrate locking and Coulomb repulsion [4, 5].

Here we present STM results from the adsorption of well-defined mixture of (*R, S*)-phenylglycine onto the Cu(110) surface pre-covered with oxygen, in the attempt to understand the interactions between the amino acid molecule with the oxygen copper complex and the effect of the presence of the oxygen on the overlayer structures formed by phenylglycine at room temperature.

Chemisorption of oxygen on a Cu(110) surface is known to result in a characteristic (2 × 1) periodic structure at room temperature. In this process, dissociated oxygen

atoms interact with copper atoms to form Cu-O added rows, oriented along the <100> direction of the substrate. The O-O spacing within the row is 3.61 Å, while the spacing between neighbouring rows amounts to 5.2 Å [6]. Shown in Figure 5.1a are the double Cu-O rows appearing as chains of bright circular protrusions. The termination sites of the added Cu-O rows usually show high reactivity at low temperature. These sites are capable of inducing oxidation reactions in the presence of H_2O [7], hydrocarbons [8]; oxydehydrogenation of ammonia has been reported on Cu(110) and Cu(111) surfaces [9-11], leading to the formation of chemisorbed imide species. At room temperature, deposition of pyridine on a Cu(110) surface pre-adsorbed with oxygen shows an increase in the inter-row spacing from 5.1 to 7.7 Å [12]. Evidence of direct N-O interaction was confirmed by XPS data; STM images showed that a molecular ring is oriented perpendicular to the surface to facilitate the formation of pyridine-oxygen complex.

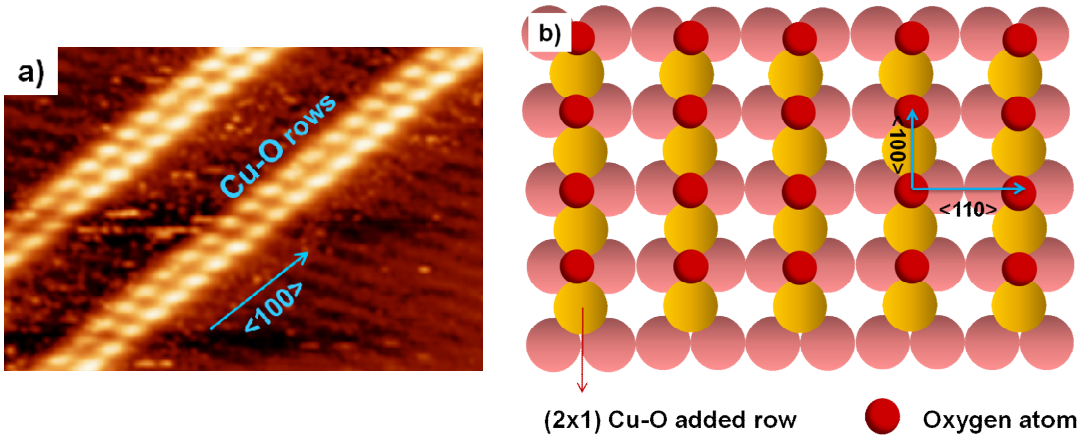

Fig. 5.1: a) STM image of the ordered oxygen rows formed on the Cu(110) surface (0.92 V, 0.90 nA, 6.9 × 4.6 nm^2). b) Schematic illustration of the p(2 × 1) added oxygen rows on the Cu(110) surface, red ball represents the oxygen atoms, they adsorb on the short bridge site of the reconstructed (2 × 1) copper substrate.

It is interesting to study the interaction of small bio-active molecules like adenine and phenylglycine molecules with the oxygen rows on Cu(110) surfaces, since both contain an amino group which could be oxidized by oxygen, leading to the formation of N-O bonds; it may also form hydrogen bonds with the adsorbed oxygen atoms when interacting in a weaker manner. In addition, different interaction mechanisms

are expected because in the adsorption of adenine on the Cu(110) surface, the strong intermolecular hydrogen bonds are the main driving force accounting for the formation of ordered overlayer structures, while the strong adsorbate-substrate interaction, mediated by intermolecular hydrogen bonding is responsible for the networks observed for phenylglycine adsorbed on Cu(110) surfaces.

5.2 Experimental

The experiments were carried out in a UHV system equipped with a rear view LEED and quadrupole mass spectrometer. Clean Cu(110) surfaces were obtained by repeated Ar^+ sputtering and annealing (800 K) cycles. The cleanliness of the surface was assessed and confirmed by the appearance of large areas of flat terraces. The racemic mixture of phenylglycine was placed in the glass tube of the home-built evaporator, attached to the chamber via a gate valve. Oxygen was introduced to the chamber via a leak valve on the gas line.

5.3 Results and discussions

5.3.1 (*S, R*)-phenylglycine on p(2 × 1)O/Cu(110) surfaces

An STM image of O-Cu rows decorated with phenylglycine molecules and a small area of phenylglycine molecular islands is given in Figure 5.2. This image was obtained after dosing a small amount of the racemic mixture of phenylglycine onto the Cu(110) surface per-covered with a small amount of oxygen at room temperature. The oxygen (2 × 1) periodic rows, appearing as depressed stripes along the <100> direction of the substrate, are easily distinguished from the bright protrusions which are recognized as molecular features of phenylglycine. The distinct difference in the contrast between these features is believed to be due to the apparent height difference and electron conductance between the phenylglycine molecules and the oxygen atoms. Within the oxygen rows, the inter-atomic distance and the spacing between neighbouring rows remain unchanged, this might indicate that phenylglycine molecules do not interact with oxygen atoms in a very strong manner. The majority of

the phenylglycine molecules show preference to grow along the oxygen rows while only a very small number of molecules forms patches in the neighbouring area. The tendency for arranging themselves close to the oxygen rows suggests that the presence of adsorbed oxygen can influence the arrangement of phenylglycine molecules on the Cu(110) surface. Inter-molecular interactions between oxygen atoms in the rows and attached phenylglycine molecules, along with the contribution from the substrate-adsorbate interactions arising from the coordination of phenylglycine to the copper atoms through its functionalities, are suggested to account for the ordered structures observed in the STM images.

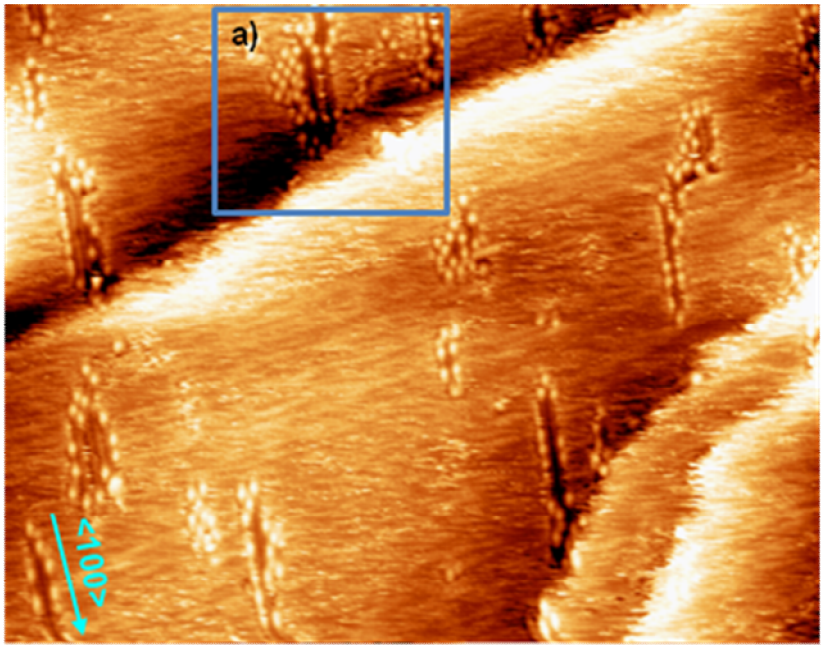

Fig. 5.2: Molecular domains and phenylglycine decorated added Cu-O rows at a low coverage (0.13 nA, -1.15 V, 73 × 58 nm^2). Selected area, **a),** indicates the coexistence of small phenylglycine patches with oxygen rows.

Shown in Figure 5.3a is a magnified image of the selected area in Figure 5.2**a)**, showing the small phenylglycine molecular domain. Within the domain, a centred nearly rectangular unit cell is identified, which has the vector **a** oriented *ca.* 10^o away from the <110> direction and the vector **b** aligned along the <100> direction of the Cu(110) substrate; a C_2 symmetry is assigned to the unit cell. The cross-sectional

dimension of the circular spot is measured to be approximately 7.0 Å; this size is close to the lateral dimension of an isolated phenylglycine anion, 5.5 Å, Figure 5.3b, the geometry of which is optimized using DFT methods and B3LYP functional with 6-31G*(d) basis set. The value suggests that the phenyl ring may be oriented nearly flat lying on the surface, which gives rise to a larger footprint than that of the standing up orientation. This finding is consistent with the suggested adsorption geometry for phenylglycine at low coverage, according to the RAIRS results. In analogy with glycine [13-15] and alanine [16-19], the simple amino acids, the adsorbed species are considered to exist in anionic form with the deprotonated hydrogen atoms leaving from the surface as H_2 following recombination. Additionally, the adsorbed molecules bind with the copper atoms via both oxygen atoms of the carboxylate group along the <110> direction; this leaves one of the hydrogen atoms of the amino group pointing upwards, while the other is pointing towards the surface plane to facilitate the formation of a hydrogen bond with the oxygen atoms of the carboxylate group of neighbouring molecules. It is difficult to distinguish the respective chirality of each phenylglycine molecule merely from the molecular appearance observed from the STM images, because both enantiomers would yield the same projection size for flat-lying adsorption geometry.

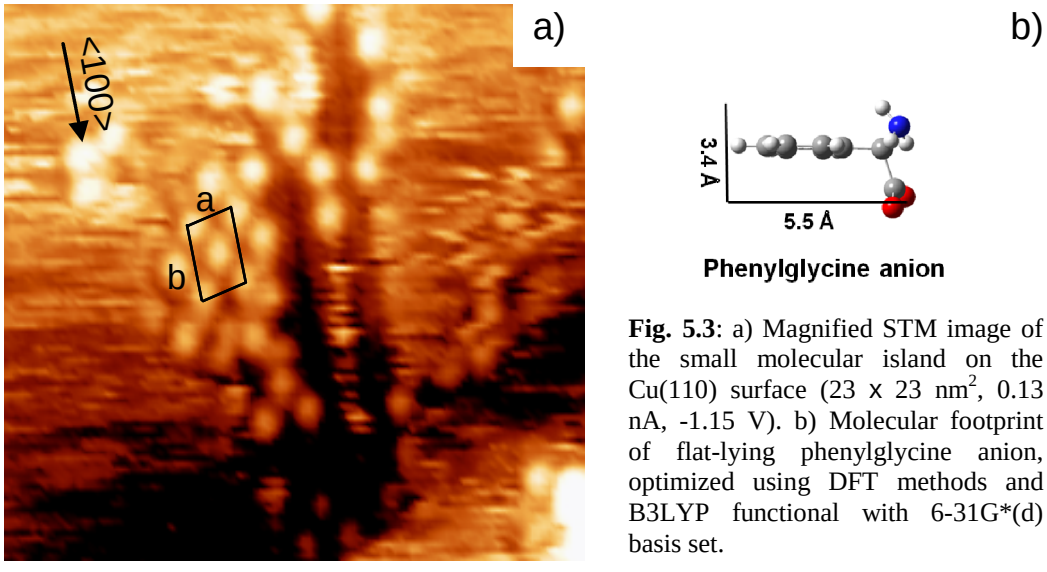

Fig. 5.3: a) Magnified STM image of the small molecular island on the Cu(110) surface (23 x 23 nm^2, 0.13 nA, -1.15 V). b) Molecular footprint of flat-lying phenylglycine anion, optimized using DFT methods and B3LYP functional with 6-31G*(d) basis set.

Within the unit cell, the intermolecular separation along the vector **a** is approximately 11.2 ± 0.3 Å and **b** is equal to 15.7 ± 0.3 Å, the size of unit cell is approximately 19 times larger than the unit mesh of the underlying Cu(110) substrate. The distances between the centred molecule and the adjacent ones along the two diagonals of the unit cell are about 8.1 ± 0.3 Å and 10.6 ± 0.3 Å. These inter-molecular distances are too large to give rise to favourable inter-adsorbate interactions originating from the hydrogen bonding. Therefore, the small area of ordered structure is an outcome of the delicate balance between the strong substrate-adsorbate interactions, due to the coordination of oxygen atoms of the carboxylate group with copper atoms, and the π-metal interaction arising from the flat-lying phenyl rings and copper substrate.

According to the measured values of the unit cell vectors, this overlayer structure is incommensurate with the substrate lattice. However, given the proposed adsorption geometry suggested at low coverage, the bonding requirement, demanded by the carboxylate group, is anticipated to result in a commensurate structure. Therefore, this discrepancy, especially with the vector aligning along the <110> direction, may imply either different adsorption sites for the carboxylate group, or possible rearrangement of the outermost copper atoms to make the local bonding of molecules to equivalent sites. Similar findings have been revealed regarding the adsorption of phenylglycine on a Cu(110) surface at saturation coverage upon annealing at 450 K [1, 2]. In the study, reconstruction in the outermost Cu layer may produce an overlayer structure with 20 atoms so that each O and N atom of the adsorbate is coordinated to a separate Cu atom. Here, we are more likely to believe that the rearrangement of copper atoms may occur in order to make all the oxygen atoms of the carboxylate group coordinate on preferential on-top sites along the <110> direction.

Based on the above analysis, we derived the structural model for the observed overlayer structures shown in Figure 5.4. In the proposed structural model, at the corners of the unit cell, all oxygen atoms of the carboxylate group are placed at the on-top sites, which are in favour of the binding between oxygen atoms and copper atoms. The calculated distance of the **a** vector is 10.8 Å, and of the **b** vector is 14.4 Å, both values are 1-2 Å shorter than the corresponding measured values, but are considered reasonable within the experimental error. The unit cell has an angle of *ca.* 115°, in good agreement with that of the measured angle. In addition, the distance

between the centred molecule that has to be accommodated closely to the on-top site, and its adjacent ones, **d1** and **d2**, are 10.6 Å and 7.3 Å, both are also in good agreement with the associated measured separations. As determined from the molecular arrangements, no intermolecular hydrogen bonding is expected in the adsorbed layer due to the slightly larger intermolecular distance. Strong adsorbate-substrate interaction and the partial π-metal interactions arising from the phenyl rings with metal surface are considered instead as the driving force behind the observed ordered structures. According to the proposed molecular arrangements on the substrate, where the centred molecule is assumed to have opposite chirality, two glide planes along the <110> direction are identified, which relate the molecules of opposite chirality together via the translational and reflectional operations. In this suggested model, all the intermolecular distances are calculated approximately in terms of the unit cell lattice of the Cu(110) substrate.

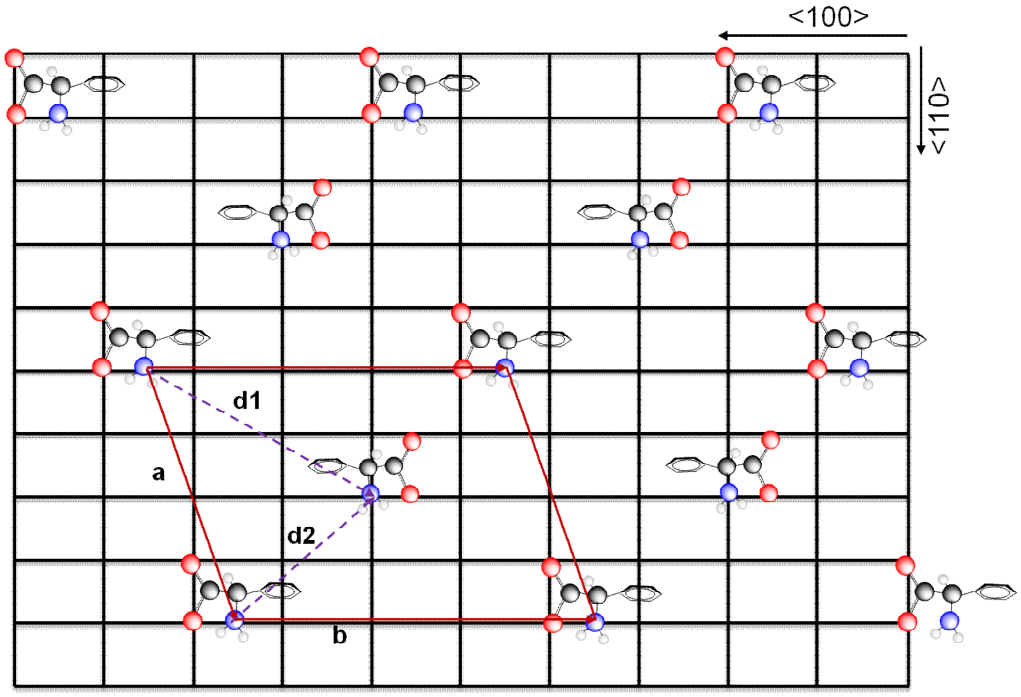

Fig. 5.4: Proposed structural model and molecular registry for the small molecular islands formed by (*R, S*)-phenylglycine molecules on the Cu(110) surface at low coverage; **a** and **b** are the unit cell vectors, **d1** and **d2** are the intermolecular distance along the diagonals.

In this proposed structural model, all oxygen atoms of the carboxylate group in the unit cell are placed on the preferential on-top sites, except that of the centred molecule that is accommodated closely to an on-top site in order to generate a perfect centred unit cell. However, it is believed that in the actual adsorption process, slight rearrangement of the substrate atoms may occur so that the bonding requirement of the oxygen atoms of the carboxylate group to the copper atoms are satisfied; this might also account for the incommensurate overlayer structures observed in STM. At low coverage, the substrate-adsorbate interactions, originating from the binding of oxygen atoms of the carboxylate with the copper, and the π-metal interactions, are main driving force accounting for the formation of the small ordered molecular islands. This is different from the overlayer structures observed at saturation coverage, which are considered to be an outcome of the compromise between the strong adsorbate-substrate bindings required by the carboxylate group and N atoms, and the intermolecular hydrogen bonds [1, 2]. Additionally, it is difficult to assign the chirality of centred molecule merely from the STM. However, as far as the suggested structural model is concerned, molecules of either chirality can give rise to the same molecular arrangements on the surface.

5.3.2 (*R, S*)-phenylglycine decorated added Cu-O rows

Shown in Figure 5.5a, is the close-up STM image of the added Cu-O rows that are decorated by randomly distributed phenylglycine molecules appearing as circular protrusions. As seen from the image, phenylglycine shows a strong preference to grow at both ends of the oxygen rows, while alongside these rows they are more likely to exist in pairs. There are no apparent variations in the inter-row distance of the Cu-O rows as determined from the image. Therefore, we assume that phenylglycine molecules are connected with the Cu-O rows mainly through hydrogen bonds formed between one of the hydrogen atoms of the amino group and the oxygen atoms forming the rows. The relative chirality corresponding to each protrusion cannot be determined because of the low resolution of the STM images. Considering the suggested flat-lying adsorption geometry, both enantiomers are expected to give rise to the same projection on the surface plane.

In the Figure 5.5b, structural model for the phenylglycine molecules decorating the oxygen rows is proposed. The orientation of each enantiomer is restricted by not only the binding requirements of two oxygen atoms of the carboxylate group with the copper substrate along the <110> direction, but also by the hydrogen bonds forming between the hydrogen atoms of the amino group and the oxygen atoms in the Cu-O added rows. DFT geometry optimization shows that H···O distance is *ca.* 2.1 Å in anionic phenylglycine; this might give rise to a less favourable N-H···O interaction in the overlayer. However, since the adsorption of oxygen on Cu(110) surfaces leads to the formation of (2 × 1) oxygen island on the top layer, the surrounding surface where the phenylglycine is adsorbed is not reconstructed; it is mono-atomic, *ca.* 1.28 Å lower than the topmost layer of added Cu-O rows [20]. As a result, this may facilitate the hydrogen bond interactions between the hydrogen atoms of the amino group and the oxygen atoms existing in the middle of the added Cu-O rows or at the ends of them. Also due to the enhanced activity of these terminal oxygen atoms, phenylglycine molecules are more likely to appear at both ends of the oxygen chains. It is believed that there is not a rule governing the specific chirality of each phenylglycine molecule attached to the rows; the hydrogen bonding can be formed between the oxygen atom and the phenylglycine molecules of either chirality randomly.

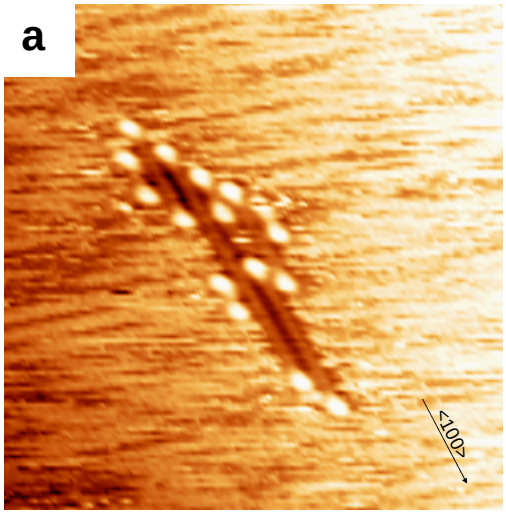

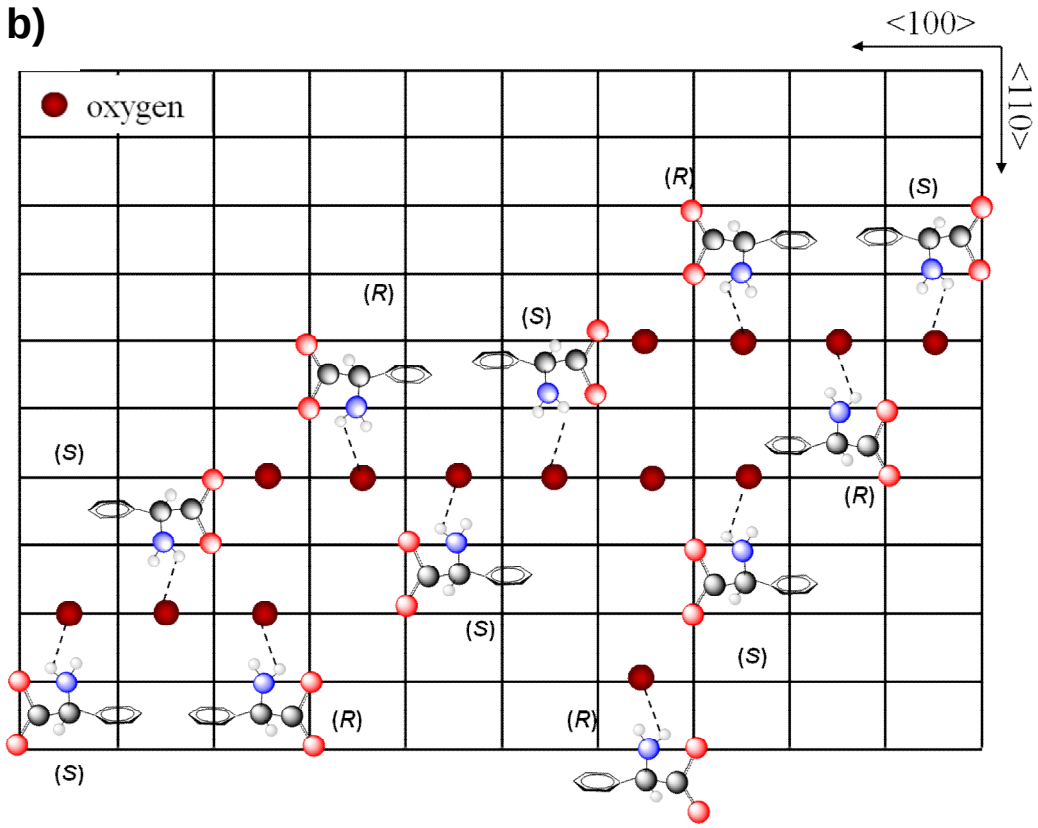

Fig. 5.5: a) STM image of phenylglycine decorated added Cu-O rows (0.18 nA, -0.84 V, 13.2 × 13.2 nm^2), phenylglycine molecules appear in pairs along the oxygen rows, but as individual feature at both ends. b) Proposed arrangement of phenylglycine molecules decorating the Cu-O rows, handedness (*R*, *S*) of phenylglycine molecule is placed randomly along the added oxygen rows that are indicated with red balls.

5.3.3 Adenine co-adsorbed on p(2 × 1)O/Cu(110) surfaces

Adenine molecules display different behaviour after being co-deposited onto the Cu(110) surface pre-covered with oxygen. The presence of small amounts of oxygen, forming Cu (110)-O (2 × 1) domains aligned along one of the <100> high symmetry

direction of the substrate, seemed not to affect the formation of adenine chains, except that adenine molecules show a strong tendency to decorate the ends of the O-Cu chains. As shown in the STM image, Figure 5.6a and b, differently from the isolated phenylglycine molecules found alongside the oxygen rows, the protrusion features, much bigger than a single adenine adsorbed species in size, correspond to short adenine dimer chains and dimer or trimers, as a consequence of the strong ability of adenine to form a variety of intermolecular double hydrogen bonds. The inset image in Figure 5.6b shows the adenine dimer chains at a high resolution. Previous studies suggest that the stronger intermolecular interaction, arising from double H-bonds, and the relatively weak adsorbate-substrate interaction between the amino group and copper atoms are responsible for the formation of ordered chain features [3]. In these adenine chiral chains, even though the $-NH_2$ group is available to connect with the oxygen rows by forming N-H···O hydrogen bond. The strength of this bond is not sufficient, in comparison with the double intermolecular double hydrogen bonds, to influence the self-assembly of adenine on Cu(110) surfaces. This results in the formation of dominant ordered molecular dimer chains after annealing at 470 K.

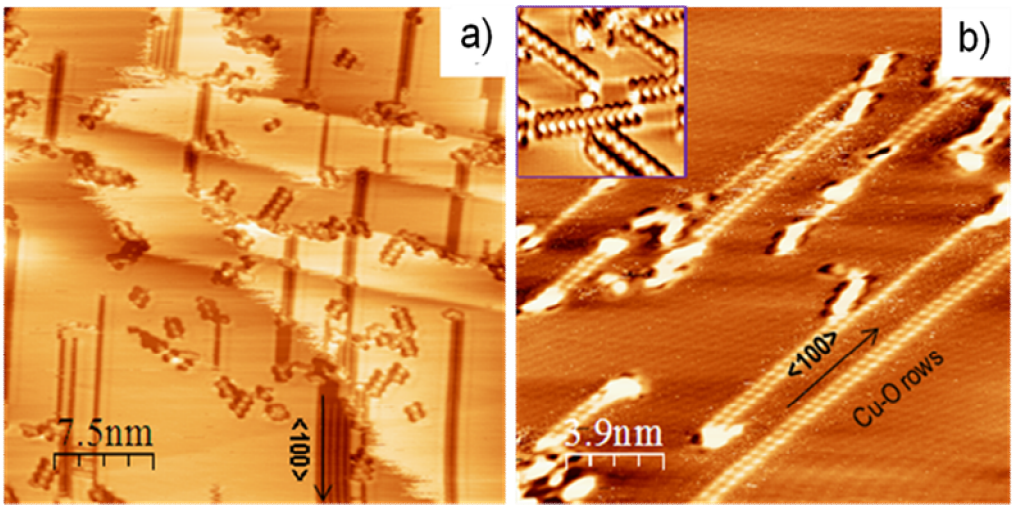

Fig. 5.6: Adsorption of adenine onto the Cu(110) surface pre-covered with added O-Cu rows. a) Co-existence of chiral related short dimer chains and ordered long oxygen rows appearing as depressed features (-1.34 V, 0.70 nA, 38 × 38 nm^2). b) Image of oxygen rows decorated with adenine clusters on both ends. (0.92 V, 0.90 nA, 18 × 18 nm^2), inset image shows the adenine chiral chains at molecular resolution (-1.12 V, 0.45 nA, 14 × 14 nm^2).

5.4 Conclusions

In summary, phenylglycine molecules adsorb in anionic form on the p(2 × 1) O-Cu(110) surface, they bind with the substrate via both the oxygen atoms of the carboxylate group at low coverage; this leaves the phenyl ring lying nearly parallel to the surface. This conclusion is consistent with the experimental findings revealed using RAIR spectra. The observed ordered molecular arrays result from the strong substrate-adsorbate interactions, originating from the binding of the oxygen atoms of the carboxylate functionality with the copper atoms, as well as the ring-metal interactions. The longer intermolecular distance rules out the existence of intermolecular hydrogen bonds which are commonly found in molecular networks formed by amino acid molecules [1, 2]. The nearly flat-lying phenyl ring, suggested for the molecular adsorption geometry at low coverage, is in favour of the π-metal interactions which contribute to the stabilization of short- range molecular networks.

Co-deposition of (*R, S*)-phenylglycine and adenine onto the Cu(110) surfaces pre-covered with oxygen, revealed that, at low coverage, phenylglycine tends to interact with oxygen rows as individual motif through the hydrogen bonding formed between amino groups and oxygen atoms. In comparison, adenine showed strong preference to form short dimer chains at the ends of the oxygen rows due to its stronger ability to form intermolecular double hydrogen bonds. The apparent difference in their behaviours upon co-deposition with oxygen is due to their unique interaction mechanisms responsible for the formation of each of the ordered overlayer structure.

5.5 References

1. Q. Chen, C. W. Lee, D. J. Frankel and N. V. Richardson, *PhysChemComm* 9, **1999**, 05986.
2. Q. Chen, D. J. Frankel, C. W. Lee and N. V. Richardson, *Chemical Physical Letters* 349, **2001**, 167.
3. Q. Chen and N. V Richardson, *Nature Materials* 2, **2003**, 324.
4. S. Blankenburg and W. G. Schmidt, *Phys. Rev. Lett.* 99, **2007**,196107.
5. S. Blankenburg and W. G. Schmidt, *Phys. Rev.* B 78, **2008**, 233411.
6. F. Besenbacher and J. K. Norskov, *Prog. Surf. Sci*. 44, **1993**, 5.
7. A. F. Carley, P. R. Davies, M. W. Roberts, N. Shukla, Y. Song and K. K. Thomas, *Appl. Surf. Sci.* 81, **1994**, 265.
8. A. F. Carley, A. Chambers, P. R. Davies, G. G. Mariotti, R. Kurian and M. W. Roberts, *Faraday Discuss* 105, **1996**, 225.
9. B. Afsin, P. R. Davies, A. Pashuski and M. W. Roberts, *Surf. Sci. Lett*. 259, **1991**, L 724.
10. A. Boronin, A. Pashuski and M. W. Roberts, *Catal. Lett*. 16, **1992**, 345.
11. B. Afsin, P. R. Davies, A. Pashuski and M. W. Roberts, *Surf. Sci*. 284, **1993**, 109.
12. A. F. Carley, P. R. Davies, R. V. Jones, G. U. Kulkarni and M. W. Roberts, *Chem. Commun*. **1999**, 687.
13. S. M. Barlow, K. J. Kitching, S. Haq and N. V. Richardson, *Surf. Sci*. 401, **1998**, 322.
14. J. Hasselstrom, O. Karis, M. Weinelt, N. Wassdahl, A. Nilsson, M. Nyberg, L. G. M. Pettersson, M. G. Samant and J. Stohr, *Surf. Sci*. 401, **1998**, 221.
15. N. A. Booth, D. P. Woodruff, O. Schaff, T. Giessel, R. Lindsay, P. Baumgartel and A. M. Bradshaw, *Surf. Sci*. 397, **1998**, 258.
16. J. Williams, S. Haq and R. Raval, *Surf. Sci*. 368, **1996**, 303.
17. S. M. Barlow, S. Louafi, D. Le Roux, J. Williams, C. Muryn, S. Haq and R. Raval, *Langmuir* 20, **2004**, 7171.
18. S. M. Barlow, S. Louafi, D. Le Roux, J. Williams, C. Muryn, S. Haq and R. Raval, *Surf. Sci*. 590, **2005**, 243.
19. D. I. Sayago, M. Polcik, G. Nisbet, C. L. A. Lamont and D. P. Woodruff, *Surf. Sci*. 590, **2005**, 76.
20. X. C. Guo and R. J. Madix, *Surf. Sci.* 367, **1995**, L95.

CHAPTER VI
Conclusions and Outlook

6.1 Conclusions

The aim of this thesis has been to investigate the adsorption behaviours of adenine and (*R, S*)-phenylglycine molecules, in terms of molecular orientation, substrate-adsorbate and intermolecular interactions, on Cu(110) surfaces. The samples were prepared by depositing molecules onto the Cu(110) surface via vacuum chemical vapour deposition under various experimental conditions in order to understand the effect of experimental parameters, *e.g.* surface coverage, annealing temperature, deposition rate, and pre-adsorption of oxygen, on the molecular self-organization on the surfaces. The adlayer structures were characterized by STM and RAIRS in combination with other surface sensitive techniques and DFT calculations; some gas-phase structural models are proposed. The following are the main conclusions drawn from the experimental results:

In Chapter III, it is found that the adsorption behaviour of adenine on Cu(110) surfaces is strongly influenced by the corresponding experimental parameters.

1. In a dense monolayer, adenine molecules formed ordered 2D chain structures aligning along the <110> direction. The small unit cell dimension suggested by the corresponding LEED patterns implies adenine is oriented with its planar ring tilted significantly toward the surface normal; the orientation is consistent with the observation of strong NH_2 scissor vibrations in the RAIR spectra.
2. Upon increasing the annealing temperature, adenine overlayer structures evolve from disordered molecular islands at room temperature to longer chains aligning along the <110> direction, coexisting with disordered molecular clusters. Well ordered chiral related chains formed after the annealing temperature was increased to 490 K. In this process, significant molecular diffusion induced by annealing gives rise to the various self-organized structures which are stabilized by the intermolecular interaction. In all these phases, adenine is suggested to lie flat on the surface.

3. Depositing adenine onto the substrate maintained at 490 K resulted in new ordered mirror reflection domains. In the chiral domains, chemisorbed species were suggested to bind with the copper substrate mainly via the ring imino N(7) atoms with partial contribution from the amino N atoms and copper interaction. The intermolecular H-bonds formed between dimers, $\mathbf{A_5A_5}$ and $\mathbf{A_2A_2}$, or $\mathbf{\bar{A}_5\bar{A}_5}$ and $\mathbf{\bar{A}_2\bar{A}_2}$, are suggested to be responsible for the growth of longer chains, while the relatively strong substrate-adsorbate interactions account for the formation of large domains. The binding nature of adenine with copper favours a flat lying molecular orientation.

4. Upon dosing adenine at low deposition rate and high coverage *ca.* 0.70 ML, ordered adlayer structures composed of new ladder chains and 1D linear chains along the <110> direction, in addition to the chiral chains long the (±1, 2) directions, were observed. The formation of the new chain structures is suggested to be related to the significant molecular aggregation arising from the low deposition rate. Driven by annealing, adenine molecules have the preference to form the stable dimers, $\mathbf{A_5A_5}$ **or** $\mathbf{\bar{A}_5\bar{A}_5}$; then these dimers have equal possibility to connect with each other via one of the four available H-bonding sites, 1, 2, 3 and 6, giving rise to the co-existence of various structures. The initial registry of the dimer on the Cu(110) substrate, along with the directional intermolecular H-bonds, is suggested to govern the growth direction of the chains. From the proposed gas-phase models, molecules are suggested to adsorb in flat-lying or slightly up-tilted orientation, and all the N atoms of the amino groups are placed at on-top sites or closely to on-top site, in order to facilitate the N-Cu interaction.

5. At very low coverage upon annealing to 440 K, a number of adenine dimers and trimers oriented in different directions, as well as short chiral chains composed of two or four pairs, were obtained. The co-existence of mirror related dimers and trimers that are related via either mirror reflection along the high symmetry directions of the substrate or C_2 rotation symmetry, revealed that the formation of chiral chains along the (±1, 2) direction starts with the formation of a dimer, to which a single diffusing adsorbate of the same chirality connects via the second type of double H-bond, 6. Longer chains formed upon further diffusion of these small molecular units driven by annealing to 490 K.

6. The intramolecular contrast variations of adenine adsorbates in the chiral chains along the (±1, 2) directions can be influenced by such factors as the adsorption of adsorbate onto the tip apex during scanning, the different orientation of the chains with respect to the tip scanning direction, in particular changing the magnitude and polarity of the tip-sample bias. At room temperature and 70 K, STM images show that the chiral chains aligning closely along the fast scanning direction are characterized by bright spot features arranged in parallel, while the chains, regardless of the chirality, growing at a certain angle with respect to the fast scanning direction consist of elongated features. Low temperature STM images also revealed that the adsorbates composed of the chains display different contrast in comparison to the isolated adsorbate because of the extensive intermolecular interactions. Proposed structural models for these adsorbates suggest that the long dimension of the isolated adsorbate is aligned almost along the <100> direction, which is different to the ones in the chains. Hence, molecular re-orientation is required upon re-organization of these isolated adsorbates to form the chains. Comparison of the adenine frontier molecular orbitals with the bias-dependent images of a single adenine adsorbate suggests that tunneling of adenine adsorbed on the Cu(110) surface occurs via a resonance mechanism arising from the coupling of the molecular orbitals with the tip and sample Fermi levels.

In chapter IV, detailed investigation of the adsorption behavior of (*R, S*)-phenylglycine on the Cu(110) surface using RAIRS suggests that the molecular orientation changes as a function of the surface coverage. At low coverage, phenylglycine is suggested to bind with the copper atoms via both the oxygen atoms of the carboxylate group at equidistance along the <110> direction of the Cu(110) substrate; this leaves the phenyl ring lying nearly flat on the surface. Upon increasing coverage, due to the limited free surface space, a new upright adsorption geometry is suggested. In this phase, phenylglycine is coordinated with the substrate via the amino N atom and one of the oxygen atoms of the carboxylate, whilst leaving its phenyl ring standing up. This binding nature is analogous with these suggested for other amino acids adsorbed on Cu(110) surfaces at high coverage. At saturation coverage, the observation of C=O vibrations in the RAIR spectra indicates the appearance of intact phenylglycine molecules on the surfaces.

In chapter V, depositions of a small amount of (*R*, *S*)-phenylglycine and adenine onto the p(2 × 1) O-Cu(110) surfaces were studied using STM. Some phenylglycine molecules form ordered molecular arrays and others prefer to decorate the added oxygen rows. Within the molecular arrays, phenylglycine is suggested to orient with the phenyl ring lying flat at the surface, which is in agreement with the experimental findings revealed by RAIRS at low coverage. The relatively large inter-molecular separation between adjacent adsorbates rules out the formation of intermolecular H-bonds. However, the aromatic ring-metal interactions, in addition to the strong substrate-adsorbate interactions originating from the binding of the oxygen atoms of the carboxylate functionality with the copper atoms, might account for the ordering of the adlayer structures. Additionally, formation of oxygen-rows decorated by individual adsorbed phenylglycine molecules indicates the formation of H-bonds between amino groups of the phenylglycine molecules and the oxygen atoms. Comparison is made with analogous structures observed for adenine molecules co-deposited onto oxygen pre-covered Cu(110) surfaces. Different from phenylglycine, adenine forms short chiral chains observed at the ends of the oxygen rows. This suggests intermolecular H-bonds, rather than substrate-adsorbate interactions, are responsible for the formation of the corresponding ordered self-assembled structures.

6.2 Outlook

Future research based on the work presented in this thesis would be the co-deposition of (*R*, *S*)-phenylglycine or other amino acids, *e.g.* glycine or alanine, with the adenine dimers and trimers at very low coverage, with the aim to investigate the chiral interaction at molecular level. It is believed these adsorption experiments carried out at a low coverage will be helpful not only in determining the associated molecular orientation on the Cu(110) surfaces, but also in understanding the preferential chiral interactions of other amino acids with the chemisorbed adenine species.

6.3 Papers under preparation

1. Self-assembly of adenine on Cu(110) surfaces at low deposition rate
2. Contrast variations of adenine chains and monomers on Cu(110) surfaces